OPTICAL SORTING AND PHOTO-TRANSFECTION OF MAMMALIAN CELLS

Patience Mthunzi

A Thesis Submitted for the Degree of PhD
at the
University of St. Andrews

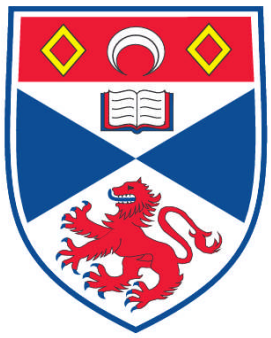

2010

Optical Sorting and Photo-transfection of Mammalian Cells

Patience Mthunzi

Optical Trapping Group

School of Physics and Astronomy

University of St Andrews

St Andrews, KY16 9SS

Scotland, UK

Optical Sorting and Photo-transfection of Mammalian Cells

Patience Mthunzi

Thesis for the degree of Doctor of Philosophy

Optical Trapping Group
School of Physics and Astronomy
University of St Andrews
St Andrews, Fife
KY16 9SS
Scotland, UK

February 2010

Declarations

I, Patience Mthunzi, hereby certify that this thesis, which is approximately 50 000 words in length, has been written by me, that it is the record of work carried out by me and that it has not been submitted in any previous application for a higher degree.

I was admitted as a research student in April 2006 and as a candidate for the degree of Doctor of Philosophy in April 2006; the higher study for which this is a record was carried out in the University of St Andrews between 2006 and 2010.

Date …….Signature of Candidate ……....

I hereby certify that the candidate has fulfilled the conditions of the Resolution and Regulations appropriate for the degree of Doctor of Philosophy in the University of St Andrews and that the candidate is qualified to submit this thesis in application for that degree.

Date ……. Signature of supervisor ……...

In submitting this thesis to the University of St Andrews we understand that we are giving permission for it to be made available for use in accordance with the regulations of the University Library for the time being in force, subject to any copyright vested in the work not being affected thereby. We also understand that the title and the abstract will be published, and that a copy of the work may be made and supplied to any bona fide library or research worker, that my thesis will be electronically accessible for personal or research use unless exempt by award of an embargo as requested below, and that the library has the right to migrate my thesis into new electronic forms as required to ensure continued access to the thesis. We have obtained any third-party copyright permissions that may be required in order to allow such access and migration, or have requested the appropriate embargo below.

The following is an agreed request by candidate and supervisor regarding the electronic publication of this thesis:

Access to printed copy and electronic publication of thesis through the University of St Andrews.

Date ……

Signature of candidate ……..

Signature of supervisor …….

Abstract

Recently, laser light sources of different regimes have emerged as an essential tool in the biophotonics research area. Classic applications include, for example: manipulating single cells and their subcellular organelles, sorting cells in microfluidic channels and the cytoplasmic delivery of both genetic and non-genetic matter of varying sizes into mammalian cells. In this thesis several new findings specifically in the optical cell sorting as well as in the photo-transfection study fields are presented. In my optical cell sorting and guiding investigations, a new technique for enhancing the dielectric contrast of mammalian cells, which is a result of cells naturally engulfing polymer microspheres from their environment, is introduced. I explore how these intracellular dielectric tags influence the scattering and gradient forces upon these cells from an externally applied optical field. I show that intracellular polymer microspheres can serve as highly directional optical scatterers and that the scattering force can enable sorting through axial guiding onto laminin coated glass coverslips upon which the selected cells adhere. Following this, I report on transient photo-transfection of mammalian cells including neuroblastomas (rat/mouse and human), embryonic kidney, Chinese hamster ovary as well as pluripotent stem cells using a tightly focused titanium sapphire femtosecond pulsed laser beam spot. These investigations permitted advanced biological studies in femtosecond laser transfection: firstly, the influence of cell passage number on the transfection efficiency; secondly, the possibility to enhance the transfection efficiency via whole culture treatments of cells thereby, synchronizing them at the mitotic (M phase) as well as the synthesis phases (S phase) of the cell cycle; thirdly, this methodology can activate the up-regulation of the protective heat shock protein 70 (hsp70). Finally, I show that this novel technology can also be used to transfect mouse embryonic stem (mES) cell colonies and the ability of differentiating these cells into the extraembryonic endoderm.

Acknowledgements

Firstly, I would like to thank the Almighty God for blessing my experiments, for the financial support throughout my PhD and for granting me the wisdom and day to day strength I needed to complete this PhD.

I would also like to thank both my supervisors, Prof. Kishan Dholakia and Dr. Frank Gunn-Moore, your assistance with my work is sincerely appreciated. Thanks also for the fantastic opportunity to work with you and learn from you. I want you to always remember that you contributed a great deal in the academic development of a girl from Soweto, which makes me feel forever indebted to you! Now to the two people I have utmost respect for, the legendary Professors: Wilson Sibbett and Malcolm Dunn. I never felt invisible or insignificant in your presence, you always stopped to say hello! That meant a lot to me, thank you for being so kind and welcoming. A big THANK you to the following people as well, Lynn (Dr. Pat!), madam Vene (darling), Graham Milne and Steve Lee. Although you're not part of the Optical Trapping group anymore, I'll never forget all the help and guidance you offered me in the optics labs. I would also like to thank Dr. S, American Dave in Scotland, what can I say???... ☺ … Dude, you're the BEST, mate! It would be a big mistake not to say THANKS to the bonnie lassies (Lotte, Eva, Kirsty and Laura) in the Gunn-Moore group, you girrrls are awesome! You made working at the Bute a pleasure for me. I also thank Tina Briscoe (you were so much fun to be around!☺) and the elusive Brian Powell for their invaluable help in the lab.

Much gratitude also goes to the Council for Scientific and Industrial Research (CSIR), National Laser Centre (NLC) for funding my PhD. Thanks to the NLC's management for their support during my time in St. Andrews.

On a personal note, I would like to thank my mom, my sis and Margaret Horton, your belief in me made me believe in myself. This thesis is dedicated to you. My friends back in South Africa, NGIYABUYA majita!!!

Table of Contents

v. Cell synchronization by Thymidine and Colcemid

vi. Preparation of stably transfected HSP-CHO-K1 and HSP-NG108-15 cells

vii. mRNA photo-transfection procedure

viii. Statistical analysis of data

Appendix C

Materials, cell culturing and plasmid DNA preparation for stem cell photo-transfection

i. Experimental setup

ii. Pluripotent stem cells used

iii. Cell culturing

iv. Plasmid DNA preparation

Abbreviations

BMSC	Bone marrow stem cells
BB	Bessel beam
CCD	Charged Coupled Camera
CHO-K1	Chinese Hamster Ovary
CW	Continuous Wave
C2GM	FDCP-mix C2GM
DEAE	Dextran Diethylaminoethyl-Dextran
DEP	Dielectrophoresis
DNA	Deoxyribonucleic Acid
Ds-Red	Discodeum Red
EGFP	Enhanced green fluorescent protein
ES	Embryonic stem
ExE	Extraembryonic endoderm
FACS	Fluorescent-activated cell sorting
Fgrad	Gradient force
Fscatt	Scattering Force
fs	Femtosecond
FWHM	Full Width at Half Maximum
GFP	Green Fluorescent Protein
HEK-293	Human embryonic kidney cells
HL60	Human promyelocytic leukemia
HSC	Haematopoietic stem cells
Hsp 70	Heat shock protein 70
ICM	Inner cell mass
LIF	Leukemia inhibitory growth factor
MACS	Magnetic-activated cell sorting
μFACS	Microfluorescent-activated cell sorting
mES	Mouse embryonic stem cells
ML	Mode-Locked

M-phase	Mitotic phase
mRNA	Messenger RNA
NA	Numerical Aperture
NIR	Near-Infrared
ns	Nanosecond
PBS	Polarizing Beam Splitter
PCR	Polymerase chain reaction
pDNA	plasmid DNA
ps	Picosecond
RPE	Retinal pigment epithelial
RNA	Ribonucleic Acid
rRNA	Ribosomal RNA
rtPCR	Reverse transcriptase polymerase chain reaction
SEM	Scanning Electron Microscope
SHG	Second Harmonic Generation
S-phase	synthesis phase
TEM_{00}	Gaussian beam mode
tRNA	Transfer RNA
UCB	Umbilical cord blood
UV	Ultra-Violet
2D	2 Dimensions
3D	3 Dimensions

Chapter 1

Introduction

1.1 Preface

Lasers are highly coherent, monochromatic light beams that may be focused into a small spot size (~µm). Depending on the energy level scheme, the population inversion, an essential step in lasing, can be either short lived or maintained continuously. In the latter mode of operation, the continuous wave (CW) regime, the laser output is relatively constant with respect to time. On the contrary, the pulsed mode of operation results in a laser output that varies with respect to time, characteristically giving high peak powers (figure 1.1).

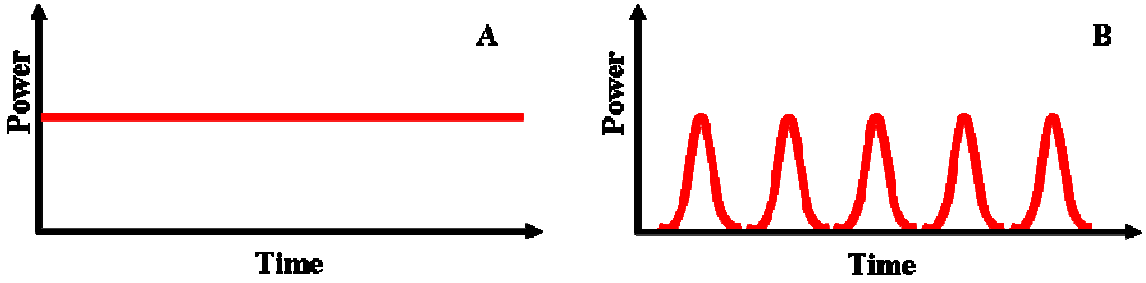

Figure 1.1: (A) profile of CW laser output with respect to time while (B) denotes the output profile of a pulsed laser relative to time.

Both these modes of laser operation have promoted an abundance of innovative techniques in the biophotonics research arena. For instance, since the conception of optical traps in 1970 (1), the first observation of single beam trapping of dielectric particles (2), and the first demonstration of optical tweezers in manipulating biological species by Arthur Ashkin *et al*, 1987 (3), the use of lasers has fuelled the development of key advances at cellular scale. Optical forces responsible for such micromanipulation are

induced by the transfer of momentum between the incident light field and transparent micro-particle under investigation. Optical forces of a CW laser light beam spot can for example, be exploited to either hold (when the beam is tightly focused) or deflect (in a weakly focused beam spot) tagged biological materials. These two scenarios are depicted in figure 1.2.

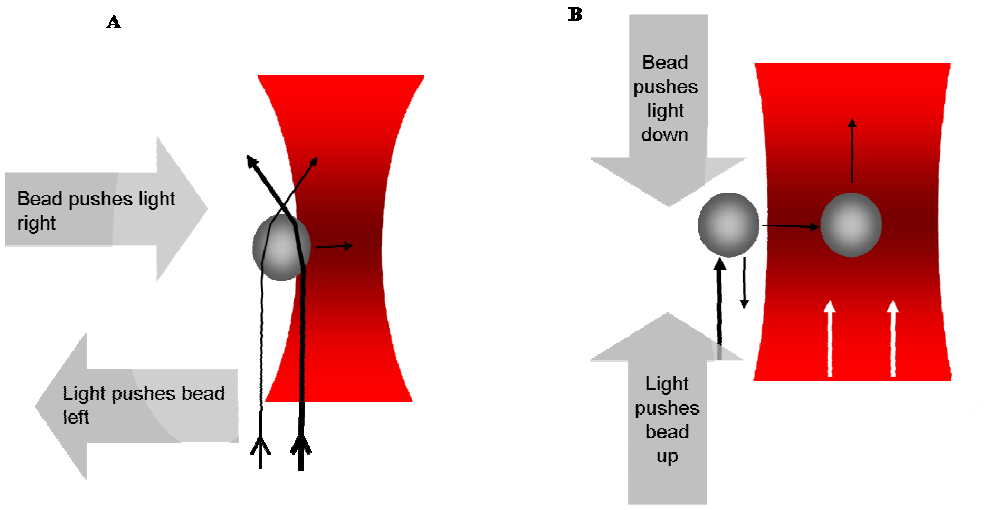

Figure 1.2: In a tightly focused beam spot (A), transparent microparticles of high refractive index can be held trapped in the region of highest beam intensity. On the contrary, optical deflection (guiding) of microparticles (B) is possible in a weakly focused beam.

Thus, CW laser sources mainly dictate optical tweezing (trapping), guiding and sorting experiments as they rarely induce the two-photon effect mainly administered by pulsed laser sources. Separately, the properties of pulsed lasers pronounces them uniquely suited to creating nonlinear effects necessary for generating inventive approaches for optical imaging, sensing, nanosurgery and laser-assisted cell transfection. In this chapter, I introduce the two major areas of my thesis where lasers of different regimes can be employed, namely: optical cell sorting, and photo-transfection of mammalian cells.

1.1.1 Mammalian cell sorting

In a mixed population of cells, the ability to sort and separate rare cells such as for example, stem cells from bone marrow cells is very attractive in biology and medicine. There are various methods of separating and sorting cells of interest, some including commercial cell separation methods such as fluorescent-activated cell sorting (FACS) and magnetic-activated cell sorting (MACS) (4). Both of these macroscopic cell sorting techniques possess high specificity and selectivity because they consist of extremely precise immunoreactions between the membrane marker proteins and labeling antibodies. However, these technologies make use of large amounts of analyte volumes, millions of cells and are expensive to run. On the other hand, non-immunological methodologies determine and separate types of cells according to their size, shape and other physical properties (5). But, these passive cell sorting techniques demonstrate a low specificity for cell separation, as cells do not remarkably show differences between each cell type with the exception of their immunological properties.

Newly emerging optical cell sorting schemes promise sorting of rare or precious cell samples in nanoliter volumes of analyte, indeed this offers prospects for potential measurements of precious biological materials examples including stem cells as well as cancer cells. In this thesis, a new microscopic fluid flow-free passive cell sorting method is presented, this makes use of a two dimensional Gaussian CW laser beam geometry in a simple micro-sample chamber that allows the sorting of a mixed population of mammalian cells.

1.1.2 Photo-transfection of mammalian cells

Several cell transfection systems such as chemical (cationic polymers and lipids), viral or physical approaches have been developed to advance uptake of foreign genes and other exogenous matter into mammalian cells (6). However, they each have limitations, viral vectors for an example possess strong gene transfection features on mammalian cells but, can incur risks such as a random recombination or immunogenicity (7). Cationic polymers and lipids on the other hand, interact with the negatively charged DNA through

electrostatic interactions resulting in polyplexes and lipoplexes successively, the major consequence of utilizing these particularly in systemic delivery, are their aggregation, instability and toxicity (8). While these vectors have a low immunogenic response, the possibility of selected modifications and the capacity to carry inserts as large as 52 kilobases. Their employment *in vivo* requires systematic administration which has been reported to escalate in a toxic response and is therefore incompatible with clinical applications (8). Yuan, 2008 reported on the advantages of some of the physical approaches used for gene therapy, drug submission and their potential application on vaccine administration. The report states that sonoporation on chick embryos is superior to electroporation, with the latter presenting risks of lethal damages (9).

For both *in vitro* and *in vivo* procedures, a gene, drug and/or vaccine delivery scheme possessing a minimum cytotoxicity and immunogenic response, which can be applied under sterile tissue culture protocols and can also offer targeted treatment of individual cells, organelles and organs, is highly desirable. Optical cell transfection, henceforth known as photo-transfection, satisfies these criteria. In this thesis I present novel photo-transfection studies, entailing the photo-transfection of new cell lines including pluripotent stem cells and investigations towards improved photo-transfection efficiency using femtosecond (fs) laser pulses.

Both the optical cell sorting and photo-transfection topics in tandem with their adaptability to portable micro sample chambers form a key part of the broader vision of the Biophotonics research area on a global scale.

1.2 Synopsis of thesis

Seven chapters are transcribed within this thesis. Chapter 1, as already outlined, summarizes some of the uses of optical forces and fs laser pulses in Biophotonics. Chapters 2 and 3 focus on optical cell tweezing and guiding projects. Explicitly, in Chapter 2, the forces governing the optical tweezing procedure are described in detail.

Mechanisms for the two approaches followed in optical tweezing particles of different sizes, namely, the Mie and Rayleigh regimes are offered. The Rayleigh regime ($a<<\lambda$; where a = diameter of the tweezed particle and λ = the wavelength of the tweezing beam) is followed where the particle size is smaller than the wavelength of the tweezing beam; in contrast, in the Mie ($a>>\lambda$) regime the particles have diameters larger than the wavelength of the tweezing beam see figure 1.3 below.

Figure 1.3: In the Mie regime the diameter of the particle to be manipulated is large compared to the wavelength of the tweezing beam and in the Rayleigh regime the particle is much smaller than the wavelength of light used for tweezing.

The chapter then proceeds to explain measurements of the optical trap efficiency and gives illustration on constructing a basic optical tweezing setup. Following this, optical trapping using a tightly focused 3D Gaussian (TEM_{00} mode) beam profile of colloidal particles is demonstrated. Thereafter a review of the laser beam trapping wavelengths suitable for optical treatment of biological material to avoid photo-damage is presented. Then, the employment of optical forces in optical cell guiding and/or deflection as well as optical cell sorting is explored. A description of the arrangement of a two-dimensional TEM_{00} mode beam optical trap utilized for optical guiding purposes is given. Finally a review of optical cell sorting with specific emphasis on immunological (both macroscopic and microscopic) versus non-immunological as well as with fluid flow

versus without fluid flow optical sorting schemes is outlined.

Chapter 3 covers laboratory data and the analysis of the theoretical concepts surrounding the particular experiments. Initially this chapter introduces the concept of phagocytosis as an intracellular tagging technique to improve the dielectric property of cells. Thereafter a comprehensive description of experimental work involving microsphere-cell incubation, cell viability measurements, microsphere detection by fluorescence and confocal microscopy and finally microsphere quantification using Labview particle tracking is presented. To study the effect of these intracellular dielectric tags on the scattering and gradient forces during three dimensional trapping where the beam is tightly focused and the gradient force overcomes the scattering force, the trapping efficiency of cells encapsulating the different numbers of microspheres compared to those without engulfed spheres is determined. The chapter moves on to display that, in a diverging beam optical field, where the scattering force overcomes the gradient force, the intracellular polymer microspheres serve as highly directional optical scatterers. Hence, axial optical guiding (pushing in the direction of laser beam propagation) of cells engulfing a varying number of spheres compared to those without dielectric tags is enhanced by strong scattering forces from these cells. Finally in this chapter, the improved axial guiding nature of cells with spheres is capitalized upon for levitating the intracellularly tagged cells onto laminin coated coverslips thereby optically sorting them from the rest of the cell sample lacking the dielectric tags.

Chapters 4 to 6 are based on fs laser assisted transfection work or photo-transfection as it is called in this thesis. Specifically, chapter 4 begins by explaining the biological significance of cell transfection, detailing the plasma membrane composition of eukaryotic cells and transport mechanisms of biomolecules through the plasma membrane. This chapter then continues to give a review of the different modes of developed cell transfection strategies including an emphasis to laser assisted transfection techniques. Finally, in chapter 4 the mechanisms of fs transfection are briefly described.

Both Chapters 5 and 6 provide laboratory data of fs laser assisted mammalian cell transfection. Chapter 5 begins by explaining measurements of the fs beam profile and pulse duration in a basic TEM_{00} mode beam setup. Thereafter, the experimental part starts by reporting on the different cell lines successfully photo-transfected with the Discodeum red (DsRed2-Mito) and enhanced green fluorescent protein (EGFP) plasmid DNA including the previously difficult to transfect neuroblastoma cell lines. This chapter then addresses various aspects which influence the photo-transfection efficiency, such as the change in optical parameters (average power output (irradiance) and time of beam exposure on the cell sample), culture passage number, and the stages of the cell division cycle. Following this, studies investigating potential cellular stress responses and/or the cytoprotective role of hsp70 post photo-transfection are performed. Lastly in this chapter, a study reporting on the introduction of mRNA, which is directly translated upon reaching the cytosol without crossing the nuclear membrane, is presented.

Chapter 6 details the photo-transfection as well as the differentiation of pluripotent stem cells. Initially in this chapter an introduction of stem cells and their employment as a therapy is explored. The chapter then continues in explaining the use of stem cells as a cell-based therapy. Experimental results displaying successful photo-transfection of E14g2a mouse embryonic stem cells using pDsRed2-Mito plasmid DNA are offered. Finally, laboratory data showing differentiation of these cells to the extraembryonic endoderm using the pCAGSIH-Gata-6 plasmid through photo-transfection is reported.

To finish, chapter 7 summarizes the content and discussions within this thesis, with special emphasis on the novel aspects of this work and its potential impact to future experimental projects in the optical cell tweezing, cell sorting and photo-transfection research fields. The last portion of this concluding chapter outlines the publication status and conference presentations of the work presented in this thesis.

References

1. A. Ashkin, "Acceleration and Trapping of Particles by Radiation Pressure," *Physical Review Letters* **24**, 156-159 (1970)
2. A. Ashkin, J.-M. Dziedzic, J. E. Bjorkholm and S. Chu, "Observation of a single-beam gradient force optical trap for dielectric particles," *Optics Letters* **11**, 288-290 (1986)
3. A. Ashkin and J. M. Dziedzic, "Optical Trapping and Manipulation of Viruses and Bacteria," *Science* **235**, 1517-1520 (1987)
4. D. L. Siegel, T. Y. Chang, S. L. Russell and V. Y. Bunya, "Isolation of cell surface-specific human monoclonal antibodies using phage display and magnetically-activated cell sorting: applications in immunohematology," *Journal of Immunological Methods* **206**, 73-85 (1997)
5. P. R. C. Gascoyne and J. Vykoukal, "Particle separation by dielectrophoresis," *Electrophoresis* **23**, 1973-1983 (2002)
6. C. P. Yao, Z. X. Zhang, R. Rahmanzadeh and G. Huettmann, "Laser-based gene transfection and gene therapy," *IEEE Trans. Nanobiosci.* **7**, 111-119 (2008)
7. T. Ito, Y. Koyama and M. Otsuka, "Analysis of the surface structure of DNA/polycation/hyaluronic acid ternary complex by Raman microscopy," *Journal of Pharmaceutical and Biomedical Analysis* **51**, 268-272 (2010)
8. M. Morille, C. Passirani, A. Vonarbourg, A. Clavreul and J. P. Benoit, "Progress in developing cationic vectors for non-viral systemic gene therapy against cancer," *Biomaterials* **29**, 3477-3496 (2008)
9. T. F. Yuan, "Noninvasive vaccination: From the perspective of sonoporation," *Vaccine* **26**, 4109-4110 (2008)

Chapter 2

Optical forces for tweezing, guiding and sorting of biological and colloidal particles

Introduction

In this chapter, a brief history of the different optical trap geometries including the dual beam trap, the levitation trap and an optical tweezers trap is described. Following this, the gradient and scattering forces responsible for the 3D optical tweezing procedure are described in detail. Then the mechanisms for trapping Mie (the ray optics approach) and Rayleigh particles, as well as a detailed description of measurements of the optical trap efficiency (the Q-value method), are offered. Construction of a basic optical tweezing apparatus using a diode laser (658 nm, average power 50 mW) is given, with the use of each optical element in the trap explained. Next, I demonstrate simple optical trapping using a tightly focused 3D TEM_{00} mode beam profile of colloidal (3 μm polymer microspheres) particles achieved using this trap. Although laser light sources of different wavelengths can be utilized for building optical tweezers and for successfully trapping colloidal particles, normally, near infrared laser wavelengths are suitable for conducting biological studies. Therefore, a brief review of the laser beam trapping wavelengths appropriate for optical treatment of biological material to avoid photo-damage is presented.

Since using a less tightly focused Gaussian beam may permit either horizontal or vertical (depending on the direction of beam propagation) optical deflection ("pushing") of particles via radiation pressure. The employment of optical forces in cell guiding (transporting) as well as sorting is explored in this chapter. Firstly, Gaussian beam propagation properties such as the beam diverging angle and Rayleigh range are briefly explained. Then a description of the arrangement of a 2D Gaussian beam optical trap utilized for guiding and eventually sorting purposes is shown. Finally, a review of optical cell sorting techniques is outlined with specific emphasis on active (both macroscopic

and microscopic), passive, fluid-flow and flow-free sorting schemes.

2.1 Optical Traps

2.1.1 Overview of the different optical traps

An optical trap or “optical tweezers” as it is normally called, allows use of optical forces to either stably trap (hold) or deflect (guide) nano-scale and micro-scale particles (1, 2). Light as a photon entity carries momentum, a property that is utilized for the operation of optical tweezers. When light interacts with a minute particle, it can exchange both energy and momentum with the particle. The force exerted on the particle is equal to the momentum transferred per unit time. Since optical tweezers exert piconewton (10^{-12} N) size order forces, they lack the ability to manipulate macroscopic sized objects but have been shown to manipulate various microscopic materials including whole mammalian cells and their intracellular structures such as DNA, chromosomes and protein motors. Three of the earliest trapping geometries are depicted in figure 2.1 below, the first one, (figure 2.1 (A)) demonstrated in 1970 is the counter propagating beam trap. Then in 1974, stable single beam optical levitation traps (figure 2.1 (B)) were demonstrated, where transparent, dielectric spheres of high refractive index were manipulated (3). Optical traps reported during this time depended on radiation pressure force from a laser beam to stably hold particle in the axial plane either against a counter-propagating beam or against gravity. The transverse gradient force held the particle in the center of the Gaussian beam. Figure 2.1 below illustrates these types of traps compared to an optical tweezers trap.

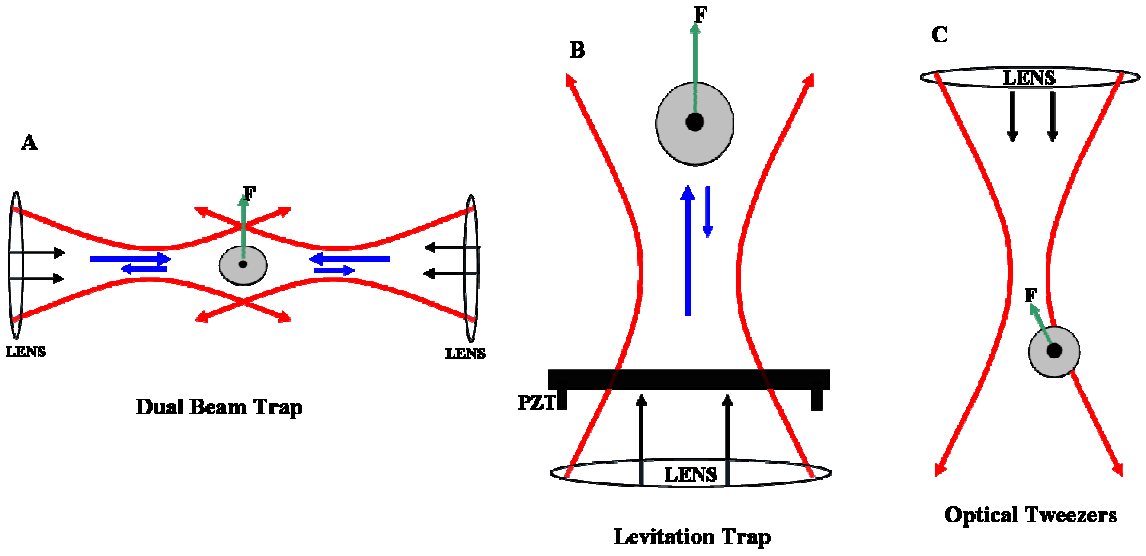

Figure 2.1: (A) is a dual beam or counter propagating trap, where lateral confinement is governed by the counter-propagating beams. (B) is a vertical levitation trap, in this geometry the Gaussian beam intensity distribution provides lateral trapping and the optical scattering force dominates the gradient force (2D trap). Finally (C) is an optical tweezers or gradient force trap. In this case the optical gradient forces are enough to overcome scattering force resulting in three-dimensional trapping of particle.

Optical traps of a wide variety based on the basic scattering and gradient forces of radiation pressure for the tweezing of neutral dielectric particles have been demonstrated (4-6). In the 1980s, stable single beam three dimensional trapping of particles with varying diameters suspended in water came to fore, through using a single tightly focused laser beam (figure 2.1 (C)) (7). This single beam gradient trap known as “optical tweezers” can be used for trapping atoms, as well as the full spectrum of Mie and Rayleigh particles. Also, it employs only a single tightly focused beam in which the axial gradient force dominates the axial stability. Section 2.2 below give a description of the roles of the gradient and scattering forces in such a 3D trap, explaining trapping of the Mie and Rayleigh particles, and finally displays how the trap efficiency of an optical tweezers system is determined.

2.2 Optical forces for trapping

2.2.1 Gradient and scattering forces in a 3D trap

Three dimensional optical traps are generated by tightly focusing a laser beam with an objective lens of high numerical aperture (NA) (8, 9). The arising optical force is said to be divided into two important components known as the gradient force (F_{grad}) (in the direction of the spatial light gradient) and the scattering force (F_{scat}) (in the direction of light propagation). In a TEM_{00} mode beam the latter can be thought of as a photon exerting a force on the particle in the direction of light propagation while the gradient force tends to draw the particle towards the center of the focal region (9, 10). Balance between the two forces results in the axial equilibrium position of a trapped particle to be located slightly beyond the focal point (10). Optical tweezers therefore work because the transparent microparticles with a higher index of refraction than their suspending medium are pulled to the region of maximum laser intensity. The particle (microsphere or cell) thus trapped in the beam can be moved about by moving the laser focal spot to manipulate its position. Two different approaches are needed to further elucidate the forces driving the optical trapping process, one based on the ray optics for particles is the Mie regime, and the other based on the electric field associated with light for Rayleigh particles (see section 2.2.2).

2.2.2 Interaction of light and Mie particles

To calculate the forces acting upon a dielectric particle with a diameter larger than the wavelength of the trapping light beam, the ray optics approach is used. To model how the laser beam impinges with the transparent particle, a bundle of rays is utilized; with each ray weighted according to the light intensity it possesses (i.e. the closer to the region of higher light intensity of the Gaussian beam pattern (Figure 2.2 A), the higher the light intensity of the ray and the thicker its weight).

A photon of wavelength λ has a momentum:

$$\overline{p} = \frac{h}{\lambda} \qquad \text{or} \qquad \hbar k \qquad (2.1)$$

where, h is Planck's constant, $\hbar$ is $h/2\pi$ and k is the wave number. On interacting with light through, for example, reflection or refraction, an object causes light to change direction. The change in momentum of the light will raise an equal but opposite change of momentum on the object. Within the Mie regime, if a transparent microscopic particle is situated within a gradient of light, the refraction of rays of differing intensity (due to gradient) through the particle results in a change in total momentum of the existing light beam and hence a corresponding reaction force on the particle, which draws the particle into the region of highest light intensity of the beam (see Figure 2.2 (A) below). A balance is reached and the particle is held in the centre of the beam as the rays of light passing through and exiting the particle reach equilibrium with no overall change in momentum of the beam. This trapping force is due to the transverse gradient force which is a result of the Gaussian intensity distribution of the laser mode, however an axial gradient is also required in order to lift the particle and manipulate it in three dimensions.

In the case of axial trapping i.e. in the z direction (vertical plane), off-axis rays come in at an angle towards the particle and gain momentum in the direction of beam propagation. This change in momentum leads to a force which pushes the sphere upwards against the direction of beam propagation towards the focal region of the beam resulting in a trapping force in the z-direction, and thus a three dimensional optical trap. The equilibrium position is reached when the scattering force and gravity (which both act to push the sphere downwards) is balanced by the axial gradient force (which pushes the sphere upwards) (Figure 2.2 (B)).

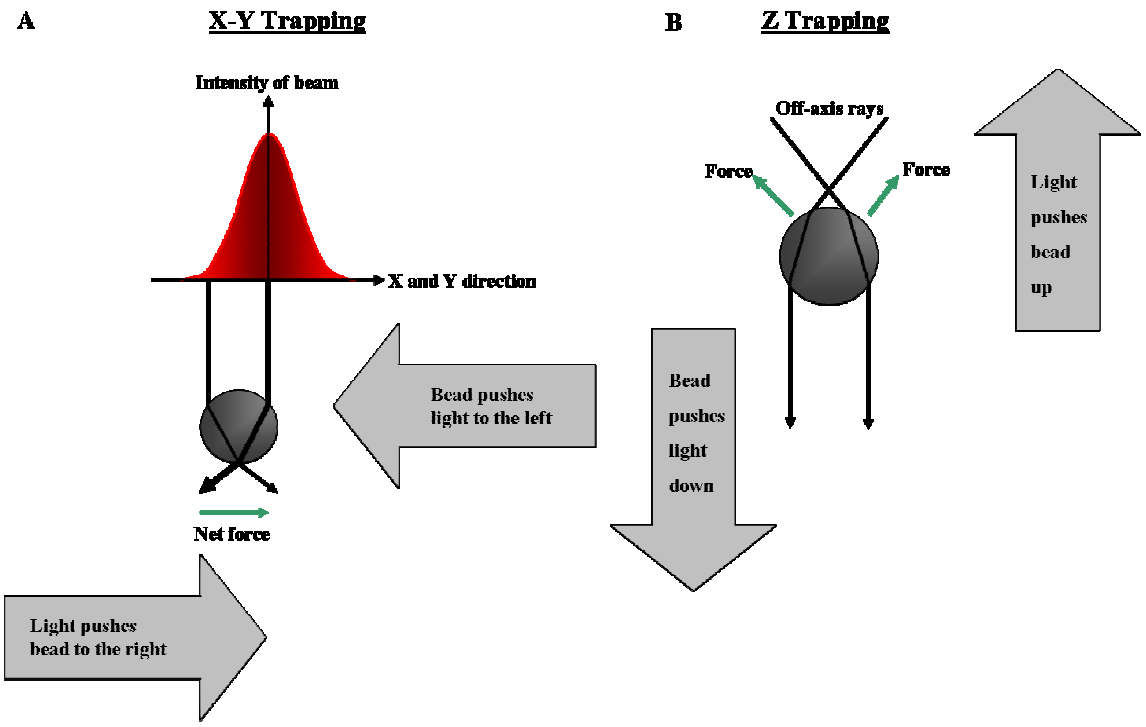

Figure 2.2: In an upright trap, the force arising from the laser beam equal the pull of gravity. For particles to be tweezed in 3D, it is imperative to exert a longitudinal force in the same direction as the laser and a transverse force at right angles to the beam. The transverse force results from having the laser intensity at the central axis of the beam. (A) If the dielectric object is of a high refractive index than the surrounding medium, and is placed to the left of the central highest intensity portion of the beam, it results in more light rays to be refracted from the right to the left as they pass through the object and not vise versa. The net effect is to transfer momentum to the beam in the left direction and the particle experiences an equal but opposite force drawing it towards the centre of the beam (right direction) according to Newton's third law of motion. (B) Off-axis rays contribute to axial trapping by being refracted in the direction of beam propagation. A force is exerted on the particle of equal size but opposite direction to the change of momentum of the light (8).

2.2.3 Trapping Rayleigh particles

Particles with a much smaller diameter compared with the wavelength of the tweezing beam satisfy the Rayleigh regime. As a result of the minute sizes of Rayleigh particles, the ray optics approach is not appropriate to calculate the tweezing forces as only a fraction of the wave has an effect on the particle. For these particles it is better to consider the force in terms of the electric field in the region of the trapped particle.

Upon being placed in an electric field, a polarisable particle will experience an electric dipole moment in response to the electric field of light and is attracted to intensity gradients in the electric field towards the focus (if the polarisability is positive, i.e. relative refractive index > 1). The energy of the system will be at a minimum when the particle moves to wherever the field is highest and that is at the focus.

Both the colloidal and cellular micro particles used in the experimental work of this thesis comprise diameters larger that of the laser wavelength of the tweezing beam and therefore, lie primarily in the Mie regime.

2.2.4 Optical trap efficiency

The well known Q value method is employed to quantify the trapping strength; it is an easy and rapid procedure by which the quality (efficiency) of the trap is determined. This method works by dragging a known trapped particle through a sample medium and recording the terminal velocity at which the particle leaves the trap (see illustration in figure 2.3 below). This is achieved by simply translating the motorised stage where the sample chamber is held at a known velocity and thereafter calculating the velocity at which the particle falls out of the trap. During the process at which the sample stage is translated and the object falls out of the trap, the Stokes drag force, F_{Stokes} is equal to the optical force exerted on the particle, F_{trap}. Using a motion controller, it is possible to manoeuvre the sample stage at a constant velocity. The sample chamber usually consists of a glass slide (bottom) and a top glass coverslip separated by a vinyl spacer (~ 100 µm depth, diameter = 12 mm). The dielectric particles to be trapped are normally suspended in water.

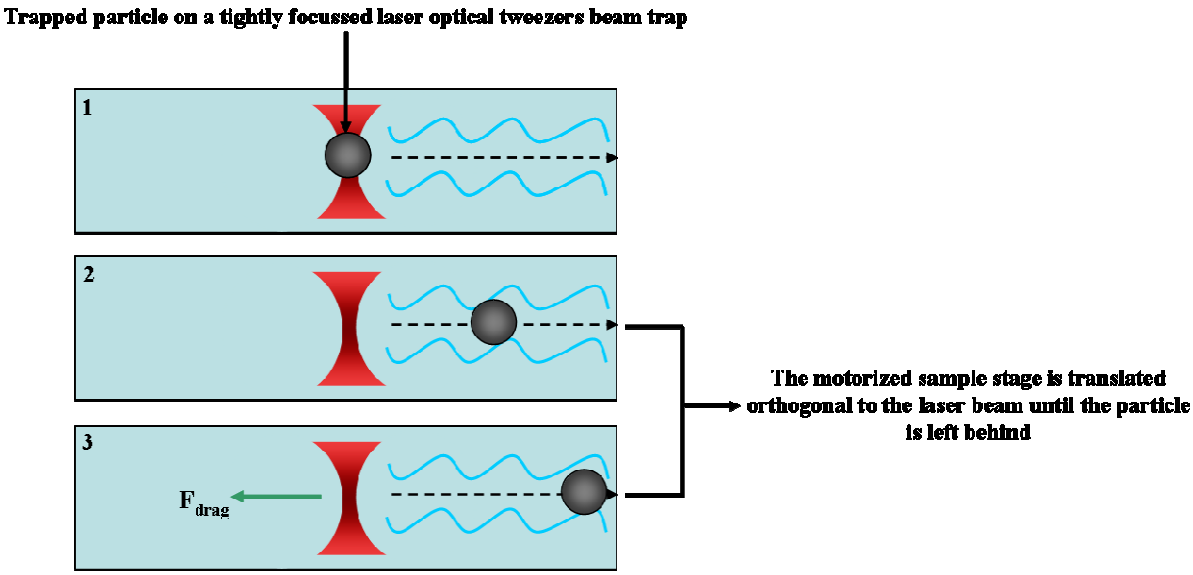

Figure 2.3: The drag force opposes the relative motion of a particle through a fluid, acts in the direction opposite to the oncoming flow velocity and depends on the velocity.

$$F_{Stokes} = 6\pi\eta r v \qquad (2.2)$$

This is the maximum force that the optical trap can exert at the specified laser power and will typically be of the order of 10^{-12} N (11). Where η is the viscosity of the medium, r is the particle diameter, and v is the velocity of the particle with respect to the fluid, exceeds the applied trapping force. The critical velocity for removal of the trapped particle scales linearly with the laser power in the optical trap (as shown in equation 2.3 below). The trapping efficiency of any optical tweezers configuration is usually described in terms of a dimensionless parameter Q, the fraction of momentum transferred to the trapping force from the trapping laser beam, which is related to the force on the particle, F_{trap}, the power output of the laser, P, c the speed of light, and the refractive index of the surrounding medium, n_m through the relationship:

$$F_{trap} = \frac{Qn_m P}{c} \qquad (2.3)$$

Since the Stokes drag is equal to the optical force exerted on the particle;

$$F_{Stokes} = F_{trap} \tag{2.4}$$

therefore,

$$6\pi\eta r v = \frac{Q n_m P}{c} \tag{2.5}$$

and,

$$Q = \frac{6\pi\eta r v c}{n_m P} \tag{2.6}$$

Previously researchers have reported on both the axial (Q_{axial}) as well as the lateral ($Q_{\text{lat.}}$) trapping efficiencies of microparticles to quantify the degree to which these particles are effectively trapped (12). For optical forces acting on a small dielectric particle, Q values tend to be in the range 0.03 to 0.1 (13). Data on Q values for a variety of experimental optical trapping geometries consisting of differing laser beam shapes is available in the literature, though this work has been mostly performed using microspheres (14-16). Within conventional optical tweezers Q_{axial} is usually an order of magnitude smaller than $Q_{\text{lat.}}$ (17).

In chapter 3 I calculate the Q value of an optical trap experimentally by measuring the maximum velocity that intracellularly tagged mammalian cells can be dragged through a viscous medium. First in the following section, I describe the construction of a basic optical tweezing setup.

2.3 Basic optical tweezing system

2.3.1 Building optical tweezers

Assembly of an optical tweezers system can be achieved with standard optical components. In order to expand, reflect and steer the tweezing beam at the back aperture of the delivering objective lens, sets of lenses and mirrors were arranged in the beam path of an optical tweezers system. In order to obtain the necessary diffraction-limited spot at the beam focus, as the laser beam is emitted, it must be expanded to either exactly match or slightly overfill the back aperture of the delivering objective lens. In addition, the ability to steer the beam is crucial to enable beam tilting at the back aperture. Lee *et al*, 2007 (14) report on the necessary guidelines on constructing and characterizing a basic single beam tweezing setup. Figure 2.4 below illustrates an optical tweezers setup which consisted of a 658 nm, 50 mW diode laser. The beam spot emitted with a 1.5 mm diameter was magnified through a simple two plano-convex lens telescope L1 and L2 (f = 50 mm and f = 150 mm respectively) to ~ 5 mm. The beam was then reflected on a flip mirror M placed at 45^{o} to the incident laser beam path.

Mirrors M1 and M2 were used in conjunction to align the beam optimally through the microscope objective. Mirror M2 located the beam onto mirror M1, which was conjugate with the back aperture of the objective. Therefore, manipulating M1 allowed tilting of the beam in the back aperture of the objective, thus allowing lateral movement of the focused beam spot in the focal plane. M1 (the beam steering mirror) was therefore used to get the beam through the objective. A simple 1:1 telescope arrangement, the optical relay system that consist part of the optical conjugates set was used to steer the laser beam spot. This comprised of two identical plano-convex lenses, L3 and L4 (f = 100 mm each), which were displaced by the sum of their focal lengths, so that an incident parallel beam produces a parallel output of the same beam diameter (13, 18). By placing these lenses with their flat surfaces facing one another, spherical aberration was minimized without resorting to expensive aplanatic lenses.

If L3 was pushed towards L4, then, movement in the axial (z-) direction occurred because the parallel beam entering the telescope (at the back of L3) became divergent after leaving L4. This pushed the focal spot away from the objective and deeper into the specimen. Conversely, if L3 was pulled away from L4 in the axial direction, the light from the telescope became convergent, bringing the focus towards the objective. Movement of lens L3 in the x-y plane, perpendicular to the optical axis, produced a deflection in the light leaving the lens in essence rotating the beam. If the lens L4 was imaged into the back of the objective aperture, then this rotation occurred in a conjugate plane to the objective aperture, resulting in a translation of the laser beam spot (19). To give the smallest possible spot size at the focus, which is imperative for stable three dimensional trapping, a 100X oil immersion objective lens with a high NA i.e., 1.25 NA was employed (10). By translating the xyz stage on which the sample was placed, the sample can be moved. A dichroic mirror positioned at 45^{o} reflected the incident laser beam into the microscope objective but also allowed white light to pass through and an image to be formed on the charge coupled device (CCD) camera which can be viewed on a computer monitor. The setup was filtered by mounting a neutral density filter in the mouth of the CCD camera to limit saturation as a result of excessive transmission of the laser light. Below the sample stage was a 35 W halogen lamp that provided incoherent illumination of the sample.

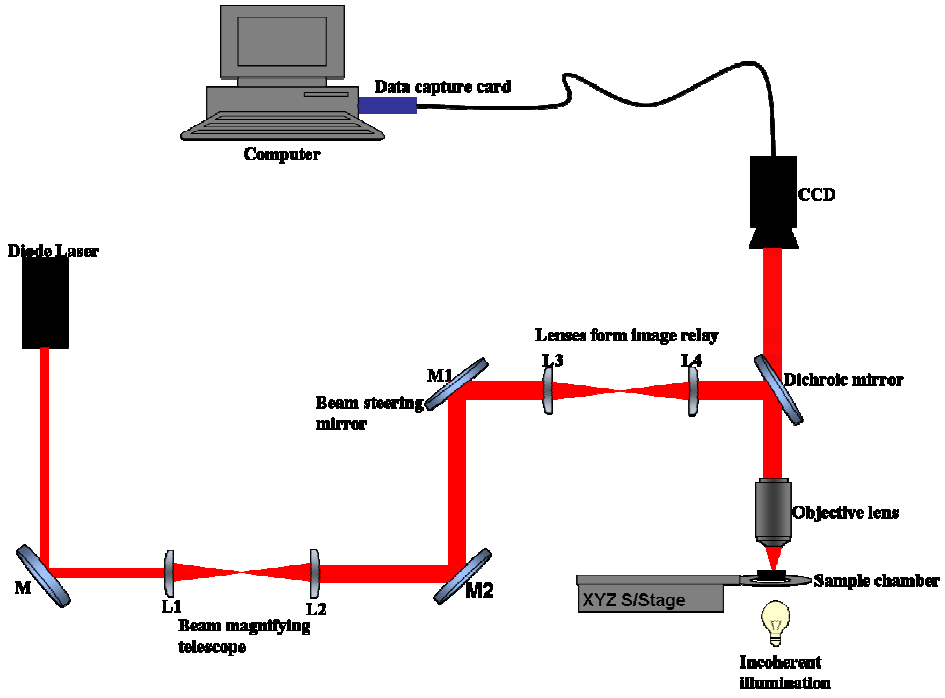

Figure 2.4: A display of a basic optical trapping device produced using a diode 658 nm diode laser with maximum output power of 50 mW. Such a setup is useful for colloidal trapping applications rather than biological applications since it consists of a visible laser light that may be absorbed in biological material and result in heating and therefore cause optical damage (optocution). Radiometric effects were avoided by suspending relatively transparent particles in transparent medium (water).

To image the beam a glass slide with some index matching oil was used. The filter between the objective and the CCD camera was removed during this stage. By translating a slide up and down at the sample cell plane a pattern of the focused light beam was seen. The incoherent light beam was left off during this point and once a spherical beam image was acquired at the sample stage only then could trapping be tested. After building and aligning the setup illustrated in figure 2.4, it was used for tweezing of 3 µm polymer spheres with a refractive index (n) 1.56 (see figure 2.5 below).

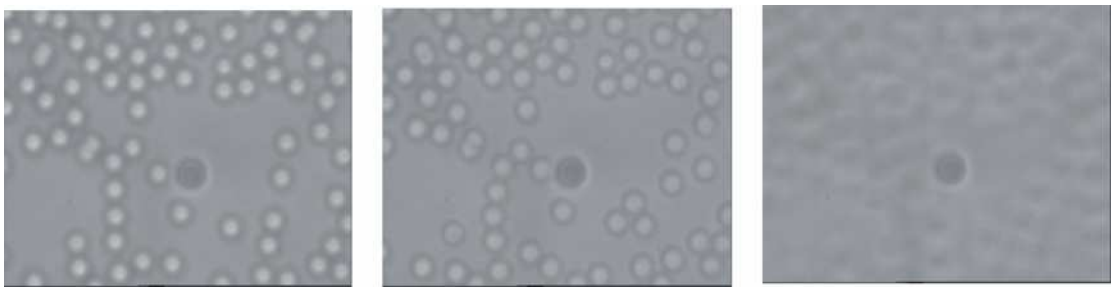

Figure 2.5: Pictures from the CCD camera displaying z-trapping of 3 µm polymer micro spheres using the optical tweezers illustrated in figure 2.4, the particles experience axial guiding by the trapping forces of laser light and migrates in the z-direction of the trap.

Figure 2.5 above illustrates the simple tweezing of polymer microspheres (diameter = 3 µm) utilizing a 658 nm diode laser system. Optical tweezers have had widespread application in biological studies as they offer, “non-invasive” precise micromanipulation of a specimen in a closed sterile environment. The response of biological cells to an applied laser beam is largely dictated by the laser wavelength as well as the laser power. Thus, Ashkin in the first studies with tweezers for biological material, recognized that near infrared (NIR) laser trapping could reduce photo-induced damage in biological cells when compared to traps made using visible light (20). Therefore to prevent the photo-damage (photobiological) effects escalating; most trapping, guiding, sorting and porating lasers operate in the NIR region of the light spectrum. Since the late 1980s a huge variety of cells and intracellular structures have been trapped and manipulated using optical tweezers. Outlined below is a summary of laser wavelength influences for biological matter.

2.4 Laser wavelength and biological material

2.4.1 Laser wavelength suitable for biological studies

The interaction of light with both biological and colloidal material can result in the refraction, reflection, absorption as well as scattering of the incident light rays. For biological species, whether individual cells, organelles or even tissue, such light-matter interactions can be subtle and may initiate a chain of events. In biological materials these interactions can also lead to the manifestation of physical, thermal, mechanical and chemical effects, or some combination of them. The absorption of light by biological materials (cells, for example) can cause damage as it may induce an excessive temperature rise or additional thermally generated (radiometric) forces amounting from temperature gradients within the material (21). For this reason the choice of laser wavelength for optical treatment of biological matter is critical. Section 2.4.2 gives a detailed description of the absorption of light in cells.

2.4.2 Laser light absorption in cells

Biological cells are rich in proteins which are responsible for a diversity of functions, from carrying oxygen, to complex processes such as providing a light-induced neurological response for vision. The building blocks of proteins are the alphabetic or aromatic (containing ring structures) amino acids. The former absorb the ultra-violet (UV) light of wavelengths shorter than 240 nm. However, aromatic amino acids including phenylalanine, tyrosine and tryptophan absorb at wavelengths longer than 240 nm but well below the visible region of the light spectrum. In addition to light absorption by constituent amino acid residues, protein bonding such as the polypeptide bonds and the disulfide linkages are also absorptive contributing to the total protein absorption of light. Proteins also contain chromophores which provide strong absorption bands; examples include the heme group (in hemoglobin) as well as the *cis*-retinal (in case of retinal proteins). The absorption peaks for hemoglobin fall around 280 nm, 420 nm, 540 nm and 580 nm. To further illustrate typical absorption coefficients for bio-matter (skin cells, whole blood, etc) Figure 2.6 below exhibits the absorption characteristics of these species, including that of water.

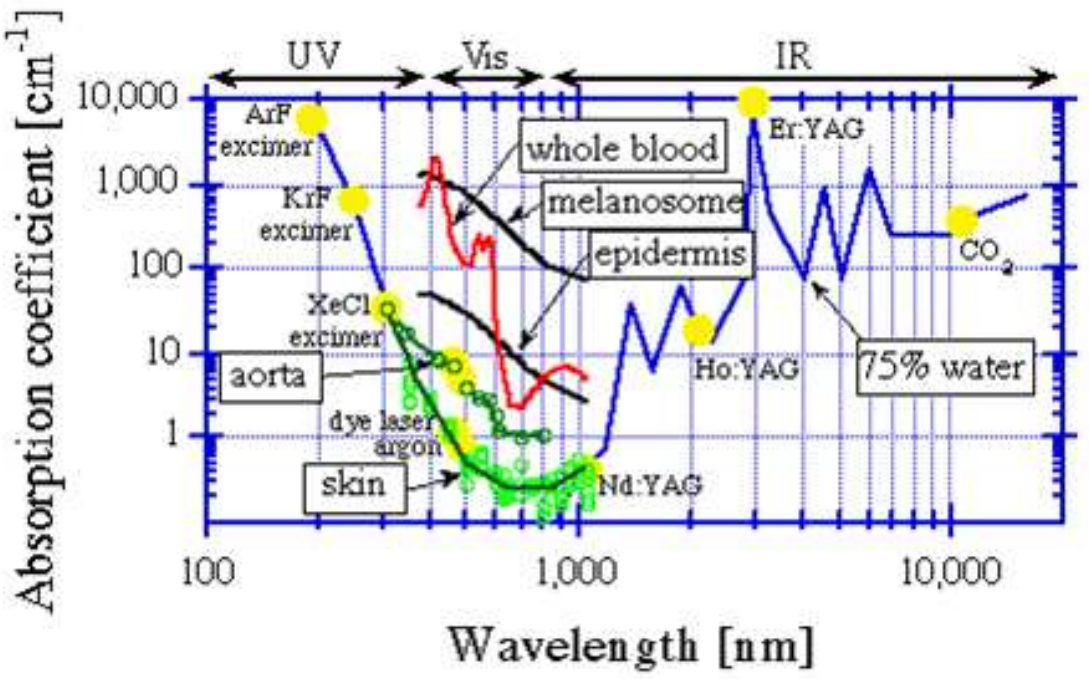

Figure 2.6: The absorption spectra of some biological species (online access date - 19.11.09 (22)). In the UV region, there is an increase in absorption of light with shorter wavelengths due to protein, DNA and other molecules. In the IR region, the increase in absorption of light with longer wavelengths results from the tissue water content. There is minimal absorption in the red and NIR.

Aside from proteins, other cellular components also absorb light. Purines and pyrimidines, the basic components of DNA and RNA absorb light ranging from 230-300 nm and carbohydrates have absorption coefficients below 230 nm. A cellular component exhibiting absorption in the visible is NADH, with the absorption peaks around 270 nm and 350 nm. Although water has no absorption bands or peaks from UV to NIR, it starts weakly absorbing light above 1.3 µm with more pronounced peaks at ≥ 2.9 µm and very strong absorption at 10 µm, the wavelength of a carbon dioxide laser beam. Typically most cells display good transparency between 800 and 1300 nm hence most biological investigations are performed with lasers operated at these wavelengths as well.

Nonetheless, Vorobjev *et al*, 1993 (23) examined the wavelength dependence of optical trapping in the NIR region of the spectrum in order to determine the potential damage of the trapping wavelength due to absorption. They reported that when using a tunable titanium-sapphire laser at 130 mW of power at the beam focus to irradiate chromosomes, maximum damage occurred when irradiating at intermediate wavelengths of 760 – 765 nm while there existed minimum sensitivity to irradiation performed at 700 and 800 – 820 nm. To further investigate the influence of laser wavelength in mammalian cells, Liang *et al*, 1996 (24) found a change in the cloning efficiency of Chinese hamster ovary (CHO) cells during treatment at different wavelengths. Explicitly, their findings showed maximum clonability at 950 – 990 nm and least clonability at 740 – 760 and 900 nm. Then, Neuman *et al* 1999 (25), later looked at the impact of trapping fields from 790 – 1064 nm on *E. coli* bacteria. They discovered that the action spectra for photo-damage exhibited minima at 830 and 970 nm and maxima at 870 and 930 nm.

Such data in literature reports therefore encourages a case specific investigation of optical damage to biological systems, since the mechanisms of photodamage are not well understood. To avoid photo-toxicity (photo-thermal effects in cells) as a result of light absorption, the cell lines and other biological samples used in this thesis were optically treated (trapping, guiding, sorting and porating) in the NIR to the early IR (780 – 1070 nm) regions of the light spectrum.

The next sections address optical guiding, to achieve the desired optical deflection and/or transportation of microparticles, the optical scattering force must predominantly overcome the gradient force. Section 2.5 below starts by giving the principles governing two dimensional Gaussian beam traps that are used for optical guiding experiments.

2.5 Optical forces for guiding or deflecting

2.5.1 Optical guiding using a Gaussian beam

Using a less tightly focused (slightly diverging) Gaussian beam propagating either horizontally or vertically it is possible to move a particle by optically "pushing" it along using radiation pressure, this concept is known as optical guiding and/or transporting (1). Refraction of light through the particle acts to draw the particle to the most intense region of the beam. This radially confines the particle in two dimensions within the beam.

2.5.1.1 Gaussian beam propagation

Gaussian beams consist of a single maximum centered along the beam propagation direction, diverging at an angle (see equation 2.7) away from beam waist w_0. The diverging angle θ can be described by the following expression:

$$\theta = \frac{\lambda}{\pi w_0} \tag{2.7}$$

where λ is the wavelength of the laser light. The Rayleigh range, Z_R, of a Gaussian beam (equation 2.8) is a standard length by which the divergence of the beam is measured. This is the distance wherein the cross-sectional area of the beam waist doubles (see fig. 2.7).

$$Z_R = \frac{\pi w_o^2}{\lambda} \tag{2.8}$$

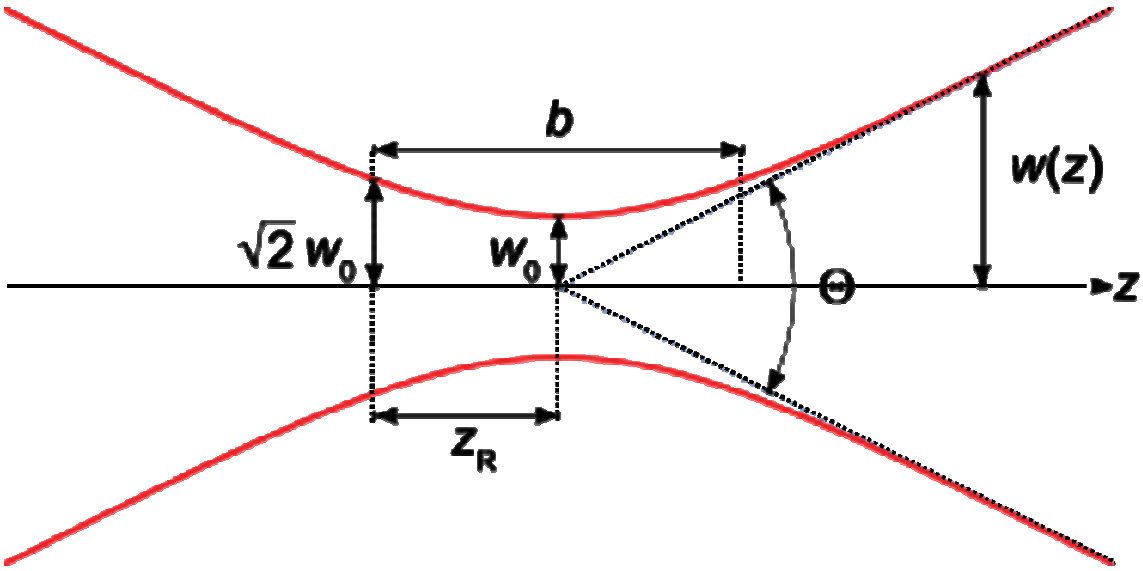

Figure 2.7: The beam waist w_o and Rayleigh range Z_R of a Gaussian beam are depicted. The beam width $w(z)$ is given as a function of the axial distance, b is the depth of beam focus and Θ is the total angular spread (online access date - 10.11.09 (26)).

For a laser of wavelength of 1070 nm and a beam waist of 5 µm, the Rayleigh range of a Gaussian beam can be calculated to obtain 73 µm. The crucial difference for optical guiding, compared with optical trapping, is how tightly focused the beam is. In optical guiding the scattering force dominates the gradient force. Section 2.5.2 below discusses how such two dimensional guiding Gaussian beams setups are created.

2.5.2 Gradient and scattering forces in a 2D trap

A two dimensional optical trap built using an objective lens of low numerical aperture, presents a slightly diverging beam that can be employed in optical guiding experiments. In this case a less tightly focused beam causes a change in the dominant force, resulting in the axial gradient force becoming much reduced so that the scattering force dominates, thereby allowing particle guiding (figure 2.8).

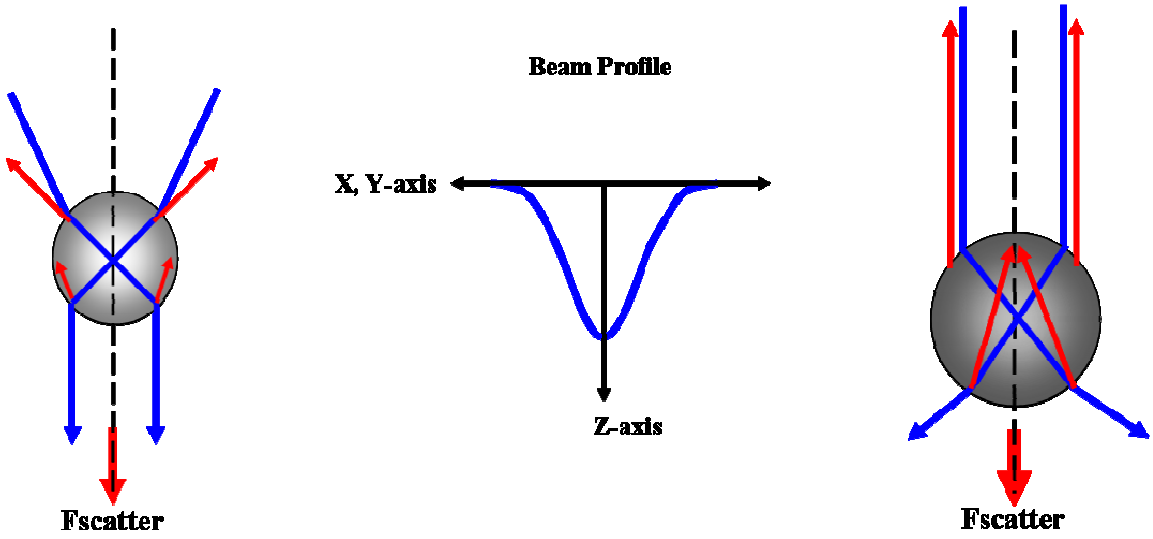

Figure 2.8: A sphere central to the tightly focused (converging) TEM_{00} beam (left). Depicted in the image on the right is a sphere on a weakly focused (diverging) Gaussian beam that experiences a scattering force in the z-direction. This force arises due to partial reflections from the incident light as it interacts with the surface of the sphere.

As with the tightly focused beam, the gradient force localizes a particle radially to the region of highest intensity. Here, a less tightly focused beam can be deemed parallel to the propagation axis in the focal region. The rays creating confinement in the z-direction are not as strong, inducing a much weaker gradient force. In chapter 3, I demonstrate how this weakly focused Gaussian beam arrangement is used in the actual sorting of mammalian cells. This is performed through enhanced guiding of cells tagged intracellularly with dielectric microparticles onto laminin coated coverslips and thus separating them from the non-tagged cells.

Firstly, in section 2.5.3, I briefly review the application of optical forces particularly to cellular material giving an overview of the types of studies performed, with emphasis upon optical cell sorting.

2.5.3 Optical cell sorting overview

Among cell manipulation techniques, technologies for cell separation and isolation with high specificity are restricting the rapid growth of cell biology because cell populations are frequently heterogeneous and the cells of interest are suspended in a solution or mixed with different types of chemicals, biomolecules and cells. To allow availability of physiological information needed for the identification and characterization of individual cells in biomedical research, specific cell sub-populations often require isolation or purification from the sample solution containing a complex mixture of various cell types (27, 28). Examples include the selective isolation and cloning of genetically modified cells for genomic and proteomic studies, separation of differentiated versus undifferentiated cells and sorting cells from patient samples for developing new cell lines (29). In clinical oncology and biomedical research, the ability to rapidly and accurately perform the enrichment and isolation of both rare and not so rare populations of cancer and stem cells from large mixtures of contaminating cells is highly desirable (30, 31). Cell sorting via optical sources at the microfluidic scale is highly attractive; various literature reports display the possibility of transporting and sorting mammalian cells in optical tweezing setups (28, 32-34). Sorting cells of interest is another area where optical forces may play a key role, though not necessarily in direct trapping but in deflecting or guiding given cells to a reservoir. Firstly a distinction between active and passive cell separation methods is made, and then fluid-flow as well as flow-free optical sorting methods briefly described.

2.5.3.1 Active cell sorting methods

Active sorting and uses an external marker e.g., dielectric marker attached via immunological means or the use of a fluorescent marker e.g., green fluorescent protein (GFP) to differentiate between the cell types present. Examples of this type of immunological sorting at the macroscopic scale are based on commercial cell separation methods such as FACS and MACS (35).

FACS machines can detect and sort cells according to a large number of parameters, and readily sort cells at rates in the order of 10^5 cells per second (36). In a FACS device, cells contained in liquid droplets are discharged from an acoustic vibrating nozzle and streamed through a detection region. In the detection region, the light scattering and fluorescence properties of a given cell are recorded onto photodetectors as the cell transverses a laser beam. The cells may be tagged with appropriate fluorescent markers (fluorescently labeled monoclonal antibodies), allowing specific cells to be recognized. If the light scattered from a cell corresponds to the chosen fluorescence signal, an electrical charge is applied to the droplets containing the selected cells. One or more droplets are then separated from the main stream of droplets into a collection chamber. In the same fashion, droplets containing different cell types are directed toward separate collection vials by a static electrical field (37). In this process, the FACS machine can also record the cell size, volume or viscosity (granularity), DNA or RNA content as well as the presence of surface antigens or internal proteins. FACS has a variety of uses and has found application in the diagnosis of leukaemia, lymphoma and immunodeficiencies.

The MACS cell-sorting technique is mostly used in immunology (35), and offers a direct and rapid separation between two cell types. Prior to the magnetic separation process, the cells are incubated with paramagnetic micro beads that are coated with the appropriate antibodies. This permits them to preferentially attach to the cells that are expressing the specific surface antigens in the sample. Subsequently the cells of interest may be sorted by use of an externally applied magnetic field. This technique is reliant upon the need for suitable antigens on the cell surface allowing the paramagnetic beads to accurately bind to or “tag” cells of interest. Furthermore, the number of paramagnetic beads that can be used in parallel is more limited than for FACS.

Both the FACS and MACS cell sorting techniques possess high specificity and selectivity because they consist of extremely precise immunoreactions between the membrane marker proteins and labeling antibodies. Another advantage of FACS and MACS cell sorting schemes is the achievement of high-throughput cell separation. This fact not only means that there is a requirement of large numbers of cells for efficient separation, but

immunologically isolated cells may often experience damage during follow on processes such as the elution of cells from the capturing antibodies, and additionally overall these cell separation systems are bulky and expensive. New technologies for cell sorting are emerging; these can be used with rare or precious cell samples in nano-liter or micro-liter volumes. For such minute analyte volumes, innovative sorting methodologies that readily deal with small sample volumes and are easily adapted to microfluidic environments are necessary. So, in contrast to the macroscopic sorting schemes previously mentioned, the next portion of this sub-section therefore describes a recent active sorting technique performed in a micro sample chamber (microscopic active-sorting).

In this example active optical sorting exists, where the combination of optical forces typically with microfluidics aims to replicate more bulky FACS machines but in a more compact geometry. Specifically, in the study of Wang *et al*, 2005 (38), a microFACS (μFACS) system that used a microfluidic cartridge and a laser at 488 nm to excite fluorescence, and a subsequent 1064 nm laser to extract the sorted cells in a microfluidic flow was developed. This therefore produced a fluorescence-activated microfluidic cell sorter. The researchers assessed the performance of this device on live, stably transfected HeLa cells that expressed a fused histone-green fluorescent protein. Viability was measured by evaluation of the transcriptional expression of two genes, *HSPA6* and *FOS*, known indicators of cellular stress, and no detrimental effects on the cells from the optical sorting were observed. Another example is shown in figure 2.9 (39) below, where the principle of active cell sorting via optical forces in such μFACS devices is illustrated. Several groups have implemented microfluidic forms of FACS, as mentioned in the review by Andersson and Berg (40). The methods used for cell identification are similar to those of macroscopic FACS machines. Hydrodynamic focusing is used to generate a laminar cell flow into a detection area, and subsequent deflection into the appropriate extraction channel is performed by electrical or optical switches. At the microfluidic scale level, the requirement of separating cells from micro liter samples may lead to a reduced throughput compared to that obtained in macroscopic sorting apparatus.

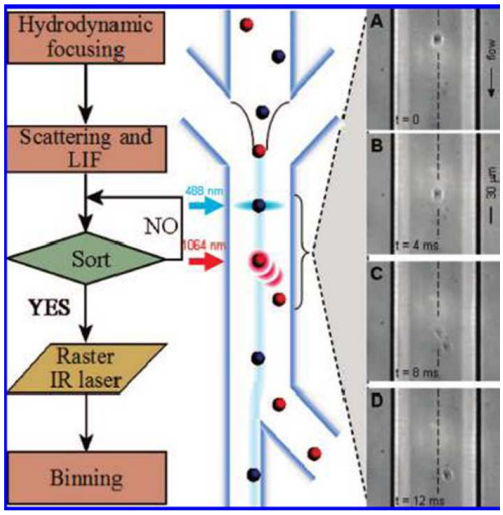

Figure 2.9: Principle and illustration of µFACS based on optical forces. The hydrodynamically focused macrophage: (A) is detected by forward scattering; (B) enters the IR laser spot; (C) is deflected by optical gradient forces; (D) and finally is released in a different laminar flow stream (reprint by permission from *Analytical Chemistry* (39)).

2.5.3.2 Passive (non-immunological) cell sorting techniques

Passive sorting is a type of non-immunological technique where the selection and separation of cells occurs purely by their differing physical (intrinsic properties) response to the light field. In these methods, the type of cells are determined and separated according to their cell size, shape and other physical properties. Non-immunological cell sorting techniques demonstrate a low specificity for cell separation, as cells do not show remarkable differences between each cell type with the exception of their immunological properties. Examples of such passive sorting in a microscopic environment, include the case where a Bessel light beam was used by Paterson *et al*, 2007 (33) to separate red and white blood cells based on their intrinsic properties. There are several methods of generating a Bessel light beam and in this case an axicon, a non-diffractive optical element with a conical shape was illuminated with an incident 1064 nm Gaussian beam to generate a Bessel beam (33, 41). Since the whole area of incident light beam is utilized when creating the resultant Bessel light pattern ($Z_R = \pi D_0^2/4\lambda$, where D_0 is the beam waist diameter), transmission is high with negligible amount of light lost on lens

reflection. This makes use of an axicon an effective choice of generating the Bessel beam.

In this study a mixture of equal quantities of lymphocytes and erythrocytes were suspended in complete cell culture medium and placed in a sample chamber. These cells were then illuminated using a Bessel beam with the central core size of 5.0 µm and average laser powers ranging from 300 up to 800 mW. During laser illumination, it was reported that the erythrocytes got locked in the outer rings of the beam while the bigger and more spherical lymphocytes got drawn into the center of the beam, were optically separated from the red blood cells and collected in a micro-capillary tube (figure 2.10).

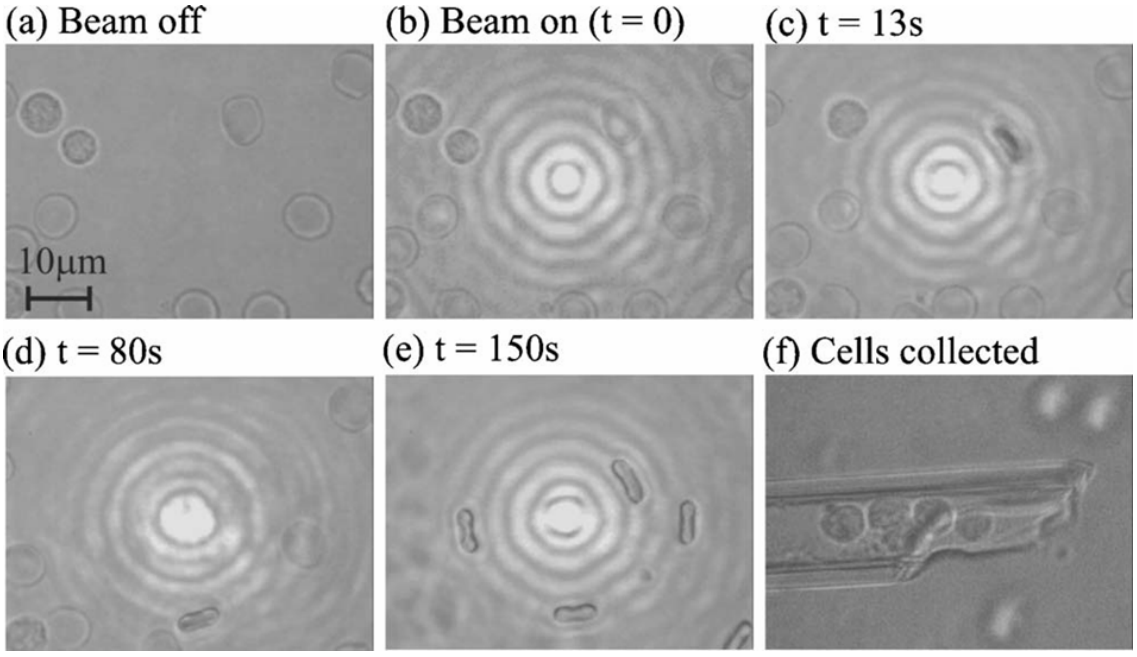

Figure 2.10: Sorting of lymphocytes from erythrocytes in a Bessel light beam (a-e), lymphocytes migrate to the central core of the beam and can be collected into a micro-capillary tube (f). However, because of their disc like shape, erythrocytes are trapped flipped on the outer rings of the beam which possess lower power compared to the central core (e) (reprint by permission from *Applied Physics Letters* (32)).

2.5.3.3 Optical sorting methods with fluid flow

This is another microscopic sorting case where a combination of microfluidic flow and optical forces are used for sorting purposes. Both biological and colloidal particles may be driven by flow over the potential energy landscape (light pattern); an example of such a process is optical chromatography where particle separation occurs due to the balance between the optical and fluid forces. Usually a laser beam is mildly focused by a long focal length lens (rather than a high numerical aperture objective) into a fluid channel containing the sample of interest (illustrated in figure 2.11 below) (42).

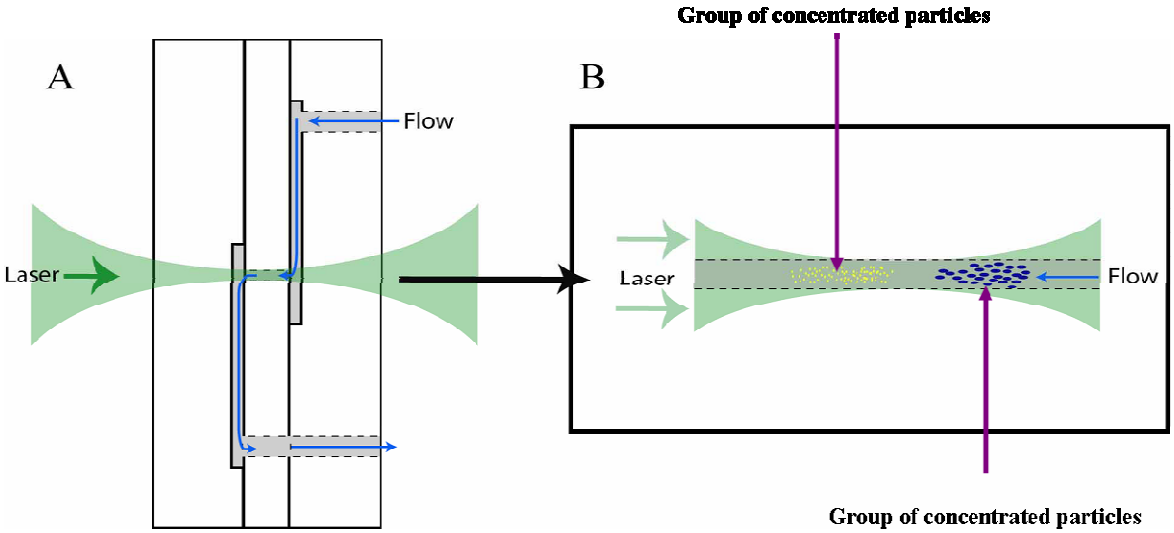

Figure 2.11: Depicts the optical chromatography glass micro-flowcell. (A) shows the construction of the microfluidic device with the pathway for fluid (grey) entering and exiting the separation channel, and the laser beam focused through the channel. In (B), sample separation is demonstrated where the sample particles are constrained to the focal point of the beam by the size of the separation channel that is filled by the laser beam focus (reprint by permission from *Optics Express* (42)).

In their optical chromatography experiments, Hart *et al*, 2007 (42) reported using a 1064 nm ytterbium fiber laser aligned with the microfluidic flow cell mounted on a linear x-y-z translation stage to demonstrate the ability to concentrate spores of *Bacillus anthracis* (6 X 10^7 spores/ml) and in another experiment, 2 µm polystyrene beads (4 X 10^7

particles/ml) both suspended in water. Basically in this flow cell, the fluid flow with the sample of interest enters the device and moves across to the laser separation channel where it interacts with a mildly focused laser beam (focused using a 100 mm focal length lens). At this point, as is shown in figure 2.11 (B), the laser beam fills the channel, therefore all particles in the fluid experience optical pressure. The separation channel size of 50 µm diameter and 500 µm length was completely filled with the focused beam. When the beam is left on, the particles are retained concentrated in the separation channel. On switching the beam off, the concentrated stream of particles are then released; see data displaying the concentration of 2 µm spheres in figure 2.12. Following crossing through the laser separation region, the fluid exits the device where it can be collected with the separated particles for additional analysis.

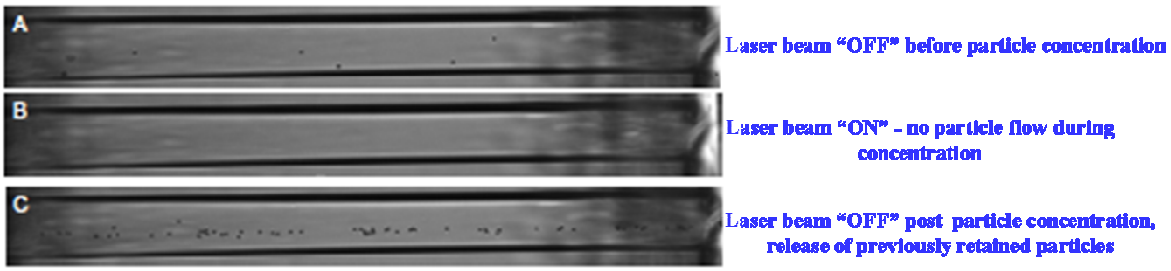

Figure 2.12: Illustrate the concentration of 2 µm polymer microspheres with 0.9 W of a 1064 nm laser beam focused into the 50 µm optical chromatography channel. In (A) the liquid containing the spheres is introduced as a constant flow at a flow rate of 3.1 µl per hour (beam "off"). When the beam is switched "on", there are no visible spheres within the channel as they are concentrated outside (B). After three minutes of microsphere retention, the beam is switched "off" and the concentrated stream of spheres is released into the channel (C) (reprint by permission from *Optics Express* (42)).

2.5.3.4 Flow-free optical sorting methods

A method using the optical fields to separate objects in the absence of any flow is now explored. In the absence of flow microparticles are normally trapped, unless the trap potential is engineered such that it is shallow leading to production of a metastable state which causes the particles to escape due to thermal activation from the optical potential well. Assays during flow-free sorting procedures are normally performed in simple micro-sample chambers, typically consisting of a glass slide or glass bottom petri dish

(bottom) and a coverslip (top). No expensive pumps, specialized micro-chambers and micro-fabrication of channels coupled to electrodes are necessary in this case. An example of flow-free sorting was demonstrated by Paterson *et al*, (33) in this work they report on enhanced passive sorting of externally tagged human promyelocytic leukaemia cells (HL60) within a mixed cell population using a propagation invariant ("non-diffracting") Bessel beam pattern. This beam profile has a central core that propagates for a distance much greater than the Rayleigh range of a Gaussian beam. The bottom of their sample chamber consisted of a type-1 thickness glass coverslip (0.13-0.17 mm thick X 22 X 50 mm), a vinyl spacer of thickness 80 µm and the top was a second glass coverslip (0.13-0.17 mm thick X 18 X 18 mm). Pulled glass capillaries (outer diameter = 20 µm, inner diameter and 10 µm) were used in combination with the sample chambers to collect the optically guided and sorted cells (33). During cell sorting, they filled the sample chamber with 20 µl of sample analyte which was a mixed population of tagged and non-tagged HL60 cells and illuminated it with a Bessel beam (250 mW, 1064 nm ND: YVO4 laser). On interacting with the beam the HL60 cells externally tagged with 5 µm streptavidin-coated silica spheres, were reported to have a faster migration rate from the outer rings to the central core of the beam compared to the non-tagged cells. In addition, on reaching the central core, tagged HL60 cells were reported to guide a vertical distance of 160 µm in just 6 seconds compared to 37 seconds vertical guiding time of the non-tagged cells. This enhanced guiding feature of tagged HL60 cells was then used to passively sort them from the non-tagged cell population in a flow-free fashion using a Bessel beam. Following optical sorting, they reported on the collection of ten optically guided tagged HL60 cells in a pulled glass micro-capillary filled with 0.1 % trypan blue for monitoring cell viability (33) (figure 2.13). Their results displayed no compromise to cell viability, thus, confirming successful sorting, collection and then recovery of healthy HL60 cells, achieved in a simple fluid flow-free cell sorting chamber.

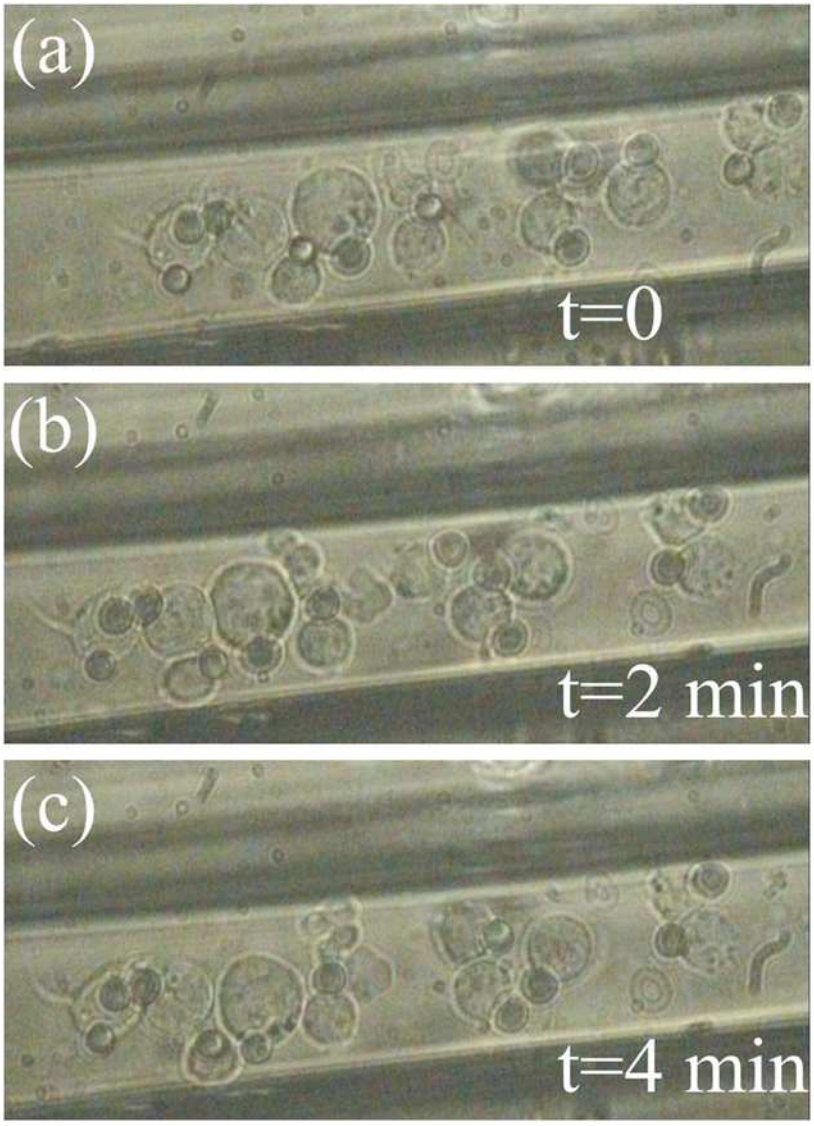

Figure 2.13: Depicts extracellularly tagged HL60 cells post collection in a glass capillary tube filled with trypan blue to test cell viability following optical treatment. These tagged cells were optically guided and subsequently sorted from the non-tagged cell population in a flow-free Bessel beam passive sorting chamber. After collection the cells were allowed to incubate in the presence of the viability dye for a few minutes (0, 2 and 4). The cells did not stain blue even after 4 minutes of dye incubation, indicating that both capillary collection as well as laser irradiation during guiding and sorting did not compromise cell viability (reprint by permission from *Journal of Biomedical Optics* (33)).

It is worth mentioning that during flow-free passive sorting; a large difference in size or refractive index between cell types is required in order for effective separation and sorting to occur. The heterogeneity within or between most cells types does not consist of large enough differences, particularly, in refractive index. Therefore to improve cell sorting, typically in flow-free methods, cells are normally tagged with dielectric particles of high refractive index such as silica or polymer microspheres.

2.6 Summary

Optical traps have allowed developments of a huge wealth of Biophotonics studies. In this chapter the different types of optical traps originally employed in earlier experiments were mentioned. Then a detailed study of the principles, use and construction of the three dimensional optical tweezers trap was presented. Single beam trapping or tweezing of polymer microspheres through a 658 nm diode laser setup was displayed. I then elucidated the reason most laser sources utilized to optically treat biological matter are usually operated on NIR region of the light spectrum. Optical deflecting or guiding in a two dimensional Gaussian beam optical guiding trap was displayed.

The different types of microscopic cell sorting technologies mentioned (μFACS, Bessel beam passive sorting, optical chromatography and flow-free Bessel beam sorting) in this chapter show the many possibilities associated with the use of optical forces for promoting cell sorting studies. In contrast to traditional macroscopic cell sorting methodologies (e.g. FACS, MACS, etc), minute volumes and low cell concentration numbers are used with microscopic sorting techniques. This therefore makes these methods very useful, particularly in investigations involving clinical samples or precious cell lines that are difficult to culture and expand into large populations. For example, only a few cells are sufficient for many downstream applications such as *in vitro* cloning or polymerase chain reaction (PCR). Added benefits of microscopic sorting schemes include the ease at which they could be integrated into microscopes and other optical elements, which may lead to a new generation of multi-functional workstations in

biophotonics laboratories. In the following chapter, I will present my experimental data demonstrating a new fluid flow-free 2D optical cell guiding and sorting technique. In contrast to the flow-free work reported by Paterson *et al*, 2007 (33), during my studies a weakly focused Gaussian beam was used to sort cells with phagocytosed (intracellularly tagged) microspheres from a non-tagged cell population in a flow-free micro-chamber made of a type zero glass bottom petri dish and a top coverslip. During optical guiding, the tagged cells were retained (got attached) onto a laminin coated coverslip (top of the chamber), collected through separating the top coverslip from the rest of the sample chamber and successfully re-cultured for further analysis.

References

1. A. Ashkin, "Acceleration and Trapping of Particles by Radiation Pressure," *Physical Review Letters* **24**, 156-159 (1970)
2. A. Ashkin, "Optical trapping and manipulation of neutral particles using lasers," *Proc Natl Acad Sci U S A* **94**, 4853-4860 (1997)
3. A. Ashkin and J. M. Dziedzic, "Stability of Optical Levitation by Radiation Pressure," *Appl. Phys. Lett.* **24**, 586-588 (1974)
4. A. Ashkin, "Applications of Laser-Radiation Pressure," *Science* **210**, 1081-1088 (1980)
5. A. Ashkin and J. P. Gordon, "Stability of Radiation-Pressure Particle Traps - an Optical Earnshaw Theorem," *Optics Letters* **8**, 511-513 (1983)
6. A. Ashkin and J. M. Dziedzic, "Observation of Radiation-Pressure Trapping of Particles by Alternating Light Beams," *Physical Review Letters* **54**, 1245 (1985)
7. A. Ashkin, J.-M. Dziedzic, J. E. Bjorkholm and S. Chu, "Observation of a single-beam gradient force optical trap for dielectric particles," *Optics Letters* **11**, 288-290 (1986)
8. K. Dholakia, G. Spalding and M. MacDonald, "Optical tweezers: the next generation," *Phys World* **15**, 31 (2002)

9. N. B. Simpson, K. Dholakia, L. Allen and M. J. Padgett, "Mechanical equivalence of spin and orbital angular momentum of light: An optical spanner," *Optics Letters* **22**, 52-54 (1997)

10. K. C. Neuman and S. M. Block, "Optical Trapping," *Review of Scientific Instruments* **75**, 2787-2809 (2004)

11. N. Malagnino, G. Pesce, A. Sasso and E. Arimondo, "Measurements of trapping efficiency and stiffness in optical tweezers," *Optics Communications* **214**, 15-24 (2002)

12. H. Felgner, O. Muller and M. Schliwa, "Calibration of Light Forces in Optical Tweezers," *Applied Optics* **34**, 977-982 (1995)

13. J. E. Molloy and M. J. Padgett, "Lights, action: optical tweezers," *Contemp. Phys.* **43**, 241-258 (2002)

14. W. M. Lee, P. J. Reece, R. F. Marchington, N. K. Metzger and K. Dholakia, "Construction and calibration of an optical trap on a fluorescence optical microscope," *Nature protocols* **2**, 3226-3238 (2007)

15. A. T. O'Neill and M. J. Padgett, "Axial and lateral trapping efficiency of Laguerre-Gaussian modes in inverted optical tweezers," *Opt. Commun.* **193**, 45-50 (2001)

16. N. B. Simpson, D. McGloin, K. Dholakia, L. Allen and M. J. Padgett, "Optical tweezers with increased axial trapping efficiency," *Journal of Modern Optics* **45**, 1943-1949 (1998)

17. N. B. Simpson, L. Allen and M. J. Padgett, "Optical tweezers and optical spanners with Laguerre-Gaussian modes," *J. Mod. Opt.* **43**, 2485-2491 (1996)

18. C. L. Kuyper and D. T. Chiu, "Optical trapping: A versatile technique for biomanipulation," *Applied spectroscopy* **56**, 300a-312a (2002)

19. S. M. Block, "Construction of Optical Tweezers," *Cells: A laboratory Manual* **2**, 2136-3136 (2006)

20. A. Ashkin, J. M. Dziedzic and T. Yamane, "Optical Trapping and Manipulation of Single Cells Using Infrared-Laser Beams," *Nature* **330**, 769-771 (1987)

21. A. Ashkin and J. M. Dziedzic, "Optical Trapping and Manipulation of Viruses and Bacteria," *Science* **235**, 1517-1520 (1987)

22. http://omlc.ogi.edu/classroom/ece532/class3/muaspectra.html,

23. I. A. Vorobjev, L. Hong, W. H. Wright and M. W. Berns, "Optical Trapping for Chromosome Manipulation - a Wavelength Dependence of Induced Chromosome Bridges," *Biophysical Journal* **64**, 533-538 (1993)

24. H. Liang, K. T. Vu, P. Krishnan, T. C. Trang, D. Shin, S. Kimel and M. W. Berns, "Wavelength dependence of cell cloning efficiency after optical trapping," *Biophysical Journal* **70**, 1529-1533 (1996)

25. K. C. Neuman, E. H. Chadd, G. F. Liou, K. Bergman and S. M. Block, "Characterization of photodamage to Escherichia coli in optical traps," *Biophysical Journal* **77**, 2856-2863 (1999)

26. http://en.wikipedia.org/wiki/Gaussian_beam,

27. C. T. Ho, R. Z. Lin, H. Y. Chang and C. H. Liu, "Micromachined electrochemical T-switches for cell sorting applications," *Lab on a Chip* **5**, 1248-1258 (2005)

28. P. Mthunzi, W. M. Lee, A. Riches, C. T. A. Brown, F. J. Gunn-Moore and K. Dholakia, "Intracellular dielectric tagging for improved optical manipulation of mammalian cells," *IEEE, Selected Topics in Quantum Electronics* **16**, 608-618 (2009)

29. H. Shadpour, C. E. Sims and N. L. Allbritton, "Enrichment and Expansion of Cells Using Antibody-Coated Micropallet Arrays," *Cytometry Part A* **75A**, 609-618 (2009)

30. O. Lara, X. D. Tong, M. Zborowski and J. J. Chalmers, "Enrichment of rare cancer cells through depletion of normal cells using density and flow-through, immunomagnetic cell separation," *Experimental hematology* **32**, 891-904 (2004)

31. N. Uchida, D. W. Buck, D. P. He, M. J. Reitsma, M. Masek, T. V. Phan, A. S. Tsukamoto, F. H. Gage and I. L. Weissman, "Direct isolation of human central nervous system stem cells," *Proceedings Of The National Academy Of Sciences Of The United States Of America* **97**, 14720-14725 (2000)

32. L. Paterson, E. Papagiakoumou, G. Milne, V. Garces-Chavez, S. A. Tatarkova, W. Sibbett, F. J. Gunn-Moore, P. E. Bryant, A. C. Riches and K. Dholakia, "Light-induced cell separation in a tailored optical landscape," *Appl. Phys. Lett.* **87**, 123901 (2005)

33. L. Paterson, E. Papagiakoumou, G. Milne, V. Garces-Chavez, T. Briscoe, W. Sibbett, K. Dholakia and A. C. Riches, "Passive optical separation within a 'nondiffracting' light beam," *J Biomed Opt* **12**, 054017 (2007)

34. K. Dholakia, W. M. Lee, L. Paterson, M. P. MacDonald, R. McDonald, I. Andreev, P. Mthunzi, C. T. A. Brown, R. F. Marchington and A. C. Riches, "Optical separation of cells on potential energy landscapes: Enhancement with dielectric tagging," *IEEE J. Sel. Top. Quantum Electron.* **13**, 1646-1654 (2007)

35. D. L. Siegel, T. Y. Chang, S. L. Russell and V. Y. Bunya, "Isolation of cell surface-specific human monoclonal antibodies using phage display and magnetically-activated cell sorting: applications in immunohematology," *Journal of Immunological Methods* **206**, 73-85 (1997)

36. S. F. Ibrahim and G. van den Engh, "High-speed cell sorting: fundamentals and recent advances," *Curr Opin Biotech* **14**, 5-12 (2003)

37. G. P. Nolan, S. Fiering, J. F. Nicolas and L. A. Herzenberg, "Fluorescence-activated cell analysis and sorting of viable mammalian cells based on beta-D-galactosidase activity after transduction of Escherichia coli lacZ," *Proc Natl Acad Sci U S A* **85**, 2603-2607 (1988)

38. M. M. Wang, E. Tu, D. E. Raymond, J. M. Yang, H. C. Zhang, N. Hagen, B. Dees, E. M. Mercer, A. H. Forster, I. Kariv, P. J. Marchand and W. F. Butler, "Microfluidic sorting of mammalian cells by optical force switching," *Nat. Biotechnol.* **23**, 83-87 (2005)

39. T. D. Perroud, J. N. Kaiser, J. C. Sy, T. W. Lane, C. S. Branda, A. K. Singh and K. D. Patel, "Microfluidic-Based Cell Sorting of Francisella tularensis Infected Macrophages Using Optical Forces," *Analytical Chemistry* **80**, 6365-6372 (2008)

40. H. Andersson and A. van den Berg, "Microfluidic devices for cellomics: a review," *Sensors and Actuators B-Chemical* **92**, 315-325 (2003)

41. J. Arlt, V. Garces-Chavez, W. Sibbett and K. Dholakia, "Optical micromanipulation using a Bessel light beam," *Optics Communications* **197**, 239-245 (2001)

42. S. J. Hart, A. Terray, J. Arnold and T. A. Leski, "Sample concentration using optical chromatography," *Opt. Express.* **15**, 2724-2731 (2007)

Chapter 3

Phagocytosis for intracellular dielectric tagging and the enhanced optical guiding and sorting of mammalian cells

Introduction

In the previous chapter, I described 2D Bessel light beam passive cell sorting using extracellular tagging as an example of a possible flow-free cell sorting scheme. This chapter introduces the concept of phagocytosis as a new type of mammalian cell tagging procedure to promote improved optical guiding and flow-free sorting in a 2D Gaussian beam trap. Firstly, I outline the difference and/or advantages between the extracellular and intracellular dielectric tagging procedures, giving examples of where each tagging technique has been successfully employed. Then I proceed to my own studies involving phagocytosis as an intracellular tagging method of choice, where, I perform experiments to quantify, detect and assess the viability of the cell-sphere phagocytosis. These investigations include the tracking of microspheres within cells via Labview particle tracking, trypan blue exclusion dye assays and eventually, imaging techniques such as fluorescence microscopy and confocal laser scanning microscopy. The initial studies were performed with Chinese hamster ovary (CHO-K1) cells but three more cell lines were used in this chapter namely, the retinal pigment epithelial cells (RPE), human promyelocytic leukemia (HL60) cells and haematopoietic FDCP-mix C2GM (C2GM) cells.

Following these characterization experiments, I next report the effect of the intracellular dielectric tags on the scattering and gradient forces during three dimensional trapping, where the trapping efficiency of cells encapsulating the different numbers of microspheres are compared to those without the spheres. Using a diverging beam optical field (2D trap) the intracellular polymer microspheres are seen to act as highly directional optical scatterers; hence, axial optical guiding of cells that have engulfed a varying number of spheres is enhanced by a strong scattering force from these cells, as compared

to those containing no spheres. Finally in this chapter, the improved axial guiding nature of cells with internalized spheres is achieved by levitating the intracellularly tagged cells onto laminin coated coverslips thereby capturing and optically sorting them from the rest of the cells lacking the dielectric tags.

3.1 Extracellular versus intracellular tagging

3.1.1 Refractive index of the material to be manipulated

The measure of how much the speed of light is reduced inside a particular medium (compared to light traveling in air) is known as the refractive index (n) of that medium. When light rays cross an interface from air to a glass or any other transparent material of high refractive index, they not only experience a change in direction via refraction, but also get partially reflected by the surface of the material. For this reason, materials of high refractive index are amenable to optical trapping, guiding as well as sorting methods. When dealing with optical forces and biological materials, the ability of light to exert forces may be hindered by the relatively low refractive index difference between, particularly, a cell and its surrounding medium. The low refractive index difference may make it difficult to ensure cell manipulation based on the native cellular response, as the scattering and gradient forces exerted are not strong enough to initiate significant cell manipulation, guiding and sorting without the use of high laser powers. One way of avoiding this hurdle is by altering the dielectric contrast of cells through attaching dielectric particles to the cell surface so that these act as tags or “micro-handles” to be used during optical treatment. This process of extracellular tagging has been previously explored in literature for optically manipulating a wealth of different biomolecules and whole cells (1-5). Although successfully utilized, the process of extracellular tagging is very complex requiring careful consideration of the surface chemistry. This introduces the need for use of expensive antibodies and highly specific ligands. Herein, I present a new cellular tagging approach by which cells naturally engulf dielectric particles via a process known as phagocytosis. Particle uptake in this manner results in an intracellular tagging scheme which is achieved through simple cell-particle incubation without

additional costly reagents. The two approaches known to enhance the refractive index of biological species thereby significantly improving their optical treatments i.e. the extracellular and intracellular dielectric tagging techniques are described in the following sub-sections.

3.1.1.1 External (extracellular) dielectric cell tagging

Optical manipulation of biological species relies on specimen tagging mostly using extracellular attachments with a prominent refractive index, compared to that of the suspending medium. These attachments are then used as handles between the trapping beam and the actual particle under investigation. For instance, the trapping force of CATH.a cells, a neuronal cell line was increased by over 270 % via a one-to-one coupling of these cells to carboxylated polystyrene beads (1). In another experiment researchers reported, irregularly shaped diamond particles, n = 2.4, when treated with 0.01 % poly-L-lysine which promotes adhesion of cells to solid substrates, and used these as optical handles providing improved degrees of freedom to manipulate cells and molecular assemblies (2). Paterson *et al*, 2005 reported enhanced optical trapping of a T-cell subpopulation of mononuclear cells through attachment of Streptavidin-coated 5.17 µm diameter silica microspheres. This enabled them to optically separate and collect lymphocytes into a microcapillary, from a mixed population of cells containing erythrocytes (3). Figure 3.1 is a schematic representation of extracellular cell tagging. Such forms of dielectric sphere tagging processes are a well established method in manipulation of macromolecules (4). However another disadvantage is that these methods can be time consuming. In addition, during the optical manipulation experiments, microspheres externally attached to the cell surface often disengage from the cells once exposed to the forces of the laser trapping beam, as a result of weak cell-sphere binding affinity. Also, this mode of cell tagging is not very effective since in some experiments, only 1:100 cells get successfully tagged. It would, therefore, be a significant step for optical cell sorting, and more general optical manipulation methodologies to explore a simplified method for enhancing cell manipulation.

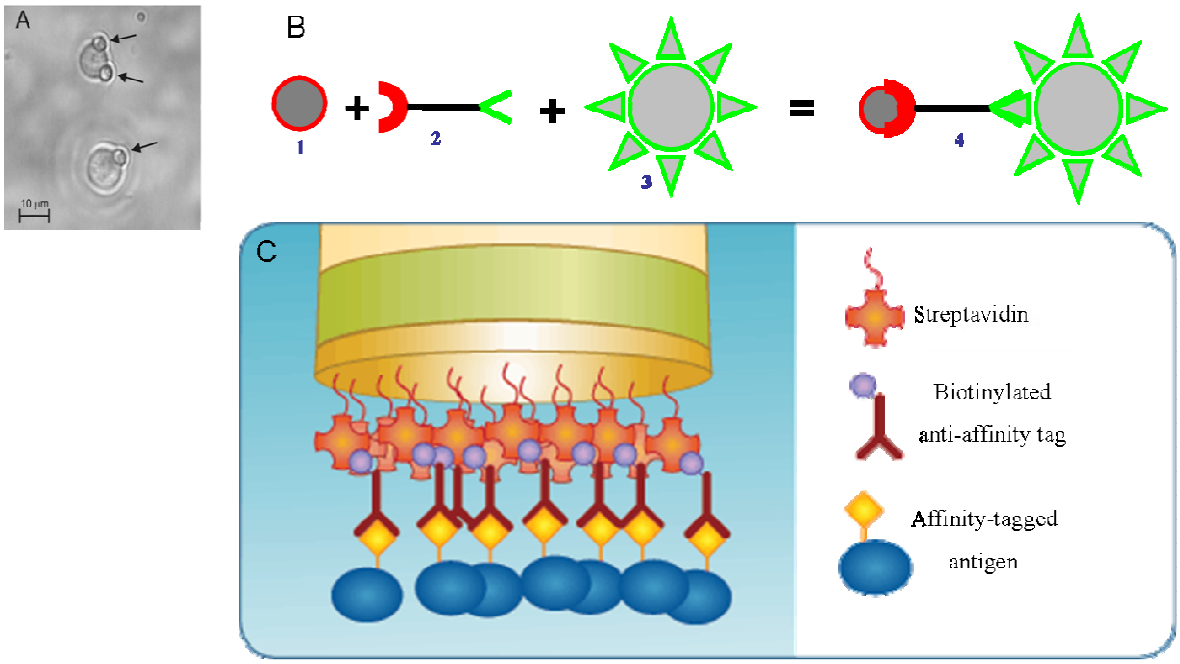

Figure 3.1: (A) Streptavidin-coated, silica microspheres of a 5.17 µm diameter (pointed by black arrows – B1) were attached to the T-cell subpopulation of mononuclear cells (B3) via a mouse CD2 primary antibody and a secondary biotinylated antimouse antibody (B2) attachment to form a complex depicted in B4. Image (C) further illustrates the binding procedure (online access date - 30.12.09 (6)). Attaching silica microspheres, targeted to a specific subpopulation of cells via antibody-antigen binding enhances this method of cell separation as the microspheres react to the optical landscape more strongly than cells (3).

To achieve this and overcome all of the challenges around extracellular tagging, another tagging approach that provides more stable, non-toxic handles that can be acquired via a natural cellular process known as phagocytosis is presented in section 3.1.1.2. This efficient intracellular dielectric tagging fashion is inexpensive and the tagging protocol (Appendix A (iv) page A3) requires no complex, time consuming immunological steps.

3.1.1.2 Intracellular dielectric cell tagging

Internalization of a foreign body by a cell is a process that can be categorized as phagocytosis ("cell eating") (7). Compared to receptor mediated endocytosis (internalization of small particles e.g. macromolecules and viruses) and pinocytosis (uptake of fluid and solutes "cell drinking") (8), phagocytosis is the uptake of relatively large particles > 0.5 µm into vacuoles by mechanisms that are clathrin independent and usually require actin polymerization (9, 10). The phagocytic process can be divided into sequential events, starting with the recognition of the particle by dedicated receptors on the phagocyte. Opsonic receptors such as the Fcγ receptor (FcγRs) are among the well-characterized phagocytic receptors (11). Particle engulfment is therefore triggered by the clustering of FcγRs which results in a local and oriented polymerization of actin filaments that encourages the plasma membrane to form an invagination which wraps the particle within pseudopods. A contractile force is then generated by the cell body (figure 3.2) specifically to attract and pull a particle into the protrusion of the cell plasma membrane. Once within the cell, the phagosome (the vesicle containing the ingested material), is degraded by lysosomes which are acidic and rich in hydrolytic enzymes. There are numerous reported studies in the literature on the engulfment of inert, degradable on non-degradable particles such as microspheres (polymer, latex and silica) (12-14). In unicellular organisms phagocytosis can be utilized for nutritional purposes (15). Conversely, in higher organisms, phagocytes including macrophages, neutrophils and dendritic cells, facilitate the elimination of senescent cells and invading pathogens through this process. Thus phagocytosis is central to a host's defense mechanism against infective agents, and to help in tissue modeling and damage from inflammation. An interesting application utilizing this phagocytosis processes is when cells are allowed to internalize dielectric particles, thereby promoting studies in optical manipulation, trapping, guiding and sorting of mammalian cells. Recently, optical tweezers have been used in several studies investigating specific membrane binding mechanisms behind phagocytosis (16, 17). In other studies, optical tweezers have been employed to move internalized beads within fibroblasts in order to identify the anomalous diffusion scaling to the density of the microtubule network within which the bead was embedded (18).

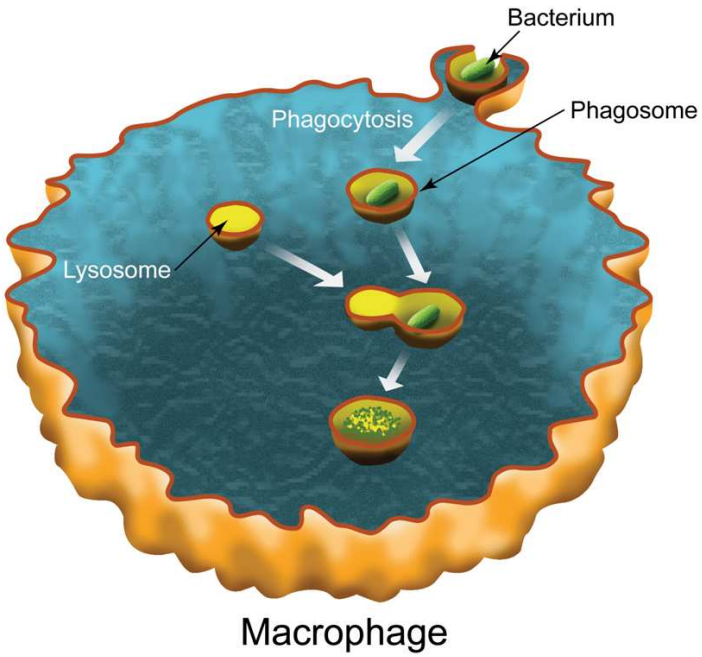

Figure 3.2: Phagocytosis is the process by which the membrane of a macrophage type white blood cell surrounds and engulfs a bacterium in a membrane-bound shell called a phagosome. Inside the cell, the phagosome fuses with a lysosome which carries digestive enzymes that destroy the bacterium. Cells also use this process for feeding purposes (online access date - 10.12.09 (19)).

The internalization of functionalised beads has also enabled intracellular studies, including calcium signalling detection (20), pH detection, force measurements and cytoskeletal rearrangements (21). Simon *et al*, 1988 (7) studied the biophysical aspects of microsphere uptake by human neutrophils. This work identified a store of excess membrane area existing on cytoplasmic granules, that may be recruited during phagocytosis for fusing to the membrane projections and promote membrane enclosure. Depicted in Figure 3.3 (A), is a cancer cell incubated with multifunctional capsules consisting of a polymer shell having certain release, permeability and adhesion properties. These capsules have an inner compartment that can be loaded with materials of different properties, examples including drugs, luminescent quantum dots or biologically active materials (22). In this study it is claimed that such capsules promise to

be the ideal system for targeted and controlled delivery system of drugs within pathological cells. Figure 3.3 (B) depicts phagocytosis of both coated and non-coated polystyrene microspheres of 750 nm diameter, into a fibroblast cell. These microspheres were found to create a well ordered 3D crystallization within a fibroblast cell when they were co-incubated at a high concentration (21). In this study, the mechanism for phagosome crystallization was reported to be similar to classic colloidal crystallization: where, in a thermal bath, colloidal crystallization of mutually-repulsive microspheres occurs when the microspheres' density exceeds a critical concentration. Thus, the spatial confinement caused by the cell membrane is said to be the driving force behind the crystallization. The particles become concentrated promoting crystallization when bound by the membrane and pumped into the perinuclear area via retrograde motion (movement in the direction opposite that of the cell membrane). Studies analyzing crystallite formation within cells, offer a comprehensive insight into the physical environment within cells.

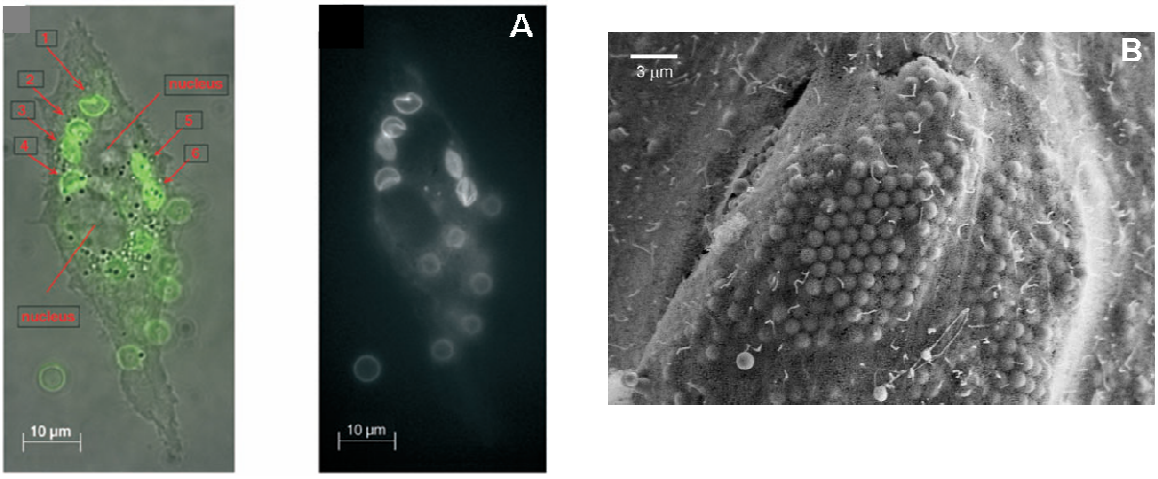

Figure 3.3: (A) shows an overlay of phase-contrast and fluorescence images of a human breast cancer cell of the cell line MDA-MB-435s with internalized capsules. The capsules are 5 mm in diameter; six capsules were counted as being phagocytosed by this particular cell (reprint by permission from *Small* (22)). (B) Displays a scanning electron microscope image of a multi-layered three-dimensional colloidal crystallite (750 nm sized particles) inside of a fibroblast cell. 750 nm and 1 µm particles are reported to form well-ordered crystallites when there are enough particles to create three dimensional structures (reprint by permission from *Soft Matter* (21)).

In addition, such investigations may provide innovative tools for studying the rearrangements, forces and stresses acting upon the cytoskeleton. An understanding of organelle-membrane interactions and cellular transport of multiple particles may also be developed by such experiments.

The process of phagocytotic internalization can be combined with a variety of intriguing physical, biochemical and optical processes. Next I explore optical studies using phagocytosis for enhancing the intrinsic dielectric contrast of different mammalian cell lines. This is where cells naturally take up polymer microspheres from their environment and thus respond more strongly to an applied optical field. I characterize the optical forces on these cells, and show that this simple, inexpensive and non-toxic internal tagging technique can be used to investigate enhanced optical manipulation and enable a simple new technique to optically sort mammalian cells. Appendix A (i) to (iv) pages A1-A3 explains the detail on cell lines used, cell culturing, microsphere preparation and cell-microsphere incubation respectively.

3.1.2 Microsphere quantification using CHO cells

Prior to optical experiments, initial studies focused on the internalization parameters of the microspheres into specifically CHO cells. Since these have been well characterized in the literature, they were also used for testing the cell viability post sphere phagocytosis, confirming microsphere uptake through fluorescent (mercury lamp) and confocal laser scanning microscopy measurements. To quantify cell–sphere uptake, the red photo-transfected CHO cells were incubated with the GF microspheres over five different time periods, namely, 3, 6, 24, 48 and 72 hrs. Following the microsphere incubations at the recorded times, non internalized (superimposed) spheres were removed by rinsing the cell monolayer twice using 2 ml complete medium, leaving approximately 200–250 µl of medium covering the sample surface to prevent the monolayer from desiccating. Samples were then analyzed via fluorescence microscopy using a 10X microscope objective lens (NA 0.25) to capture images of the fluorescing cell-sphere samples with a large field of view over different time periods (figure 3.4).

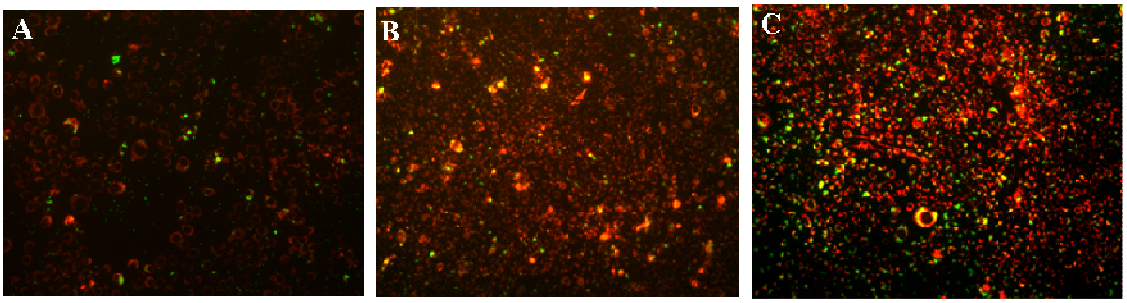

Figure 3.4: Using a color digital camera (CCD), fluorescent micrographs were captured through a 10X, NA 0.25 microscope objective for quantifying the amount of microspheres taken up by the CHO cells over different time periods. (A) an image taken 48 hours post microsphere incubation and B&C depict the cell-sphere sample area 72 hours post incubation.

These images were then imported into a Labview© particle tracking program that was written specifically to count sphere uptake per cell (written by Dr. Graham Milne in an independent PhD study). Figure 3.5 displays the quantification data of microsphere ingestion by mammalian cells, showing that maximum internalization for both the 2 and 3 µm spheres was achieved at 24 hrs post incubation with the cells. Also for both 2 and 3 µm spheres at 48 – 72 hrs, microsphere internalization drops. This result is expected as CHO cells are adherent cultures which reach saturation density as of 48 hours post seeding as is evident in images a, b and c of figure 3.4. Normally in cell cultures, at 24 hrs post seeding the nutrients in the growth medium starts depleting (23). This then alters general metabolism and biochemistry of cells which might be the reason for a decrease in microsphere uptake at 48 and 72 hrs.

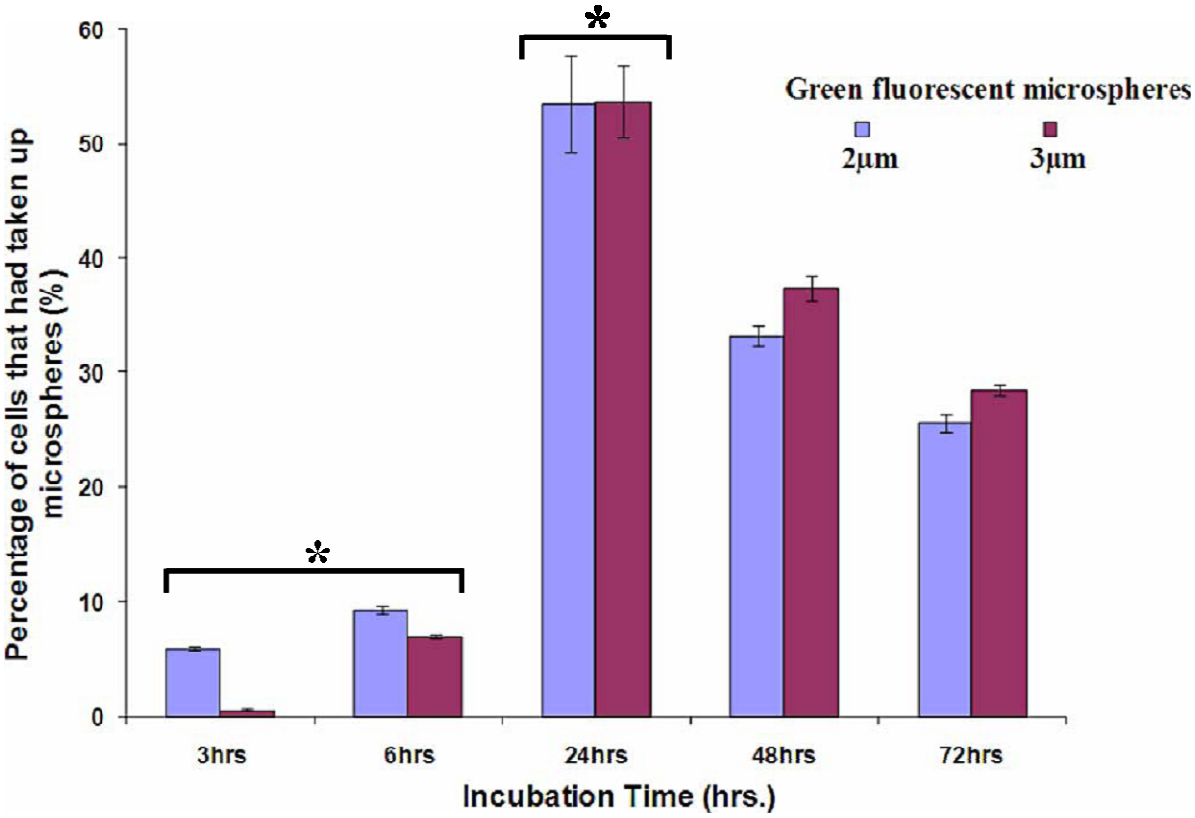

Figure 3.5: Illustrates cellular uptake of 2 and 3 µm diameter GF microspheres. The maximum number of cells that internalized microspheres occurred at 24 h post incubation for both sphere sizes. Error bars indicate the standard error of the mean (SEM) (n = 5 experiments repeated trice for each column). Using ANOVA followed by Dunnett's and Fisher's tests: * means data points are significantly different from each other in both the case for 2 and 3 µm GF spheres (reprint by permission from *IEEE Journal of Selected Topics in Quantum Electronics* (24)). Appendix A (v) pages A6-A7 shows full statistical analysis of this plot.

After quantifying microsphere ingestion by mammalian cells and noting that the maximum engulfment was possible at 24 hours post incubation, samples utilized in optical trapping and other experiments were therefore cells incubated over this time period.

3.1.3 Microsphere phagocytosis detection via fluorescence and confocal microscopy

The 24 hour incubated samples were evaluated using fluorescence as well as confocal microscopy to confirm the degree of microsphere uptake within the cells. After plating and incubating CHO cells with the different size microsphere for 24 hrs, the monolayer was left covered with roughly 250 µl of medium to prevent dehydration and fluorescent images of live cells were captured using a camera system attached to a Zeiss Axioscope (figure 3.6).

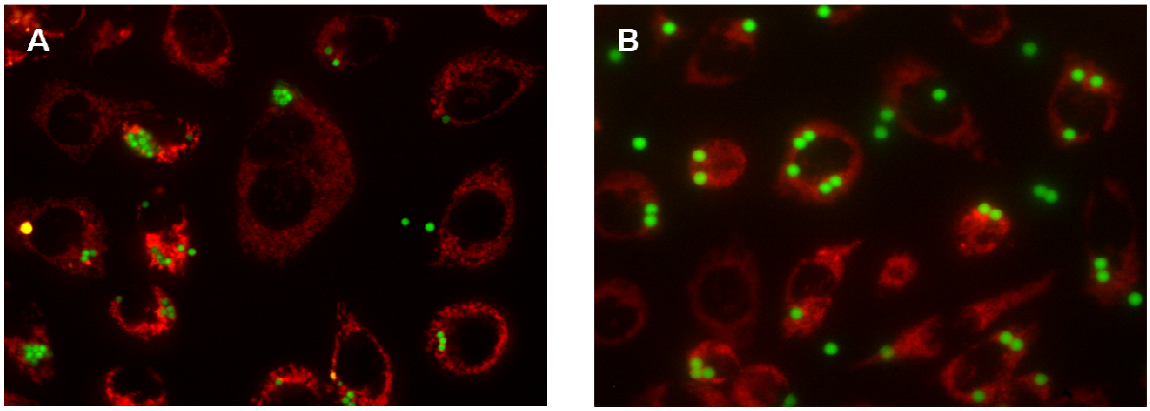

Figure 3.6: Shows a fluorescent micrograph of red fluorescing CHO cells containing 2 and 3 µm (A&B successively) green fluorescing microspheres. The images were taken using a Zeiss Axioscope microscope through dual band filter (TRITC – red and FITC – green) 24 hrs post microsphere incubation. The image was viewed through a 63X, NA 1.4 oil immersion objective lens.

To perform the confocal laser scanning microscopy experiment, an equidistant stack of images was captured in confocal laser scanning mode (CLSM) and confocal laser scanning reflectance modes (CLSRM) of live CHO cells with phagocytosed green fluorescing microspheres. By scanning many thin sections through the cell-sphere samples it was possible to detect that the 2 µm GF spheres were totally phagocytosed by the CHO cells (figure 3.7). A Leica TCS-SP2 AOBS confocal system coupled to a Leica DMIRE2 inverted microscope using a Plan Apo 63X oil immersion objective (NA 1.4) was utilized for CLSM and CLSRM imaging of the cells with spheres. A double dichroic mirror (DD488/543) was employed for CLMS imaging and an RT 30/70 (30 %

reflection, 70 % transmission) dichroic mirror was used for CLSRM. Under CLSM, the cells were excited by a 488 nm laser with collection between 500 – 780 nm. Under CLSRM, the microspheres were excited at 468 nm with collection between 533 – 553 nm. Planar images were taken at 1 µm intervals (slices) along the axial plane through the cells with engulfed spheres. Finally, 3D reconstruction of the planar stacks and digital merging of the CLSM and CLSRM image stacks were performed using the Image J program. Using the same procedure mentioned herein, data images for the CHO cells incubated with the 3 µm spheres confirmed only partial internalization of these spheres.

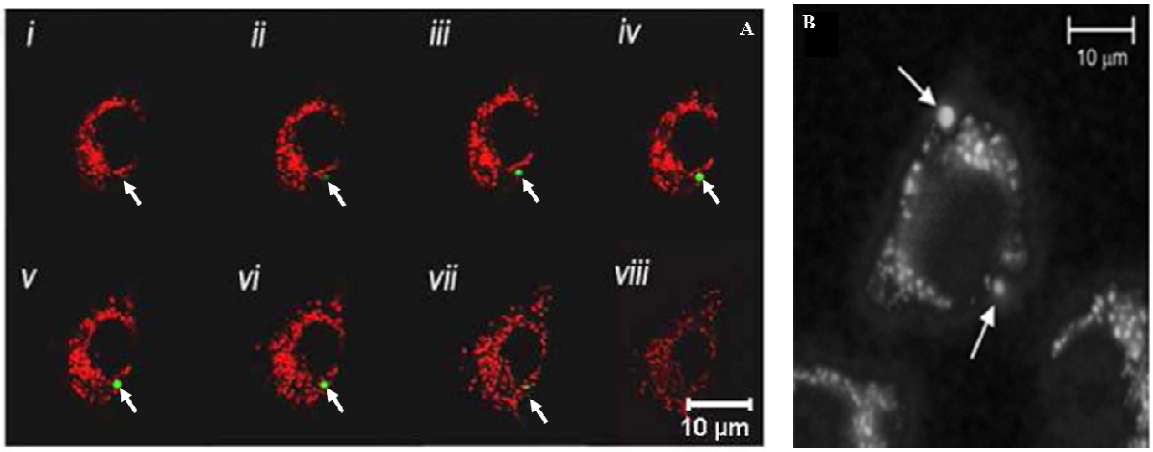

Figure 3.7: In (A) data obtained via confocal laser scanning microscopy (i)–(viii) z-scans of 1 µm confirmed total internalization (pointed by arrows) of 2 µm GF microspheres (reprint by permission from *IEEE Journal of Selected Topics in Quantum Electronics* (24)). The image in (B) is a fluorescent picture of a CHO cells with internalized 2 µm spheres, arrows point to the spheres within the cell. Both A&B were viewed using a 63X, NA 1.4 oil microscope objective lens.

3.1.4 Cell viability measurements

Once the spheres were confirmed to be inside the cells (2 µm) and/or partially embedded (3 µm), cell viability using the trypan blue exclusion viability dye assay was undertaken. Cell viability for cells incubated with spheres over the time periods indicated in section 3.1.2 was determined. This was measured by rinsing the monolayer twice with 2 ml of OPTIMEM each time post cell plating and incubation over the required time period.

After aspirating the second 2 ml of the wash medium, a 160 µl of 0.4 % trypan blue exclusion dye solution was added per dish, the samples allowed to incubate at room temperature for 5 – 15 minutes and then imaged via a home built Köhler illumination system created using a white light source (figure 3.8).

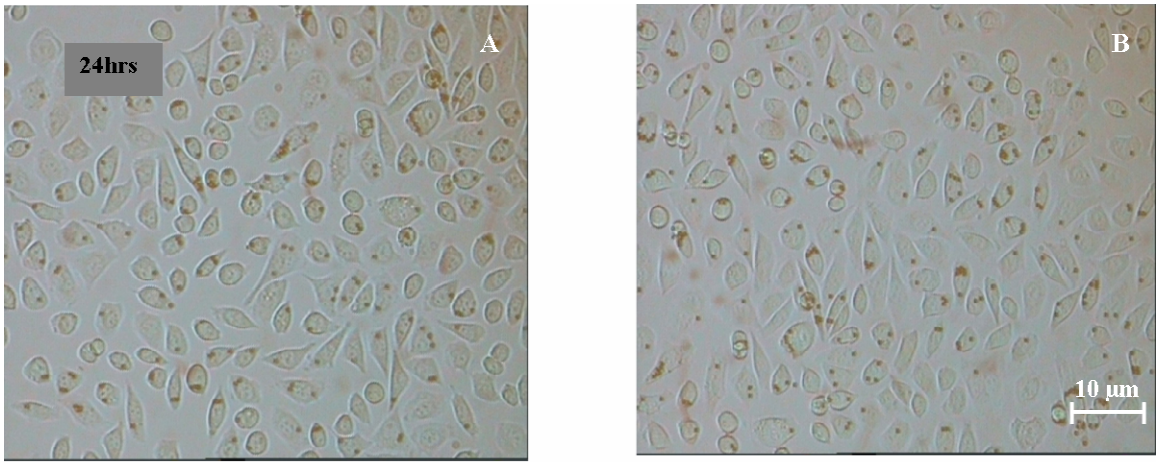

Figure 3.8: Taken fifteen minutes post incubation in 0.4 % trypan blue at room temperature and imaged via Köhler illumination (20X, NA 0.42 objective lens), is an illustration of adherent CHO cells engulfing 2 µm spheres (A) and the partially included 3 µm beads are shown in picture B. The microspheres appear as reddish-brown dots on the cells and there is no occurrence of blue staining in any of the cells, therefore this proves the CHO cells were viable after sphere phagocytosis.

This was done to acquire images with optimum resolution, minimum heating, uniform illumination field and good contrast for brightfield imaging. Trypan blue exclusion dye experiments performed on CHO cell samples incubated with microspheres over 3, 6, 24, 48 and 72 hrs; confirmed no compromise to cell viability as no cells included the dye following microsphere ingestion. Cell viability assays performed using the same procedure mentioned in this section, subsequent to optical treatment experiments to be reported in the remaining sections of this chapter also proved the cells to be viable. These trypan blue experiments were performed in order to prove that the ingestion of inert non-digestible particles (2 and 3 µm spheres) by cells was not toxic to the cells.

3.2 Gaussian beam optical cell-sphere trapping and guiding

3.2.1 Optical lateral trapping efficiency and axial guiding of cells internalizing microspheres

In chapter 2 sections 2.2.4 and 2.5.2 I introduced the concepts of optical trapping efficiency and guiding respectively, outlining the forces governing these processes. In this section the effect of the intracellular dielectric tags on the scattering and gradient forces of a stable 3D optical trap is determined. I present experimental data on how efficiently cells internalizing different numbers of polymer microspheres trap compared to those without ingested microspheres. Also, herein, I display that in a diverging beam optical field (2D trap) created using a low numerical aperture objective lens the intracellular polymer microspheres serve as highly directional optical scatterers. Hence, axial optical guiding of cells engulfing a varying number of spheres compared to those without dielectric tags is enhanced by strong scattering forces from these cells. Laboratory results for this optical guiding experiment are also presented in the following sections.

3.2.1.1 Experimental setup of the optical trapping and guiding apparatus

Using a high numerical aperture microscope objective (MO), an inverted microscope system (Nikon TE2000U), and a Prior motorized translation stage (Prior Scientific) (setup by Dr. Steve Lee in an independent PhD project), the lateral *Q*-values and the axial guiding velocities of cells both with and without internalized microspheres were measured. The trapping beam and guiding beams were both generated using a 1070-nm, 5-W fiber laser (YLM-5, IPG Photonics). For the lateral trapping studies, the Gaussian beam was magnified to slightly overfill the back aperture of the oil immersion MO (of NA 1.25, magnification 100X) to form a diffraction-limited spot that acted as a 3-D optical trap. The transverse beam waist ($w_{x,y}$) at the full-width at half maximum (FWHM), was measured to be ≈ 380 nm. The beam diameter was calculated via the direct camera technique, this method entails direct illumination of the charge-coupled-device (CCD) camera. The image of the focused spot was captured and processed using

the IMAQVision program (National Instruments). A beam steering system was formed using a conjugate lens pair where the image of the steering mirror was imaged onto the back focal plane of the MO. The 3D optical trap was maintained at a power of 22 mW.

A low NA 0.25, 10X objective was used for the cell-guiding experiment, where the transverse beam waist at FWHM was calculated to be ≈ 5µm and the power was kept at 250 mW. In this work, both the axial distance and time taken for cells with spheres guiding were determined to calculate the optical guiding velocities. Notably, as calculated using equation 2.8 (chapter 2), the Rayleigh range of the 3D trapping beam set using a high NA lens was determined to be ≈ 4.2 µm. This was distinctively short compared to that of the guiding beam which was measured using the same equation to be ≈ 73 µm. Thus, with the low NA objective, we were able to obtain a beam with a longer Rayleigh range, thus propelling the particles further along in axial direction (optical guiding) as opposed to a high NA objective producing a shorter Rayleigh range beam. As both the optical trapping and guiding experiments were setup on a commercial inverted microscope, there was a smooth transition between switching from one objective to the other without requirements of aligning the system in between the experiments. The back aperture of both the 100X and 10X Nikon objective lenses used for these studies were measured to have diameters of ≈ 8 and 14 mm respectively. For sample imaging, a CCD camera was aligned to one of the side ports of the microscope and connected to a monitor or a computer for capturing videos (see figure 3.9 A and B).

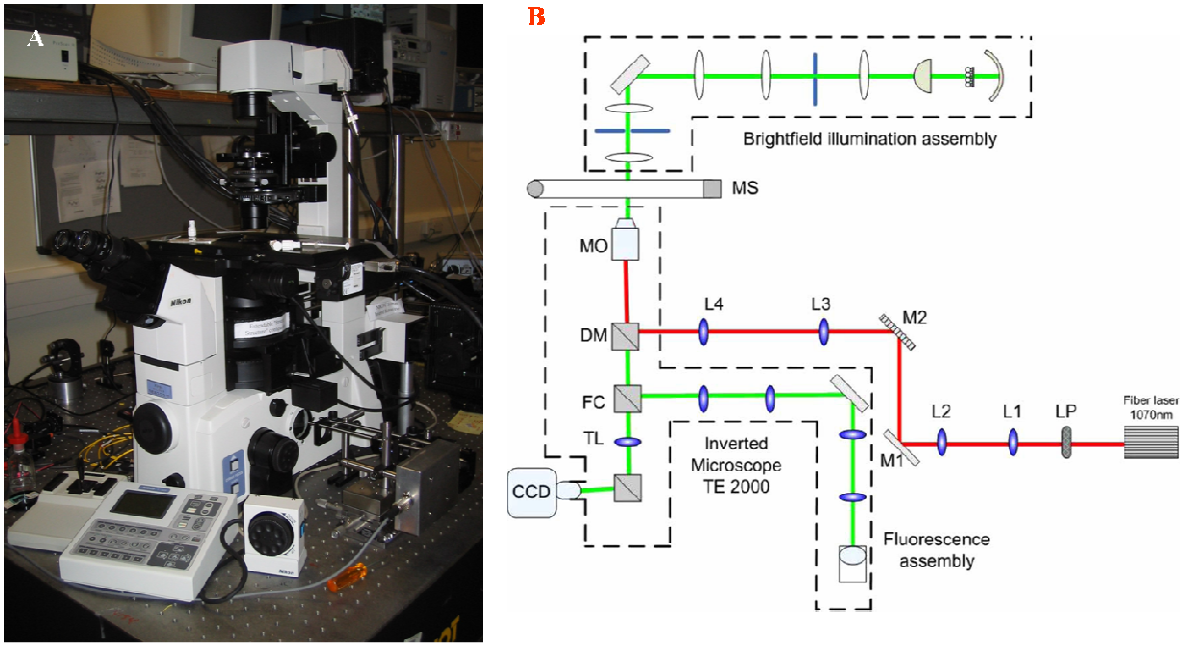

Figure 3.9: (A) is a picture of the Nikon TE2000U inverted microscope used during this project. (B) an outline of the optical tweezing and guiding setup as was aligned within the microscope. A fiber laser (5W, ytterbium-doped fiber laser, IPG) provides a Gaussian beam (M^2 < 1.1, beam diameter 1.6 mm) that is expanded by lens L1 and L2 to 9.6 mm. A linear polarizer (LP) is used to rotate the polarization of the beam. The expanded Gaussian beam is relayed through a beam steering lens system (L3 and L4), via reflecting off M1 and M2 (silver mirrors). The beam is then reflected by NIR dichroic mirror (DM) (z900dcsp, Chroma) onto the back aperture of the MO. The sample is mounted onto a motorized stage (MS). For brightfield and fluorescent illumination, we make use of the brightfield and fluorescence assembly supported by a commercial inverted microscopy (TE2000E, Nikon). FC is the fluorescence cube and TL is the tube lens. A color digital camera (CCD) (HAD, Pulnix) is used to record the microscopic images (reprint by permission from *IEEE Journal of Selected Topics in Quantum Electronics* (24)).

For the axial optical guiding studies, it was not necessary for the magnified Gaussian beam (diameter ~ 9.6 mm) to overfill the back aperture (~ 14 mm) of the low NA 10X MO. In this project there was no specific requirement for a diffraction limited optical field but rather for a less tightly focused beam geometry found essential for particle transport.

3.2.1.2 Measuring Q-Values and Guiding Velocities

Having established the optical setup as described above, I next measured the lateral Q_{lat} values and the guiding velocities of different cell types both with and without internalized microspheres. As described in chapter 2, I used the Q_{lat} value measurement technique to quantify the lateral trapping forces. A typical sample chamber used for optical tweezing consists of a microscope glass slide (BDH, Poole UK) for the base and a glass cover slip (type zero or one, 0.13 – 0.17 mm thick) (BDH, Poole UK) on the top side, sandwiched using a vinyl spacer (National Sign, Scotland, UK) with a central well between the two glass compartments. The sample itself was a total volume of 20 µl of cell-sphere dielectric entities suspended in complete culture medium dispensed within the well in the middle of a vinyl spacer.

After loading the sample chamber it was placed on the motorized sample stage over the microscope objective with a drop of index matching fluid (oil) on the bottom side of the sample chamber to contact the anterior of the objective. On viewing, the cells with phagocytosed spheres were noticed to move around in the liquid due to Brownian motion. Because the laser was properly aligned through the microscope objective, a faint image of the focused laser beam was visible at the bottom of the sample slide. By translating the beam focus into the plane of freely moving particles and manipulating the z-controller of the sample stage on the setup to translate the sample thereby matching the laser beam to the position of mobile spheres three dimensional particle trapping was achieved. This was demonstrated by the cells (or cell) with internalized spheres being pulled into the beam when the beam is placed close to their vicinity. Thereafter, the cell (with or without the phagocytosed spheres) was held in the trap and by traversing the sample stage utilizing a motion controller at constant velocity until the cell fell out of the trap (upon attaining the critical drag force velocity), the amount of momentum transferred onto the cell from the trapping beam, was established. Figures 3.10 and 3.11 shows the Q_{lat} values obtained for the different cell types but also dependent on the number of spheres that had been internalized.

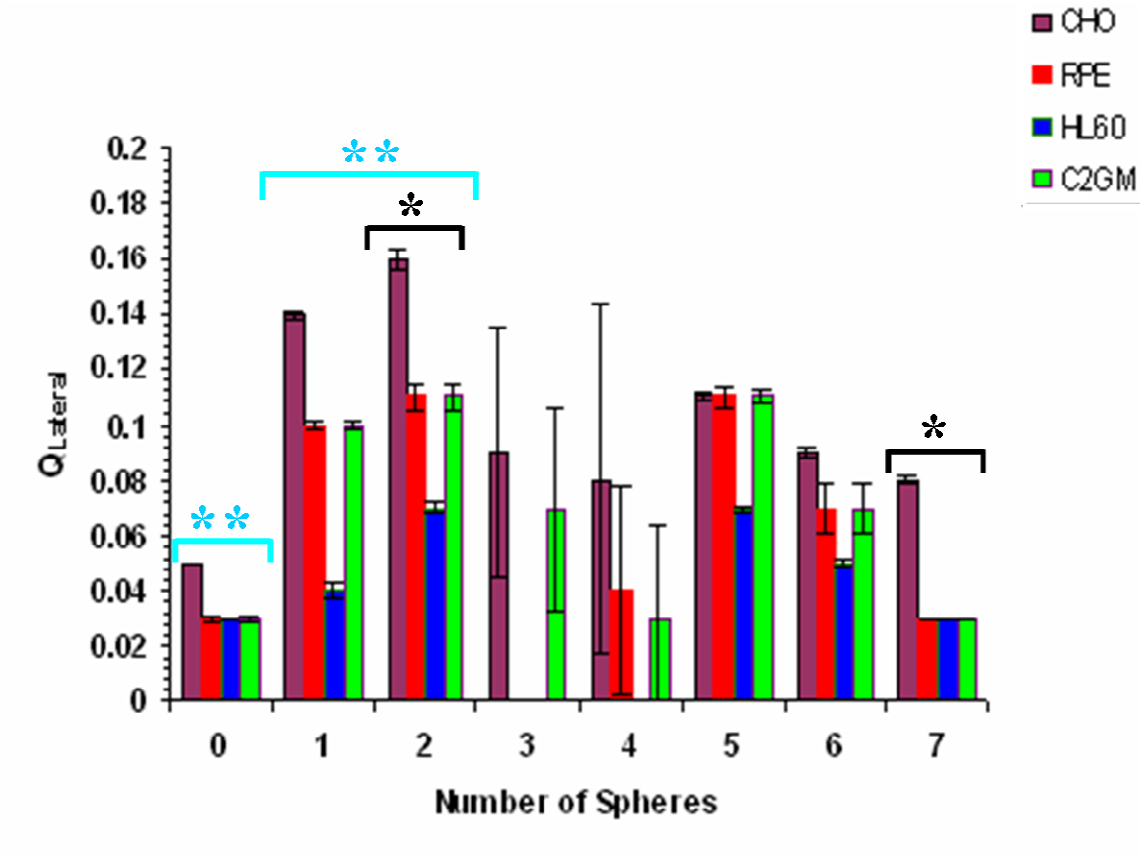

Figure 3.10: Lateral *Q*-values of different cell types containing different amounts of 2 µm polymer microspheres. In general, cells containing one or two spheres per cell, trapped with the highest efficiency. Error bars represent the SEM (n = 3, experiments repeated trice for each column). Notably, for the data of cells engulfing 3 spheres, only two samples out of the triplicate contained cells with 3 spheres for both CHO and C2GM cells. However, in all the triplicates for RPE and HL60 cells, no cells were found with three internalized spheres. Additionally, only one out of three samples tested contained cells with four phagocytosed spheres for CHO, RPE and C2GM cells. For this experiment, none of the HL60 cell samples were found containing four spheres per cell. Using ANOVA followed by Dunnett's and Fisher's tests: * and ** means data points are significantly different from each other within each of the separate cell lines (Appendix (v) pages A8-A13).

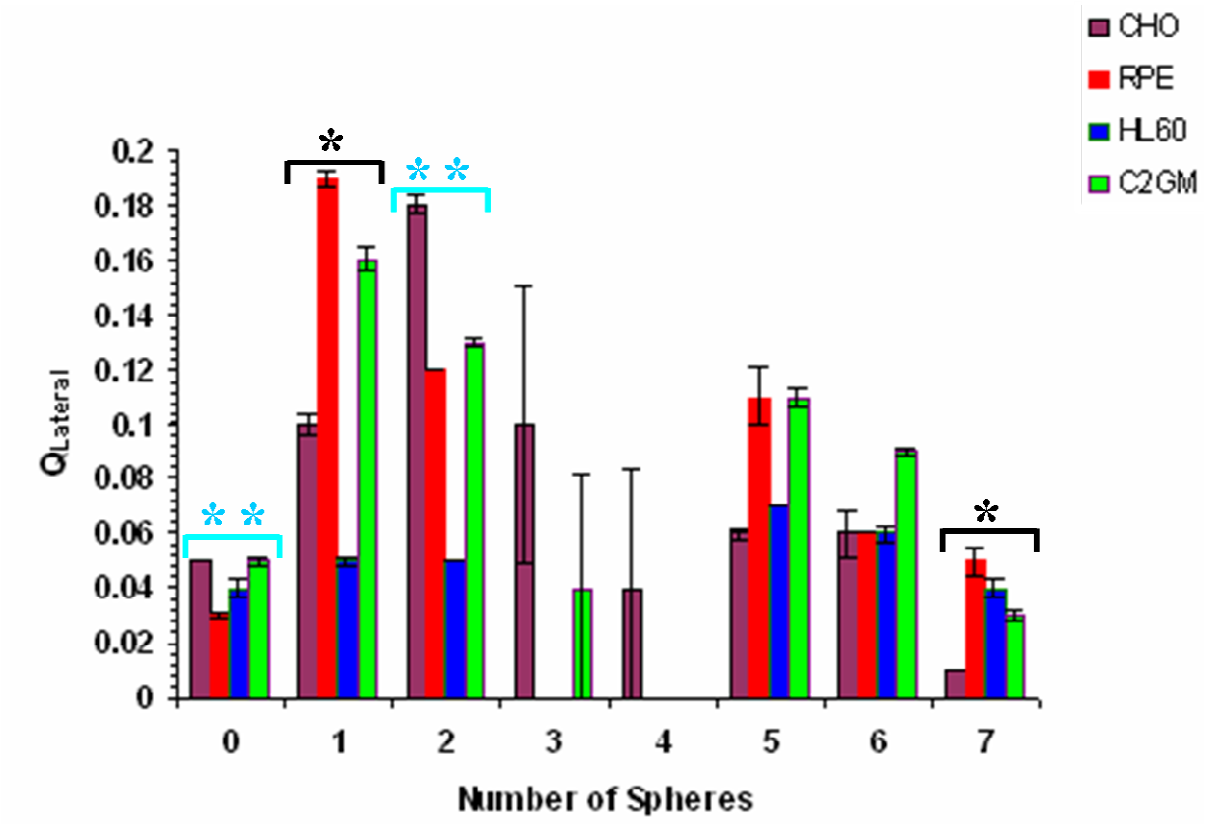

Figure 3.11: Lateral *Q*-values of different cell types containing different amounts of 3 µm polymer microspheres. Notably compared with the cell lines totally internalizing the 2 µm GF spheres, higher trapping efficiency values were obtained for cells with the partially included 3 µm spheres. Error bars represent the SEM (n = 3, experiments done in triplicates for each column). In CHO cells, two out of the three samples analysed contained cells with three internalized spheres and only one sample had cells with four engulfed spheres. Also, one of the triplicate test samples of C2GM cells contained cells with three spheres and no C2GM cells had four spheres for this experiment. In both RPE and HL60 cell samples neither three nor four polymer spheres per cell were observed to be up taken. Therefore, no trapping efficiency data is available for these cells. Using ANOVA followed by Dunnett's and Fisher's tests: * and ** means data points are significantly different from each other in each cell line (Appendix (v) pages A13-A18).

During the tweezing of the cells with either totally or partially internalized spheres, it was noted that the cell would orientate such that the microspheres (either 2 µm or 3 µm) were aligned to the tweezing beam. This then resulted in the actual trapping of the

microspheres and not necessarily the whole cell. For most cells, one to two internalized microspheres provided the highest Q_{lat} values for trapping in the lateral plane. The consistency of the Q_{lat} values was dependent on the quality of the trap and the trapped particle. Hence, the microspheres provided an increase of the lateral gradient force. Markedly, for both the 2 µm and 3 µm cells with phagocytosed spheres, the HL60 cells did not appear to respond as well as the other cell lines to the optical field and displayed a poor trapping efficiency. In addition it was noted that in all four cell lines for both the 2 and 3 µm spheres, there was lack of consistency in the presence of cells containing 3 and 4 spheres. In some cases there were no cells with 3 or 4 engulfed microspheres. This might have been due various reasons including cell age or even an undetected change in cell culture conditions within the incubator. Future studies will aim at a thorough study to investigating this issue alongside creating a rudimentary physical model that will be utilized for studying the role of sphere placement within the cell and its consequential role on the trapping efficiency.

Contrarily, by using a weakly focused Gaussian beam through a low NA objective, the axial gradient force is much reduced so that the scattering force dominates thereby allowing cells or cells with phagocytosed spheres to be deflected in the direction of beam propagation. Sample preparation for this experiment was similar to that used in the optical trapping methodology. In this experiment a dry objective was employed, therefore, I positioned the sample chamber containing cells with and without ingested microspheres on the sample stage in the beam path of a diverging Gaussian beam. By recording and observing the guiding velocity of the cells, I was able to measure that cells with polymer spheres guided an order of magnitude faster than cells without spheres. With larger numbers of ingested microspheres, I observed an increase in the guiding velocity of the cells. This increase of the guiding velocity of the cells was attributed to an increase in the axial scattering due to the presence of the ingested spheres. From this effect, a conclusion was drawn that the increase in the effective axial scattering exerted onto the cells was due to the ingested microspheres (see figure 3.12 and 3.13).

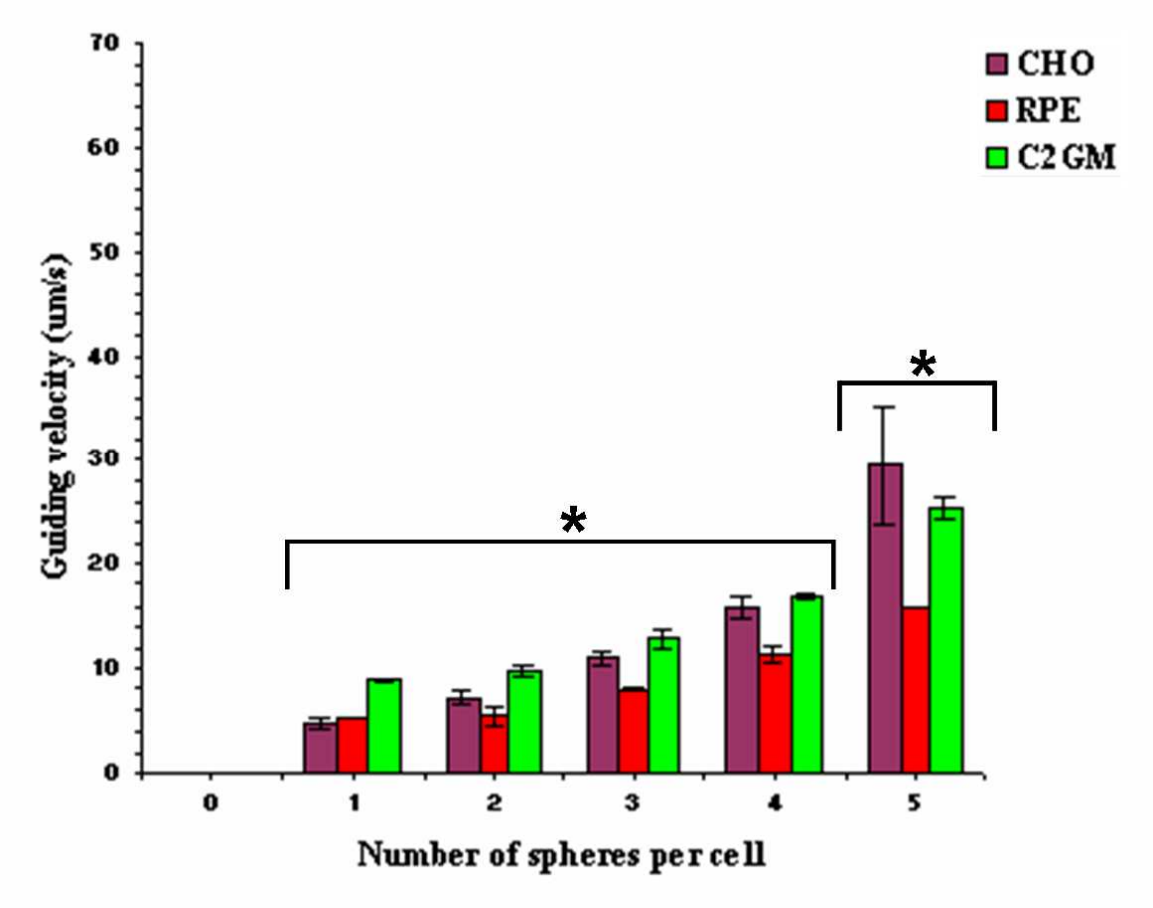

Figure 3.12: Axial cell guiding data, displaying maximum guiding velocities for cells containing different numbers of 2 µm GF spheres per cell. Cells with no spheres displayed no axial guiding. Experiments were performed in triplicates, for each data point. Error bars represent the SEM (n = 3). Using ANOVA followed by Dunnett's and Fisher's tests: * means data sets are significantly different from each other within each of the three cell lines (Appendix (v) pages A19-A22).

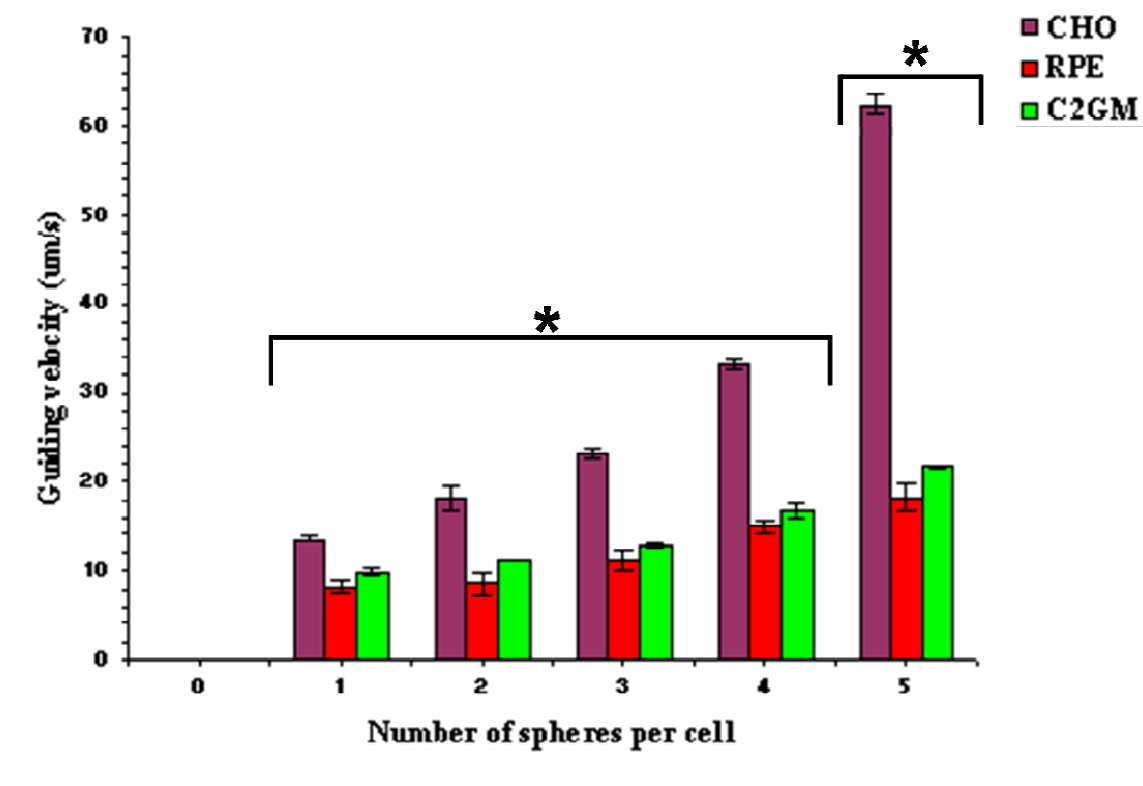

Figure 3.13: Axial cell guiding data, displaying maximum guiding velocities for cells containing different numbers of 3 µm spheres per cell. Cells with no spheres displayed no axial guiding and compared to the data in figure 3.12 previously presented, cells with 3 µm spheres showed enhanced axial guiding. Experiments were performed in triplicates and repeated three times. Error bars represent the SEM. Using ANOVA followed by Dunnett's and Fisher's tests: * means data sets are significantly different from each other in each of the different cell lines presented (reprint by permission from *IEEE Journal of Selected Topics in Quantum Electronics* (24)). See appendix (v) pages A22-A25 for full statistical analysis.

In both cells incubated with 2 and 3 µm spheres, cells with five spheres guided significantly faster than those with only one sphere, also the cells with 3 µm spheres showed profound guiding velocities compared to those incubated with 2 µm spheres. Notably, the HL60 cells either with or without 2 or 3 µm spheres displayed no axial guiding on exposure to the weakly focused light field.

3.3 Optical cell sorting using a Gaussian beam

3.3.1 Optical cell sorting through axial guiding to laminin coated coverslips

I have shown that on exposing CHO cells to a diverging optical field obtained through use of a low numerical aperture objective, cells with ingested microspheres have enhanced axial guiding (Figs. 3.12-13). Therefore, I sought to capitalize upon this feature to develop a novel optical cell sorting methodology for the separation of cells from a mixed cell population. To do this, I implemented the sorting of the cells with microspheres on a self-built inverted optical trapping setup, using analyte volumes of 100 µl as elucidated in section 3.3.1.2 to follow.

3.3.1.1 Experimental setup

A home built optical guiding apparatus was employed, where a diffracting Gaussian beam was directed upwards through a 10X objective lens (NA 0.28) (Comar, USA) towards a mixed population of CHO cells (with and without internalized microspheres) suspended between a hydrophobic glass bottom petri dish and a laminin-coated top coverslip. Only cells that had internalized microspheres were propelled axially to the top of the sample chamber and attached to the laminin-coated glass coverslips. Figure 3.14 below illustrates the home-built optical guiding setup used in this optical cell sorting experiment.

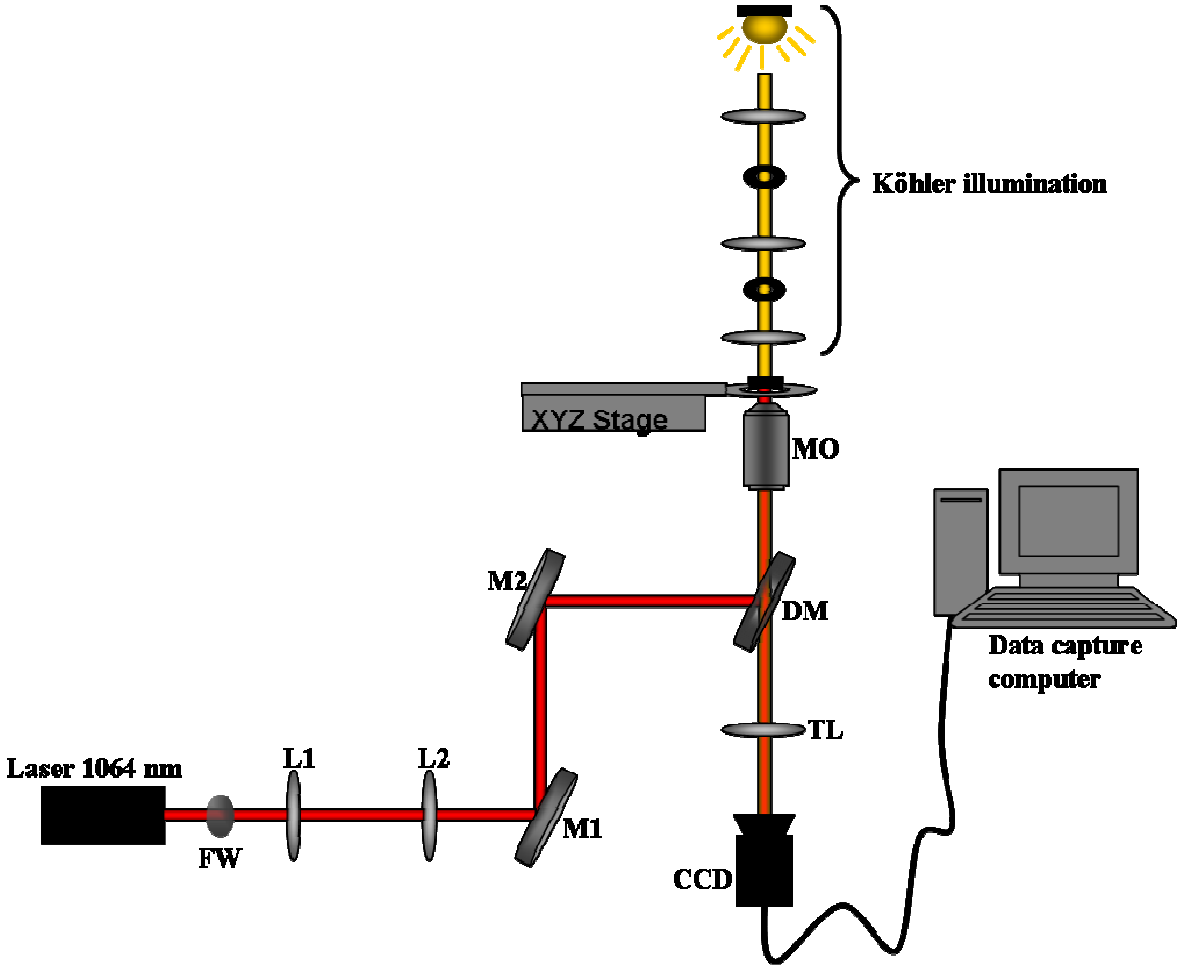

Figure 3.14: Cell sorting system built using a 1064 nm Nd:YAG laser, the beam (diameter = 1.5 mm) was emitted and the average power attenuated using a neutral density filter-wheel (FW), before expanding the beam via a two lens magnifying telescope system L1 and L2 (f = 50 and f = 200 mm) to a 6 mm diameter. Then it is reflected using members of a periscope mirrors M1 and M2 via a dichroic mirror (DM) onto the back aperture (diameter = 8mm) of low NA 0.28, 10X microscope objective (MO). The XYZ stage is the sample stage which was illuminated using Köhler illumination consisting of a light emitting diode (LED), three lenses (f = 20 mm, f = 20 and 65 mm respectively) and two diaphragm apertures. A tube lens (TL) (f = 100 mm) was positioned beneath the sample stage and focused the collected bundle of rays onto the sensor of a CCD camera through which the image forming data is transferred onto a data capturing computer.

3.3.1.2 Selective separation of CHO cells with internalized microspheres

A mixed population of CHO cells with a range of numbers of partially internalized 3 µm microspheres was trypsinised from a T25 culture flask and suspended in complete growth medium. These were strained through a 40 µm pore size filter (Millipore, UK) to obtain a mono-dispersed cell sample. The cell concentration used for the sorting experiment was calculated to be 6.2 X 10^5 cells/ml. A 100 µl of this cell sample per sorting experiment was used. Sample chambers used in these experiments consisted of 30 mm diameter type-zero glass bottom petri dishes (bottom compartment) (World Precision Instruments, Stevenage, K) and 22 mm diameter round glass type-one coverslips (top part) (BDH, Poole UK). To prevent cell adhesion to the 23 mm glass surface of the dishes, the dishes were coated with sigmacote (Sigma-Aldrich), a reagent that reacts with surface silanol groups on glass to produce a neutral, hydrophobic microscopic thin film. The coating procedure involved adding 1 ml of neat sigmacote per dish and incubating them at room temperature in a class II level Bio-hood (bio-hood) for 12 hrs, before aspirating and air drying the within the bio-hood. In contrast, the top coverslips were coated with 2 µg/cm^2 laminin solution made up in sterile tissue culture grade water (Sigma-Aldrich) to promote cell adhesion upon close physical contact (25). To coat, the coverslips were incubated in the laminin solution overnight in a 37^{o}C incubator and thereafter allowed to air dry in the bio-hood before use in experiments.

After sample preparation the sample chamber was placed on the sample stage of an inverted microscope optical setup. The sample was exposed to the beam and an average of 50 cells with ingested spheres per experiment were optically sorted and separated from the rest of the sample (figure 3.15).

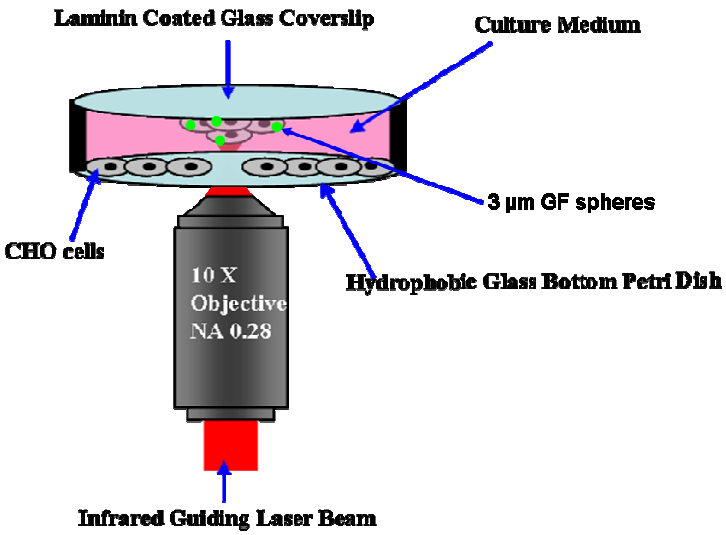

Figure 3.15: Illustrates a 1064 nm laser Gaussian guiding beam less tightly focused through a low NA objective to propel cells with intracellular dielectric tags onto the top surface on the sample chamber. This image explicitly displays cells with 3 µm spheres being optically transported onto the laminin coated glass slide whilst neat CHO cells remain on the bottom of the sample assembly without any optical treatment.

Optical guiding was achieved due to an increased axial scattering force exerted onto cells with internalized microspheres compared to those with no ingested spheres. The sorting occurred at a maximum rate 11 cells/min. Figure 3.16 shows the actual laboratory results of this experiment.

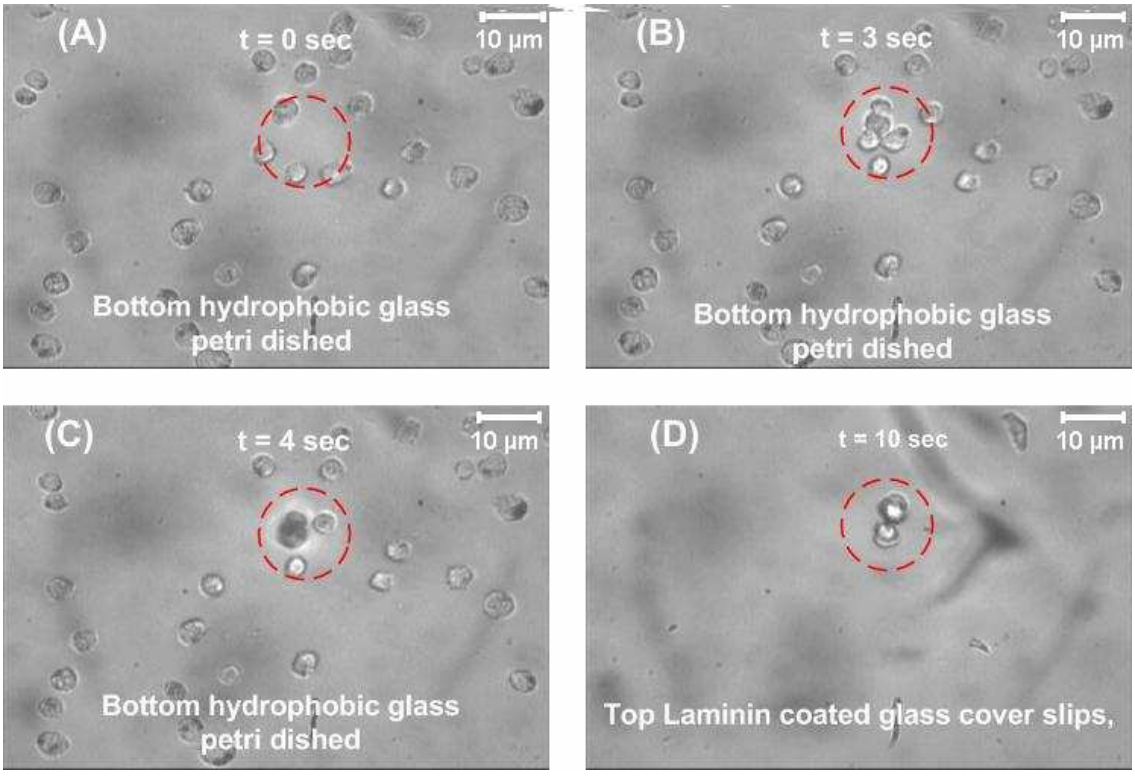

Figure 3.16: Sample chamber containing 100 µl of a mixed population (with and without ingested microspheres) of CHO cells was suspended between a hydrophobic glass bottom petri dish and laminin-coated top coverslip, while a diffracting Gaussian beam (red dotted circle) emerging from a 10X objective with NA 0.28 was illuminated toward the laminin-coated coverslip (video available). (A) and (B) CHO cells begin to migrate toward the centre of the beam. (C) CHO cells with ingested microspheres start to be axially propelled onto the top laminin-coated glass coverslip. (D) CHO cells with ingested spheres adhere to the top glass coverslip, and subsequently, can be cultured separately (reprint by permission from *IEEE Journal of Selected Topics in Quantum Electronics* (24)).

The separated cells that adhered to the laminin-coated coverslip were then further cultured by placing the coverslips into 500 µl of filter-sterilized conditioning medium (collected from routine sub-culturing of CHO cells) in 30 mm diameter plastic petri dishes at 37^{o}C with 5% CO_2 , 85% humidity, and the medium changed every 48 h. After four days of culturing, the optically sorted cells were trypsinised; their viability tested using the trypan blue exclusion dye method, and counted. A total cell count number of 1.2 X 10^3 cells/ml was obtained with 100 % viability. In figure 3.17, a brightfield image of the re-cultured CHO cells viewed with a 20X, NA 0.54 microscope objective is shown.

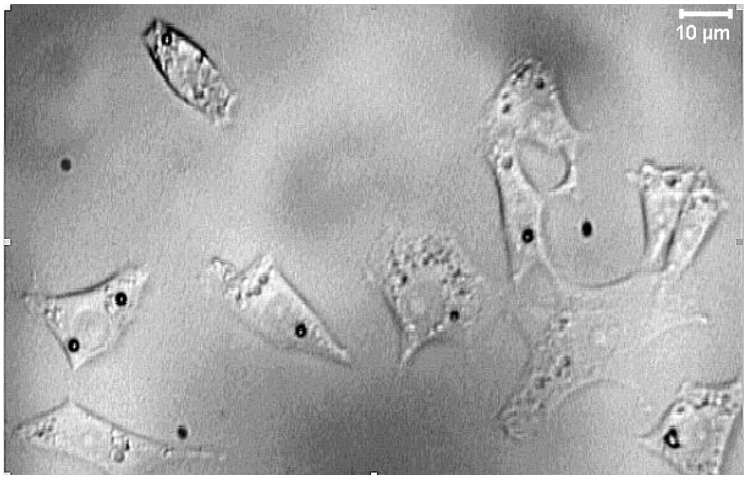

Figure 3.17 Brightfield image of a sample chamber containing re-cultured CHO cells with ingested microspheres (dark spots) viewed with a 20X objective lens of NA 0.54 (reprint by permission from *IEEE Journal of Selected Topics in Quantum Electronics* (24)).

3.4 Discussion

Effective optical trapping, guiding, and sorting of cells remain a key topic for biophotonics. The application of optical forces for the trapping, guiding and/or sorting of cells was investigated in the studies offered in this chapter. The phagocytosis process was presented as a new technique for enhancing the dielectric contrast of the mammalian cells for enhanced optical treatment. During this process cells were allowed to naturally take up non-functionalized polymer microspheres from their surroundings. Maximum engulfment for cells incubated with both the 2 and 3 µm polymer microspheres was possible 24 hrs post incubation. The extent of microsphere inclusion in cells was confirmed by fluorescence and laser scanning confocal microscopy, confirming total engulfment of the 2 µm spheres and only partial inclusion of the 3 µm spheres within the cells. I have shown that a range of different cell types (both adherent and suspension cell lines) are capable of taking up microspheres without harm. Cell viability (~ 98 %) post microsphere uptake was supported by the trypan blue exclusion dye experiments.

Therefore, it is possible to enhance the dielectric contrast of cells to promote effective optical micromanipulation of these cells by the uptake of nontoxic microspheres. Furthermore as phagocytosis is a physiological process, to achieve cell tagging this way implies minimum interference with the biological system under study. By studying how these intracellular microspheres influenced the cell's response to an applied optical field, I was able to exploit both the lateral gradient as well as the axial scattering forces to both optically trap and guide cells engulfing various amounts of microspheres compared to those cells which expressed no spheres. The optical trapping efficiency results showed that in a 3D trap, cells with one or two spheres trapped better (higher Q-values) than those with higher numbers of spheres (lower Q-values). This is due to the increased volume of cells with more that two spheres, optical tweezers can only exert picoNewton size order forces and these might not be strong enough to maneuver cells with more than two spheres. However as a result of their lower refractive index, cells without spheres trapped with a poor efficiency (typical Q-values below 0.06 for both 2 and 3 µm spheres) compared to those with spheres and therefore an enhanced dielectric contrast. Interestingly, although having phagocytosed the microspheres, compared to the other cell lines the HL60 cells displayed lower Q-values and thus a poor trapping efficiency. This apparent difference could be due to their smaller size (~10 µm) and also having a larger nucleus to cytoplasm ratio in comparison to the other cell types (26). Nonetheless, HL60 cells with spheres trapped with a significantly higher efficiency to those without any spheres at all.

Contrarily in the 2D trap, cells with the highest number (5 spheres per cell) of spheres displayed significantly stronger axial optical guiding velocities (roughly 30 µm/s and 63 µm/s for 2 and 3 µm spheres respectively) compared with those that had one or two spheres (> 20 µm/s for both 2 and 3 µm spheres). This is in because these cells had an overall increased scattering force compared to cells with a lower number of spheres or no spheres at all. HL60 cells either with or without 2 or 3 µm spheres did not respond to axial optical guiding on exposure to the weakly focused light field. This cell line was established from promyelocytic leukemia tissue. Promyelocytes have an indented nucleus it is therefore likely that the engulfed spheres may be embedded to these indented regions

in the nucleus. This could explain the reason for the poor optical guiding of these cells. However, more experiments are required to prove this theory.

The enhanced optical guiding behaviour of cells in my investigations was used to successfully sort cells via a simple, inexpensive, and nontoxic flow-free optical process. From an initial concentration of 6.2 X 10^5 cells/ml, roughly 50 cells with ingested spheres were optically guided at a maximum rate of 11 cells/min. These were sorted and carefully separated from the rest of the sample, as they got attached to the laminin coated top coverslips of the sample micro-chamber. Four days following collection and re-culturing, a total number of 1.2 X 10^3 cells/ml with 100 % viability was obtained. This is indeed a very good result considering the simple design of the sample chamber used with no fluid flow or bulky microfluidic pumps. This kind of flow-free passive sorting also promoted no hydrodynamic focusing of the cells, leading to less mechanical stress normally caused by fluidic shear on the cells (5). In contrast to the previously reported flow-free passive cell sorting performed using a Bessel beam reported by Paterson *et al*, 2007 (5), where cells were externally tagged using a tedious and expensive protocol as well as collected using pulled microcapillary glass tubes, I showed that an effective flow-free sorting scheme can be realized using phagocytosis for cell tagging, a laminin coated cover slip (top of the sample chamber) for cell collection and a 2D Gaussian beam trap requiring no special optics (e.g. an axicon lens) for cell guiding.

In future, it might be possible to apply this new method to studies within, for example, the immune system, to isolate different phagocytes and non-phagocytes. It may also be possible in future studies, to sort and separate healthy versus diseased cells in this manner. Uptake of microspheres by pathogenic cells might be facilitated by modifying the surface of the spheres with specific receptor molecules that target only diseased cells.

Furthermore, since optical tweezers and/or guiding measures, have been applied in cell sorting and separation experiments they possess the potential to be the key contributing element to the success of lab-on-a-chip systems. Because microfluidics systems enable use of nano and/or micro liter sample scales, development and improvement of these

devices is of extreme importance. In the cell sorting project reported, I showed successful sorting of a mixed population of cells using only 100 µl of sample volume. This study is both time and cost effective, creating an opportunity for permitting crucial cell sorting technologies which promise the conduction of multiple biomedical tests with employment of minute amounts of reagents and sample analyte sizes. Also in cases were rare or precious cell populations are a sample of interest, lab-on-a-chip approaches may provide a more successful means of sample analysis and the current study might help in the developing of such systems. Hence, future studies will be performed towards the improvement of this technique for the microfluidic environment with computer-based analysis system (27, 28) for automated high-throughput cell sorting.

References

1. V. Saxena, "Optical microparticles as handles for optical manipulation of CATH.a cells," *Stanford Undergraduate Research Journal* **2**, 39-42 (2003)
2. C. K. Sun, Y. C. Huang, P. C. Cheng, H. C. Liu and B. L. Lin, "Cell manipulation by use of diamond microparticles as handles of optical tweezers," *J. Opt. Soc. Am. B-Opt. Phys.* **18**, 1483-1489 (2001)
3. L. Paterson, E. Papagiakoumou, G. Milne, V. Garces-Chavez, S. A. Tatarkova, W. Sibbett, F. J. Gunn-Moore, P. E. Bryant, A. C. Riches and K. Dholakia, "Light-induced cell separation in a tailored optical landscape," *Appl. Phys. Lett.* **87**, 123901 (2005)
4. M. D. Wang, H. Yin, R. Landick, J. Gelles and S. M. Block, "Stretching DNA with optical tweezers," *Biophysical Journal* **70**, SUP63-SUP63 (1996)
5. L. Paterson, E. Papagiakoumou, G. Milne, V. Garces-Chavez, T. Briscoe, W. Sibbett, K. Dholakia and A. C. Riches, "Passive optical separation within a 'nondiffracting' light beam," *J Biomed Opt* **12**, 054017 (2007)
6. http://www.fortebio.com/interactions/July_2008/,
7. S. I. Simon and G. W. Schmidschonbein, "Biophysical aspects of microsphere engulfment by human-neutrophils," *Biophysical Journal* **53**, 163-173 (1988)

8. A. Aderem and D. M. Underhill, "Mechanisms of phagocytosis in macrophages," *Annu Rev Immunol* **17**, 593-623 (1999)

9. B. Alberts, D. Bray, J. Lewis, M. Raff, K. Roberts and J. D. Watson, *Molecular Biology of the Cell 3rd edition (Garland)* 559-651 (1993)

10. S. Greenberg and S. C. Silverstein, *Paul WE (ed.) Fundamental Immunology.* 941-946 (1993)

11. P. Chavrier, "May the force be with you: Myosin-X in phagocytosis.," *Nature Cell Biology* **4**, E169-E171 (2002)

12. Y. Tabata and Y. Ikada, "Macrophage Phagocytosis of Biodegradable Microspheres Composed of L-Lactic Acid Glycolic Acid Homopolymers and Copolymers," *Journal of Biomedical Materials Research* **22**, 837-858 (1988)

13. E. Essner, J. R. Roszka and J. H. Schreiber, "Phagocytosis and Surface Morphology in Cultured Retinal-Pigment Epithelial-Cells," *Invest Ophth Vis Sci* **17**, 1040-1048 (1978)

14. R. M. Gilberti, G. N. Joshi and D. A. Knecht, "The Phagocytosis of Crystalline Silica Particles by Macrophages," *Am J Resp Cell Mol* **39**, 619-627 (2008)

15. E. Gagnon, S. Duclos, C. Rondeau, E. Chevet, P. H. Cameron, O. Steele-Mortimer, J. Paiement, J. J. M. Bergeron and M. Desjardins, "Endoplasmic reticulum-mediated phagocytosis is a mechanism of entry into macrophages," *Cell* **110**, 119-131 (2002)

16. H. Kress, E. H. K. Stelzer, G. Griffiths and A. Rohrbach, "Control of relative radiation pressure in optical traps: Application to phagocytic membrane binding studies," *Physical Review E* **71**, (2005)

17. M. B. Hallett, "Phagocytosis of optically-trapped particles: delivery of the pure phagocytic signal," *Cell Research* **16**, 852-854 (2006)

18. A. Caspi, R. Granek and M. Elbaum, "Diffusion and directed motion in cellular transport," *Physical Review E* **66**, 011916 (2002)

19. http://www.sflorg.com/sciencenews/scn110608_01.html,

20. R. M. Sanchez-Martin, M. Cuttle, S. Mittoo and M. Bradley, "Microsphere-based real-time calcium sensing," *Angew. Chem.-Int. Edit.* **45**, 5472-5474 (2006)

21. V. K. Kodali, W. Roos, J. P. Spatz and J. E. Curtis, "Cell-assisted assembly of colloidal crystallites," *Soft Matter* **3**, 337-348 (2007)

22. G. B. Sukhorukov, A. L. Rogach, B. Zebli, T. Liedl, A. G. Skirtach, K. Kohler, A. A. Antipov, N. Gaponik, A. S. Susha, M. Winterhalter and W. J. Parak, "Nanoengineered polymer capsules: Tools for detection, controlled delivery, and site-specific manipulation," *Small (Weinheim an der Bergstrasse, Germany)* **1**, 194-200 (2005)

23. W. B. Jakoby and I. H. Pastan, "Cell Culture," **LVIII**, (1978)

24. P. Mthunzi, W. M. Lee, A. Riches, C. T. A. Brown, F. J. Gunn-Moore and K. Dholakia, "Intracellular dielectric tagging for improved optical manipulation of mammalian cells," *IEEE, Selected Topics in Quantum Electronics* **16**, 608-618 (2009)

25. H. K. Kleinman, L. Luckenbilledds, F. W. Cannon and G. C. Sephel, "Use of Extracellular-Matrix Components for Cell-Culture," *Analytical Biochemistry* **166**, 1-13 (1987)

26. S. Salvioli, G. Storci, M. Pinti, D. Quaglino, L. Moretti, M. Merlo-Pich, G. Lenaz, S. Filosa, A. Fico, M. Bonafe, D. Monti, L. Troiano, M. Nasi, A. Cossarizza and C. Franceschi, "Apoptosis-resistant phenotype in HL-60-derived cells HCW-2 is related to changes in expression of stress-induced proteins that impact on redox status and mitochondrial metabolism," *Cell Death and Differentiation* **10**, 163-174 (2003)

27. I. R. Perch-Nielsen, P. J. Rodrigo, C. A. Alonzo and J. Gluckstad, "Autonomous and 3D real-time multi-beam manipulation in a microfluidic environment," *Opt. Express.* **14**, 12199-12205 (2006)

28. S. C. Chapin, V. Germain and E. R. Dufresne, "Automated trapping, assembly, and sorting with holographic optical tweezers," *Opt Express* **14**, 13095-13100 (2006)

Chapter 4

Photo-transfection of mammalian cells using femtosecond laser pulses: Review and mechanisms

Introduction

In chapters 2 and 3 the exploitation of optical forces using continuous wave laser sources for optical tweezing and cell sorting studies was explored. Pulsed laser sources also promise rapid development of research subjects such as cell nanosurgery and recently laser assisted cell transfection. Therefore, in this chapter and the next two chapters of this thesis, I present work on femtosecond (fs) laser transfection (photo-transfection). Specifically, this chapter starts by a brief review of the use of a pulsed fs laser source in biological experiments with particular emphasis on photo-transfection studies. I explain the biological meaning of cell transfection, detailing the composition of eukaryotic cell membranes, specifically the natural transport mechanisms of biomolecules through the plasma membrane. Thereafter, I review the different methods of cell transfection including chemical methods (cationic polymers and lipids), viral methods and physical methods (microinjection, biolistic particle delivery, electroporation and sonoporation). Next a particular focus is placed on pulsed laser light assisted method of cell transfection, the photo-transfection technique and its mechanisms.

To study the mechanisms for pulsed laser transfection, the concept of laser-induced optical breakdown is described to elucidate the process of free-electron plasma production in a transparent material. Multiphoton ionization responsible for the creation of the free-electron plasma is briefly described. Then, the influence of pulse duration (nanosecond, picosecond and femtosecond pulses) on mechanical effects such as cavitation bubbles and shock wave emission during laser-induced optical breakdown is outlined. An explanation on the self-healing ability of the cell plasma membrane as well as the tension reduction and patch hypotheses is offered. Finally, implications for laser effects on biological cells and tissues are presented.

4.1 Cell transfection

The introduction and subsequent expression of plasma membrane impermeable nucleic acids into eukaryotic cells is known as cell transfection. In essence, cell transfection entails the introduction of the negatively charged deoxyribonucleic acid (DNA) and ribonucleic acid (RNA) into cells which have an overall negatively charged membrane. This gene transfer and cytoplasmic expression technology is a powerful tool for studying gene function in cells and has crucial roles in medicine and biology (1). Typically there are two kinds of cell transfection, namely, transient and stable transfection. The former is for short-term nucleic acid expression, lasting for a few days in cells. Whilst in stable transfection, long-term transfection of cells is achieved with the integration of the transfected DNA into the chromosome of the foreign cell (2). During cell transfection, different approaches have been developed to facilitate uptake of foreign genes and other macromolecules specifically into eukaryotic cells (3).

A typical eukaryotic cell contains a rich array of intracellular organelles with different densities and varying amounts of internal membranes. Notably, these cells encase a nucleus which is also enclosed in a membranous nuclear envelope. The entire region between the nucleus and the outer membrane bounding the cell is known as the cytoplasm. It consists of a semi-fluid medium called the cytosol, a viscous environment where the organelles of specialized form and function are contained. Hence, for successful cell transfection, the desired nucleic acid material to be introduced into the cells is required to first traverse the plasma membrane, the highly viscous cytosol, then the nuclear membrane and finally the nucleoplasm which exceeds the cytosol in viscosity. Prior to discussing the various methodologies employed during cell transfection, the following sections give an outline of eukaryotic cell membranes, the transport of exogenous material therein.

4.1.1 The plasma membrane of eukaryotic cells

In eukaryotic cells the plasma membrane is a boundary responsible for the inward passage of sufficient oxygen and nutrients as well as the outward trafficking of cellular waste. This boundary, that segregates and protects life inside the cell from its outward surrounding environment, is a thin film of roughly 7 – 8 nm (4). Through being selectively permeable i.e. allowing certain substances to cross it more easily than others, the plasma membrane also provides overall regulation of all trafficking of materials in cells. Plasma membranes are referred to as a fluid mosaic of lipids, proteins and carbohydrates, implying that membranes rather than being static, rigidly arranged molecular structures, are flexible structures as they comprise hydrophobic interactions which are characteristically weaker compared to covalent bonds. This therefore means that most lipids and proteins in membranes can drift laterally in a plane.

Of crucial note, membranes must be fluid for their effective functioning. However, a temperature drop in cells gives rise to membrane solidification. Membrane lipid composition dictates the critical temperature at which the membrane starts to solidify, and maintain their fluid status when rich in phospholipids. These are comprised of unsaturated hydrocarbon tails because unsaturated hydrocarbons are structurally arranged more sparsely in comparison to saturated hydrocarbons which naturally pack more closely together. At 37^{o}C, the steroid cholesterol is found wedged among the phospholipids in the plasma membrane of animal cells, thus making the membranes less fluid through restricting phospholipids mobility. Also cholesterol prevents the close arrangement of phospholipids, thereby lowering the temperature required to solidify the membrane, providing membrane fluid stability. Membrane solidification alters membrane permeability resulting in enzymatic protein inactivity within the membrane which can then prevent substance transportations across the membrane. Therefore, as an adjustment to the changing temperature, a cell can alter the lipid composition of its membrane to a certain degree and avoid membrane solidification (5).

Although the plasma membrane composition mainly consists of a lipid bilayer, embedded in the fluid matrix of this lipid bilayer are many different proteins. These proteins determine most of the membrane's specific functions. The plasma membrane as well as all other organelle bounding membranes possesses various kinds of unique proteins. Nonetheless, the two major membrane protein populations are known as the integral and peripheral proteins, with the latter not embedded in the lipid bilayer but rather appearing as appendages attached to the intracellular surface of the membrane. Integral proteins on the other hand penetrate through the membrane with their hydrophobic regions surrounded by the hydrocarbon tails of the membrane lipids. In addition to membrane proteins, the plasma membrane also has carbohydrates normally restricted to its extracellular portion and responsible for cell-cell recognition. Usually the membrane carbohydrates are branched oligosaccharide i.e. short chains with fewer than 15 sugar units. In cases where oligosaccharides are covalently bonded to lipids they are referred to as glycolipids, some however, form a covalent bond with membrane proteins and are called glycoproteins (5). Depicted in figure 4.1 is a detailed cross section of the plasma membrane.

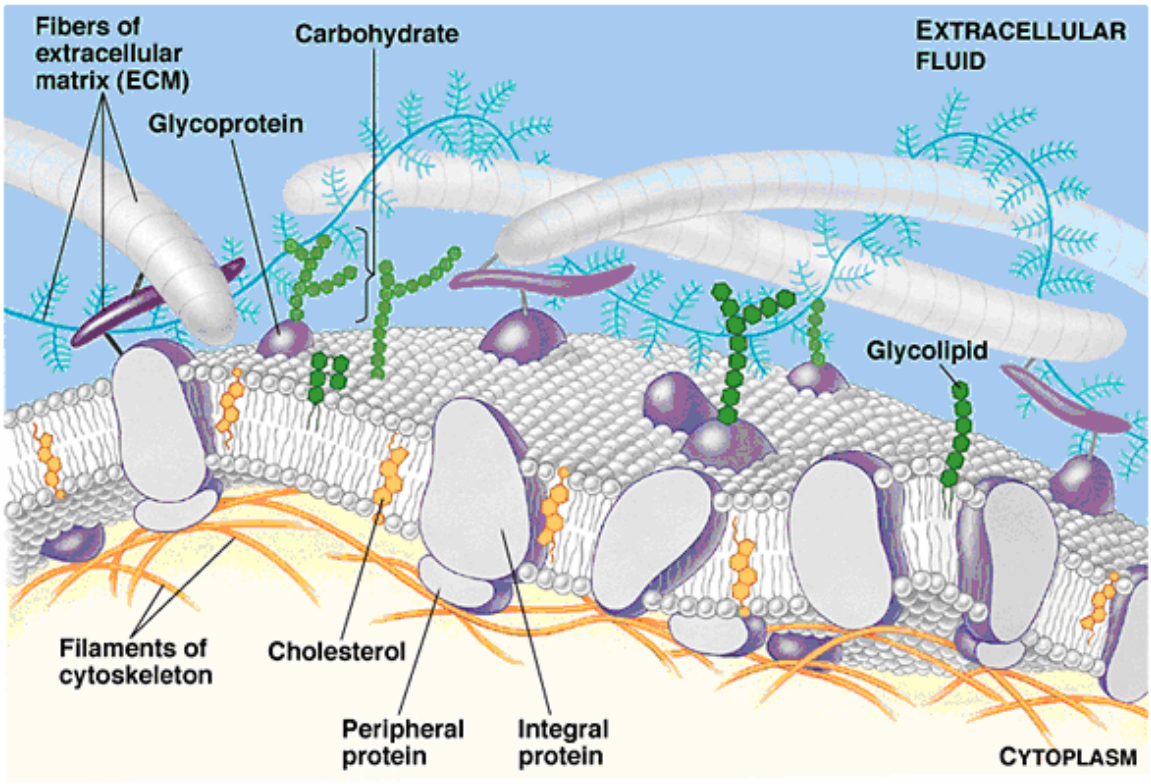

Figure 4.1: Mosaic properties of the cell membrane. A phospholipids bilayer constitutes a typical structure of animal cell membranes. With the hydrophobic fatty acids acyl tails of the phospholipids formulating the middle of the bilayer and the polar hydrophilic heads of the phospholipids expressed on either side of the membrane surface. Integral proteins are embedded in the lipid bilayer but the peripheral proteins are primarily associated with the membrane via specific protein-protein interactions. Oligosaccharides bind mainly to membrane proteins (glycoproteins), some however are found binding to the lipids to form glycolipids (online access date - 12.12.09 (6)).

The cell membrane therefore is comprised of a symmetrical assembly of proteins, lipids, glycolipids and glycoproteins which are constructed by the endoplasmic reticulum and Golgi bodies/apparatus of the cell.

4.1.2 Biomolecular transport across the cell membrane

The hydrophobic core (phospholipids tails) of the membrane hinders passage of hydrophilic ions and polar molecules. Nonetheless, hydrophobic molecules such as hydrocarbons and oxygen can freely traverse through this section of the plasma membrane. Also, small polar, uncharged molecules such as water and carbon dioxide rapidly pass through the membrane. The lipid bilayer is impermeable to larger, uncharged polar molecules (e.g. sugars such as glucose), charged atoms or molecules and even small ions such as H^+ and Na^+. The proteins embedded into the membrane play a key role in governing trafficking across the cell membrane. For instance, hydrophilic substances evade contact with the lipid bilayer by passing through transport proteins that are diversely placed along the membrane. Figure 4.2 displays a situation where integral transport proteins within the lipid bilayer membrane possess a channel which hydrophilic molecules use as a hydrophilic tunnel through the membrane.

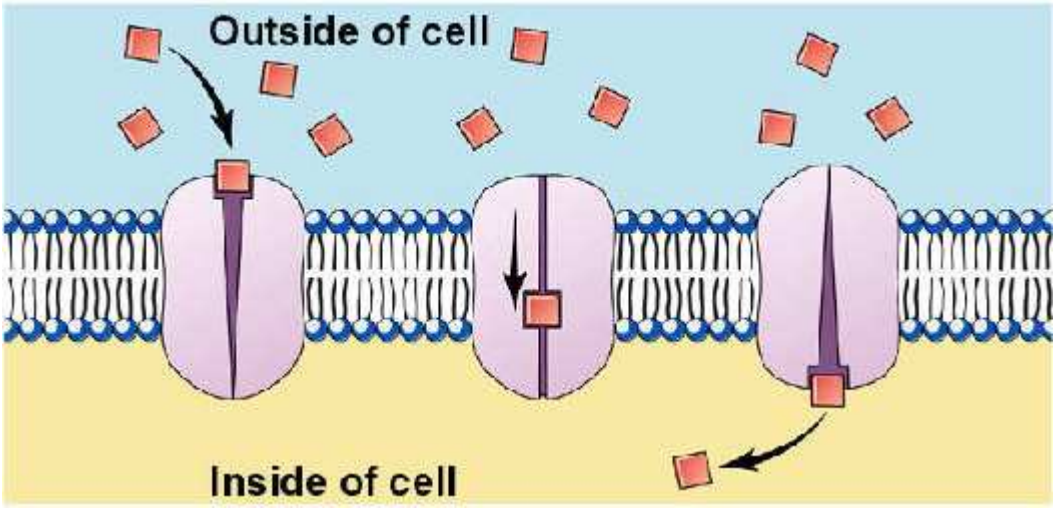

Figure 4.2: Illustrates selective trafficking of hydrophilic molecules (down the concentration gradient) from the outside of the cell through a channel that functions as a hydrophilic passageway thereby permitting intracellular placement of these molecules (online access date - 12.12.09 (7)).

Other transport proteins bind to the molecules in order to physically move them across the membrane this mode of membrane protein transportation is shown in figure 4.3 below.

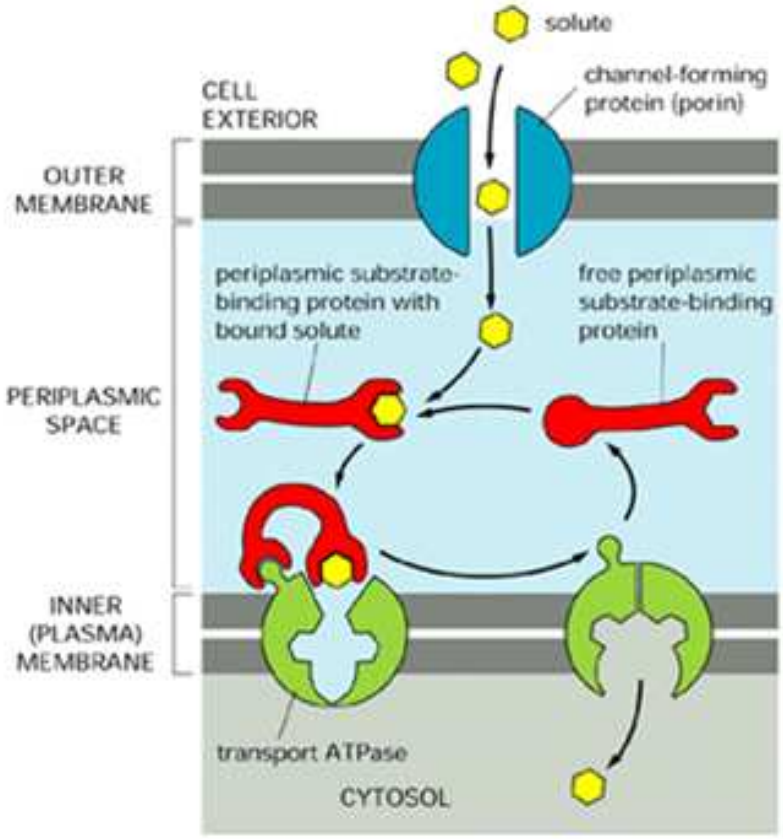

Figure 4.3: Solutes transported from the outer membrane of the lipid bilayer membrane via a periplasmic substrate-binding protein into the inner plasma membrane compartment of the plasma membrane and then eventually into the cytosol (online access date - 12.12.09 (8)).

In any of the two transport cases reported above, transport proteins are very specific for the substances they translocate, selectively permitting transportation of only certain molecules and/or class of closely related molecules. Therefore, the native selective permeability of a membrane depends on both the discriminating barrier of the lipid bilayer and the specific transport proteins embedded into the membrane. Recently, the idea of cell transfection has promoted research studies leading to the introduction of a

wealth of other exogenous material within cells. For example, the incorporation of a wide selection of potentially therapeutic agents including proteins, oligonucleotides (9), drugs such as bleomycin and cisplatin (10) has had critical applications in clinical trials studies among other things. On the other hand, cellular inclusion of biological dyes, chromophores and fluorescent markers which exhibit site specific expression in organelles and subcellular compartments is essential for cellular and/or organelle imaging, studying discrete organelles and a variety of other intracellular investigations.

Since the cell plasma membrane possesses limited permeability to all sorts of exogenous substances, these therefore fail to be naturally transported into the cell unless the membrane integrity is somehow disrupted. Nucleic acids such as DNA, mRNA and viability dyes such as trypan blue cannot be naturally transported into the cell via the previously mentioned membrane embedded proteins. These substances are all reported to be negatively charged and are physically large; i.e. trypan blue (molecular weight = 906.80524 $g.mol^{-1}$), DNA (~3.5 kb) and mRNA (~1.7 – 1.9 kb (11)). Because of the presence of anionic phosphatidylserine (PS) phospholipids found bound in the cytosolic leaflet of the cell plasma membrane (12), the cell membrane is negatively charged (13). For these reasons, different techniques have been successfully employed for assisted delivery of both cell transfection foreign genetic materials as well as a wide range of other exogenous matter.

4.2 Different modes of cell transfection

In chapter 5 of this thesis I present laboratory data involving cellular expression of trypan blue, DNA and mRNA within different kinds of mammalian cells. But before this, the various modes of cell transfection and translocation (introduction of biological stains and other non-genetic materials) methodologies are discussed in the following section.

4.2.1 Chemical reagents – cationic polymers

DEAE-dextran was one of the first chemical reagents used for the transfer of nucleic acids into cultured mammalian cells (14). DEAE-dextran is a cationic polymer that tightly associates with negatively charged nucleic acids. An excess of positive charge, contributed by the polymer in the DNA-polymer complex, allows the complex to come into closer association with the negatively charged cell membrane. Uptake of the complex is thought to be facilitated by endocytosis. Other synthetic cationic polymers have been used for the introduction of DNA into cells, including polybrene (15), polyethyleneimine (16) and dendrimers (17).

Then, in the early 1970s, calcium phosphate co-precipitation became a popular transfection technique (18). The protocol of calcium phosphate precipitation involves mixing DNA with calcium chloride, carefully adding this in a buffered saline phosphate (PBS) and allowing the mixture to incubate at room temperature. The controlled mixing generates a precipitate that is then dispersed onto the cultured cells. Here as well, the precipitate is engulfed by endocytosis into the cells and this method has been used for both transient and stable transfection procedures.

While inexpensive, both chemical transfer methods provide high (80 – 90 %) cell transfection efficiency. However, these reagents are toxic, (especially DEAE-dextran), and as a result are not suited for *in vivo* gene transfer to whole animals.

4.2.2 Cationic lipids

In 1980, artificial liposomes became the method of choice for delivering DNA into cells (19). In this case, the cationic head group of the lipid compound associates with the negatively charged phosphates on the nucleic acid. This association leads to a compaction of the nucleic acid in a liposome-nucleic acid complex, presumably from electrostatic interactions between the negatively charged nucleic acid and the positively charged head group of the synthetic lipid. Entry of this complex into the cell occurs either via endocytosis or fusion with the plasma membrane (20). Following cellular internalisation the complexes appear in the endosomes and later in the nucleus (figure 4.4).

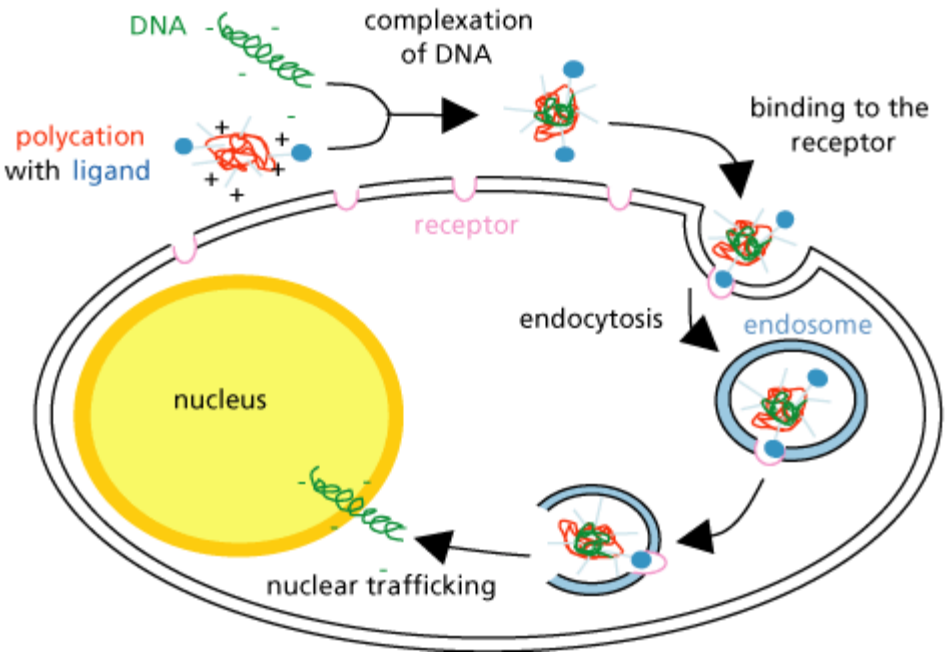

Figure 4.4 Herein a polycation with ligand complexes with a negatively charged DNA molecule. On association with the cell membrane, the complex binds onto specific receptors forming an endosome. Inside the cell the endosome is digested, resulting in the release of the contained DNA which then continues to traverse the nuclear membrane into the nucleoplasm (online access date - 14.10.09 (21)).

An overall net positive charge of the liposome-nucleic acid complex, results in a high transfection efficiency since close association of the complex with the negatively charged plasma membrane is achieved. In addition, liposome mediated delivery offers advantages such as the ability to transfect certain cell types that are resistant to calcium phosphate or DEAE-dextran, the successful delivery of RNA (11) and proteins (22). In addition, both transient and stable transfection can be performed through use of cationic lipids.

On the other hand, cationic polymers and lipids interact with the negatively charged DNA through electrostatic interactions resulting in polyplexes and lipoplexes successively. While these vectors have a low immunogenic response, the possibility of selected modifications and the capacity to carry inserts as large as 52 kilobases. Their employment *in vivo* requires systemic administration which has been reported to escalate in a toxic

response and would therefore be incompatible with clinical applications (23).

4.2.3 Viral methods

The use of viruses as possible vectors for the delivery of foreign genes into cells has also been explored. For example adenoviral vectors possess numerous key features that make them attractive for gene transfer purposes, they can rapidly infect a broad selection of human cells and achieve high levels of gene transfer; they can accommodate relatively large DNA (~7.5 kb) species and transduce these transgenes in non-proliferating cells; in addition, adenoviral vectors can be easily manipulated via recombinant DNA techniques (24). Consequently, viral vectors possess strong gene transfection features on mammalian cells, yet contrarily, adenoviral vectors have a low packaging capacity and their production is labour intensive (24). Also, the employment of these vectors comes with the risk for the potential activation of latent diseases (24), as well as a random recombination or immunogenicity (25).

4.2.4 Physical methods

Physical approaches for gene transfer were developed and used as of the early 1980s. Although making use of a fine needle to directly microinject cultured cells or their respective nuclei is an effective technique for the delivery of nucleic acids, it is also reported to be laborious (26). This method has been used to transfer DNA into embryonic stem cells that are used to produce transgenic organisms (27) and for introducing antisense RNA into C. elegans (28). The draw back of this methodology however, is that it is expensive and tedious, and is only applicable for studies requiring transfection of a few number of cells. An illustration of DNA microinjection into a mouse zygote is presented in figure 4.5 below.

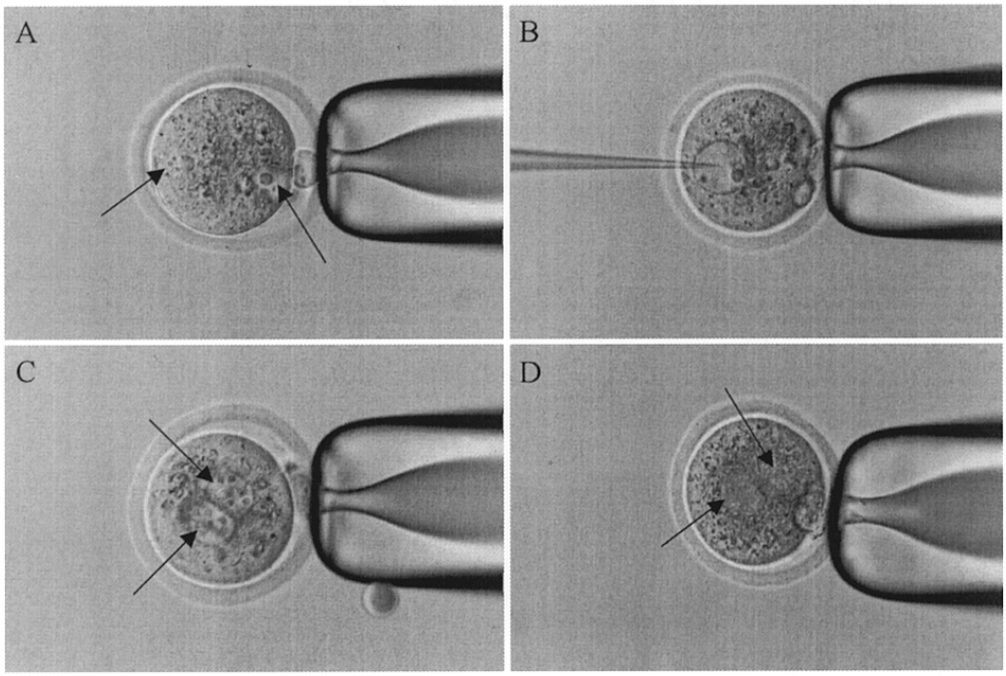

Figure 4.5: (A &C) pronuclei (arrows) developing in a mouse zygote approximately 20 and 26 hrs after injection with the human chorionic gonadotopin (hCG) to enhance super-ovulation. Image (B) displays microinjection with the fine needle shown in the left side of the image. And image (D) showing the pronuclei as they start to disappear (reprint by permission from *Experimental Physiology* (29)).

Another physical method for gene delivery is ballistic particle delivery also known as particle bombardment using a device called the gene gun. This method relies upon high velocity delivery of nucleic acids on micro-projectiles to recipient cells by membrane penetration (30). This method has been successfully employed to deliver nucleic acids to cultured cells as well as to cells *in vivo* (31-33). Ballistic particle delivery is relatively costly but the technology has also been used for genetic vaccination and agricultural applications (figure 4.6).

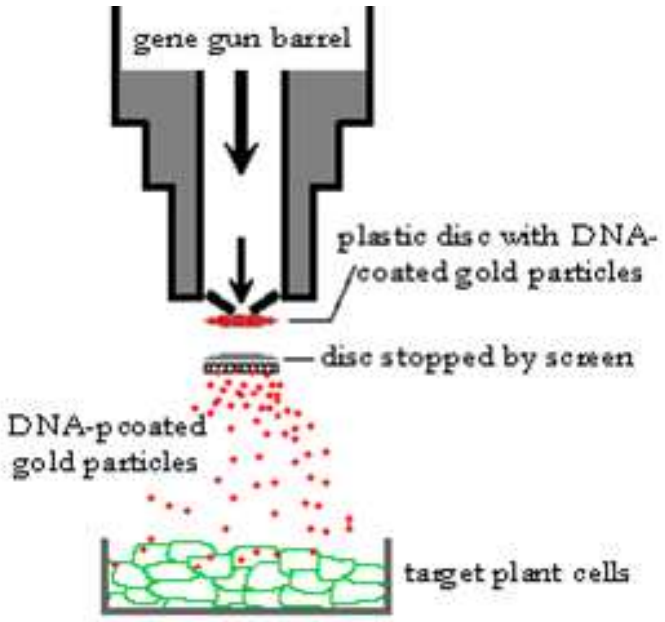

Figure 4.6: In this example, the plasmid DNA-coated gold particles are desiccated onto a plastic membrane and placed on a holder roughly 5 cm above the plant tissue within the chamber of the micro-particle gun. Once a predetermined pressure is reached, the gas is released and the disc is projected against a screen which then stops the plastic disc, but allowing only the gold particles to be released into the targeted plant cells. Upon their penetration into the cell wall, these particles then perform intracellular delivery of the plasmid DNA thereby transfecting the cells (online access date - 13.12.09 (34)).

Electroporation which was first reported for gene transfer studies into mouse cells (35), has been mostly applied in cell types such as plant protoplasts that are difficult to transfect via other means. The mechanism is based upon perturbing the cell membrane by an electrical pulse which forms transient pores that allow the intracellular passage of nucleic acids (36). The method requires fine-tuning and optimization for the duration and strength of the pulse for each type of cell used. Also, electroporation often requires more cells than chemical methods because of substantial cell death, and extensive optimization is often required to delicately balance transfection efficiency against cell viability.

Ultrasound can also be used for the introduction of genetic materials into cells: this procedure is called sonoporation. This technology utilizes the acoustic piercing of micro-bubbles to facilitate the delivery of DNA molecules (37).

As in the case of electroporation, when using this sonoporation technique cell viability must be accounted for. For instance, Yuan, 2008 reported on the advantages of some of the physical approaches used for gene therapy, drug submission and their potential application on vaccine administration. The report also states that sonoporation on chick embryos is superior to electroporation, with the latter presenting risks of lethal damages (38). Figure 4.7 depicts the electroporation as well as sonoporation transfection techniques.

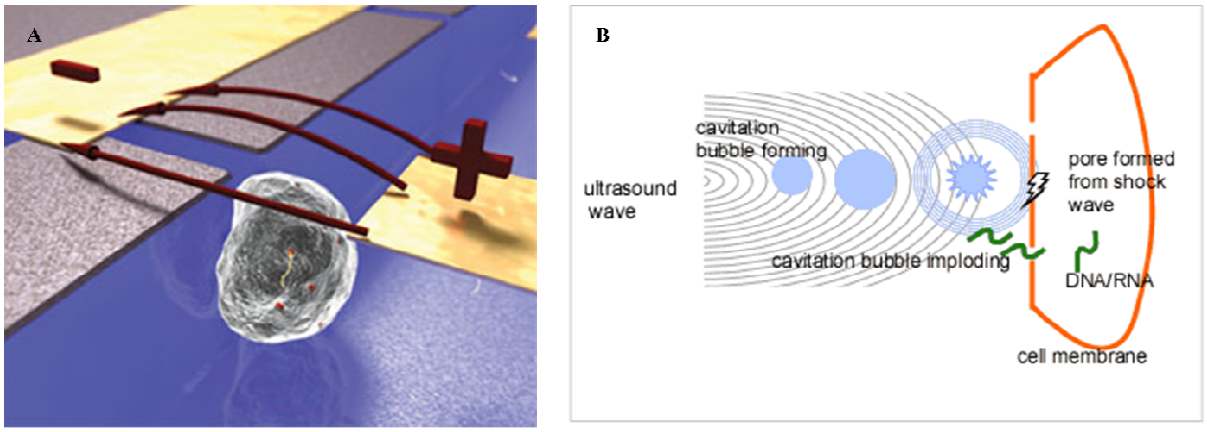

Figure 4.7: Image (A) is an illustration of an electric pulse used to create pores in a single cell that is held in a microfluidic device (reprint by permission from *Lab on a Chip* (39)). The picture in (B) shows how a tiny bubble may form and then produce a shock wave that generates pores on the cell membrane to permit entrance of genetic material into a cell (online access date - 10.12.09 (40)).

Overall each of the previously mentioned delivery systems for cell transfection features limitations and draw backs. In *in vitro* as well as *in vivo* procedures, gene, drug and/or vaccine delivery schemes possessing minimum cytotoxicity and an immunogenic response that can be applied under sterile tissue culture protocols and can offer targeted treatment of a large number of individual cells, organelles and organs among other things is highly desirable. Optical cell transfection or photo-transfection (as it is called in this thesis) using laser light satisfies these criteria.

Additional benefits are that optical transfection setups can be easily integrated with other optical techniques such as confocal laser scanning microscopy and optical tweezers systems (41, 42). For example it has been recently shown that gold nanoparticles can be optically tweezed to a desired location and subsequently introduced into mammalian cells by such photo-transfection (42). Optical transfection of mammalian cells via an axicon tipped optical fibre has also been demonstrated, thus opening the future prospect of coupling this photo-transfection methodology with endoscopes for *in vivo* applications (43).

Since the conception of photo-transfection by Tsukakoshi *et al*, 1984 (44), lasers of different wavelengths and type, ranging from CW visible sources (45-49) to pulsed infra-red (44, 50-52) sources have been widely utilised for successful introduction and expression of genetic materials into mammalian cells. CW laser transfection experiments have been mostly performed in the near UV regions of the light spectrum and this approach leads to ablative effects as a result of heating and linear photon absorption. Although diode lasers at near UV wavelengths have previously been a popular choice as they are cheap and compact, during cell transfection CW membrane perforations require considerably high irradiations which result in temperature increase at the site of irradiation. This therefore gives rise to collateral damage that is linked to compromised cell viability and consequently a high level of cell death.

In pulsed laser sources, initial cell transfection experiments involved nanosecond (ns) pulses and as compared to CW sources they provide membrane perforation at lower irradiances (44, 53, 54). The disadvantage here however is that the interaction of ns pulses with the plasma membrane has been associated with mechanical effects such as shock waves and cavitation bubbles. These can cause permanent damage at the area of interaction and collateral damage due to the linear nature of the photon absorption at the targeted region. Nonetheless, induced mechanical effects are decreased with shorter pulse durations such as picosecond (ps) and femtosecond (fs) pulses as these required much lower irradiances for membrane perforation. Optical transfection with ps pulses (55) involves plasma membrane perforation with induced mechanical effects that are milder

compared to that obtained with ns pulses. There is therefore less heating and collateral damage in this case.

The most commonly used laser source in the area of photo-transfection is the fs laser since it emits extremely short pulses and has a broad spectral range in the near infrared regime extending within the 700 – 1000 nm region. When focussed to a diffraction limited spot, fs pulses possess high peak powers and sufficient photon density to trigger non-linear effects such as multiphoton absorption of photons confined at the laser beam focus. Therefore employment of fs laser pulses for photo-transfection, offers a high degree of spatial confinement of the deposited pulses leading to precise local disruptive effects at the targeted area and very minimum collateral damage. First reported by Tirlapur *et al*, 2002 (52), fs lasers have revolutionized laser assisted cell transfection. During their experiments, a mode locked titanium sapphire laser with 100 fs pulse duration and 80 MHz repetition frequency was used to photo-transfect CHO and rat-kangaroo epithelial cells with plasmid DNA encoding the green fluorescent protein gene (52). Interaction of this tightly focussed beam with the plasma membrane of cells permitted transient membrane permeabilization and subsequent diffusion of the exogenous plasmid DNA into the cytoplasm of the cells. A number of mammalian cell lines have since been transfected using fs pulses as they do not compromise cell viability, cause minimum collateral damage and appear to be the most biologically safe mode of cell transfection.

Transient permeabilisation and subsequent introduction of both genetic and non-genetic species into mammalian cells without concomitant cytotoxicity is achieved through the exploitation of laser light. In the next section I elucidate the mechanisms responsible for this photo-transfection procedure briefly describing utilization of nanosecond versus picosecond and versus femtosecond laser pulses.

4.3 Mechanisms of femtosecond laser transfection

4.3.1 Laser-induced optical breakdown

In the literature, a wealth of information on the physical aspects governing pulsed laser-matter interaction exists. Tight focussing of laser pulses to high peak intensities onto transparent media (cells or water), leads to the production of a free-electron plasma in the medium through multiphoton or single photon processes, depending on the laser parameters. This all occurs via a process called laser-induced optical breakdown. In the theoretical model of optical breakdown described by Vogel *et al*, 2005 (56) and Sacchi *et al*, 1991 (57), the water model was treated as an amorphous semiconductor of bandgap energy Eg = 6.5 eV. The meaning of the term "free-electron" plasma, which usually describes ionization in gases, is utilized here as the abbreviated form of "quasi free" electrons which upon ionization travel from the valence to the conduction band of the water molecule.

In both solid and liquid materials the effects of optical breakdown have been well characterized. In liquids, this laser-induced optical breakdown is mainly of interest for both biological and medical applications. Also in liquids, depending on laser pulse duration, laser-induced optical breakdown amounts to the creation of both shock wave emission as well as cavitation bubbles. For example, free-electron plasma formation due to ns optical breakdown in water results in mechanical effects including the generation of intense shock waves and cavitation bubbles which contain the vaporized matter. These cavitation bubbles oscillate and subsequently collapse due to hydrostatic pressure resulting in the damage of the targeted material. But compared to ns pulses with longer pulse duration, for shorter pulses such as ps pulses, the required intensity threshold is reduced as the peak power is increased leading to minimum collateral damage in the breakdown region. Additionally, fs laser pulses have the ability to localize cellular disruption to sub-micron regimes, the low threshold energy required for cellular ablation and a lower conversion of energy into shockwaves and cavitation bubbles which lead to adverse consequences for enhancement of spatial extent of cellular damage (56, 58).

Consequently, use of fs pulses with ultra-short duration and a high repetition rate produces ultra-fine effects in the irradiated region with a high spatial resolution. For this reason, pulsed fs lasers have become the apparatus of choice for an array of precision dependent applications. These include, laser nanosurgery (whole cells as well as their subcellular organelles) and most importantly in this thesis, photo-transfection.

4.3.2 Plasma formation in transparent materials

Visible light allowed to pass through substances such as glass or water, often undergoes scattering, reflection, refraction and even absorption. In these cases the light-matter interaction seldom results in material breakdown or meltdown. This is due to the fact that ordinary light intensities possess insufficient energy to ionize any material they pass through. Nonetheless, light intensities around 10^3 W/cm^2 as is the case for fs pulses, possess sufficient photon density leading to a high possibility of multiple photons interacting with the same molecule simultaneously. It is this cooperative behaviour of multiple photons that can give rise to material ionization. The mechanisms reported to cause the production of free-electron plasma through laser-mediated optical breakdown in transparent media involve multiphoton ionization as well as avalanche ionization (cascade or impact ionization).

In multiphoton ionization, an unexcited electron simultaneously absorbs the energy of several photons (figure 4.8), so that the combined energy of these photons is sufficient to boost the electron to an excited state or may free the electron to form electron-ion plasma. Since overcoming the energy gaps in transparent materials require multiple photons, the possibility of ionization depends on incident light laser intensity to a power equivalent to the number of photons. This multiphoton ionization process requires that the photon density is high enough that the probability of absorbing multiple photons at one time is non-negligible but achievable. For example, according to Fan *et al*, 2001 (59) a plasma of order $10^{18} – 10^{20}$ electrons/cm^3 must be produced.

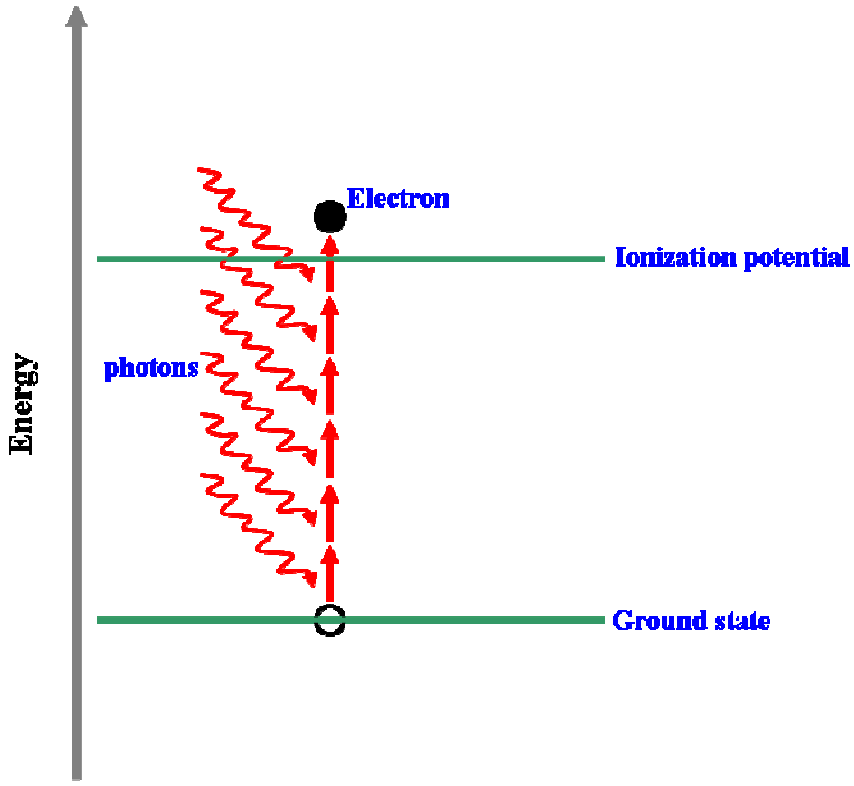

Figure 4.8: Schematic representation of the multiphoton ionization process. When the energy required for an atom or molecule to be ionized is greater than that of the incident photons, then there is a probability that multiple photons will be simultaneously absorbed and cause the transport of an electron from the ground to an excited state. This may occur provided the incident laser field is extremely intense, as is the case with ultra-short laser pulses. This multiphoton excitation phenomenon takes place when intense laser irradiation interacts with matter (60).

In summary, during laser ablation newly generated electrons transfer energy to the ions and this energy heats the material leading to vaporization in the interaction volume (multiphoton ionization). This multiphoton ionization depends on the laser intensity in the interaction volume, and requires minimum threshold intensity prior to breakdown initiation. Usually, effective material ablation is achieved when the incident laser irradiance exceeds the material breakdown threshold. The threshold relies on the ionization potential (the bandgap) of the material, the pulse duration and wavelength of the incident laser pulse (59). In the next section I discuss the mechanical effects attributed

to laser pulse duration post laser-induced optical breakdown.

4.3.3 Description of femtosecond optical breakdown in transparent media

Distilled water has been employed in most theoretical and experimental models for the investigation of laser optical breakdown; this is because water is the primary constituent of most biological materials. When laser pulses of high intensities are focused into a transparent material or medium (water, soft tissue, bone, dental material at 1 µm depths), there is the formation of laser-induced optical breakdown, amounting to the creation of both shock wave emission as well as cavitation bubbles. Generally, shock waves do not lead to morphological damage but, according to *in vitro* experimental reports shock waves can alter cell membrane permeability (61), influence cell viability (61, 62) and can cause fracturing of DNA strands (62). However, major tissue displacement and compromise resulting from cavitation bubbles has been identified as the main source of collateral damage in nanosecond photo-disruption (63).

However, the use of shorter laser pulses (e.g. fs pulses) can dramatically reduce the undesired side-effects associated with laser-induced optical breakdown. Noack *et al*, 1998 (64) presented the reason behind this observation to be associated to the fact that, pulse energy necessary for optical breakdown decreases with decreasing pulse duration. In this report, they further demonstrated the mechanical effects of the laser pulse duration post laser-induced breakdown. On using a pulse energy equivalent to a sixfold breakdown threshold during all their experiments, they reported a ~ 4 % energy transmission for the 76 ns pulse whereas ~ 52 % and ~ 59 % energy transmission was measured for the 60 ps and 300 fs pulses respectively. Meaning that for shorter pulse durations (i.e. 60 ps and 300 fs), a higher fraction of the energy is transmitted. Hence, for these shorter pulses a larger fraction of pulse energy is required to evaporate the focal volume, as a result less energy is available for mechanical processes (64). Figure 4.9 shows the cavitation bubble images obtained post laser-induced optical breakdown in high purity distilled water for laser pulses of different duration. These cavitation bubbles were reported to range in radius from 2.5 mm (76 ns pulses) to less than 50 µm (100 fs

pulses); this size reduction was attributed to the small amount of energy deposited into the focal volume of the shorter pulses. For the longer nanosecond pulses, roughly one fifth (~ 20 %) of the deposited laser pulse energy is reported to result in the creation of the cavitation bubble whereas only 6.5 % of the pulse energy gets converted to mechanical energy of the cavitation bubble amounting from the 100 fs pulses (64).

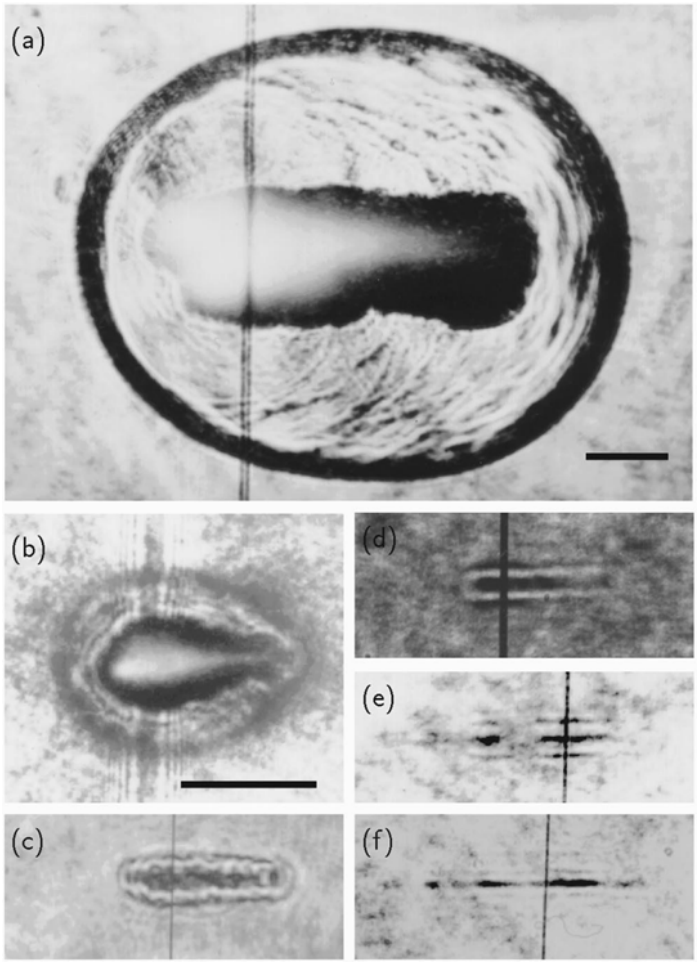

Figure 4.9: Illustrates the breakdown regions obtained via exposure of high purity distilled water to 76 ns (a), 6 ns (b), 60 ps (c), 3 ps (d), 300 fs (e) and 100 fs (f) pulses. The laser pulses possessed an energy corresponding to a sixfold breakdown threshold and were incident from the left hand side. The vertical lines across each image represent the position of the streak slit. The length of the scale was 100 µm for images (a) and (b) the rest of the images (b-f) are reported to be of equal magnification (reprint by permission from *Journal of Applied Physics* (64)).

Subsequent to laser optical breakdown, shock wave emission streak images corresponding to the different pulse durations presented in figure 4.9 were captured and these are shown in figure 4.10.

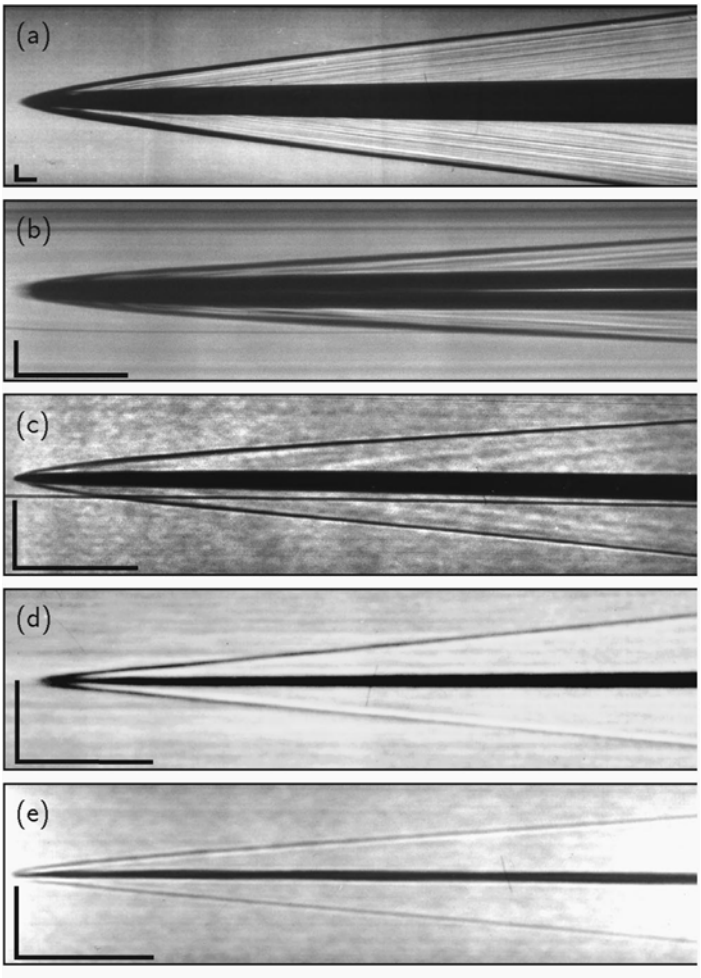

Figure 4.10: Streak image profiles of shock wave emission post laser-induced optical breakdown with pulse durations: 76 ns, 6 ns, 60 ps, 3 ps, and 300 fs corresponding to images a-e successively. In the case of the 100 fs pulses, a shock wave with poor contrast was produced thus no usable streak image could be captured. The plasma appeared as the dark central object with the two inclined dark lines above and below it indicating the outward propagation of the shock wave. The bars are scaled horizontally at 10 ns and vertically at 100 µm for each image (reprint by permission from *Journal of Applied Physics* (64)).

This data revealed that for nanosecond pulses, the shock pressures were almost double the size of those arising from the picosecond and femtosecond pulses. At sixfold threshold, the shock pressure was noted to closely follow the trend observed in the energy transmission for the different pulse durations. It is reported that with longer pulses (ns) roughly the entire pulse energy is deposited during laser induced optical breakdown. Therefore, the energy density of the resultant plasmas is very large leading to high shock pressures. On the contrary, ps and fs pulses with increased transmission, create a drastic reduction in the energy density and thus, plasmas with reduced shock pressures (64).

During laser-induced optical breakdown, significant reduction of mechanical effects such as cavitation bubbles and shock wave emission is achievable via the employment of shorter laser pulse durations. This is mostly because the threshold energy and consequently the energy available for mechanical effects are decreased for shorter laser pulses. Notably the incident pulse energy divided into transmission energy, cavitation bubble energy, shock wave energy and heat of vaporization energy, changes with decreasing pulse duration. For the longer pulses a large portion of the incident energy results into mechanical effects whilst for the shorter pulses the incident pulse energy leads mainly to the transmitted energy and heat of vaporization energy. Hence, the photo-transfection studies reported upon in chapter 5 of this thesis involves investigations using a pulsed fs laser source.

4.3.4 Membrane repair and restoration: tension reduction and the patch hypotheses

During photo-transfection experiments, plasma membrane perforation is an essential step to achieving successful cytosolic delivery of exogenous materials into mammalian cells. The question on how the cell membrane restores through the self healing process after induced permeabilization, is as crucial to answer as that on how the micro-pores are created. Literature report by McNeil *et al*, 2003 (65) presents studies on rapid repairing and resealing of plasma membrane disruption following both physiological and induced cell membrane wounding in different cell types. They report membrane resealing as an active and intricate process involving the endomembrane (intracellular membrane)

alongside both cytoskeletal and membrane fusion proteins. Where through a Ca^{2+} elicited response to plasma membrane injury and via exocytosis, the endomembrane gets deposited to the site of disruption to initiate the membrane self-healing process. Extracellular Ca^{2+} ions migrating through the membrane lesion have been reported to promote a vesicle-vesicle and vesicle-plasma-membrane fusion response (66, 67). Further, in nucleated cells the endomembrane has been said to play a critical role in rapid resealing of disrupted plasma membrane post wound infliction using a mode locked titanium sapphire laser (67).

McNeil *et al*, 2003 (65) provide evidence supporting the hypothesis that in eukaryotes; cytoplasmic vesicle-plasma membrane (i.e. Ca^{2+}-dependent exocytosis) fusion events are responsible for cell membrane repair mechanisms. They used two related hypotheses namely, tension reduction and patch formation to clarify how this rapid Ca^{2+} driven resealing procedure is achieved. In brief, the tension reduction hypothesis is supported by findings which suggest that, cell membrane wound resealing is promoted by a reduction in the membrane tension. In this instance, although the mechanism is not yet clear, exocytosis occurring at the membrane injury location is reported to be followed by a decrease in membrane tension. On the other hand, the patch hypothesis comes into play in cases where cells experience membrane disruptions of more than 1000 μm^2 size scale. Damages of this size range are reported to be survived by numerous cell kinds, whereby membrane restoration demands the replacement of an entire plasma membrane segment (65). It has been reported that the newly produced membrane which gives rise to the resultant patch is formed through a massive homotypic fusion responses (68). According to Steinhardt *et al*, 1994 (69) compared to the exocytosis-reliant membrane repair system, these fusion reactions possess a higher Ca^{2+} threshold.

Considering plasma membrane disruption repair and restoration mechanisms mentioned above, it is worth noting that plasma membrane perforations induced by fs laser pulses are of a submicron size range. Therefore, the membrane resealing mechanisms post fs photo-transfection might be an energy-intensive process requiring Ca^{2+} and intracellular vesicles. However, the resealing procedure in fs photo-transfection might not necessarily

involve formation of the membrane patch. For example, Schlicher *et al*, 2006 (70), reported that ultrasound-mediated uptake of molecules (proteins and other macromolecules) into cells via plasma membrane wounds of up to micron dimensions, are repaired within minutes by vesicle exocytosis during a Ca^{2+} rich process. Even though the response to plasma membrane permeabilization has been briefly covered in this chapter, numerous questions of particularly what happens at the molecular level during the cell self sealing process, still remain unclear. Of additional interest would be future studies on long-term changes regarding for example gene expression, in cells surviving fs induced laser perforation.

4.3.5 Implications for laser effects on biological cells and tissue

Numerous publications on the mechanisms behind the fs pulse ablation between high and low (i.e. 80 MHz vs. 1 kHz) laser oscillation repetition rates are available for fs pulse-cell interactions. This is due to the overall usefulness together with the applicability of fs laser pulses in nanosurgery to both mammalian and plant cell transfection investigations. Based on the comparison of the physical effects linked to fs laser-induced plasma formation elucidated in the previous sub-sections, it is worthwhile at this point to consider the mechanisms for both the 80 MHz and 1 kHz treatment regimes in biological materials.

In the case of 80 MHz ablation with long pulse series from fs oscillators, the pulse energy is below the threshold energy for optical breakdown with each pulse producing low density plasma. In this regime roughly $10^4 – 10^6$ pulses simultaneously interact with one specific location on the sample of interest to achieve the desired dissection or membrane permeabilization. This manner of ablation, particularly in biological material, occurs via the interaction of multiple pulses through free-electron induced chemical decomposition of the material by bond-breaking. Whereas, low repetition rates such as 1 kHz of the amplified pulse series for example, have pulse energies slightly above the threshold for transient bubble formation. In this instance, the number of pulses delivered at any one location ranges between 30 and several hundreds pulses.

Also, in this case, large plasma densities are created resulting in the formation of minute cavitation bubbles. Such cavitation bubbles have been reported to be cytotoxic and are responsible for the dissection of the biological material (71). In Figure 4.11 is shown a summary of the different low-density plasma effects and aspects of physical breakdown, alongside experimental damage, transfection and dissection thresholds on mammalian cells is presented.

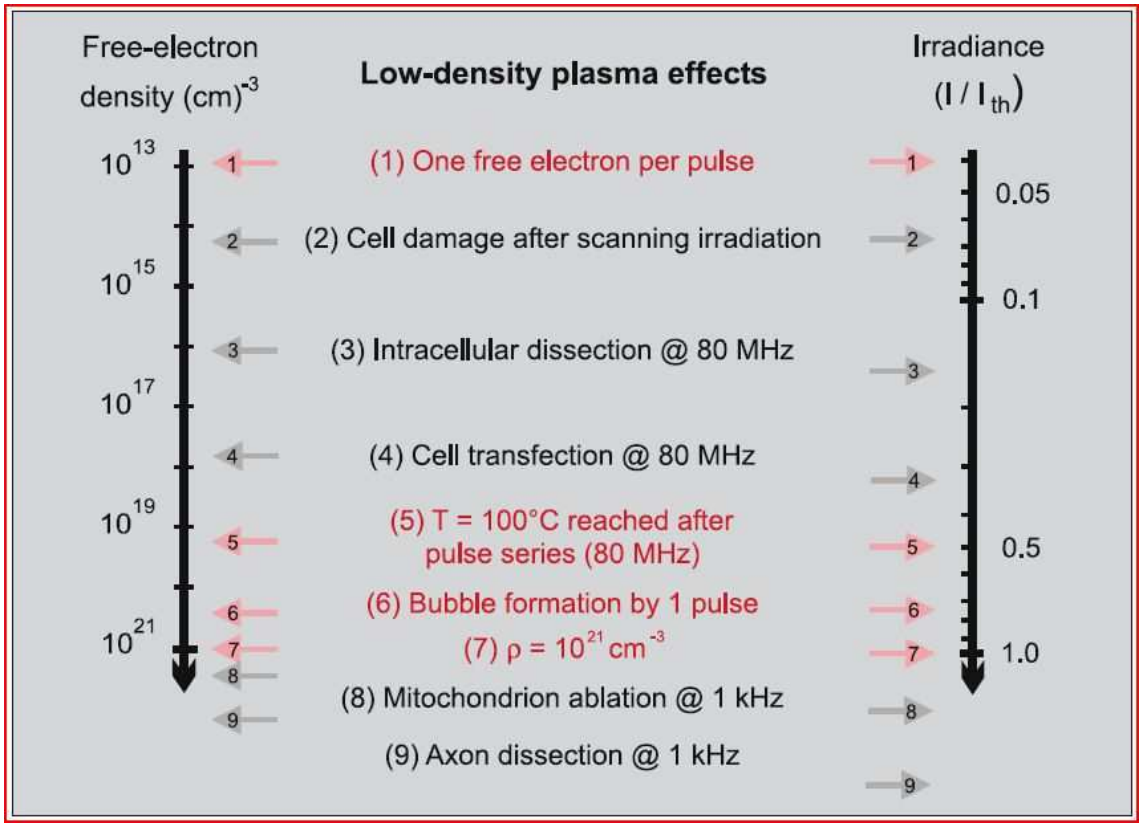

Figure 4.11: An overview of physical optical breakdown observations from fs laser pulses, the different effects are scaled by corresponding values of free-electron density and irradiance (standardized to the optical breakdown threshold I_{th} decreasing by a critical electron density of $\rho_{cr} = 10^{21}$ cm^{-3}. In the figure numbers (1), (5), (6) and (7) represent physical events or threshold criteria. (2), post scanning irradiation with 800 nm at 80 MHz, PtK2 cells were observed to possess membrane dysfunction and DNA strand breaks leading to apoptosis like cell death. (3) and (4) represents intracellular chromosome dissection and cell transfection through membrane permeabilization both performed via 80 MHz pulses from a fs oscillator respectively. (8), is the ablation of a single mitochondrion in a living cell using 1 kHz pulses. Finally (9), refers to axotomy in live *C. elegans* worms performed with 1 kHz pulses of a regenerative amplifier (reprint by permission from *Applied Physics B* (56)).

Finally, fs laser pulses win favour in photo-transfection and other biological studies due to their ability to localize cellular disruption to sub-micron resolutions, plus the threshold energies necessary for ablation are very low. Thus a lower conversion of energy into detrimental effects such as shockwaves and cavitation bubbles is kept at a minimum. In the next chapter, fs pulses focused to a diffraction limited spot using a 60 X microscope objective lens (NA, 0.8) at 80 MHz, 790 nm, 200 fs pulse duration and energy levels of ~ 0.76 nJ (peak power = 3.75 kW) are used for photo-transfection.

Notably, during my photo-transfection experiments, the bubbles observed under brightfield imaging indicates a cytotoxic dosage of cells. These bubbles were caused by the high tuning of the laser irradiance and/or intensity and the cavitation bubbles associated with the shockwave generation and cavitation of vaporized material studied by Vogel *et al*, 2005 (56) have no relation to those bubbles I observed in my experiments which were due to accumulative thermal effects. In addition, the observation of these bubbles, which have an extremely small lifetime, were employed in my experiments to indicate optical toxic doses that are undesirable and so should be avoided. Mostly, these bubbles were observed during trial experiments to assist in setting optimal parameters for photo-transfection and they were also useful for the determining Gaussian beam focus-plasma membrane alignments. Therefore, at optimum levels for photo-transfection which resulted in the enhancement of photo-transfection efficiencies, no bubble formation or cellular disruption and/or response should be visible as this will be a direct indication of cytotoxicity.

4.4 Summary

Chapter 4 was initiated by explaining cell transfection, giving details on the fluid mosaic model of plasma membranes. Thereafter, selective intracellular trafficking of hydrophilic molecules through a channel that functions as a hydrophilic passageway versus intracellular transportation by a periplasmic substrate-binding protein was explained. Due the fact that plasma membranes have highly selective permeability with a wealth of

substances lacking ability to be naturally transported through membranes, as this poses a problem during amongst other things, cell transfection studies. Herein, different means of delivering biological molecules including genes were considered. A brief review of the different technologies developed for cell transfection strategies such as chemical reagents (cationic polymers and/or lipids), viral as well as physical (microinjection, electroporation, ballistic particle delivery (gene gun) and sonoporation) methods with particular interest granted to fs laser assisted transfection (photo-transfection) techniques was presented.

Finally, in this chapter a systematic study of the mechanisms of femtosecond laser transfection was discussed. I presented a study comparing the employment of pulsed ns versus ps versus fs laser source in theoretical and experimental water models to predict possible implications in biological systems. The use of fs pulses during photo-transfection promotes generation of highly localized plasma membrane disruption, resulting in minimum damage and accuracy in membrane targeting. Laser-induced optical breakdown was described to clarify the process of free-electron plasma production in transparent material. The physical mechanism driving photo-transfection is plasma mediated optical breakdown, a process which for ultra-short pulses is almost entirely a multiphoton effect. The Ca^{2+} rich membrane self sealing process post transient cell perforation is also a critical step during photo-transfection. The influence of laser pulse duration on mechanical effects such as cavitation bubbles and shock wave emission during laser-induced optical breakdown was outlined.

Finally the mechanisms of femtosecond laser repetition rate i.e. 80 MHz versus 1 kHz on various biological applications was presented. At MHz repetition rates and lower laser irradiances, fs cellular transfection occurs because of photochemical effects caused by multiphoton plasma formation in the breakdown area. During photo-transfection, the undesirable thermal and mechanical effects are mainly caused by high irradiance levels. Chapters 5 and 6 of this thesis will involve demonstration of the photo-transfection experimental results obtained during my studies. I will present data on cell lines that have never been photo-transfected before such as the neuroblastomas (SK-N-SH and NG108-

15), embryonic kidney (HEK-293) and pluripotent stem cells.

References

1. T. Kodama, M. R. Hamblin and A. G. Doukas, "Cytoplasmic molecular delivery with shock waves: Importance of impulse," *Biophys. J.* **79**, 1821-1832 (2000)
2. Y. Gluzman, "Sv40-Transformed Simian Cells Support the Replication of Early Sv40 Mutants," *Cell* **23**, 175-182 (1981)
3. C. P. Yao, Z. X. Zhang, R. Rahmanzadeh and G. Huettmann, "Laser-based gene transfection and gene therapy," *IEEE Trans. Nanobiosci.* **7**, 111-119 (2008)
4. H. Curtis and S. N. Barnes, "Biology 5th Edition," *New York: Worth Publishers* 104 (1989)
5. T. F. Weiss, "Cellular Biophysics," *Tectonophysics* **1**, 36-44 (1996)
6. http://www.bio.miami.edu/dana/104/104F02_3.html,
7. http://www.williamsclass.com/SeventhScienceWork/CellsOrganization.htm,
8. http://219.221.200.61/ywwy/zbsw(E)/edetail5.htm,
9. M. P. Rols, "Electropermeabilization, a physical method for the delivery of therapeutic molecules into cells," *BBA-Biomembr.* **1758**, 423-428 (2006)
10. E. Phez, C. Faurie, M. Golzio, J. Teissie and M. P. Rols, "New insights in the visualization of membrane permeabilization and DNA/membrane interaction of cells submitted to electric pulses," *Biochim. Biophys. Acta.* **1724**, 248-254 (2005)
11. R. W. Malone, P. L. Felgner and I. M. Verma, "Cationic Liposome-Mediated Rna Transfection," *Proceedings Of The National Academy Of Sciences Of The United States Of America* **86**, 6077-6081 (1989)
12. T. Yeung, B. Heit, J. F. Dubuisson, G. D. Fairn, B. Chiu, R. Inman, A. Kapus, M. Swanson and S. Grinstein, "Contribution of phosphatidylserine to membrane surface charge and protein targeting during phagosome maturation," *Journal of Cell Biology* **185**, 917-928 (2009)

13. T. Yeung, G. E. Gilbert, J. Shi, J. Silvius, A. Kapus and S. Grinstein, "Membrane phosphatidylserine regulates surface charge and protein localization," *Science* **319**, 210-213 (2008)

14. A. Vaheri and J. S. Pagano, "Infectious poliovirus RNA: a sensitive method of assay," *Virology* **27**, 434-436 (1965)

15. S. Kawai and M. Nishizawa, "New Procedure for DNA Transfection with Polycation and Dimethylsulfoxide," *Molecular and Cellular Biology* **4**, 1172-1174 (1984)

16. O. Boussif, F. Lezoualch, M. A. Zanta, M. D. Mergny, D. Scherman, B. Demeneix and J. P. Behr, "A Versatile Vector for Gene and Oligonucleotide Transfer into Cells in Culture and in-Vivo - Polyethylenimine," *Proceedings Of The National Academy Of Sciences Of The United States Of America* **92**, 7297-7301 (1995)

17. J. Haensler and F. C. Szoka, "Polyamidoamine Cascade Polymers Mediate Efficient Transfection of Cells in Culture," *Bioconjugate chemistry* **4**, 372-379 (1993)

18. F. L. Graham and A. J. Van der Eb, "A new technique for the assay of infectivity of human adenovirus 5 DNA," *Virology* **52**, 456-467 (1973)

19. R. Fraley, S. Subramani, P. Berg and D. Papahadjopolous, "Introduction of liposome-encapsuled SV40 DNA into cells," *Journal of Biological Chemistry* **255**, 10431-10435 (1980)

20. X. Gao and L. Huang, "Cationic liposome-mediated gene transfer," *Gene Ther*. **2**, 710-722 (1995)

21. http://www.nano-lifescience.com/research/gene-delivery.html,

22. R. J. Debs, L. P. Freedman, S. Edmunds, K. L. Gaensler, N. Duzgunes and K. R. Yamamoto, "Regulation of Gene-Expression Invivo by Liposome-Mediated Delivery of a Purified Transcription Factor," *Journal of Biological Chemistry* **265**, 10189-10192 (1990)

23. M. Morille, C. Passirani, A. Vonarbourg, A. Clavreul and J. P. Benoit, "Progress in developing cationic vectors for non-viral systemic gene therapy against cancer," *Biomaterials* **29**, 3477-3496 (2008)

24. S. A. Vorburger and K. K. Hunt, "Adenoviral gene therapy," *Oncologist* **7**, 46-59 (2002)

25. T. Ito, Y. Koyama and M. Otsuka, "Analysis of the surface structure of DNA/polycation/hyaluronic acid ternary complex by Raman microscopy," *J Pharm Biomed Anal* (2009)

26. M. R. Capecchi, "High efficiency transformation by direct microinjection of DNA into cultured mammalian cells," *Cell* **22**, 479-488 (1980)

27. E. Bockamp, M. Maringer, C. Spangenberg, S. Fees, S. Fraser, L. Eshkind, F. Oesch and B. Zabel, "Of mice and models: improved animal models for biomedical research," *Physiol Genomics* **11**, 115-132 (2002)

28. S. L. Wu, J. Staudinger, E. N. Olson and C. S. Rubin, "Structure, expression, and properties of an atypical protein kinase C (PKC3) from Caenorhabditis elegans - PKC3 is required for the normal progression of embryogenesis and viability of the organism," *Journal of Biological Chemistry* **273**, 1130-1143 (1998)

29. T. Rulicke and U. Hubscher, "Germ line transformation of mammals by pronuclear microinjection," *Exp Physiol* **85**, 589-601 (2000)

30. G. N. Ye, H. Daniell and J. C. Sanford, "Optimization of Delivery of Foreign DNA into Higher-Plant Chloroplasts," *Plant Molecular Biology* **15**, 809-819 (1990)

31. T. M. Klein, E. D. Wolf, R. Wu and J. C. Sanford, "High-velocity microprojectiles for delivering nucleic acids into living cells," *Nature* **327**, 70-73 (1987)

32. J. K. Burkholder, J. Decker and N. S. Yang, "Rapid Transgene Expression in Lymphocyte and Macrophage Primary Cultures after Particle Bombardment-Mediated Gene-Transfer," *Journal of immunological methods* **165**, 149-156 (1993)

33. R. Ogura, N. Matsuo, N. Wako, T. Tanaka, S. Ono and K. Hiratsuka, "Multi-color luciferases as reporters for monitoring transient gene expression in higher plants," *Plant Biotecnology* **22** 151-155 (2005)

34. http://artsci.wustl.edu/~anthro/blurb/Backgrounder.html,

35. T. K. Wong and E. Neumann, "Electric field mediated gene transfer," *Biochem Biophys Res Commun* **107**, 584-587 (1982)

36. K. Shigekawa and W. J. Dower, "Electroporation of Eukaryotes and Prokaryotes - a General-Approach to the Introduction of Macromolecules into Cells," *Biotechniques* **6**, 742-751 (1988)

37. Y. Z. Song, T. Hahn, I. P. Thompson, T. J. Mason, G. M. Preston, G. H. Li, L. Paniwnyk and W. E. Huang, "Ultrasound-mediated DNA transfer for bacteria," *Nucleic Acids Research* **35**, - (2007)

38. T. F. Yuan, "Noninvasive vaccination: From the perspective of sonoporation," *Vaccine* **26**, 4109-4110 (2008)

39. A. Valero, J. N. Post, J. W. van Nieuwkasteele, P. M. ter Braak, W. Kruijer and A. van den Berg, "Gene transfer and protein dynamics in stem cells using single cell electroporation in a microfluidic device," *Lab on a Chip* **8**, 62-67 (2008)

40. http://clearlyexplained.com/answers/sonoporation.html,

41. D. Stevenson, F. Gunn-Moore, C. Campbell and K. Dholakia, "Transfection by optical injection," *The Handbook of Photonics for Biomedical Science,* **Chapter 3**, 87-117 (2010)

42. C. McDougal, D. J. Stevenson, C. T. A. Brown, F. Gunn-Moore and K. Dholakia, "Targeted optical injection of gold nanoparticles into single mammalian cells," *J. Biophot.* **2**, 736-743 (2009)

43. X. Tsampoula, K. Taguchi, T. Cizmar, V. Garces-Chavez, N. Ma, S. Mohanty, K. Mohanty, F. Gunn-Moore and K. Dholakia, "Fibre based cellular transfection," *Opt. Express.* **16**, 17007-17013 (2008)

44. Tsukakoshi, Kurata, Nomiya, Ikawa and Kasuya, "A novel method of DNA transfection by laser microbeam cell surgery," *Appl. Phys. B-Photo.* **35**, 135-140 (1984)

45. H. Schneckenburger, A. Hendinger, R. Sailer, W. S. L. Strauss and M. Schmidtt, "Laser-assisted optoporation of single cells," *J. Biomed. Opt.* **7**, 410-416 (2002)

46. L. Paterson, B. Agate, M. Comrie, R. Ferguson, T. K. Lake, J. E. Morris, A. E. Carruthers, C. T. A. Brown, W. Sibbett, P. E. Bryant, F. Gunn-Moore, A. C. Riches and K. Dholakia, "Photoporation and cell transfection using a violet diode laser," *Opt. Express.* **13**, 595-600 (2005)

47. G. Palumbo, M. Caruso, E. Crescenzi, M. F. Tecce, G. Roberti and A. Colasanti, "Targeted gene transfer in eucaryotic cells by dye-assisted laser optoporation," *J Photochem. Photobio. B.* **36**, 41-46 (1996)

48. H. Schneckenburger, A. Hendinger, R. Sailer, M. H. Gschwend, W. S. Strauss, M. Bauer and K. Schutze, "Cell viability in optical tweezers: high power red laser diode versus Nd:YAG laser," *J. Biomed. Opt.* **5**, 40-44 (2000)

49. A. V. Nikolskaya, V. P. Nikolski and I. R. Efimov, "Gene printer: Laser-scanning targeted transfection of cultured cardiac neonatal rat cells," *Cell Comm. Adhes.* **13**, 217-222 (2006)

50. Y. Shirahata, N. Ohkohchi, H. Itagak and S. Satomi, "New technique for gene transfection using laser irradiation," *J. Invest. Med.* **49**, 184-190 (2001)

51. D. Stevenson, B. Agate, X. Tsampoula, P. Fischer, C. T. A. Brown, W. Sibbett, A. Riches, F. Gunn-Moore and K. Dholakia, "Femtosecond optical transfection of cells: viability and efficiency," *Opt. Express.* **14**, 7125-7133 (2006)

52. Tirlapur and Konig, "Targeted transfection by femtosecond laser," *Nature.* **418**, 290-291 (2002)

53. S. K. Mohanty, M. Sharma and P. K. Gupta, "Laser-assisted microinjection into targeted animal cells," *Biotechnol. Lett.* **25**, 895-899 (2003)

54. W. Tao, J. Wilkinson, E. J. Stanbridge and M. W. Berns, "Direct Gene-Transfer into Human Cultured-Cells Facilitated by Laser Micropuncture of the Cell-Membrane," *Proceedings of the National Academy of Sciences of the United States of America* **84**, 4180-4184 (1987)

55. K. Nawata, M. Okida, K. Furuki and T. Omatsu, "MW ps pulse generation at sub-MHz repetition rates from a phase conjugate Nd : YVO4 bounce amplifier," *Opt. Express.* **15**, 9123-9128 (2007)

56. A. Vogel, J. Noack, G. Huttman and G. Paltauf, "Mechanisms of femtosecond laser nanosurgery of cells and tissues," *Appl. Phys. B-Lasers O.* **81**, 1015-1047 (2005)

57. C. A. Sacchi, "Laser-Induced Electric Breakdown in Water," *J. Opt. Soc. Am. B-Opt. Phys.* **8**, 337-345 (1991)

58. F. H. Loesel, J. P. Fischer, M. H. Gotz, C. Horvath, T. Juhasz, F. Noack, N. Suhm and J. F. Bille, "Non-thermal ablation of neural tissue with femtosecond laser pulses," *Applied Physics B-Lasers and Optics* **66**, 121-128 (1998)

59. C. H. Fan and J. P. Longtin, "Modeling optical breakdown in dielectrics during ultrafast laser processing," *Applied Optics* **40**, 3124-3131 (2001)

60. http://hasylab.desy.de/facilities/flash/research/multiphoton_ionization/index_eng. and html.,

61. A. G. Doukas and T. J. Flotte, "Physical characteristics and biological effects of laser-induced stress waves," *Ultrasound in Medicine and Biology* **22**, 151-164 (1996)

62. K. Teshima, T. Ohshima, S. Tanaka and T. Nagai, "Biomechanical Effects of Shock-Waves on Escherichia-Coli and Lambda-Phage DNA," *Shock Waves* **4**, 293-297 (1995)

63. A. Vogel, M. R. Capon, M. N. Asiyo-Vogel and R. Birngruber, "Intraocular photodisruption with picosecond and nanosecond laser pulses: tissue effects in cornea, lens, and retina," *Invest Ophthalmol Vis Sci* **35**, 3032-3044 (1994)

64. J. Noack, D. X. Hammer, G. D. Noojin, B. A. Rockwell and A. Vogel, "Influence of pulse duration on mechanical effects after laser-induced breakdown in water," *Journal of Applied Physics* **83**, 7488-7495 (1998)

65. P. L. McNeil and R. A. Steinhardt, "Plasma membrane disruption: Repair, prevention, adaptation," *Annual Review of Cell and Developmental Biology* **19**, 697-731 (2003)

66. McNeil, "Repairing a torn cell surface: make way, lysosomes to the rescue," *Journal of Cell Science* **115**, 873-879 (2002)

67. McNeil, Miyake and Vogel, "The endomembrane requirement for cell surface repair," *Proceedings of the National Academy of Sciences* **100**, 4592-4597 (2003)

68. Terasaki, Miyake and McNeil, "Large Plasma Membrane Disruptions Are Rapidly Resealed by Ca2+-dependent Vesicle-Vesicle Fusion Events," in The Journal of Cell Biology, pp. 63-74 (1997).

69. R. A. Steinhardt, G. Bi and J. M. Alderton, "Cell membrane resealing by a vesicular mechanism similar to neurotransmitter release," *Science* **263**, 390-393 (1994)

70. R. K. Schlicher, H. Radhakrishna, T. P. Tolentino, R. P. Apkarian, V. Zarnitsyn and M. R. Prausnitz, "Mechanism of intracellular delivery by acoustic cavitation," *Ultrasound in medicine & biology* **32**, 915-924 (2006)

71. V. Kohli and A. Elezzabi, Y. , "Prospects and developments in cell and embryo laser nanosurgery," *Wiley Interdiscipl. Rev. Nanomed. Nanobiotechnol.* **1**, 11-25 (2009)

Chapter 5

Photo-transfection of mammalian cells via femtosecond laser pulses

Introduction

In chapter 4 an introduction of the delivery of membrane impermeable molecules into cells during the transfection processes, was presented alongside the mechanisms governing photo-transfection. In this chapter, laboratory data of femtosecond transfection is provided. Chapter 5 starts by briefly describing the mechanisms of DNA transcription, mRNA translation as well as protein synthesis and expression in mammalian cells during photo-transfection. Then measurements of the femtosecond beam profile and pulse duration in a basic Gaussian beam setup are explained. Thereafter, I describe the photo-transfection setup employed throughout my experiments, giving a full description of the cell sample preparation as well as the photo-transfection protocol. I also provide a description of how the photo-transfection setup was tested and optimized via trypan blue dry run (photo-translocation) experiments.

Following this a report on the different cell lines successfully photo-transfected with DsRed2-Mito and EGFP expressing DNA plasmids is presented. This includes the previously difficult to transfect NG108-15 and SK-N-SH neuroblastoma cell lines. I then address various aspects which influence the photo-transfection efficiency, such as a change in optical parameters (average power output and time of beam exposure), the culture passage number and the stages of the cell division cycle (particularly the M and S phases). Following this, studies investigating potential cellular stress responses and/or the cytoprotective role of the hsp70 post photo-transfection are described. Lastly, introduction of mRNA which is directly translated upon reaching the cytosol without crossing the nuclear membrane is presented.

5.1 From genes to protein

Since diverse forms of life share a common genetic code, it is possible to program one species to produce proteins characteristic of another species by transplanting DNA. For example during cell the photo-transfection studies reported herein, genes from jellyfish (green fluorescent protein (GFP)) and *Discosoma species* (DsRed2-Mito) are incorporated into different mammalian cells. Once successfully introduced and/or delivered into cells, these foreign genes are responsible for making specific proteins. However, a gene does not construct a protein directly; rather the connection between genetic information and protein synthesis occurs via an intricate process involving ribonucleic acid (RNA). The process involved in how genes become proteins occurs through two main steps known as transcription and translation. In eukaryotic cells, transcription is the synthesis of RNA under the direction of DNA while translation is the synthesis of a polypeptide, which occurs under the direction of mRNA (1).

In eukaryotes, the nuclear membrane decouples the processes of transcription from translation. Transcription takes place in the nucleoplasm and the newly synthesized mRNA is dispatched to the cytoplasm which is the site for the translation. Briefly, during transcription enzymes called RNA polymerases force open the two DNA strands apart and hook together the RNA nucleotides as they base pair along the DNA template (figure 5.1). The RNA polymerase works its way downstream from the initiation site, prying apart the two strands of DNA and elongating the mRNA in the 3' – 5' direction. The RNA polymerase continues to elongate the RNA molecule until it reaches the termination site end of the transcription unit. Then mRNA, a transcript of the gene is released (figure 5.1) and the polymerase subsequently dissociates from the DNA. During protein translation in the cytoplasm, the mRNA strand slides through a ribosome, a complex particle with many enzymes and other agents that facilitate the orderly linking of amino acids into polypeptide chains. Within the ribosome there is an mRNA-binding site as well as transfer RNA (tRNA) binding sites. The tRNA molecules function as interpreters during protein translation, in that each type has a specific anticodon at one end (the ribosome binding site) and a particular amino acid at the other end.

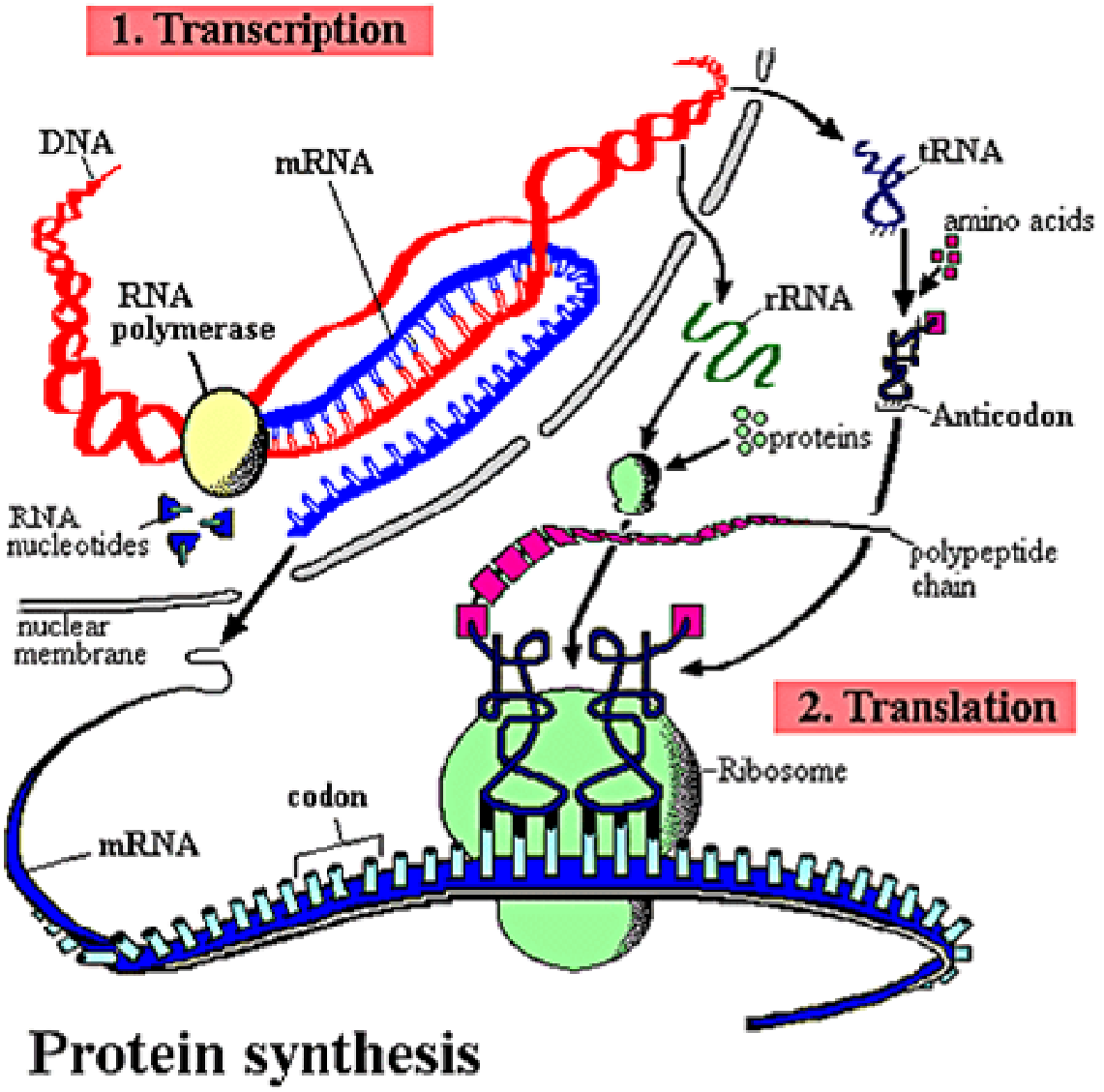

Figure 5.1: A simplified illustration of, the two main steps of protein synthesis occurring in separate compartments i.e. transcription in the nucleoplasm and translation in the cytoplasm of a eukaryotic cell. After its synthesis in the nucleus, mRNA is translocated into the cytoplasm through pores within the nuclear envelope. The function of the ribosomal RNA (rRNA) is to provide a mechanism for decoding mRNA into amino acids and to interact with the tRNAs during translation. Therefore, in the cytoplasm the mRNA molecule slips into the ribosome while the tRNA brings the amino acids to the ribosome to have them incorporated into the growing protein polypeptide chain (online access date - 23.12.09 (2)).

Thus, a tRNA fits into a binding site when its anticodon base-pairs with an mRNA codon. So, as the mRNA slides through the ribosome, codons are translated into amino acids one by one because a tRNA adds its amino acid cargo to a growing polypeptide chain when the anticodon binds to a complementary codon on the mRNA (figure 5.1). This is how the foreign genes which are normally delivered as plasmid DNA into mammalian cells during cell transfection become processed into proteins. These transcribed proteins are commonly fluorescent and can be viewed under fluorescence microscopy. Such gene transplantation (i.e. from one species to different one) experiments are crucial for numerous applications. For example bacteria can be programmed to synthesize the human protein insulin, a product that can be used to treat diabetes. Other examples include the creation of transgenic animals which can express genes from a range of other organisms and are subsequently used for studies investigating genetically inherited diseases.

In the following sections of this chapter the prospects for coupling laser light and genetic studies through the process of fs photo-transfection studies, opens doors to more novel and advanced biological investigations. The process of fs photo-transfection requires use of a tightly focused beam located on the plasma membrane of the cell to irradiate it with ultra-short pulses of higher peak powers. Thus, in section 5.2, I describe the methods utilized for characterizing the beam waist, the temporal duration of the pulsed output of the fs titanium sapphire (Ti: sapph.) laser used and full details of the experimental procedures followed during my photo-transfection experiments.

5.2 Femtosecond laser beam profile and pulse duration measurements

5.2.1 Beam profile and laser characteristics

The experimental data to be presented in the remaining chapters of this thesis were all performed using a tunable Kerr lens mode-locked Ti: sapph laser (MIRA, *Coherent*) which emits ~100 fs near infrared pulses of 80 MHz repetition rate and ~ 2 watts average power output at the laser exit aperture. The beam diameter was measured using a laser

beam profiler which was used to display and capture the transverse intensity profile of the emitted laser beam. The output beam spot size ($2w_o$) during mode-locked operation along the x direction was measured to be 1.547 mm ± 0.001 mm error and along the y direction 1.524 mm ± 0.001 mm error.

5.2.2 Pulse duration measurements

As the Gaussian laser beam pulses were emitted from the exit aperture of the Ti: sapphire laser, their temporal profile was measured directly near the exit, in the beam path before the periscope as well as at the microscope objective focus of the photo-transfection setup. The measurements were obtained via a commercial TIMEWARP, E750 (*Elliot Scientific LTD, UK*) interferometric autocorrelator that comprises an optical detector head and a control box unit. Pulse duration measurements near the exit and directly before the periscope were performed by simple horizontal alignment of the TIMEWARP detector to the beam path and recording the reading from the control unit at each of these points in the photo-transfection setup. Thus assuming the sech^2 shaped pulse, during all my photo-transfection experiments the pulse duration was measured to be ~ 116 fs near the laser exit aperture, ~ 187 fs just before the periscope and ~ 196 fs at the sample plane. This difference is because, upon traveling through the photo-transfection setup optics (particularly passing through beam splitter cubes of ~ 4 cm thickness), the laser pulse duration undergoes a small amount of temporal stretching, which results in an approximately 10 – 15 fs increase in pulse duration at 790 nm.

5.2.3 Experimental setup

The photo-transfection setup consisted of a dual objective optical system as depicted in figure 5.2. Briefly, the femtosecond laser beam pulses emitted by a titanium sapphire laser (790 nm, 80 MHz, 200 fs, average power = 60 mW at the focus) were magnified by a simple two lens telescope to match the back aperture of the 60 X air objective (*Nikon*) lens with numerical aperture (NA) 0.8. This created a diffraction limited spot of ($1/e^2$) diameter = 1.1 µm. The pulse energy at the objective front focal plane was calculated to be ~ 0.76 nJ with an associated pulse peak power = 3.75 kW. The mechanical shutter (*Newport, UK*, model 845HP-02) on the beam path was used to regulate the time of beam

exposure at the cell sample plane on an XYZ translation stage (*Newport*). The sample chamber was illuminated via a Koehler arrangement, and imaged by a Watec colour camera (WAT-250D) situated below the sample stage. Appendix B (i) to (iii), page B1-B2 explains the detail on cell sample preparation, cell culturing and plasmid DNA preparation.

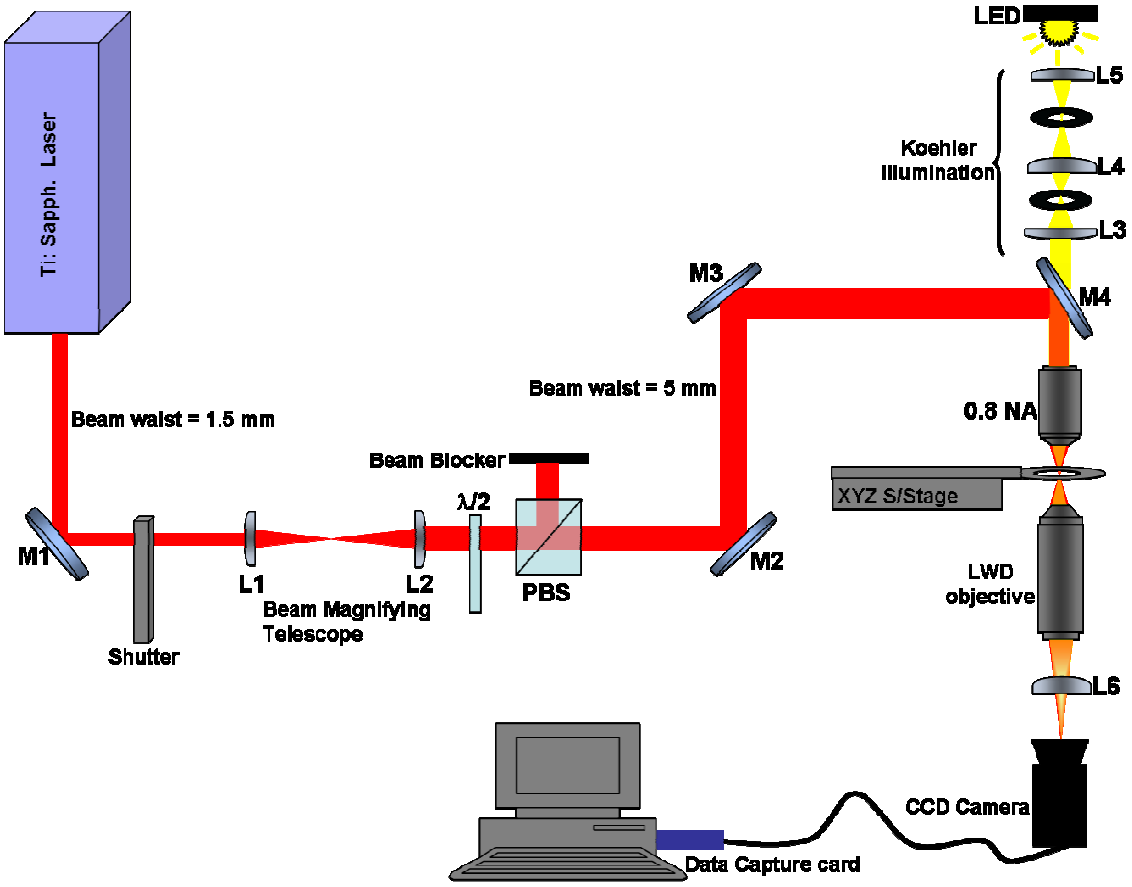

Figure 5.2: Photo-transfection setup for my studies. An infrared Gaussian beam (beam diameter ($2w_o$) = 1.5 mm) is emitted by a titanium sapphire laser bounced off mirror (M1) and expanded via lenses (L1 (f = 50 mm) and L2 (f = 175 mm). A half wave plate (λ/2) and polarizing beam splitter cube (PBS) were used to attenuate the power output, while mirrors (M2 and M3) served as a periscope. Mirror M4 reflected the beam onto the back aperture of a 60 X objective lens (NA 0.8). A light emitting diode (LED) provided sample lighting when arranged into Koehler illumination via passing through lenses (L5, L4 & L3) and two apertures. The sample imaging system consisted of: a long working distance (LWD), f = 200 mm, 50 X Mitutoyo objective lens (NA = 0.55), a tube lens (L6) and a charge coupled device (CCD) camera. These were connected to the output computer by a data capture card (reprint by permission from *Journal of*

Biomedical Optics (3)).

5.2.4 Photo-transfecting different mammalian cell lines

For photo-transfection experiments, approximately 10^4 cells in 2 ml of complete medium were seeded in 35 mm diameter type zero glass bottomed petri dishes (23 mm diameter = glass working area, from *World Precision Instruments, Stevenage, UK*). These were incubated to sub-confluence over 24 hrs in optimum growth conditions. The monolayer was washed twice with 2 ml of OptiMEM (*Invitrogen*) each time, to remove the serum. Thereafter the cells were submerged in 60 µl of serum-free medium containing 10 µg/ml of pDsRed2-Mito and/or pEGFP plasmid DNA (pDNA). The sample chamber was then covered with a 22 mm diameter type-1 coverslip (*BDH, Poole UK*). Targeted photo-transfection of individual cells was then performed via laser irradiation through administering three shots of ultra-short duration while avoiding visual cellular response (i.e. no bubble formation or cellular disruption). During this process, the top surface of the cell's plasma membrane is directly exposed to the pDNA and fs beam focus, the area where the multi-photon effect is confined (figure 5.3) (4). Alignment of the beam focus to the cell's plasma membrane therefore promotes the generation of free-electrons which photo-chemically react with the membrane resulting in the induction of transient holes (5) through which pDNA diffuses into the cytosol. Following irradiation, the DNA containing medium was aspirated, the monolayer washed once with OptiMEM, covered in 2 ml condition medium and incubated under optimum growth conditions for 48hrs before live cell fluorescence analysis.

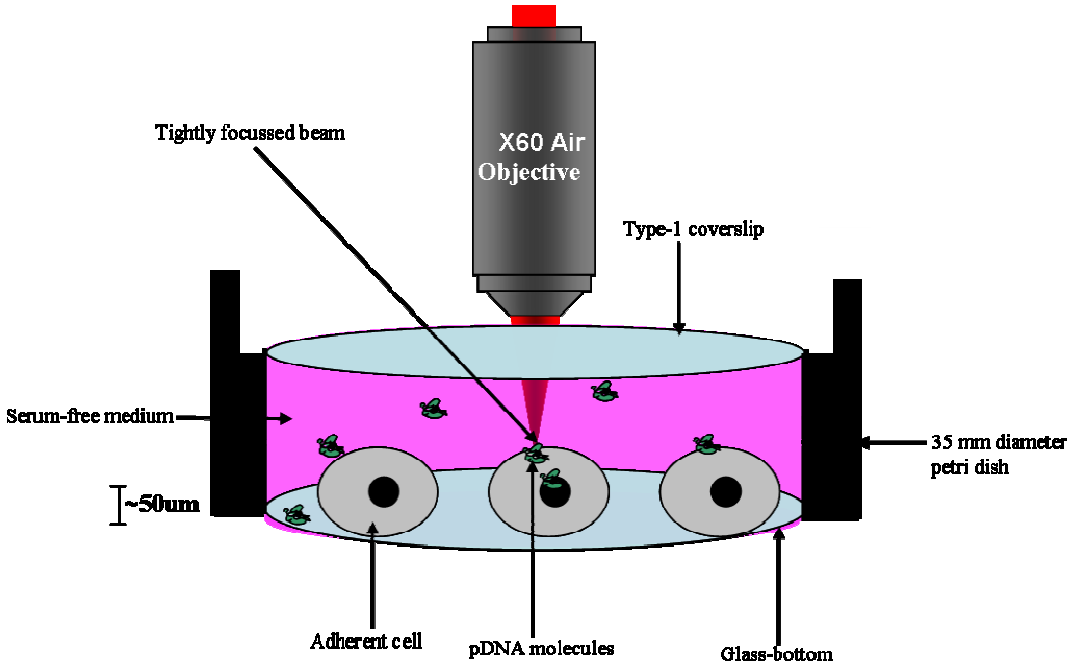

Figure 5.3: Sample chamber illustrated (~ 50 µm depth). Irradiation of the top surface of adherent cells facilitated by targeted delivery of the infrared fs laser beam permitted transient opening of the plasma membrane and subsequent diffusion of surrounding plasmid DNA (reprint by permission from *Journal of Biomedical Optics* (3)).

Subsequent to constructing and aligning the photo-transfection setup and prior to performing the intended transfection experiments, photo-translocation experiments using a membrane impermeable dye were performed. This dry run experiment was done not only to test and optimize the system but was used as a means to determine and confirm whether photo-transfection of cells caused plasma membrane perforation. Thus, a sample of CHO-K1 cells was plated and prepared as mentioned in 5.2.4 but the cell monolayer was submerged in 60 µl of 0.4 % trypan blue exclusion viability stain instead of DNA. Figure 5.4 depicts the results obtained post photo-translocation in CHO-K1 cells at 790 nm, 80 MHz, 200 fs, 40 ms and average power = 200 mW at the focus. Upon laser irradiation at power levels greater than optimal levels (50 – 60 mW), membrane perforation was achieved leading to intracellular diffusion and inclusion of trypan blue through the membrane pore. Trypan blue translocation (staining) was apparent within 30 seconds following laser irradiation.

However, no dye inclusion was observed at 50 – 60 mW even after 30 minutes of incubation in the presence of the dye subsequent to optical treatment. In addition, no photo-transfection i.e. with either DsRed2-Mito or EGFP expression plasmid occurred at the photo-toxic dosing of 200 mW. Instead, 48 hrs post cell irradiation at 200 mW resulted in the detachment of most of the monolayer from the surface of the sample chamber.

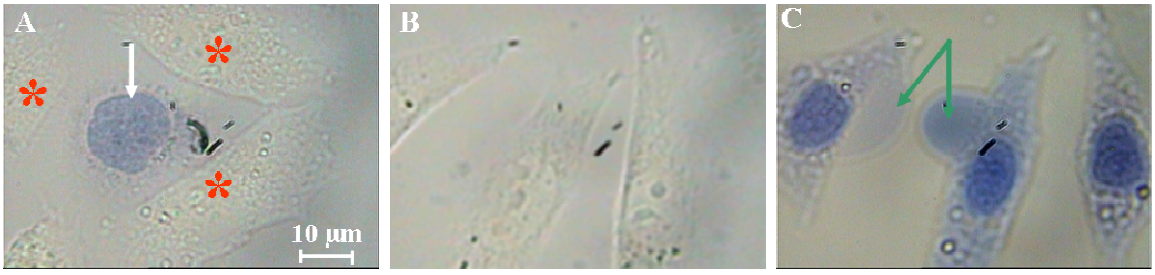

Figure 5.4: CHO-K1 cells photo-translocated with trypan blue viability dye imaged under brightfield using a 50 X Mitutoyo objective lens (NA = 0.55). In (a) * means viable cells that were neither optically treated nor did they naturally include the surrounding toxic dye five minutes post incubation in its presence. Nonetheless, the blue stained cell (white arrow) was irradiated via administering one shot at 790 nm, 80 MHz, 200 fs, 40 ms and 200 mW. And as of 30 seconds post photo-translocation and consequential membrane perforation the dye was included into the cytoplasm resulting in blue staining of the nucleus. In (B), three healthy CHO-KI cells imaged in the presence of trypan blue before photo-translocation are shown. Image (C) displays the same three CHO-K1 cells irradiated as mentioned in (A) and left incubating in the presence of trypan blue for ten minutes subsequent to optical treatment. The green arrow indicated cell blebbing ("cytoplasmic bleeding") as a result of irradiation at power levels greater than optimal level of between 50 – 60 mW power output at the beam focus.

Of note, Schlicher *et al*, 2006 (6) stated that ultrasound promotes successful delivery of molecules (protein, macromolecules, etc) into cells. They further reported that, depending on the size of the molecules, their introduction into the cytosol can persist for more than one minute following plasma membrane sonication. They therefore concluded that ultrasound-induced cellular transport occurs through plasma membrane wounds of up to micron size ranges, which get repaired by vesicle exocytosis within minutes (6). Therefore, the lack of trypan blue inclusion at powers below 200 mW could be attributed

to both the size of the molecule as well as that of the induced pore. The pore sizes induced at 50 – 60 mW may not be opened long enough to allow extensive and rapid entrance of visually detectable amounts of the trypan blue. In support of this, Chang *et al*, 1992 (7) reported that membrane holes induced via electroporation permitted cytosolic transport through 1 – 10 nm size openings, that spontaneously resealed without the involvement of special wound-repair machinery (ATP, Ca^{2+}, intracellular vesicles, etc) as reported by McNeil et al, 2003 (8). Therefore, the transiently induced membrane holes at 50 – 60 mW might be wide enough to allow the entrance of plasmid DNA molecules into the cytosol yet short lived to avoid photo-toxicity that results in cell blebbing.

Although the irradiation of cells at very high power levels allowed quick checks of the alignment of setup, beam focus-plasma membrane alignments, they also induce cytotoxicity displayed through localized visual micro-explosions (bubble formation) during the optical shots and followed by cell blebbing as shown in figure 5.4 (c). So, for my photo-transfection experiments (i.e. using pDNA) the photo-toxic parameters operating at lethal irradiances were avoided but strictly employed only for optimization purposes. For all photo-transfection experiments, irradiance thresholds (~ 50 to 60 mW) safe for optical transfection which are indicated by the lack of a visual response of the cell during optical treatments were applied.

Thus, the versatility of the photo-transfection technique under these optimum parameters of 60 mW average power output and 40 ms time of beam exposure at the cell sample plane was tested. Using these optical parameters in Table 5.1 is shown the successful transient transfection efficiency of various mammalian cell types. These include neuroblastomas (SK-N-SH and NG108-15) that have been previously described as difficult to transfect by conventional transfection technologies examples including, the lipid based gene delivery methods (9).

Throughout my experiments, the transfection efficiency (%) was calculated according to Tsukakoshi et al, 1984 (10) and Stevenson et al, 2009 (11) using the expression: N_{cor} = ((E/D).100)/X_D. Where N_{cor} = the population corrected transfection efficiency, E = number of cells transiently expressing the pDNA after a suitable amount of time has passed, D = number of cells dosed on a given experiment and X_D = the ratio of proliferation that has occurred in the dosed cells between dosing and the measurement of expression (see appendix B (iv) page B2 for example).

Table 5.1: Summary of the cell lines photo-transfected at 60 mW and 40 ms with a gene encoding red fluorescent protein (pDsRed2-Mito). Experiments were performed in triplicate with a minimum of 150 individual cells treated per experiment. The transfection efficiency (%) values reported were corrected as previously described (reprint by permission from *Journal of Biomedical Optics* (3)).

Cell type	Tissue of origin	Transfection efficiency (%)
CHO-K1	Ovary (hamster)	63 (2500 cells treated)
HEK-293	Kidney (human)	52 (2000 cells treated)
NG108-15	Brain (mouse/rat)	40 (1500 cells treated)
SK-N-SH	Brain (human)	45 (1500 cells treated)

5.3 Optical parameters and cell transfection efficiency

A study directly comparing the influence of utilizing varying optical parameters during photo-transfecting was conducted in order to show their effect on the cell transfection efficiency. In these investigations to obtain optimum optical parameters for photo-transfection, different optical parameters were tried and tested including photo-transfecting at 130 mW/ 40, 30, 20 and 10 ms (i.e. keeping the average power output constant while altering the pulsed beam time of exposure). Different power outputs (ranging from 130 to 40 mW) at the beam focus while keeping the time of exposure constant at either 10 or 40 ms were also tested. In separate experiments average power output was reduced to 60 mW and kept constant whereas the time of beam exposure at

the focus, varied between 40, 30, 20 and 10 ms. Notably, two different sets of optical parameters employed proved successful. One possibility resulting in reduced transfection efficiency involved treatment of cells with 130 mW average power coupled with a 10 ms beam exposure time at the focus. The other regime, which resulted in a two-fold increase in transfection efficiency compared to the one mentioned above, was photo-transfecting with a 60 mW average power at the focus and 40 ms duration. Figure 5.5 depicts the results of this experiment in CHO-K1 cells. A similar experiment was run on HEK-293 cells and displayed complementary results as in the case of CHO-K1 cells (figure 5.6). In each of the figures below, experiment number plotted in the x-axis referrers to the different experiments performed per time period and repeated in triplicate.

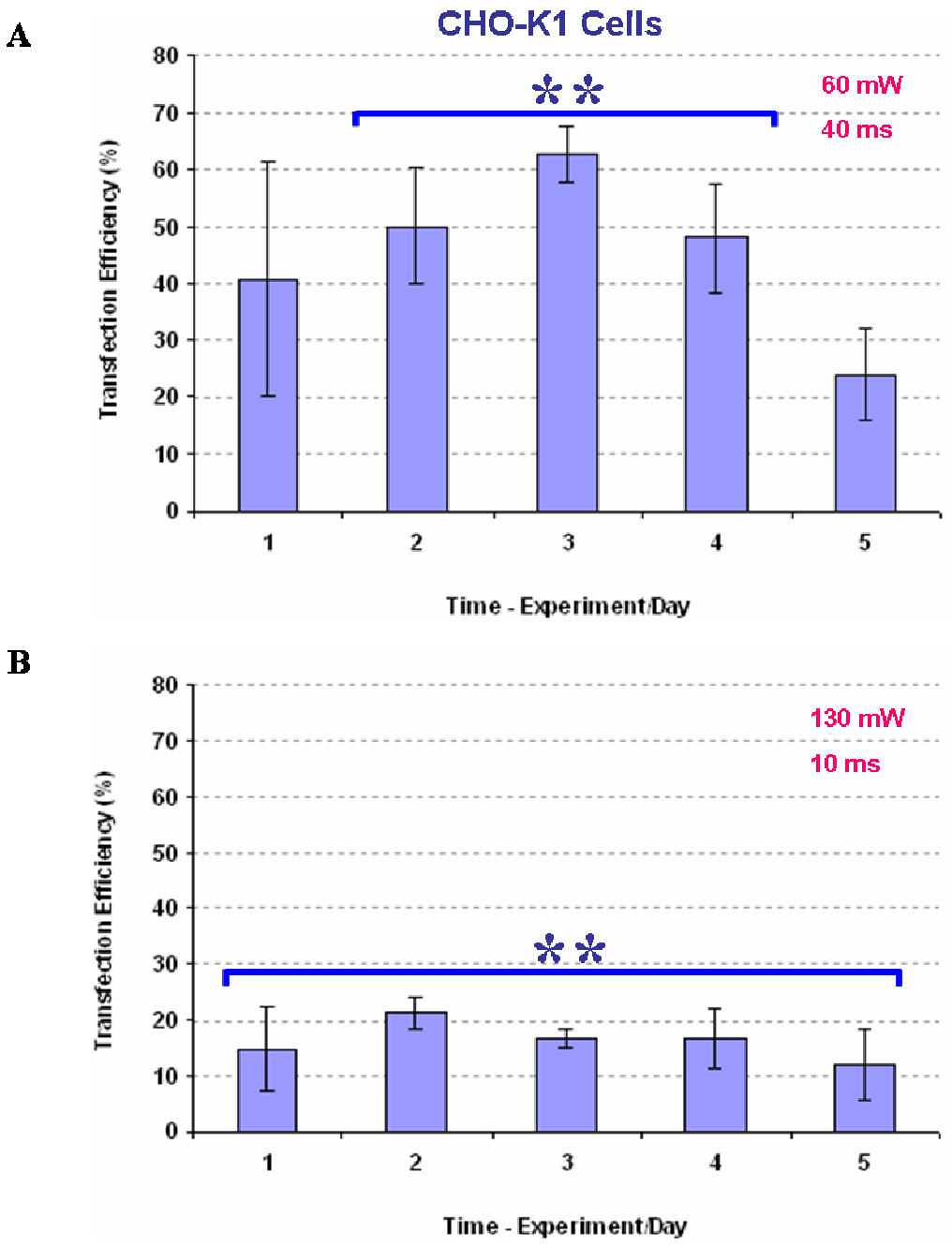

Figure 5.5: Cells photo-transfected with pDsRed2-Mito at 60 mW and 40 ms (A), show a two fold increase in transfection efficiency when compared to those irradiated at 130 mW and 10 ms (B). The data herein presents the corrected transfection efficiency calculated as mentioned before. Error bars represent the SEM (n = 3 experiments of 50 dosed cells). Using ANOVA followed by Dunnett's and Fisher's tests, ** means the data sets between image (A) and image (B) were significantly different from each other (Appendix B (viii) pages B6-B7 shows full statistical analysis of this plot).

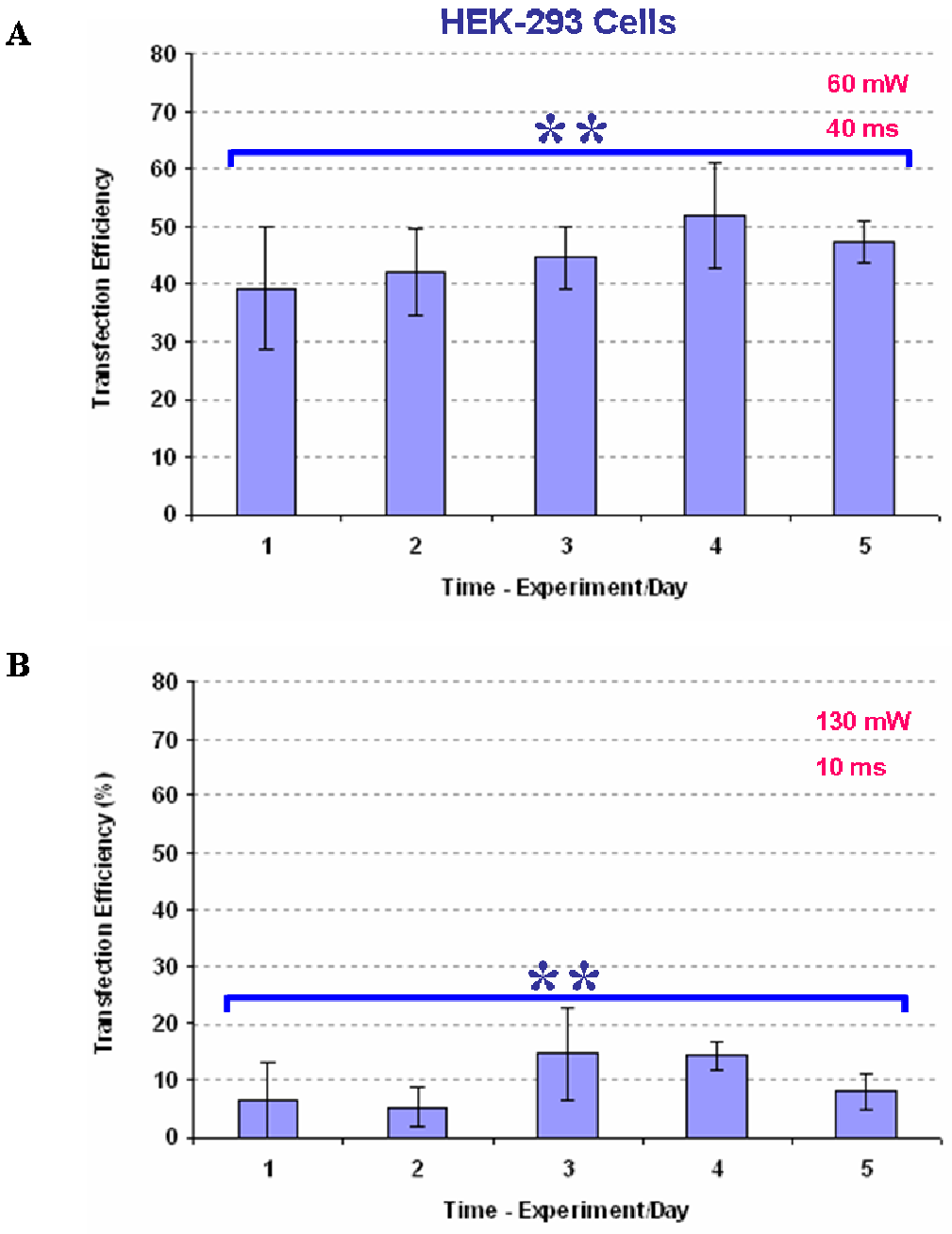

Figure 5.6: Results from photo-transfecting HEK-293 cells with 10 µg/ml of pDsRed2-Mito at 60 mW and 40 ms (A) and 130 mW and 10 ms (B). Although a different cell line is employed in this case, the data obtained using the two different sets of optical parameters complemented the data presented in figure 5.5. The SEM (n = 3 experiments of 50 dosed cells) is represented by the error bars. ANOVA analysis alongside Dunnett's and Fisher's tests ** illustrated that, data presented in image (A) was significantly different from that given in image (B) (Appendix B (viii) pages B7-B8).

Most neuroblastoma cell lines are derived from highly malignant tumors (12). However, many neuroblastoma cell lines remain hard to transfect with established protocols, hindering consecutive analysis. Indeed in sub-section 5.2.4 photo-transfection was shown to be a valuable tool for nucleic acid delivery in a wide variety of cell types. Notably, the capability to photo-transfect neuroblastoma cells with nucleic acid molecules of choice at relatively high efficiency while maintaining cell viability is essential for elucidating various biochemical pathways and other genetic studies. Therefore in order to potentially improve the transfection efficiency, I compared using different optical parameters for the transfection of neuroblastoma cell lines SK-N-SH and NG108-15. The average power output of 130 mW at the sample plane and 10 ms time of beam exposure proved to be a photo-toxic dose for NG108-15 and SK-N-SH cells as no fluorescence was detected on analyzing the cells 48 hrs post photo-transfection. Cell detachment, death and lyses in both cell lines were observed at this dose. However, successful transfection was obtainable on treatment with 60 mW and 40 ms in these neuroblastoma cell lines. Figures 5.7 and 5.8 depict SK-N-SH and NG108-15 cells respectively, 48 hrs post photo-transfection using either the pDsRed2-Mito or pEGFP plasmid DNA.

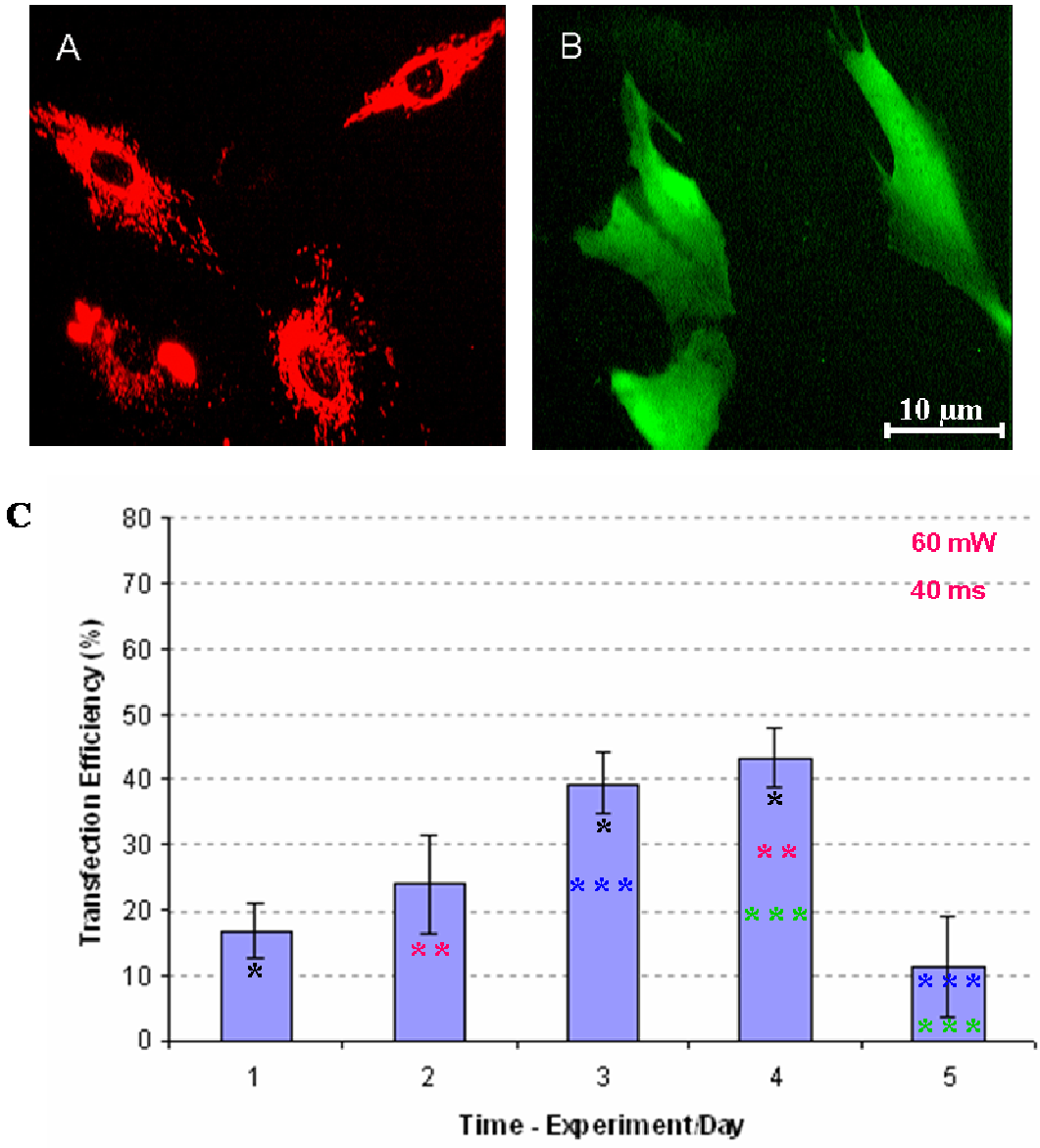

Figure 5.7: Fluorescent images of SK-N-SH neuroblastoma cells photo-transfected with 10 µg/ml of plasmid DNA, DsRed2-Mito (A) and EGFP (B). Proteins expressed 48 hours post laser treatment at 60 mW and 40 ms, the plot (C) illustrated the transfection efficiency achieved post optical treatment with pDsRed2-Mito. The error bars represent the SEM, where n = 3 experiments of 50 cells treated. Using ANOVA followed by Dunnett's and Fisher's tests *, ** and *** means that data points are significantly different from each other (Appendix B (viii) pages B9-B10).

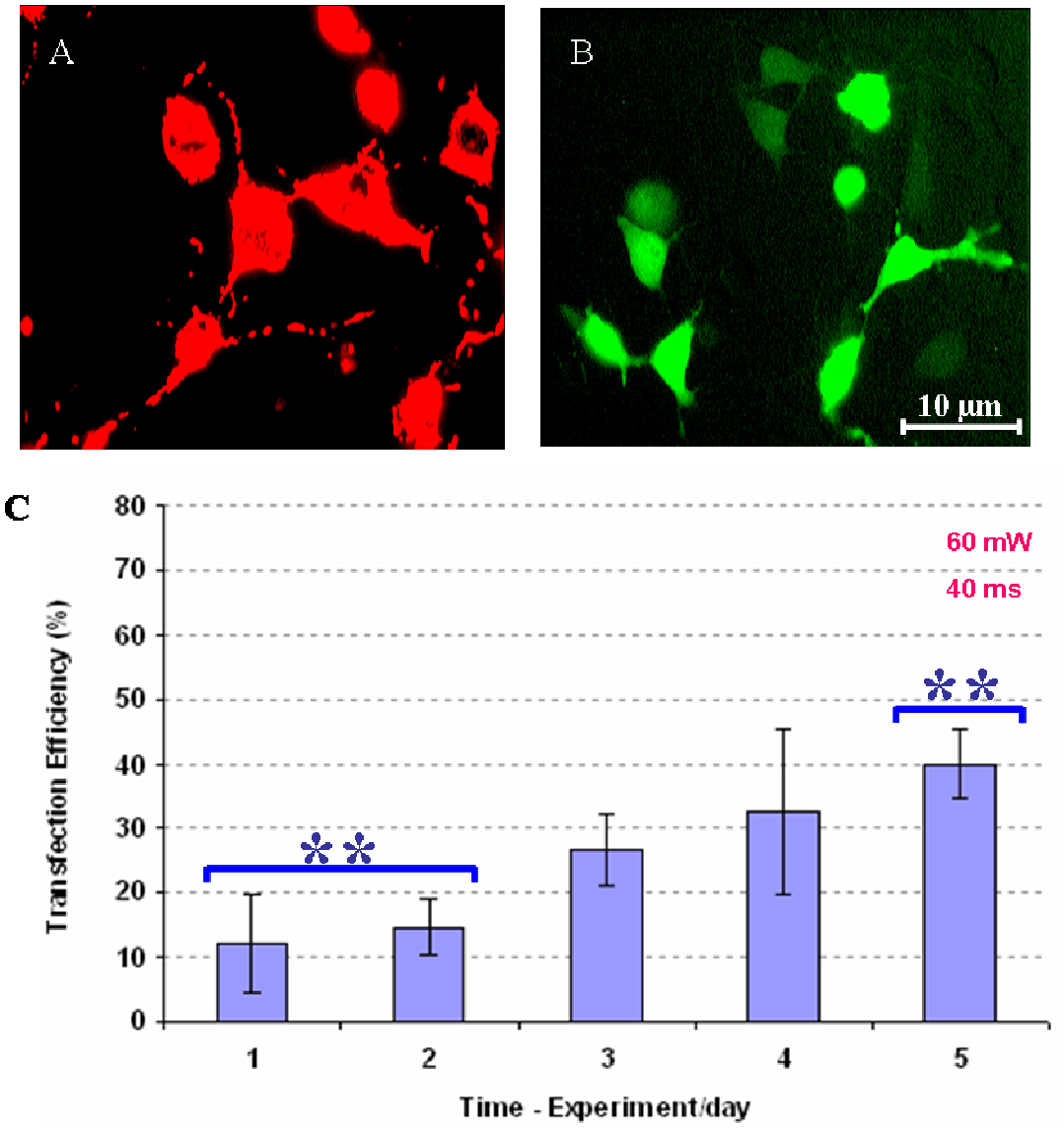

Figure 5.8: Both the DsRed2-Mito (A) and EGFP (B) plasmid DNA (10µg/ml) could be successfully transiently photo-transfected into NG108-15 cells to express the respective proteins 48 hrs post optical treatment at 60 mW and 40 ms. Image (C) is the numerical analysis of cells photo-transfected with pDsRed2-Mito where 50 cells were dosed per experiment and each experiment repeated trice, hence the error bars represent the SEM. ANOVA with both Dunnett's and Fisher's tests showed that the data points labeled with ** are significantly different from each other (Appendix B (viii) pages B10-B11).

5.4 Culture passage number and photo-transfection efficiency

The extent of sub-culturing a cell line is often expressed as a "passage number". This process of passaging causes mechanical injury to cells followed by changes in gene expression (13). Generally, in transfection experiments the passage number of cell lines can affect not only the transfection efficiency, but also protein expression (14). Compared to those in lower passage numbers, cell lines at higher passage numbers undergo alterations in cell morphology, response to stimuli, growth rates, protein expression, transfection and signalling (15-20). Mechanisms for passage number effects vary. However, according to Ryan 2007 (21), cells in culture are cells under stress from being in an alien environment. Ryan further reports that genetic engineering and cell line transfection poses additional stress on cultured cells. Genetic engineering forces a cell to express foreign proteins, and expression of these non-native proteins at high levels requires energy from the cells. Hence, expression or over-expression of artificially introduced genes forces the cells to redirect energy required for cell growth and subsequently leads to a slower than normal growth rate. In addition as the cells proliferate and are sub-cultured, the stress of culture creates a selective pressure (21). For *in vitro* investigations the cell line quality is essential for successful experimentation and avoiding the use of cells that have been in culture too long is critical. Therefore I investigated the effect of passage number on photo-transfection efficiency.

The plasmid DsRed2-Mito was photo-transfected into CHO-K1 and HEK-293 cells of different culture passage number. As can be seen in figure 5.9 (A), in CHO-K1 cells from passage 19 through to 30, then the efficiency is between 40 – 60 % peaking at approximately passage number 28, but this dropped significantly once the cells were at passage number 34. This effect was also shown with HEK-293 cells (figure 5.9 (B)), as there was a significant increase in the photo-transfection efficiency from passage 8 through to 26. At P26 there was a peak of ~53 % transfection efficiency which then started to decrease from passage 31. Therefore this confirmed that, as with other transfection techniques, the passage number of a cell line plays a significant role in establishing the efficiency of photo-transfection.

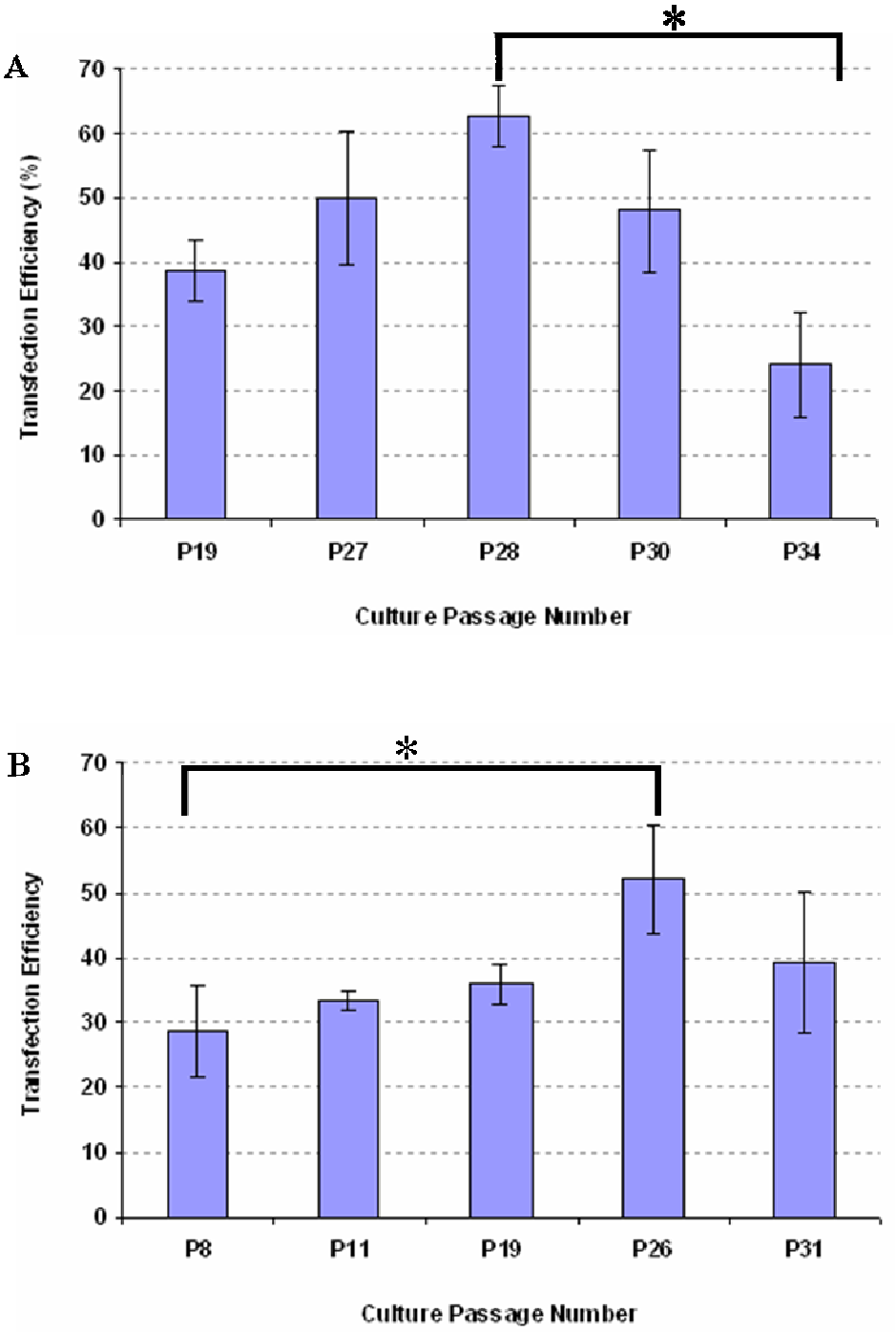

Figure 5.9: CHO-K1 (A) (reprint by permission from *Journal of Biomedical Optics* (3)) and HEK-293 (B) cells photo-transfected at an average power of 60 mW and 40 ms time of exposure illustrates the influence of culture passage number on the photo-transfection efficiency. Error bars represent SEM (n = 3 experiments of 50 treated cells). Using ANOVA followed by Dunnett's and Fisher's tests: * means data sets are significantly different from each other within each cell line (Appendix B (viii) pages B11-B13).

Future photo-transfection experiments of cells at different passage numbers will involve studies investigating whether there might be a change in the refractive index of cells that photo-transfect with maximum efficiency (i.e. the cells resulting in the peak of each plot in figure 5.9). Change in *n* might be brought about by an increase in the number of cells at maybe the S phase of the cell cycle as a result of the change in intracellular protein: DNA ratio.

5.5 The cell division cycle and photo-transfection efficiency

In this section the possibility to enhance the transfection efficiency via chemically aligning cells so they display a common property is explored. The process by which a series of events within a cell leads to its division and duplication (replication) to daughter cells is described as the cell division cycle (figure 5.10). The actual division (cytokinesis) state is known as mitosis (M) phase, while the non-dividing stages are collectively called the interphase. Interphase is further sectioned into three stages, namely, first gap (G1), DNA synthesis (S) and second gap (G2) phases. Through the use of whole-culture synchronisation approach, Brunner *et al*, 2000 (22), previously conducted a study analysing the cell cycle dependence of six different gene transfer systems. Their findings indicated a clear and comparable variation in transfection efficiency between cells transfected in late S/G2 phases to those treated at the G1 phase for five of the transfection systems investigated.

Improvement of both transient and stable cell transfection efficiencies was also achieved by Goldstein *et al*, 1989 (23) through synchronizing cells in the G2/M phase and then treating them with butyrate. This combination allowed a decrease in the electroporation voltage and DNA concentration while greatly enhancing the transfection efficiency. In addition, Musiani *et al*, 1983 (24) showed that cultures infected in S phase with DNA from different strains of the human cytomegalovirus, the efficiency of transfection was higher than cells infected in G2, M and G1 phases respectively.

Therefore I explored whether changes in the cell cycle could also influence photo-transfection efficiency. In my experiments, cells were reversibly arrested at the M and S phases. To synchronize the cells at the M phase colcemid was used. This is a drug which through its binding to a tubulin dimmer, inhibits polymerization of microtubules and forces the cycling cells to accumulate in pro-metaphase-like state (25, 26). Also addition of colcemid to the cells prevents the centrioles from organizing the microtubules, which are necessary for chromosome migration to the poles during cell division (27).

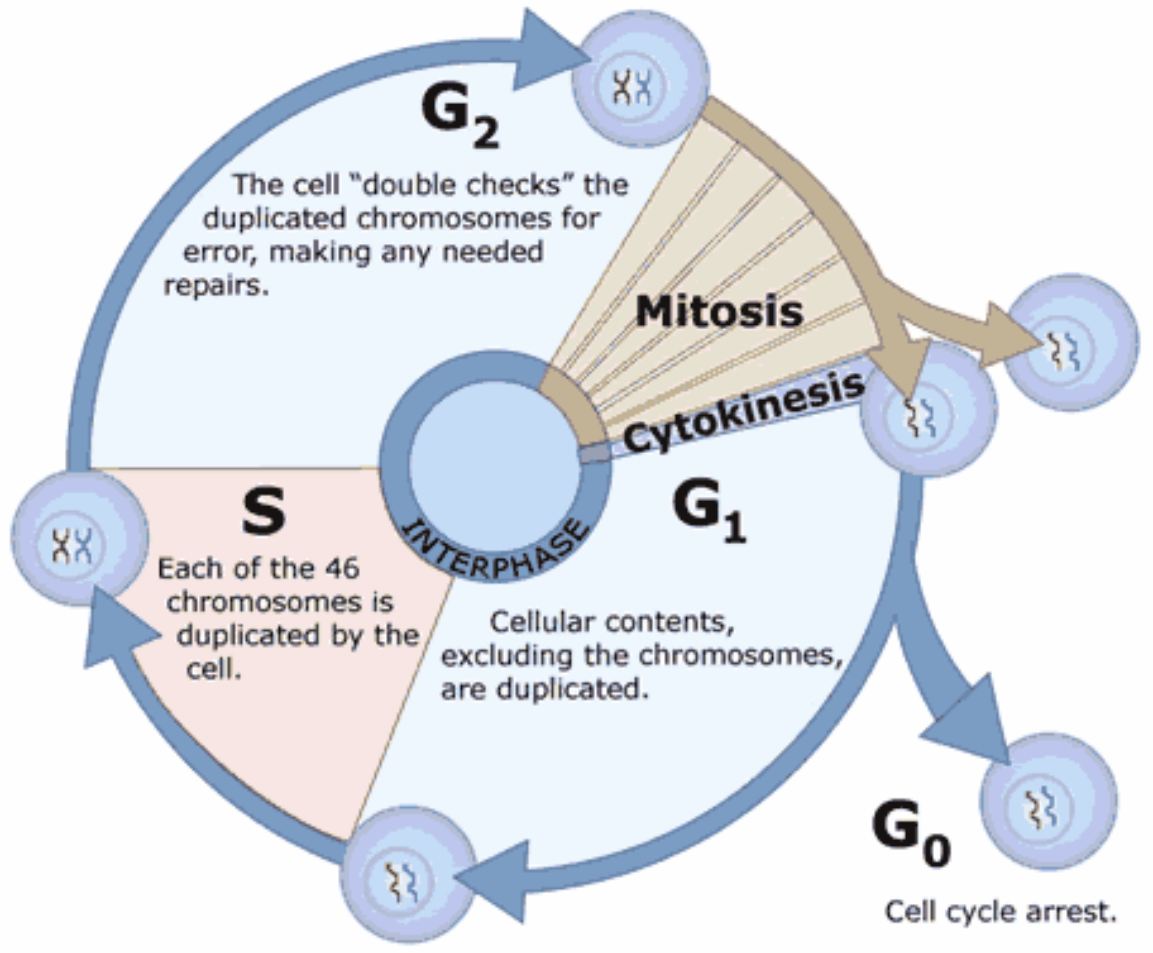

Figure 5.10: Illustrates the cell division cycle where G1 is the growth phase the cell enters when it senses growth signals. During the S phase the DNA is synthesized and in the G2 phase the cell arranges and checks chromosomes. There is a major checkpoint in G2 to ascertain that DNA replication has successfully occurred, if not a normal cell undergoes apoptosis. In the M phase once the mitosis chromosomes are

drawn apart by molecular motors, the cell divides. There is also a checkpoint here that ensures that chromosomes are correctly attached to the spindles before segregation takes place. Cells that are not dividing leave the cell cycle and stay in the G0 phase (online access date - 23.12.09 (28)).

A double thymidine treatment which primarily arrests cells with an S-phase DNA content was also performed to achieve synchronization at the S phase. Briefly this works as thymidine is taken up by cells and subsequently phosphorylated to thymidine-monophosphate (IMP) and thymidine-triphosphate (TIP). The accumulation of TIP then results in a feedback inhibition of other nucleoside triphosphates, particularly deoxycytidine-triphosphate (dCTP) which is critical for DNA synthesis (29). Detailed cell synchronization protocols followed during my experiments are described in appendix B (v), page B3 In figure 5.11 the results of CHO-K1 and HEK-293 cells synchronized at the M and S phases of the cell division cycle are shown and provide evidence of the influence of cell synchronization on the photo-transfection efficiency.

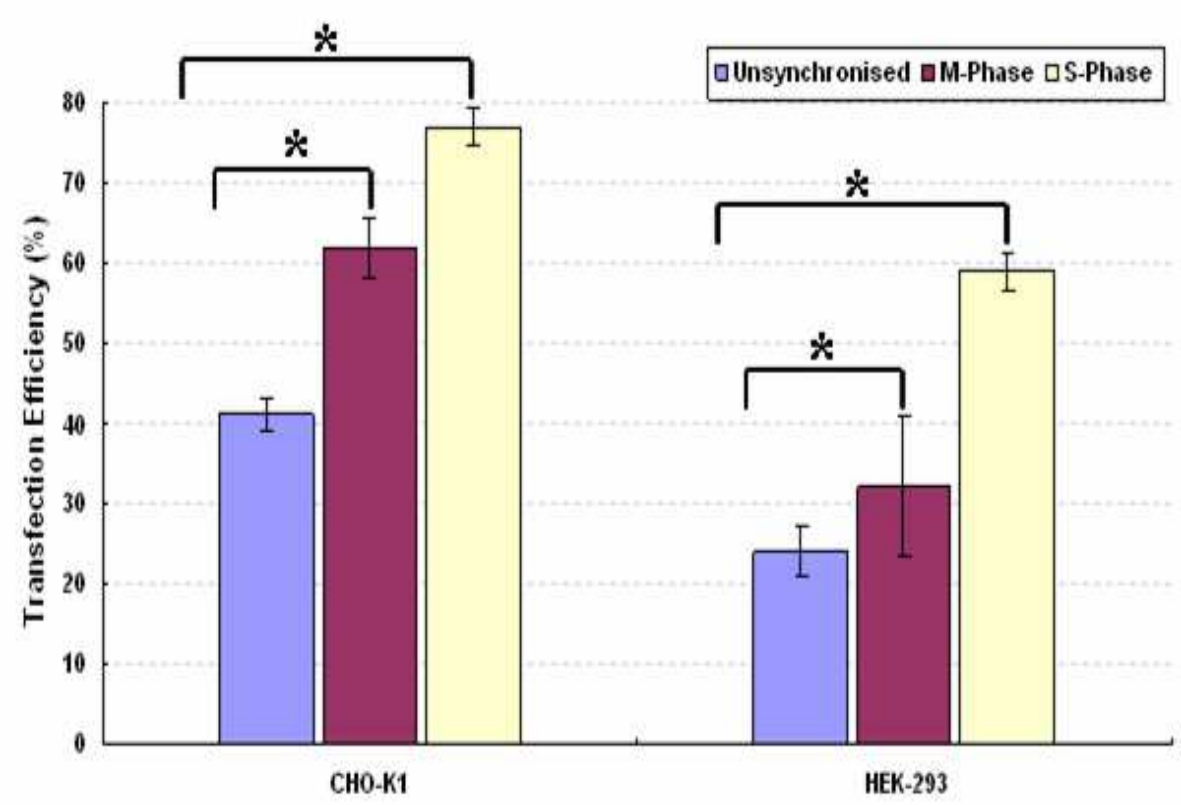

Figure 5.11: Arresting CHO-K1 and HEK-293 at the M-phase gave a higher photo-transfection compared to cells treated while at random stages of the cycle. However, arresting at the S-phase gave highly enhanced photo-transfection efficiency; this was observed in both cell lines. The corrected values of transfection efficiency are presented. Error bars represent the SEM (n = 3 experiments of 50 dosed cells). Using ANOVA followed by Dunnett's and Fisher's tests: * means data sets are significantly different from each other within the different cell lines. Appendix B (viii) pages B13-B15 shows full statistical analyses of this data. Reprint by permission from *Journal of Biomedical Optics* (3).

5.6 Investigation of cellular stress induced post photo-transfection

Next, I performed a study investigating potential cellular stress responses post photo-transfection. The up-regulation of the stress sensing heat shock protein 70 (hsp70) was tested during photo-transfection of mammalian cells. Heat shock proteins are a family of functionally related stress proteins whose synthesis is enhanced through subjecting cells to elevated temperatures or other stresses (30). Members of this stress protein family particularly hsp70 are highly responsive to temperature variations.

Hsp70 is a molecular chaperone and plays a key role in a complex of genetic network that allows the organism to respond to lethal effects of stress (31). Schlesinger 1990 (32), report that in mammalian cells, hsp70 is also synthesized for several other reasons than just to indicate heat shock stresses. Various literature reports have indicated no compromising of the cell viability in photo-transfected cells (33). This is particularly the case when using infrared laser beam as a delivering tool since thermoelastic and/or heating effects are not a major consideration (5).

However, to explore whether intracellular stress responses are activated by this process, I made use of HSP-CHO-K1 and HSP-NG108-15 cells. These are mammalian cells which had been previously stably transfected with the promoter of the heat shock protein 70 (hsp70) fused to the green fluorescent protein (GFP). Thus for these cells when they are exposed to a cellular stress e.g. an increase in temperature between 39 and 45^{o}C, the heat shock promoter hsp70 is activated and hence GFP is synthesized and the cells fluoresce green. Appendix B (vi), page B3 gives a full description on the stable transfection of CHO-K1 and NG108-15 cells with the HSP70 promoter gene. The results in figure 5.12 show that when the cells were heat shocked by incubating them in a 45^{o}C oven for half an hour, upregulation of the hsp70 gene promoter occurred for both HSP-CHO-K1 and NG108-15 cells, but there was a difference when they were exposed to the laser treatment (i.e. 60 mW, 40 ms). The laser irradiated HSP-NG108-15 cells displayed no GFP synthesis and expression meaning no up-regulation of the hsp70 promoter, while for HSP-CHO-K1 cells there was a detectable switching “on” of the hsp70 promoter gene. Morphological differences between these two types of cell lines may explain the reason for this result obtained after cells were laser irradiated.

CHO-K1 cells normally have a top surface that bulges up and is axially deeper providing easier targeting during photo-transfection shots but this cell feature also causes easier micro-explosion and/or photo-damage if the beam focus is improperly aligned to the cell surface. On the other hand when compared to CHO-K1 cells, NG108-15 cells are more naturally flat (shallow z-direction) making it slightly harder to align the plasma membrane with the beam during photo-transfection in this case.

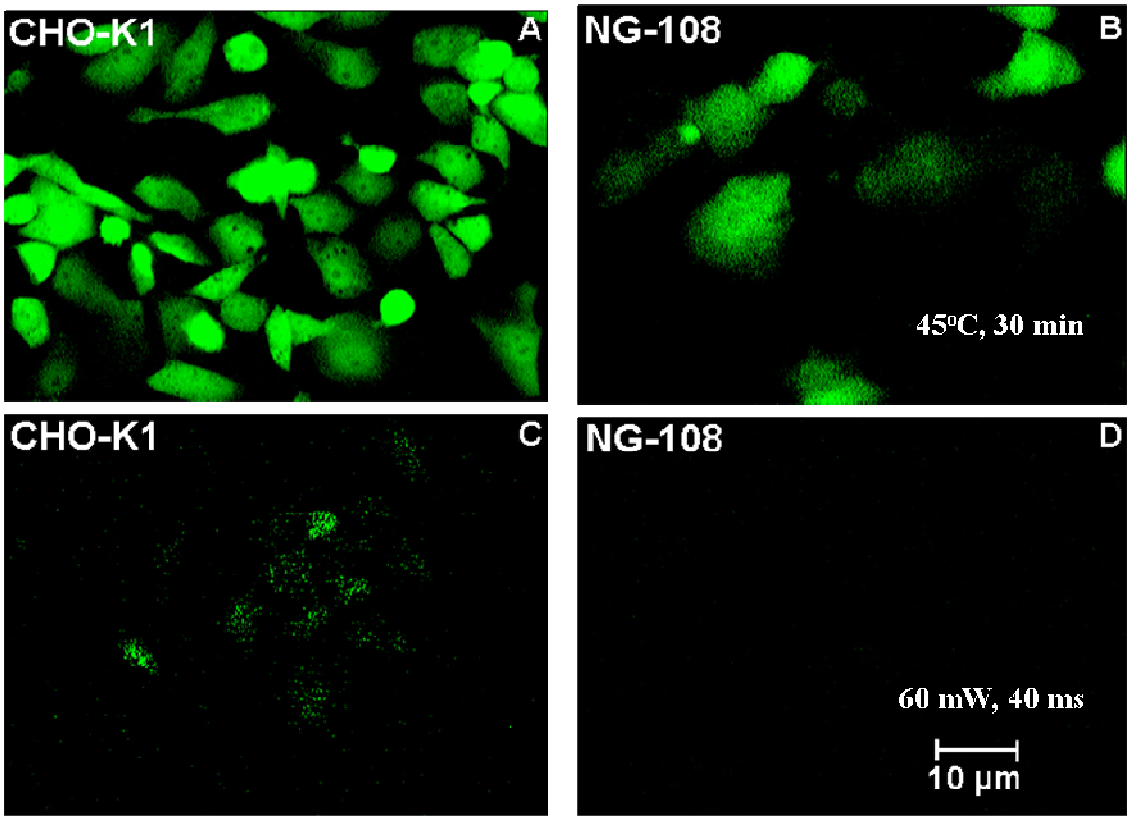

Figure 5.12: Captured images of stably transfected HSP-CHO-K1 and HSP-NG108-15 cells. Displayed in images A & B are fluorescent cells as a result of heat induced (incubated at 45°C, for 30 min) hsp-70 upregulation. In pictures C & D the cells were irradiated at 60 mW and 40 ms in the absence of DNA. In the case where the cells were irradiated HSP-NG108-15 (D) cells displayed no GFP synthesis and expression meaning no upregulation of hsp70 occurred, while HSP-CHO-K1 (C) cells indicated a slight (~ 23 % - quantified via Matlab) "on" switching of the hsp70 promoter gene.

5.7 Photo-transfection with messenger RNA (mRNA)

Earlier in this chapter I described the transcription and translation procedures, showing the processing of genes into proteins post the introduction of foreign pDNA into eukaryotic cells. In this section the introduction of mRNA which is delivered directly into the cytosol via photo-transfection is described. Although both DNA and RNA are nucleic acids they have two major structural differences. These differences include dissimilarity in the five-carbon (pentose) sugar component of the nucleotides. Deoxyribose, the sugar component of DNA, has one less hydroxyl group than ribose, the sugar component of

RNA. The second difference is in the selection of nitrogenous bases. Adenine (A), guanine (G) and cytosine (C) are common to both nucleic acids. However, thymine (T) is unique to DNA as a different base called uracil (U) is unique to RNA (figure 5.13).

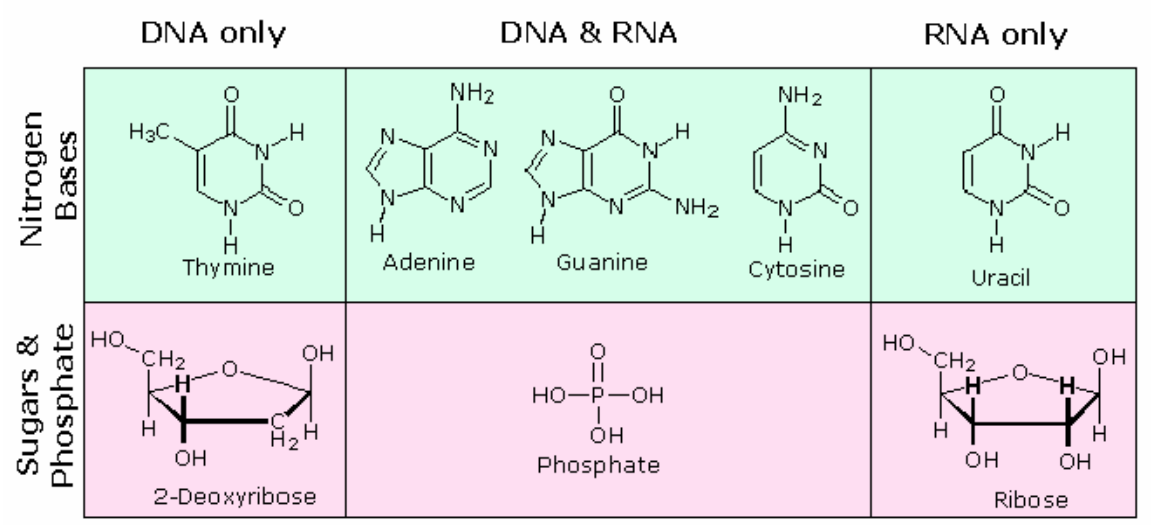

Figure 5.13: DNA (deoxyribose nucleic acid) and RNA (ribose nucleic acid) are both nucleotide polymers. These molecules are very similar but there are some distinct differences between them. Both molecules are helical structures but DNA is a double helix whereas RNA is a single helix. DNA is made up of the nucleotides Adenine (A), Thymine (T), Cytosine (C) and Guanine (G). RNA is also made up of A, G and C but T is replaced with Uracil (U). Another distinct nucleotide difference between them is that DNA has one less oxygen on the 5 carbon sugar than RNA; this accounts for the difference in their names. Deoxyribose simply refers to a ribose sugar lacking an oxygen molecule (online access date - 26.12.09 (34)).

Because of its inherent structural stability particularly when inserted into plasmids, in most transfection experiments DNA has mainly been a genetic material of choice. Contrarily, use of RNA for transfection purposes in the past was avoided due to its rapid nuclease degradation during *in vitro* experiments as well as the inability to obtain it in sufficient amounts. Nonetheless, since Malone *et al*, 1989 (35) reported on the successful use of cationic lipids to deliver mRNA into NIH 3T3 mouse cells, there has been several examples of the employment of RNA in the field of gene therapy. In fact, transfection of *in vitro-transcribed* mRNA into targeted cells and/or their subcellular regions is an

efficient method to achieve transient transgene expression. Once delivered to the cytoplasm, mRNA is rapidly translated and in contrast to expression DNA plasmids, with mRNA transfection there is no requirement for nuclear transfer. This advantage not only allows protein expression within minutes after the intracellular introduction of RNA (36, 37), but also opens an opportunity to successfully target even quiescent and post-mitotic cells which lack the cell cycle-dependent breakdown of the nuclear envelope (22). Cytoplasmic processing of RNA thus implies that mRNA can be relied upon to express therapeutic proteins within slowly dividing or post mitotic (non-cycling) cells. The other attraction to using RNA instead of DNA for transfection is its lack to integrate into the host genome, meaning no risk for insertional mutagenesis, an important advantage during clinical gene therapy trials (38).

Several transfection agents have been employed for the intracellular delivery of mRNA in cells. Mainly reported in literature is the use of cationic lipids (39, 40). But some reports mention the use of polycations for mRNA delivery, examples include poly (L-lysine) (41). Interestingly, exogenous mRNA can be selectively introduced into eukaryotic cells via photo-transfection. Barrett *et al*, 2006 (36), reported on targeted photo-transfection of mRNA into rat hippocampal neurons. In this study they demonstrated the effect of the site specific delivery of *Elk1* mRNA, where photo-transfection of this transcript into the cell's dendrite resulted in cell death whilst the cells remain viable through introduction of *Elk1* mRNA into the cell's body. This behaviour of cells was attributed to the possibility of having different post-translational modifications occurring in dendrites versus those taking place in the cell body. From the findings of Barrett *et al*, 2006 (36) fascinating biological investigations are coming into illumination. Also with photo-transfection playing a special role of allowing region specific targeting of cells, specific biological consequences of a local cellular environment can be analysed in detail. In another literature report, Wu *et a*l, 2007 (37) dendrites are described to account for most postsynaptic sites in the nervous system. They further report that dendrites also possess an active role of the local splicing and translation of RNA. In addition they present information that soma free dendrites are able to translate proteins and that dendrites are capable of removing introns of precursor mRNA.

Through all this information they concluded that protein translation from the RNA moving between the nucleus and the dendrite versus translation directly from dendritic RNA will result into varying cellular events. Such findings create a niche for even more fundamental biological questions and with technologies such as photo-transfection that allow site specific addressing and subsequent delivery of different types of exogenous naked nucleic acids into cells, numerous biological questions can be answered. Since there is a crucial requirement towards the understanding of mRNA photo-transfection experiments, during my studies I performed preliminary experiments aimed at optimizing the photo-transfection conditions required for targeted delivery of mRNA into CHO-K1 cells. Appendix B (vii), page B4 explains the methodology followed during this experiment.

Subsequent to mRNA photo-transfection, the cells were monitored under fluorescence microscopy in the presence of a FITC filter every half an hour for the first 12.5 hours post laser treatment after which they were then analysed on six hour intervals. It was noted that from roughly six to eight hours following mRNA photo-transfection, the cells started displaying a weak and punctuate fluorescence signal that became more prominent and uniform with time as the cells received further incubation at $37^{o}C$, 6 % CO_2 and 85 % relative humidity. At roughly 12 hours post treatment fluorescence signal was strong enough to capture images (figure 5.14) of the transfected cells as well as to quantify the mRNA transfection efficiency. Notably, at roughly 18 to 24 hours the fluorescence signal started to fade away and was completely diminished at roughly 36 – 42 hours. The results shown in figure 5.14 indicate successful protein translation following optical introduction of the *in vitro* transcribed EGFP mRNA even though this occurred within the first 12 hrs of treatment rather than within minutes as reported in literature. The other crucial observation to note is the time course dependent increase and subsequent decrease of the synthesized protein together with its consequent green fluorescence signal during this experiment.

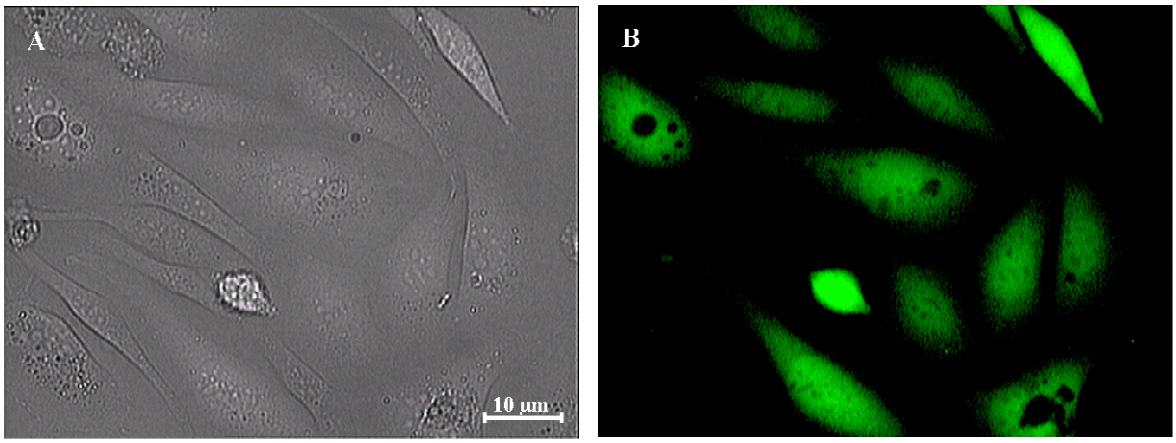

Figure 5.14: Preliminary data of live CHO-K1 cells photo-transfected at 60 mW and 40 ms with 15 µg/ml of *in vitro transcribed* EGFP mRNA. Image (A) is the brightfield picture and (B) its fluorescent version captured using a 20X objective lens of NA 0.54 twelve hours following photo-transfection. The transfection efficiency calculated as previously mentioned (section 5.2.4 and appendix B (vi)) was ~ 35 %.

5.8 Discussion

Photo-transfection is becoming an applicable transfection technology. This technique allows the delivery of both molecular and non-molecular particles of various sizes into mammalian cells. Key characteristics to this all optical methodology include its ability to keep cell viability intact, retain the quality of genetic materials being introduced, producing a minimum immunogenic response and its use under sterile tissue culture protocols. During all the photo-transfection experiments undertaken in my studies three different types of negative controls were run. These were labelled: 1. laser /no DNA, i.e. cells irradiated using the laser conditions mentioned above (60 mW, 40 ms) in the absence of DNA, 2. DNA /no laser, i.e. cells allowed incubating at room temperature in 60 µl of transfection mixture (10 µg/ml DNA or 15 µg/ml mRNA made up in OptiMEM) for ± 20 min and 3. No DNA /no laser, i.e. cells allowed incubating at room temperature in 60 µl OptiMEM for ± 20 min. For all three negative controls no fluorescence was detected, meaning no intracellular transportation of any exogenous material was possible. This observation led to a confirmation that merely bathing cells in the presence of whatever foreign naked genetic or non-genetic matter does not amount to its intracellular

inclusion in the absence of perforation. Thus during the photo-translocation (dry run with trypan blue) experiments, the induction of transient pores on the cell plasma membrane allowed the intracellular accumulation of the trypan blue viability dye with the influx occurring in a matter of seconds after optical treatment. Although the trypan blue experiment was performed at high laser irradiation energies, this experiment displayed successful membrane permeabilization and intracellular diffusion of the extracellular dye. Due to realized cell blebbing subsequent to cell irradiation at 200 mW and 40 ms during the photo-translocation studies and to therefore preserve cell viability, the different types of cell lines were photo-transfected using lower power setting (irradiance).

The ability to specifically tailor the optical transfection conditions and parameters during photo-transfection renders this technique versatile. This statement is supported by the data presented in all the results in this chapter. Whereas on photo-transfecting neuroblastomas, it was discovered that identifying optimal laser time of exposure as well as the average power output was of critical importance. This was because at more photo-toxic conditions, (e.g. 130 mW, 10 ms) the neuroblastoma cells could not be transfected but they rather died. It is worth noting that, Martinez et al, 2003 (9) in their electroporation studies discovered that compared to non-neuronal cells, neurons were more difficult to transfect. They attributed this finding to the fact that neurons recover more poorly from permeabilization and also express transgenes less effectively compared to other cell types. Neurons are also reported as one of the examples of non-renewing cell types (42). The poor behaviour of neuroblastomas post treatment at 130 mW/ 10 ms might therefore be associated with the fact that this optical dosing did induce irreparable damage leading to the slight cellular recovery post permeabilization. However, both CHO-K1 and HEK-293 cells did successfully photo-transfect at 130 mW and 10 ms although it was with a lower efficiency compared to a gentler treatment of 60 mW and 40 ms. This behaviour of the different cell types to the different transfection conditions elucidate that during photo-transfection studies, cell sensitivity can be accounted for and the conditions can be specifically optimised. Targeted delivery addressing individual cells during photo-transfection is also an exceptional feature. This is because morphological change particularly in adherent cells is influenced by range of biochemical

changes within the cells. For example, adherent cells round up either during cytokinesis or when dying. The ability to then during an experiment target distinctively spindled or stellate shaped cells increases the attraction of photo-transfection as a method of choice when working with adherent cell lines.

It appears that there is a strong dependency of the photo-transfection efficiency to the cell passage number. Therefore for future studies, it is imperative to establish the passage number under which a cell line is at to optimise transfection efficiency. The effects of passage number on cell lines are intricate and can be influenced by factors such as the type of cell line, the tissue and species of its origin, and also the culture conditions of the cells (21). As results my studies indicate, a passage considered high for one cell type may not necessarily lead to any significant passage effects in another. On analyzing the transfection efficiency data obtained and presented from particularly the bell-like shapes of figures in 5.5 (A), 5.6 (B) and 5.7 (C), it became apparent that there is a certain optimum point where the transfection efficiency reaches a peak after which it begins to decline. Hughes *et al*, 2007 (43) state that, when kept in culture for an extended period cell lines show a reduced or altered function thereby failing to represent reliable models of their original source material. It is known that on working with cell populations specifically cells grown as *in vitro* cultures, that no two cells are exactly the same. And this population inhomogeneity in cultured cells can be brought about via a number of changes, including culture passage numbers. The difference in passage number peaks may also be attributed to a difference in the number of cells in metaphase per passage during the time the experiments are performed. For an example, Yu *et al*, 2006 (44) in their cell cycle analysis studies, revealed that mouse fetal fibroblast cells at passage 3 contained the highest % of metaphase cells compared with mouse oviductal epithelial cells and mouse granulosa cells at the same passage. Therefore, the fact that the cells are also at different stages of the division cycle also plays a role here.

My results also demonstrated the influence of the metabolic state of the cells on transfection efficiency. In fact, in cells photo-transfected while synchronised at the S phase, the efficiency of transfection was significantly higher than in cultures treated

while synchronised in the M phase and even those in a non-arrested state. Notably a photo-transfection efficiency of ~ 80 % for CHO-K1 rivals many chemically induced methodologies. This observation therefore demonstrates that the photo-transfection efficiency reflects cell cycle dependency. This effect was also reported for the improvement of both transient and stable cell transfection efficiencies using electroporation technology, where cells were synchronized in the G2/M phase and then treating them with butyrate (23). This combination allowed a decrease of electroporation voltage and DNA concentration while greatly enhancing the transfection efficiency. Brunner et al, 2000 (22), reported that transfection efficiency is strongly dependent on the cell cycle phase with S/G2 cells giving 30 to 500 fold greater levels of transfection than G1 cells. My results showed that arresting cells at two different stages of the cell cycle can significantly enhance photo-transfection efficiency, with those arrested in the S-phase the most efficient. The reasons for this are dependent on the processes occurring in the different phases of the cell cycle. In the M-phase, the nuclear membrane disappears and as a result gene transfection efficiency increases as plasmid DNA can easily access the nuclear machinery (22, 45). Whilst in the S-phase, this is the point in the cycle where DNA is synthesized, thus plasmid DNA will be also copied and transcribed increasing its overall copy number and thus subsequently allowing more transcription.

Although photo-thermal stresses play no role in cells photo-transfected through pulsed infra-red laser beams, cell thickness (axial depth) may contribute to negligible cellular stress and /or damage during laser treatment. This is displayed by my data of when HSP-CHO-K1 and HSP-NG180-15 cells were irradiated in the absence of plasmid DNA. The HSP-NG108-15 cells which are axially flat compared to the HSP-CHO-K1 cells expressed no upregulation of the hsp70 promoter gene. It is worth noting that, even in the positive control that was incubated at 45^{o}C HSP-NG108-15 (figure 5.12 B) displayed a milder upregulation of the hsp70 promoter gene compared to the HSP-CHO-K1 cells. This result illuminates the fact that, cell thickness (roundness) somehow plays a role in triggering potential minor cellular stress during photo-transfection experiments. On the contrary though, hsp70 induction has been reported to provide a cytoprotective role (46, 47). For example, in literature it is reported that HSPs are expressed in the stomach and

possess a protective influence against mucosal injury (47). This finding should therefore not be disregarded, as the upregulation of the hsp70 promoter especially in the irradiated HSP-CHO-K1 cells may be associated with cellular protection rather than cellular damage.

Notably, in contrast to other methodologies, photo-transfection permits the delivery and expression of small molecules including mRNA into specific subcellular regions within cells (36), and also the ability of targeting individual cells within a population of cells. Although in my mRNA photo-transfection studies protein expression was fully detectable as of 12 hrs post photo-transfection rather than within minutes. This might have been because the experiment was performed using non-neuronal cells with the CHO-K1 cells not necessarily photo-transfected on the dendrite. Wu *at al*, 2007 (37) revealed that the protein translation time courses in soma and dendrites can differ. They further report that during their investigations, upon metabotropic receptor (a subtype of membrane receptors at the surface or in vesicles of eukaryotic cells) activation, a slow increase in GFP fluorescence takes place in the soma, whereas that in the dendrite shows a much more rapid increase. Hence in cells such as CHO-K1 which are normally irradiated on the cell body (soma) and lack prominent dendrites as those present in neurons, protein expression took muck longer. In addition it is also reported that the difference in the dynamics of protein synthesis in dendrites as opposed to those in soma proposes that for RNA translation, the location might serve different roles in cellular function (37). In my investigations the fluorescence intensity was seen to vary during the different time periods of analysis and it initially appeared in a punctuate fashion (interspaced fluorescent patches) before becoming uniform throughout the cells. This heterogeneous nature for protein translation might be linked to the dispersed location of the ribosomes within the cytoplasm and the time-dependent increase of protein expression has been reported in literature (36).

In summary I have shown that fs laser photo-transfection has the ability of becoming a standard transfection method, as it now has the ability of transfecting cells at a high efficiency, a wide variety of cell-types, but with the additional capability of being

targeted when required. I explored new parameters about this process, initially showing that this technology can be applied to a variety of different cell types. Now in the next chapter I will display the capability to photo-transfect successfully mouse embryonic stem (mES) cells both in a targeted manner but also with the ability of transforming these cells into a new cell type.

References

1. D. Voet and J. G. Voet, Biochemistry, John Wiley & Soons (1995).
2. http://elizabetholin.tripod.com/central_dogma_of_life.htm,
3. P. Mthunzi, K. Dholakia and F.Gunn-Moore, "Phototransfection of mammalian cells using femtosecond laser pulses: optimization and applicability to stem cell differentiation " *J Biomed.Opt.* **15**, 041507 (2010)
4. X. Tsampoula, V. Garces-Chavez, M. Comrie, D. J. Stevenson, B. Agate, C. T. A. Brown, F. Gunn-Moore and K. Dholakia, "Femtosecond cellular transfection using a nondiffracting light beam," *Appl. Phys. Lett.* **91**, 053902-053903 (2007)
5. A. Vogel, J. Noack, G. Huttman and G. Paltauf, "Mechanisms of femtosecond laser nanosurgery of cells and tissues," *Appl. Phys. B-Lasers O.* **81**, 1015-1047 (2005)
6. R. K. Schlicher, H. Radhakrishna, T. P. Tolentino, R. P. Apkarian, V. Zarnitsyn and M. R. Prausnitz, "Mechanism of intracellular delivery by acoustic cavitation," *Ultrasound in medicine & biology* **32**, 915-924 (2006)
7. D. C. Chang, B. M. Chassy, J. A. Saunders and A. E. Sowers, "Guide to electroporation and electrofusion," *New York: Academic Press* (1992)
8. P. L. McNeil and R. A. Steinhardt, "Plasma membrane disruption: Repair, prevention, adaptation," *Annual Review of Cell and Developmental Biology* **19**, 697-731 (2003)
9. C. Y. Martinez and P. J. Hollenbeck, "Transfection of primary central and peripheral nervous system neurons by electroporation," *Method Cell Biol.* **71**, 339-351 (2003)
10. Tsukakoshi, Kurata, Nomiya, Ikawa and Kasuya, "A novel method of DNA

transfection by laser microbeam cell surgery," *Appl. Phys. B-Photo.* **35**, 135-140 (1984)

11. D. Stevenson, F. Gunn-Moore, C. Campbell and K. Dholakia, "Transfection by optical injection," *The Handbook of Photonics for Biomedical Science,* **Chapter 3**, 87-117 (2010)

12. G. M. Brodeur and R. C. Seeger, "Gene amplification in human neuroblastomas: basic mechanisms and clinical implications," *Cancer Genet Cytogenet* **19**, 101-111 (1986)

13. A. C. Passaquin, W. A. Schreier and J. Devellis, "Gene-Expression in Astrocytes Is Affected by Subculture," *International Journal of Developmental Neuroscience* **12**, 363-372 (1994)

14. L. Jacobsen and P. Hughes, "Effects of passage number on cell line transfection," *Biochemica* **3**, 32 (2007)

15. M. Esquenet, J. V. Swinnen, W. Heyns and G. Verhoeven, "LNCaP prostatic adenocarcinoma cells derived from low and high passage numbers display divergent responses not only to androgens but also to retinoids," *J Steroid Biochem Mol Biol* **62**, 391-399 (1997)

16. H. S. Yu, T. J. Cook and P. J. Sinko, "Evidence for diminished functional expression of intestinal transporters in Caco-2 cell monolayers at high passages," *Pharmaceutical research* **14**, 757-762 (1997)

17. M. J. Briske-Anderson, J. W. Finley and S. M. Newman, "The influence of culture time and passage number on the morphological and physiological development of Caco-2 cells," *Proc Soc Exp Biol Med* **214**, 248-257 (1997)

18. I. Behrens and T. Kissel, "Do cell culture conditions influence the carrier-mediated transport of peptides in Caco-2 cell monolayers?," *Eur J Pharm Sci* **19**, 433-442 (2003)

19. Y. Sambuy, I. Angelis, G. Ranaldi, M. L. Scarino, A. Stammati and F. Zucco, "The Caco-2 cell line as a model of the intestinal barrier: influence of cell and culture-related factors on Caco-2 cell functional characteristics," *Cell Biology and Toxicology* **21**, 1-26 (2005)

20. C. M. Chang-Liu and G. E. Woloschak, "Effect of passage number on cellular response to DNA-damaging agents: cell survival and gene expression," *Cancer Lett* **113**,

77-86 (1997)

21. ATCC, "Passage number effects in cell lines," *ATCC Technical Bulletin* (2007)

22. S. Brunner, T. Sauer, S. Carotta, M. Cotten, M. Saltik and E. Wagner, "Cell cycle dependence of gene transfer by lipoplex, polyplex and recombinant adenovirus," *Gene Ther.* **7**, 401-407 (2000)

23. S. Goldstein, C. M. Fordis and B. H. Howard, "Enhanced transfection efficiency and improved cell survival after electroporation of G2/M-synchronized cells and treatment with sodium butyrate," *Nucleic Acids Res.* **17**, 3959-3971 (1989)

24. M. Musiani and M. Zerbini, "Influence of cell cycle on the efficiency of transfection with purified human cytomegalovirus DNA," *Arch Virol* **78**, 287-292 (1983)

25. M. N. Jha, J. R. Bamburg and J. S. Bedford, "Cell-Cycle Arrest by Colcemid Differs in Human Normal and Tumor-Cells," *Cancer Research* **54**, 5011-5015 (1994)

26. E. W. Taylor, "The Mechanism of Colchicine Inhibition of Mitosis. I. Kinetics of Inhibition and the Binding of H3-Colchicine," *J Cell Biol* **25**, SUPPL:145-160 (1965)

27. R. Kuriyama, "Effect of colcemid on the centriole cycle in Chinese-hamster ovary cells," *J. Cell Sci.* **53**, 155-171 (1982)

28. http://www.le.ac.uk/ge/genie/vgec/images/cellcycle.png,

29. P. J. O'Dwyer, S. A. King, D. F. Hoth and B. Leyland-Jones, "Role of thymidine in biochemical modulation: a review," *Cancer Res.* **47**, 3911-3919 (1987)

30. I. J. Benjamin and D. R. McMillan, "Stress (heat shock) proteins: molecular chaperones in cardiovascular biology and disease," *Circ. Res.* **83**, 117-132 (1998)

31. O. Lipan, J. M. Navenot, Z. Wang, L. Huang and S. C. Peiper, "Heat shock response in CHO mammalian cells is controlled by a nonlinear stochastic process," *PLoS Comput. Biol.* **3**, 1859-1870 (2007)

32. M. J. Schlesinger, "Heat shock proteins," *J. Biol. Chem.* **265**, 12111-12114 (1990)

33. D. Stevenson, B. Agate, X. Tsampoula, P. Fischer, C. T. A. Brown, W. Sibbett, A. Riches, F. Gunn-Moore and K. Dholakia, "Femtosecond optical transfection of cells: viability and efficiency," *Opt. Express.* **14**, 7125-7133 (2006)

34. http://www.cem.msu.edu/~reusch/VirtualText/Images3/dna_rna1.gif,

35. R. W. Malone, P. L. Felgner and I. M. Verma, "Cationic Liposome-Mediated Rna Transfection," *Proceedings Of The National Academy Of Sciences Of The United States*

Of America **86**, 6077-6081 (1989)

36. L. E. Barrett, J. Y. Sul, H. Takano, E. J. Van Bockstaele, P. G. Haydon and J. H. Eberwine, "Region-directed phototransfection reveals the functional significance of a dendritically synthesized transcription factor," *Nat. Methods.* **3**, 455-460 (2006)

37. C. W. Wu, F. Zeng and J. Eberwine, "mRNA transport to and translation in neuronal dendrites," *Analytical and bioanalytical chemistry* **387**, 59-62 (2007)

38. T. J. L. Van De Parre, W. Martinet, D. M. Schrijvers, A. G. Herman and G. R. Y. De Meyer, "mRNA but not plasmid DNA is efficiently transfected in murine J774A.1 macrophages," *Biochemical and Biophysical Research Communications* **327**, 356–360 (2005)

39. D. Lu, R. Benjamin, M. Kim, R. M. Conry and D. T. Curiel, "Optimization of Methods to Achieve Messenger-Rna-Mediated Transfection of Tumor-Cells in-Vitro and in-Vivo Employing Cationic Liposome Vectors," *Cancer Gene Ther* **1**, 245-252 (1994)

40. K. Kariko, A. Kuo and E. S. Barnathan, "Overexpression of urokinase receptor in mammalian cells following administration of the in vitro transcribed encoding mRNA," *Gene Ther.* **6**, 1092-1100 (1999)

41. K. J. Fisher and J. M. Wilson, "The transmembrane domain of diphtheria toxin improves molecular conjugate gene transfer," *Biochemical Journal* **321**, 49-58 (1997)

42. McNeil, Miyake and Vogel, "The endomembrane requirement for cell surface repair," *Proceedings of the National Academy of Sciences* **100**, 4592-4597 (2003)

43. P. Hughes, D. Marshall, Y. Reid, H. Parkes and C. Gelber, "The costs of using unauthenticated, over-passaged cell lines: how much more data do we need?," *Biotechniques* **43**, 575-586 (2007)

44. J. N. Yu, S. F. Ma, D. Q. Miao, X. W. Tan, X. Y. Liu, J. H. Lu and J. H. Tan, "Effects of cell cycle status on the efficiency of liposome-mediated gene transfection in mouse fetal fibroblasts," *J Reprod Dev* **52**, 373-382 (2006)

45. M. Golzio, J. Teissie and M. P. Rols, "Cell synchronization effect on mammalian cell permeabilization and gene delivery by electric field," *Biochim. Biophys. Acta.* **1563**, 23-28 (2002)

46. K. Tanaka, T. Namba, Y. Arai, M. Fujimoto, H. Adachi, G. Sobue, K. Takeuchi, A. Nakai and T. Mizushima, "Genetic evidence for a protective role for heat shock factor

1 and heat shock protein 70 against colitis," *J. Biol. Chem.* **282**, 23240-23252 (2007)

47. T. Shibata, T. Arisawa, T. Tahara, D. Yoshioka, N. Maruyama, H. Fujita, Y. Kamiya, M. Nakamura, M. Nagasaka, M. Iwata, K. Takahama, M. Watanabe, I. Hirata and H. Nakano, "Protective Role of Genetic Polymorphism of Heat Shock Protein 70-2 for Gastric Cancer Risk," *Digest Dis. Sci.* **54**, 70-74 (2009)

Chapter 6

Photo-transfection and the differentiation of embryonic stem cells

Introduction

In chapter 5 I showed that femtosecond lasers can be used to photo-transfect a range of different cell lines proving the versatility and applicability of this methodology. Herein I show for the first time that this novel technology also allows transfection of mouse embryonic stem (mES) cell colonies. Stem cells are thought to be capable of advancing current therapies for tissue regeneration and/or engineering, which makes the cell-based technology very attractive. Thus, in this chapter mES cell colonies were not only photo-transfected to express a gene encoding red fluorescent protein, but also induced to differentiate into a specific tissue type via photo-transfection with the Gata-6 transcription factor. Initially in this chapter an introduction of stem cells and their employment as a therapy is described.

Thereafter, I illustrate the photo-transfection setup employed throughout the mES cell experiments, describing the cell sample preparation as well as the photo-transfection protocol. Then, the experimental results showing successful photo-transfection of E14g2a mouse embryonic stem cells using pDsRed2-Mito plasmid DNA are described. Following this, I present laboratory data showing the photo-transfection and subsequent differentiation of these pluripotent cells into extraembryonic endoderm (ExE) using a transcriptional factor, Gata-6 plasmid. This cellular differentiation result was supported by an observable morphological alteration of E14g2a colonies and also by a biochemical analysis using reverse transcriptase PCR (rtPCR) to monitor the upregulation of Gata-4 transcription factor and the downregulation of Oct-4 and Nanog pluripotency transcriptional factors, thus proving stem cell differentiation.

6.1 Stem cells, their use as a cell-based therapy

Organ transplants are now a routine procedure. However, with the shortage of organ donors and potential immunological rejection, these are the two major challenges leading to transplant failure. Several possible solutions to both these problems are being tried and tested. Autologous grafts, involving the harvesting of tissue from one part of the body to repair another are often performed to avoid immunological rejections. Another possible solution to avoid potential immunological rejections and that also eliminates the necessity of employment of whole organs and/or tissue, is the use of special cells called stem cells. As stem cells are undeveloped (non-specialized) cells, they possess the ability to become any type of cell and so form any type of tissue including bone, muscle, nerve etc. This is because of their self-renewal and pluripotency characteristics which renders them with the potential to advance current therapies in tissue regeneration and/or engineering. Hence, with stem cell therapy, the idea is to somehow isolate such cells, multiply and process them *in vitro* to eventually utilize them in the replacement of damaged tissue. Many disease conditions could then be treated in this manner.

There are many different types of stem cells and these are present at all stages of an organism's life from the early embryo to adult stages. Nonetheless the ideal option in facilitating stem cell based therapy would be through the isolation of embryonic stem from a patient, which might be difficult for treatment of adult patients. But technologies such as the nuclear transfer (cloning) technique have provided a platform for reversing the normal direction of cell differentiation; resulting in the reprogramming of the nucleus of an adult cell, thus allow suitable stem cells to be engineered from an adult cell. The two potential methods for obtaining suitable stem cells for cell-based therapy which are also ideal for patient-specific purposes are illustrated in figure 6.1.

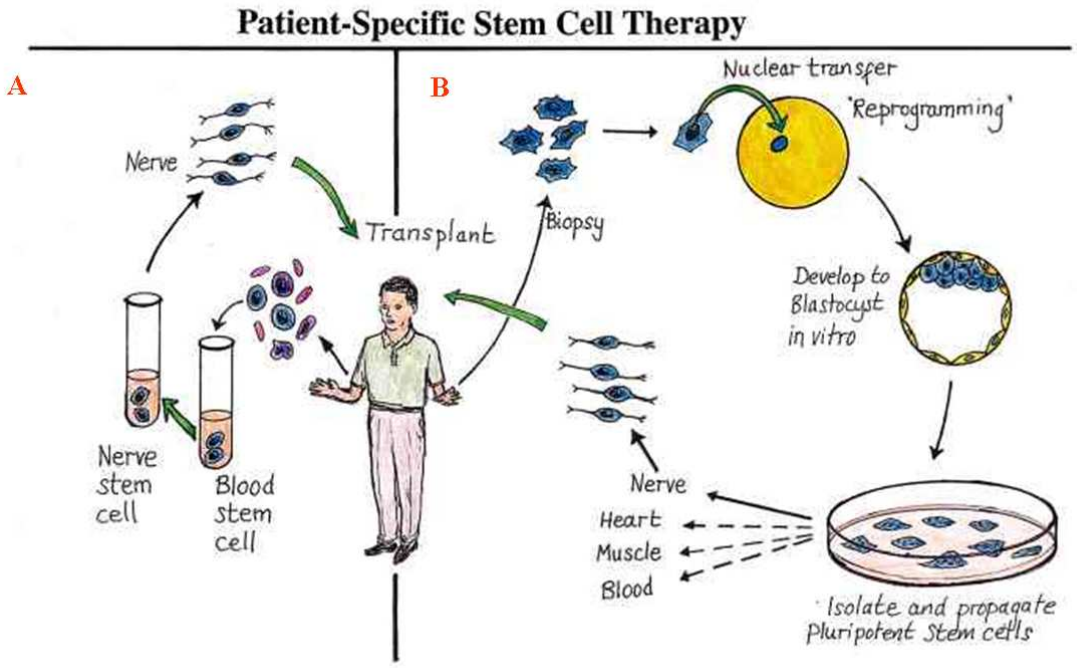

Figure 6.1: In (A) on the left side of the figure, stem cells are obtained for therapy via redirecting one type of adult stem cells into another i.e. blood to nerve stem cells in this example. In (B) on the right side, an adult cell is reprogrammed into an early embryo cell to generate the necessary stem cells (online access date – 7. 1.10 (1)).

One of these methods involves the isolation and subsequent reprogramming of one kind of stem cells into another type of stem cell. For instance, in figure 6.1 (A) is depicted blood stem cells converted into nerve stem cells, which in turn could be used to cure various kinds of nerve cell disorders. On the contrary, cell nuclear replacement technology is where a biopsy is collected from a patient and by nuclear transfer, reprogramming of an adult cell into an early embryo is achieved (figure 6.1 (B)). The latter is achieved through removing the oocyte's (unfertilized egg) own nucleus and replacing it with that of an adult donor cell's nucleus resulting in the artificial creation of an embryo. The availability of the embryonic stem cells would then be through an *in vitro* culturing of the blastocyst stage and the later harvesting of its inner cell mass. Embryonic stem cell differentiation performed using a host of various techniques would then permit the formation of various cell types relevant for cell based therapies that are also patient-

specific. Some of the diseases for which stem cell research is projected to benefit are: heart disease, spinal cord lesions, non-union of fractured bones, Parkinson disease, Huntington disease, type 1 diabetes, corneal & retinal lesions, motor neuron disease, cerebrovascular disease, Alzheimer disease and muscular dystrophy (2).

One of the advantages of the use of laser light for investigating biological materials, particularly stem cells, is that it promotes limited use of reagents and chemicals that can interfere with the physiological properties of these therapeutic cells. More work on optical manipulation of stem cells further endorses the fact that there is normally minimal requirement for use of chemicals during optical experiments used in studying and answering biological questions. Uchugonova et al, 2008 (3) investigated the two-photon excited autofluorescence of multipotent human stem cells and the onset of collagen production of differentiated cells through detection of second harmonic generation signals at 435 nm. In this paper they also report that multiphoton microscopes hold novel non-invasive ability for marker-free optical stem cell characterization. Further in their other paper they reported on the optical cleaning of stem cells based on highly precise multiphoton processing using ultrashort near infra-red fs laser pulses. This was performed to isolate single cells of interest in order to inactivate undesirable single cells within three dimensional stem cell clusters (4). Thus, the ability to photo-transfect embryonic stem cells is highly desirable, especially because this transfection technique promotes the introduction of chemical-free naked pDNA.

The two major kinds of mammalian stem cells comprise of embryonic stem cells (from embryos) as well as adult stem cells (mainly from bone marrow). Generally embryonic stem cells are able to differentiate into all of the different specialized embryonic tissue. On the contrary, adult stem cells act towards the body's repair system, replenishing specialized cells as well as maintaining the normal turnover of regenerative organs such as blood, skin, intestinal tissue, etc. Stem cells vary in the diversity of their differentiation descendants and are classified as totipotent (zygote stem cell), pluripotent (embryonic stem cells), multipotent (adult stem cells) (5). During my studies I made use of pluripotent mouse embryonic stem (mES) cells, these were both photo-transfected to

express a foreign plasmid and were also optically induced to differentiate into a new cell type.

In both *in vivo* and *in vitro* investigations preservation of mainly pluripotent stem cells is of critical importance. As a result, recent literature reports on the dedifferentiation techniques allowing the reprogramming of fully differentiated cells into induced pluripotent stem cells that closely resemble ES cells in their developmental potency. Nuclear replacement technology (figure 6.1 (B)) is one way of achieving this but Takahashi *et al*, 2006 (6) demonstrated the induction of pluripotent stem cells from mouse embryonic and adult fibroblasts by introducing (via retroviral transduction) into these cells four pluripotency transcription factors known as Oct3/4, Sox2, c-Myc and Klf4 under ES cell culture conditions. These four and various others (e.g. Nanog) are crucial factors that are necessary to maintain pluripotency and a key feature reflecting the developmental capacity of ES cell lines is that in early embryo they express such markers of pluripotency. Therefore core transcription factors are required and essential to maintain the undifferentiated state in ES cells. These factors activate genes that are necessary for ES cell survival and proliferation while repressing target genes that are activated only during differentiation.

Stem cell based-therapy, their properties, differentiation pattern and lineage commitment are all essential biology topics currently under significant investigation in literature. However, there still remains a pressing necessity to answer the biological questions concerning how the renewal and differentiation programs are operated and regulated at the genetic level. Genetic manipulation such as delivery of exogenous gene expression or knockout with small interfering RNA (siRNA) is relatively rare in ES cells. The ability of ES cells and adult stem cells to differentiate into specific cell types holds immense potential for therapeutic use in cell and gene therapy. Realization of this potential depends on efficient and optimized protocols for genetic manipulation of stem cells.

The remainder of this chapter presents experiments where I investigated photo-transfection of pluripotent stem cells and also optically induced differentiation of these cells.

6.2 Photo-transfection of pluripotent stem cells using a femtosecond laser

Several non-viral gene delivery methods for mES cells such as liposome based vectors; electroporation and nucleofection have been developed to avoid the safety issues of viral vector based gene transfer. Previous literature reports 20 – 70 % ES cell transfection efficiency using the effectene liposome based transfection system (7). Further, Ward *et al*, 2002 (8) reported 50 – 80 % transfection efficiency expression of plasmid EGFP in five undifferentiated mES cells lines (BL/6III, D3, E14TG2a, MESC20 and 129) on using the lipofectamine transfection reagent in mES cells. Another study displayed that using EGFP as a reporter gene, nucleofection produced a ten fold transient transfection efficiency (i.e. 63.66 %) of mES cells compared to 6.41 % transfection efficiency achieved via electroporation (9).

Photo-transfection is becoming an attractive methodology for the transfection of stem cells as these cells are important for cell-based therapies. The first optical transfection of stem cells was reported by Uchugonova *et al*, 2008 (10) where they report on preliminary data obtained during optical transfection of individual human pancreatic and salivary gland (multipotent) stem cells using sub-20 femtosecond laser pulses of mean powers < 7 mW (figure 6.2). They further reported that the transfection of stem cells is a major challenge for transfection technologies using either a chemical, mechanical or electrical means. In their experiments, it was claimed that this problem was overcome by gently creating transient nanoholes in the cellular membrane by low power i.e. 5 – 7 mW (66 – 93 pJ at 75 MHz) and 50 – 100 ms of sub-20 fs laser pulses which resulted without any collateral damage and disturbance of the self-repairing potency of these cells (10). Compared to delivering 200 fs laser pulses as was the case in my photo-transfection experiments, these ultra-short pulses of sub-20 fs duration have a very short time

bandwidth which allows for significantly higher peak power to be obtained per pulse even at very low irradiances (average power).

Figure 6.2: Photo-transfected human salivary gland stem cells imaged three days after laser transfection in the presence of 0.2 µg of pDNA vector pEGFP-N1 suspended in 5 ml extracellular medium (reprint by permission from *Optics Express* (10)).

Using sub-20 fs laser pulses for their photo-transfection studies allowed precise membrane perforation, in the absence of collateral damage and a transfection efficiency of 70 – 80 % in multipotent stem cell lines. During my experiments using 200 fs, 50 mW and 40 ms laser pulses at the beam focus, mouse embryonic stem cell colonies were not only photo-transfected to express a gene encoding red fluorescent protein (pDsRed2-Mito), but also induced to differentiation into ExE via photo-transfection with the Gata-6 transcription factor. Appendix C (pages C1-C2) covers the methodology followed for pluripotent stem cell culturing and plasmid preparation.

6.3 Sample preparation and photo-transfection

For photo-transfection experiments, the E14g2a cells were seeded at approximately 10^6 cells/ml and plated in gelatin coated 35 mm diameter type zero glass bottomed petri dishes (23 mm diameter = glass working area, *World Precision Instruments, Stevenage, UK*). These cells were suspended in 2 ml of complete growth medium when incubated to sub-confluence over 24 hrs in optimum growth conditions.

Then the cell colonies were carefully washed twice with 2 ml of serum-free KDMEM each time, to remove the serum. Thereafter they were submerged in 60 µl of serum-free medium containing 10 µg/ml of pDsRed2-Mito plasmid DNA (pDNA). The sample chamber was then covered with a 22 mm diameter type-1 coverslip (*BDH, Poole UK*). Targeted photo-transfection of individual cell colonies was then performed via laser irradiation through administering three shots of ultra-short duration while avoiding a visual cellular response. Irradiation of the adherent stem cell colonies facilitated by targeted delivery of the infrared fs laser beam pulses (50 mW and 40 ms) permitted diffusion of surrounding plasmid DNA into individual groups of stem cells per colony. Following laser irradiation the DNA containing medium was aspirated, the stem cell colonies washed once with serum-free KDMEM, covered in 2 ml complete medium and incubated under optimum growth conditions for 48 hrs before live cell colony fluorescence analysis and imaging.

6.4 Expression of pDsRed2-Mito in E14g2a cell colonies post photo-transfection

In my studies a 25 % transfection efficiency of mES cell colonies using the DsRed2-Mito plasmid DNA was achieved. Figure 6.3 below depicts successful photo-transfection of non-differentiated pluripotent E14g2a stem cells, also indicating the possibility of the selection and targeted treatment of specific cells within a mass of cells.

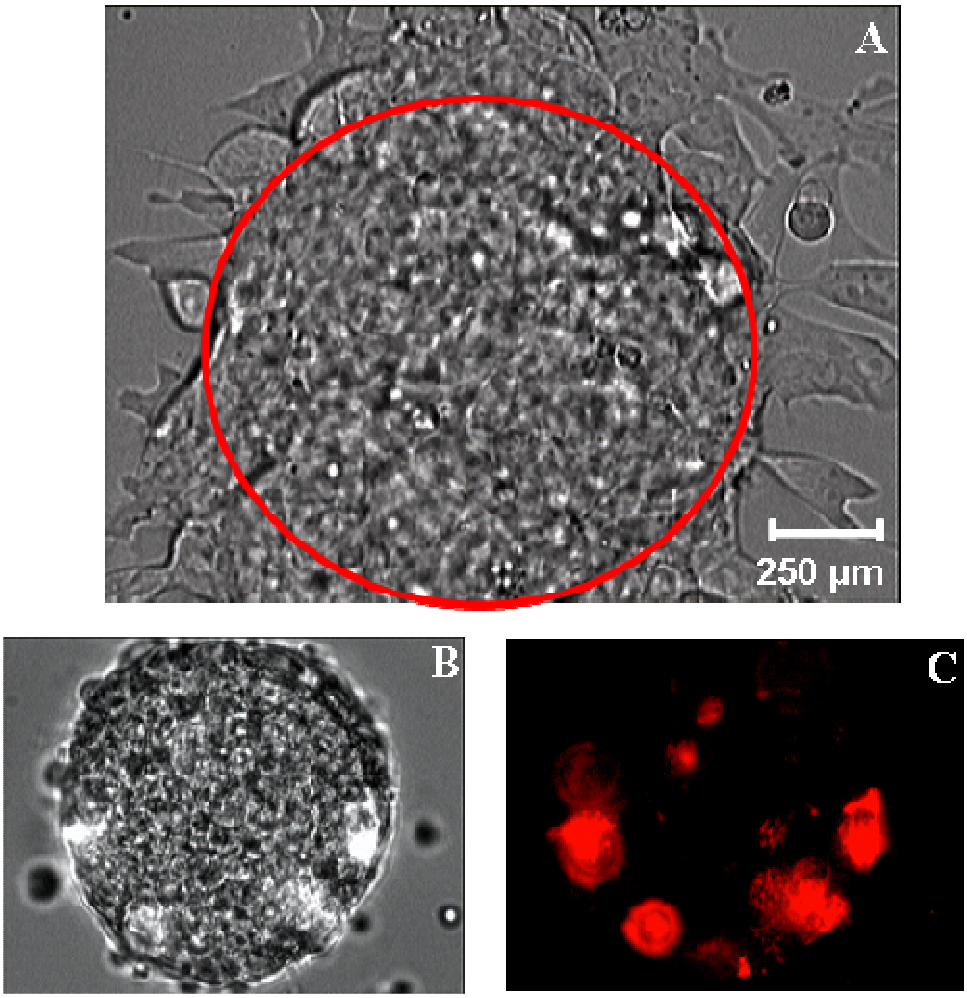

Figure 6.3: A 50 X Mitutoyo long working distance objective lens (NA 0.55) was used to capture image A displaying a brightfield view of the E14g2a cells. Surrounded within the red circle is the sample of interest i.e. the non-differentiated cell colony. 10 µg/ml of DsRed2-Mito pDNA was photo-transfected into these cells at 50 mW and 40 ms. 48 hrs later a 10 X Nikon objective lens (NA 0.25) was employed to capture images B (brightfield image) and C (fluorescent image) in the presence of a TRITC filter cube (reprint by permission from *Journal of Biomedical Optics* (11)).

6.5 Investigating stem cell differentiation via photo-transfection

Following successful photo-transfection of the pluripotent cells, the possibility of taking this technology an important step further was explored. Previously I have commonly photo-transfected a fluorescent reporter gene into various mammalian cells. However, within the field of stem cell biology it would be a significant step forward to use

physiologically relevant genes. Indeed, Uchugonova et al, 2008 (3) reported on an urgent requirement in stem cell research on technologies for noninvasive, marker-free observation of growth, proliferation and stability of living stem cells under physiological conditions. In their studies, through the detection of second-harmonic generation signal, they investigated two-photon excited autofluorescence of human stem cells and the onset of collagen production of differentiated cells.

Expressed in the ExE are numerous transcription factors, GATA factors and hepatocyte nuclear factors (HNFs). Both Gata-6 and Gata-4 are reported to be master regulator candidates because loss of function of either of these factors results in loss of function of all HNFs (12). Notably, mES (E14g2a) cells can be differentiated into extraembryonic endoderm by the activation of the transcriptional factor Gata-6. Thus, using the sample preparation and photo-transfection parameters established in both section 6.3 and appendix C, the endoderm associated transcription factor Gata-6 gene was optically introduced into E14g2a cells. Specifically, post seeding and plating as previously mentioned, these cells were photo-transfected with 15 µg/ml of naked Gata-6 expressing plasmid DNA at 40 ms pulse duration, 50 mW average power levels at the focus. After laser treatment the cells were rinsed with serum free KDMEM and incubated in optimum growth conditions in complete medium without LIF but selecting with 200 µg/ml of hygromycin (*Invitrogen, UK*). The LIF-free medium was changed every two days. As a result of the Gata-6 induced differentiation events, a morphological change in E14g2a cells 96 hrs post optical treatment was observed. Figure 6.4 displays pictures of this result, showing an altered morphology of E14g2a colonies producing identifiable individual cells with spindle and stellate shaped morphology which is characteristic of extraembryonic endoderm tissue (12, 13).

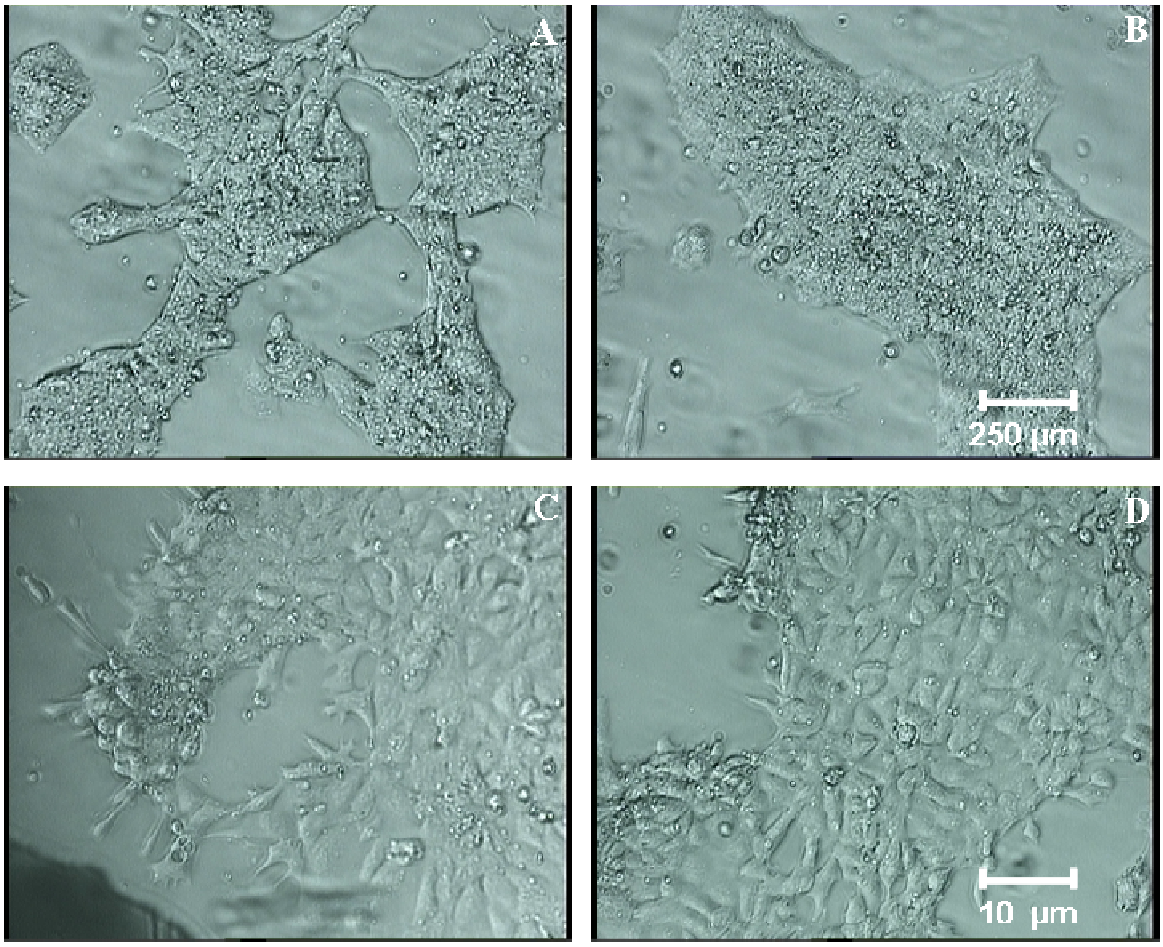

Figure 6.4: Photographs A & B (negative controls) are brightfield images of the E14g2a cell colonies 48 hrs post routine sub-culturing, growing in the presence of LIF. Obtained 96 hrs after photo-transfection at 50 mW, 40 ms with the Gata-6 vector, images C & D are the morphologically altered E14g2a cells selected in the presence of LIF. All pictures were captured through a 10 X Nikon microscope objective lens (NA 0.25) (reprint by permission from *Journal of Biomedical Optics* (11)).

To biochemically confirm this morphological change the differentiated cells were tested by reverse transcriptase PCR (rtPCR) for the expression of key transcriptional factors. To achieve this, total RNA was isolated from differentiated ES cells by trizol reagent (Invitrogen, UK). For rtPCR analysis, cDNA was synthesized from 5 µg of total RNA, with an oligo-dT primer and transcriptor reverse transcriptase (RT) (*Roche, UK*). One twentieth of the single strand cDNA products were utilized for each PCR amplification experiment. PCR was performed according to the manufacture's instructions using the

readymix taq PCR reaction kit (*Sigma, UK*). Primer (*Eurofins, UK*) sets (Gata-4 = 469 bp, Oct-4 = 455 bp and Nanog = 425 bp) described by Fujikura *et al*, 2002 (12) were used at 10 picomoles (pmol) and 40 cycles per reaction. In figure 6.5 the upregulation of Gata-4 (marker towards cell differentiation) and downregulation Oct-4 and Nanog (pluripotency marker) transcription factors is demonstrated.

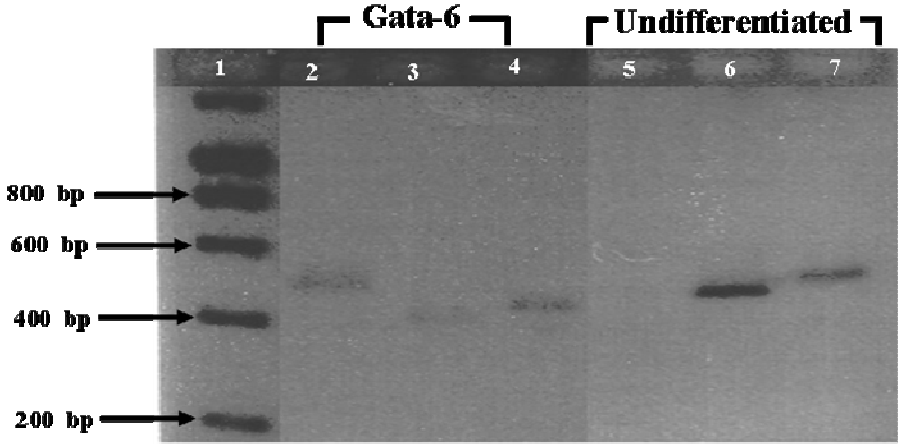

Figure 6.5: rt-PCR analysis of germ layer markers. Lane 1: Molecular weight marker: Hyperladder 1 molecular weight marker (*Bioline*), Lane 2: rtPCR product for Gata-4, Lane 3: rtPCR product for Oct-4, Lane 4: rtPCR product for Nanog gene transcripts in differentiated cells (Gata-6). Lane 5: rtPCR product for Gata-4, Lane 6: rtPCR product for Oct-4, Lane 7: rtPCR product for Nanog gene transcripts in undifferentiated cells. This experiment was repeated three times (reprint by permission from *Journal of Biomedical Optics* (11)).

The results confirm that the stem cells have been differentiated as can be seen: firstly the amplification of Gata-4 (lane 2) in the Gata-6 photo-transfected cells as compared to the undifferentiated cells (lane 5) and secondly down-regulation of both Oct-4 and Nanog (lanes 3 & 4) in the differentiated cells as compared to the undifferentiated cells (lanes 6 & 7). These observations are in agreement with what has been previously observed and reported for these transcription factors (12). To further verify successful ES cell differentiation following optical delivery of the Gata-6 transcription factor, future

experiments will involve direct sequencing of the PCR products (more in particular the Gata-4 band) from the agarose gel slices.

6.6 Discussion

In this chapter the possibility to use new photo-transfection parameters for targeted transient transfection of mES cells was explored for the first time. Previously, electroporation and liposome-mediated methods were the most commonly used methods to transfect mES cells. However, electroporation has been reported to have typical transient mES transfection efficiency of less than 10 % (9). Although offering improvement to both the stable and transient mES transfection efficiencies, chemical transfection via reagents can lead to the change in metabolism of these cells and limit their use as a cell-based therapy. For example, liposome-based methods are reported to promote ES cell differentiation since the protocol of this cell transfection method requires that the cells be exposed to serum free conditions (9). The risk of spontaneous differentiation of stem cells under serum-free conditions could lead to heterogeneity within the ES cell population, hence, complicating and altering *in vitro* stem cell investigations. Stem cell differentiation means loss in "stemness" and gain in specialization, as a result, transfection reagents might lead to loss of the very critical mES cell properties. For instance the ability to maintain their potency and expression of stem cell markers such as Oct4, Sox2, Nanog, Sall4, CDX2, TEA, etc, post genetic manipulation is desirable. This is because these and many more transcription factors are responsible for preserving cell lineages and preventing stem cell plasticity.

The experimental data presented in this chapter shows how an all optical system as photo-transfection (naked pDNA introduction) can be used for genetic introduction into pluripotent cells. Thus, the problems of cytotoxicity and stem cell population heterogeneity resulting from using other cell transfection methodologies can be avoided. Compared to the optical parameters used by Uchugonova *et al*, (10) of 5 – 7 mW (66 – 93 pJ at 75 MHz) and 50 – 100 ms of sub-20fs laser pulses, during my investigations ~

200 fs laser pulses (790 nm) at 50 mW (0.76 nJ at 80 MHz) and 40 ms were employed to successfully introduce the DsRed2-Mito reporter gene with 25 % efficiency in pluripotent stem cells. This result is very interesting as ES cell lines can assist in the understanding of pathological diseases including the origin of cancers, testing the efficacy of drugs and in monitoring the development of genetic disorders. For instance, for genetic disorders human ES cell lines could be constructed from affected blastocysts identified at pre-implantation genetic testing.

Notably, the protocol used in my studies has the capability to photo-transfect successfully mES both in a targeted manner but also with the ability of transforming these cells into a new cell type. The controlled ability of ES cells and adult stem cells to differentiate (non-spontaneous differentiation) into specific cell types holds immense potential for therapeutic use in cell and gene therapy. Both the morphological and biochemical results displayed by figures 6.4 & 6.5 prove that E14g2a cells can be optically induced to differentiate into extraembryonic endoderm by the activation of the transcriptional factor Gata-6. There was downregulation of the pluripotency transfection factors (Oct4 and Nanog) in the differentiated cells. Also the production of the cell differentiation transcription factor, Gata-4, post introduction of Gata-6 confirmed successful differentiation of the E14g2a cells. The capability to optically induce stem cell differentiation at will indeed guarantees a non-invasive and marker-free treatment of mES cells. This is a very attractive result as the genetic manipulation such as delivery of exogenous genes is relatively rare in ES cells. Photo-transfection therefore provides an ideal method for transfecting both pluripotent and multipotent stem cells. However, future studies will concentrate on making the technology more efficient.

References

1. http://easyweb.easynet.co.uk/~sfl/rlb_stem.htm,

2. B. E. Tuch, "Stem cells: A clinical update," *Australian Family Physician* **35**, 719-721 (2006)

3. A. Uchugonova and K. Konig, "Two-photon autofluorescence and second-harmonic imaging of adult stem cells," *J. Biomed. Opt.* **13**, 054068 (2008)

4. A. Uchugonova, A. Isemann, E. Gorjup, G. Tempea, R. Buckle, W. Watanabe and K. Konig, "Optical knock out of stem cells with extremely ultrashort femtosecond laser pulses," *J Biophotonics* **1**, 463-469 (2008)

5. P. C. Park, S. Selvarajah, J. Bayani, M. Zielenska and J. A. Squire, "Stem cell enrichment approaches," *Semin Cancer Biol* **17**, 257-264 (2007)

6. K. Takahashi and S. Yamanaka, "Induction of pluripotent stem cells from mouse embryonic and adult fibroblast cultures by defined factors," *Cell* **126**, 663-676 (2006)

7. L. Bugeon, N. Syed and M. J. Dallman, "A fast and efficient method for transiently transfecting ES cells: application to the development of systems for conditional gene expression," *Transgenic Res* **9**, 229-232 (2000)

8. C. M. Ward and P. L. Stern, "The human cytomegalovirus immediate-early promoter is transcriptionally active in undifferentiated mouse embryonic stem cells," *Stem Cells* **20**, 472-475 (2002)

9. U. Lakshmipathy, B. Pelacho, K. Sudo, J. L. Linehan, E. Coucouvanis, D. S. Kaufman and C. M. Verfaillie, "Efficient transfection of embryonic and adult stem cells," *Stem Cells* **22**, 531-543 (2004)

10. A. Uchugonova, K. Konig, R. Bueckle, A. Isemann and G. Tempea, "Targeted transfection of stem cells with sub-20 femtosecond laser pulses," *Opt. Express.* **16**, 9357-9364 (2008)

11. P. Mthunzi, K. Dholakia and F.Gunn-Moore, "Phototransfection of mammalian cells using femtosecond laser pulses: optimization and applicability to stem cell differentiation " *J Biomed.Opt.* **15**, 041507 (2010)

12. J. Fujikura, E. Yamato, S. Yonemura, K. Hosoda, S. Masui, K. Nakao, J. Miyazaki and H. Niwa, "Differentiation of embryonic stem cells is induced by GATA factors," *Genes Dev.* **16**, 784-789 (2002)

13. P. Mthunzi, K. Dholakia and F.Gunn-Moore, "Photo-transfection of mammalian cells using femtosecond laser pulses: optimisation and applicability to stem cell differentiation," *Journal of Biomedical Optics* **15**, (2010)

Chapter 7
Conclusion

This thesis presented 6 chapters starting with a short introduction of the impact of laser sources of different regimes in the Biophysics research. A brief discussion on the employment of optical forces to tweeze, as well as sort mammalian cells was provided. In addition, pulsed fs laser-assisted cell transfection (photo-transfection), which is a non-invasive and innovative technique was also presented. These in conjunction with other Biophotonics applications are helping to illuminate our understanding of single cell and biomolecule structure and function. All of which are critical subjects for the establishment of solutions to complex biochemical, biophysical and biomedical problems.

In chapter 2, I outlined the forces governing the optical tweezing procedure; specifically the mechanisms for trapping Mie particles as during all my experiments the diameter of the materials to be manipulated was large compared to the trapping or guiding beam. A description of how the optical trap efficiency is measured was described to create an understanding of the Q-value experimental data reported in chapter three. Thereafter the construction of a basic optical tweezing setup was provided, followed by a demonstration of 3D optical trapping (dominant gradient force) of 3 μm polymer microspheres using a diffraction limited beam spot of a 658 nm diode laser (page 20-21). To avoid photo-damage (optocution) of biological material during optical treatments NIR lasers were mostly used and therefore an overview of the laser wavelengths suitable for biological material was provided. The employment of optical forces in optical cell guiding and/or deflection as well as optical cell sorting was also explored. In addition a comprehensive study was presented describing the arrangement of a two dimensional TEM_{00} mode beam optical trap, with a prominent scattering force utilized for optical guiding purposes. Finally a review was outlined of optical cell sorting with a specific emphasis on immunological (both macroscopic and microscopic) versus non-immunological as well as optical sorting schemes with and without fluid flow. This was described to highlight the

advantages and disadvantages of each methodology.

Experimental results on optical trapping, guiding and sorting of intracellularly tagged mammalian cells during my studies were described in chapter 3. The refractive index of various mammalian cell lines commonly used in biological laboratories was enhanced by allowing the cells to phagocytose 2 and 3 µm polymer spheres (n = 1.59). During phagocytosis a series of biochemical events leads to the engulfment of particles found within the extracellular environment. In my studies, uptake of the inert polymer spheres promoted a cheap, toxic-free and less tedious tagging approach for the effective optical trapping, axial guiding and subsequent sorting of mammalian cells. Cell viability measurements via trypan blue viability assays confirmed the intracellular dielectric tagging approach to be safe and scanning laser confocal microscopy techniques detected internalized microsphere (pages 53-54) which were quantified using Labview particle tracking (figure 3.5, page 51). Therefore using this novel procedure, the influence of the intracellular dielectric tags on the scattering and gradient forces during three dimensional trapping and optical guiding experiments was demonstrated for the first time. My results indicate that, the optical trapping efficiency of cells which had encapsulated microspheres in a diffraction limited beam spot obtained through the use of a high NA lens was higher than that of non-tagged cells (page 59-60). This is because cells lacking the dielectric tags have a low refractive index and so have poor optical trapping capability. Although, this 3D optical trap had a smaller Rayleigh range and trapping beam spot, it was able to successfully trap both tagged and non-tagged cells as it is with this geometry that the gradient force is stronger than the scattering force. My results show that in a bigger laser beam spot with a larger Rayleigh range, then using a low NA lens, the intracellular dielectric tags function as highly directional optical scatterers. Therefore, the axial optical guiding of cells that engulf a varying number of spheres compared to those without dielectric tags is enhanced (figures 3.12-3.13). In this optical arrangement, particle guiding rather than trapping was observed since the scattering force was stronger than the gradient force. This was further endorsed by the observation of lack of guiding of cells without microspheres while those tagged were axially deflected at faster (~ 30 to 60 µm/s) velocities.

Finally in this chapter, the improved axial guiding nature of cells with spheres was manipulated for levitating the intracellularly tagged cells onto laminin coated coverslips thereby optically sorting them from the rest of the cell sample. Therefore these studies provide the basis of a new technique where cells could be passively sorted in flow-free micro-sample chambers (roughly 80 µm depths) which would be a significant step forward in cell sorting experiments where the analyte size is in the micro liter volumes size range. This would be important in scenarios when using precious or rare biological samples. In addition these studies are cheap and could be adapted to microfluidic channels for the sorting of diseased cells from healthy cells.

Chapters 4 to 6 of this thesis were based on fs laser photo-transfection. Specifically, chapter 4 begins by explaining the biological significance of cell transfection, detailing the plasma membrane composition of eukaryotic cells in order to describe the complexity of the movement of exogenous matter through this boundary. As the hydrophobic core of the plasma membrane prevents the passage of the hydrophilic material some molecules are therefore impermeable to the plasma membrane. Protein transport systems that are highly specific for the substances they translocate, can permit selective transport. The chapter summarized the most developed cell transfection technologies emphasizing the advantages and disadvantages of each method. In addition, a description was provided on the implications for laser effects on biological cells and tissues. At MHz repetition rates and irradiances levels well below the optical breakdown, the interaction of fs pulses with the cell's plasma membrane leads to localized multiphoton ionizations which progressively results in free electron plasma formation. At these low irradiances, cumulative thermal effects play no role, since the time of duration of the pulses is shorter than the time scale of any thermal effects. The mechanism behind fs laser transfection is therefore predicted to be due to photochemical effects which results in membrane perforation, high resolution pore formation with minimum collateral damage (1).

Both chapters 5 and 6 demonstrate the novel photo-transfection experimental data obtained during my studies. Chapter 5 was started by explaining the molecular biology of how genes become proteins via describing the transcription and translation processes.

This was done in order to elucidate how foreign genes introduced into mammalian cells during the transfection process end up expressed by the receptive cells as fluorescent proteins. Following this, measurements of the femtosecond beam profile and pulse duration in a basic TEM_{00} beam upright photo-transfection setup were taken. Thereafter, the different cell lines were successfully photo-transfected with the DsRed2-Mito and EGFP expressing plasmid DNA. This included the previously difficult to transfect neuroblastoma cell lines which therefore indicated the versatility and applicability of the photo-transfection technique (Table 5.1, page 119). This chapter then addressed various aspects which influence the photo-transfection efficiency, such as the change in optical parameters i.e. the irradiance level (average power output) and time of beam exposure at the beam focus, to show that at lower irradiances higher transfection efficiency can be achieved compared to at higher irradiances (page 121-122). Also for sensitive cell types such as neuroblastomas no transfection was possible at higher irradiances of 130 mW and 10 ms time of beam exposure. At low irradiance levels and short time duration of the laser beam pulses at the focus, there are no cumulative thermal effects that may compromise cell viability and consequently the photo-transfection efficiency. So the optimum laser dose producing transfection efficiency between 40 and 60 % depending on the cell line under investigation was 60 mW and 40 ms beam exposure time at the laser focus. The results concerning the culture passage number indicated that the cell's age is critical during photo-transfection experiments as at higher passage numbers the transfection efficiency dropped (figure 5.9, page 127). At high passage numbers, cells undergo alterations in cell morphology, response to stimuli, growth rates, protein expression and signaling (2-4). Cell transfection poses additional stress on cultured cells since the expression of foreign proteins requires energy from the cells. Hence, the expression of the photo-transfected genes forces the cells to redirect energy required for cell growth and subsequently leads to a slower than normal growth rate. This might explain the drop in the photo-transfection efficiency obtained when CHO-K1 and HEK-293 cells were treated at higher passage numbers (beyond P34 and P31 in CHO-K1 and HEK-293 cells respectively). In addition, the metabolic state of the cell also influences the photo-transfection efficiency and can be manipulated to improve the efficiency. This was achieved by synchronizing the cells at distinctive stages of the cell division cycle.

Specifically, those which had been synchronized in the S-phase were most efficient (page 131). The reasons for this are dependent on the processes occurring in the different phases of the cell cycle. In the M-phase, the nuclear membrane disappears and as a result gene transfection efficiency increases as plasmid DNA can easily access the nuclear machinery. Whilst in the S-phase, this is the point in the cycle where DNA is synthesized, thus plasmid DNA will also be copied and transcribed therefore increasing its overall copy number and thus subsequently allowing more transcription. Notably a photo-transfection efficiency of ~ 80 % for CHO-K1 rivals many chemically induced methodologies.

During pulsed NIR laser transfection at MHz repetition rates, thermoelectric and/or heating effects are not a major consideration (1). To test this I used cell lines that were stably transfected with the stress sensing hsp70 promoter gene that is highly responsive to elevated temperatures or other stresses (5). The results indicated that there was no upregulation in the HSP-NG108-15 (figure 5.12, page 133) cells however hsp70 was switched on in the HSP-CHO-K1 cells (figure 5.12, page 133). This result might be associated with the observation that HSP-CHO-K1 cells occur to be axially thicker (rounder) compared to the morphologically flat HSP-NG108-15 cells. Cell thickness provides easier targeting of the cell membrane during targeted fs transfection shots. But also during experiments, rounder cells were observed to be more prone to laser focus-membrane interaction misalignments, which can result in micro-explosions as a result of micro-pore formation. The high resolution pore formation supports the idea that fs photo-transfection is a highly localized effect with minimum collateral damage. However, even at 60 mW and 40 ms mismatches between the fs laser beam focus and the cell plasma membrane during Gaussian beam photo-transfection, produce photochemical and cumulative thermal effects resulting in visual micro-pore formation and subsequent cell damage. For this reason, during Gaussian beam photo-transfection precise laser beam focus-plasma membrane alignments are a very critical requirement. Upregulation of the hsp70 gene in HSP-CHO-K1 cells may also be indicative of the cell's biochemical protection as the induction hsp70 can provide a cytoprotective role (6, 7). To further demonstrate versatility of the photo-transfection technique, the delivery and expression of

mRNA which is directly translated upon reaching the cytoplasm was also achieved. Results for this experiment demonstrated that although highly susceptible to nuclease degradation, mRNA could be successfully photo-transfected into CHO-K1 cells with 35 % transfection efficiency (page 137). In addition compared to plasmid DNA which normally takes 48 hrs before protein expression is observed, using mRNA protein expression was achieved 12 hrs post photo-transfection. For example, Barrett *et al*, 2006 (8), reported on targeted photo-transfection of mRNA into rat hippocampal neurons with protein expression achieved as early as half an hour post photo-transfection.

Finally in chapter 6, novel experimental data on the photo-transfection as well as differentiation of pluripotent stem cells was presented. I started the chapter by describing the use of stem cells as a cell-based therapy. This was done to highlight the importance of stem cells and the reason why it is essential to avoid use of chemicals during their *in vitro* handling and treatment. Although the employment of stem cells as a cell-based therapy offers the ability to revolutionalize the biomedical and gene therapy research fields, more experiments are required to further develop their genetic manipulation by expressing exogenous genes or gene knockout using siRNA. Therefore the development of optimized protocols for the genetic manipulation of stem cells would be highly desirable and so, I attempted to photo-transfect mES cells. I achieved the successful photo-transfection of E14g2a mES cells using pDsRed2-Mito plasmid DNA with approximately 25 % transfection efficiency (figure 6.3, page 155). Since photo-transfection promotes the delivery of naked plasmid DNA into cells, this technique can then be used to prevent problems of cytotoxicity and spontaneous differentiation associated with using other cell transfection techniques. In addition both morphological (figure 6.4, page 157) and biochemical (figure 6.5, page 158) data showed that differentiation of these cells into the ExE using the pCAGSIH-Gata-6 plasmid through photo-transfection was successfully achieved. This is a very significant result as the controlled ability of ES cells and adult stem cells to differentiate into specific cell types holds immense potential for therapeutic use in cell and gene therapy.

Considering projects reported in this thesis, future studies are aimed at more innovative laser light assisted Biophotonics investigations. For the optical cell sorting projects, since the polymer microspheres that were used in my investigations were non-digestible, future studies will involve using biodegradable spheres of higher refractive index (for example, the poly (dl-ε-caprolactone) microspheres (*Polysciences, Inc.*)). This will allow further analysis and characterization of the collected intracellularly tagged cells. In addition the adaptation of the intracellular cell tagging scheme to optically sorting cells in microfluidics and/or optical chromatography chambers with higher throughput might be pursued. By functionalizing the microspheres, it may also be possible in future studies to sort and separate healthy versus diseased cells. Uptake of microspheres by pathogenic cells might be facilitated by modifying the surface of the spheres with specific receptor molecules that target only the diseased cells. Future work will also involve modeling the spatial guiding of cells with spheres to investigate the intricate processes occurring at fundamental level.

For the photo-transfection work, since mRNA can be relied upon to express therapeutic proteins within slowly dividing or post mitotic (non-cycling) cells. Future studies might involve more mRNA photo-transfection experiments with the possibility to target quiescent and post-mitotic cells which lack the cell cycle-dependent breakdown of the nuclear envelope. Additionally, mRNA transfection poses no risk for insertional mutagenesis this might lead to future investigations involving the introduction of mRNA into pluripotent stem cells. Also, because within the field of stem cell biology, the capability to use more physiologically relevant genes examples including, stem cell markers such Oct4, Sox2, Nanog, Sall4, CDX2, TEA, etc. would be a significant step forward. Future studies will be therefore addressing this requirement. Since gene knockout methods serve as a powerful tool to understand the function of genes, another possible project may include photo-transfecting small interfering RNA (siRNA) into pluripotent stem cells. Manipulating the level of gene expression in these ES cells might assist in understanding the specific signaling pathways involved in their specification and differentiation processes. Photo-transfection efficiency of 25 % was obtained during my mES cell studies this might be improved in future studies by photo-transfecting using a

Bessel light beam (BB) instead of a Gaussian beam. Tsampoula *et al*, (9) demonstrated that using this non-diverging beam for photo-transfection eliminated the critical requirement for laser focus-plasma membrane alignment. Their results showed that when assuming the threshold for successful transfection efficiency to be 20 %, the axial range over which successful transfection is obtained using the BB was over twenty times greater compared to the TEM_{00} mode beam. For this reason, using the BB for photo-transfecting the E14g2a cell colonies might help enhance the transfection efficiency.

During the photo-translocation experiments, the induction of transient pores on the cell plasma membrane allowed the intracellular accumulation of the trypan blue viability dye with the influx occurring in a matter of seconds after optical treatment. This was due to successful membrane permeabilization and intracellular diffusion of the extracellular dye. However to study laser threshold energies required to reliably permeabilised a cell with a certain set of pulse parameters, future experiments will involve using propidium iodide instead of trypan blue. This should also allow direct determination of whether the cell is immediately lysed or it recovers, to thereafter die via the process of cell apoptotisis.

Minimum use of chemicals is not only attractive to stem cell research, arresting cells (CHO-K1 and HEK-293) at the S-phase and M-phases using thymidine double blocks and colcemid respectively was not only invasive but also time-consuming. Literature reports that using scanning and transmission electron microscopes indicated an increased height and roundness of adherent rat kangaroo cells (PtK2) in late anaphase (second last stage of the M-phase) (10). Thus, with the aim of developing a non-invasive method of estimating growth activity of adherent cells, Ito *et al*, (10) investigated the correlation between the laser phase shift determined using phase-shifting laser microscopy and the cell cycle phase of CHO cells. Their results showed that in the G2/M-phase, the laser phase shift was higher compared to that of cells in the G1/S-phase. In addition on determining the refractive indices of these cells, the refractive index of the G2/M cells was measured to be 1.47 while that of cells in the G1/S cells was 1.45. They used these refractive indices to calculate the height of the G2/M cells (2.24 ± 0.32) which was higher than the height of G1-phase (1.71 ± 0.32) and S-phase (1.63 ± 0.41) cells.

Future photo-transfection projects might therefore involve using imaging techniques for detecting the cell cycle phase of adherent cells rather than drugs or chemicals which may alter the biochemistry of cells and their plasma membrane.

Finally, as previously mentioned within this thesis laser light sources have played a huge role in the development of innovative Biophotonics research area. The major goal of most of these projects is aiming towards providing answers within the biomedical field. Therefore more laser-tissue and/or laser-cell interaction studies are required to promote an understanding of single cell and/or molecule structure and function. This could provide insight into the biochemistry of diseased cells and help develop valuable treatment regimes for a whole host of diseases.

Publications

Journal publications

1) K. Dholakia, W. M. Lee, L. Paterson, M.P. MacDonald, R. McDonald, I.Andreev, P. Mthunzi, C. T. A. Brown, R. F. Marchington and A. C. Riches, "*Optical separation of cells on potential energy landscapes: enhancement with dielectric tagging*", IEEE Journal of Selected Topics in Quantum Electronics **13**, 1646 – 1654, 2007.

2) P. Mthunzi, W. M. Lee, A. C. Riches, C.T.A. Brown, F. J. Gunn-Moore, and K. Dholakia, "*Intracellular dielectric tagging for improved optical manipulation of mammalian cells*"**,** IEEE Journal of Selected Topics in Quantum Electronics **16** (3), 608-618, 2009.

3) P. Mthunzi, K. Dholakia and F. Gunn-Moore, "*Photo-transfection of mammalian cells using femtosecond laser pulses: optimisation and applicability to stem cell differentiation*", Journal of Biomedical Optics, **15** (2), 041507 (1-7), 2010. Selected for

publication in: Virtual Journal of Ultrafast Science (Chemistry and Biophysics), **9** (8), 2010

4) P.C. Ashok, R.F. Marchington, P. Mthunzi, T. F. Krause and K. Dholakia, "O*ptical chromatography using a photonic crystal fiber with on-chip fluorescence excitation*", Optics Express **18** (6), 6396 – 6407, 2010. Selected for publication in: The Virtual Journal for Biomedical Optics (Microfluidics and Nanofluidics), **5** (7), 2010.

Attended Conference

1) CLEO/Europe conference-EQEC 2009: Conference on Lasers and Electro-Optics (CLEO) and European Quantum Electronics Conference (EQEC), Munich, ICM, Germany, "*Photo-transfection of mammalian cells via femtosecond laser pulses*", 14 -19 June, 2009 (Oral presentation).

References

1. A. Vogel, J. Noack, G. Huttman and G. Paltauf, "Mechanisms of femtosecond laser nanosurgery of cells and tissues," *Appl. Phys. B-Lasers O.* **81**, 1015-1047 (2005)
2. H. S. Yu, T. J. Cook and P. J. Sinko, "Evidence for diminished functional expression of intestinal transporters in Caco-2 cell monolayers at high passages," *Pharmaceutical research* **14**, 757-762 (1997)
3. M. J. Briske-Anderson, J. W. Finley and S. M. Newman, "The influence of culture time and passage number on the morphological and physiological development of Caco-2 cells," *Proc Soc Exp Biol Med* **214**, 248-257 (1997)
4. C. M. Chang-Liu and G. E. Woloschak, "Effect of passage number on cellular response to DNA-damaging agents: cell survival and gene expression," *Cancer Lett* **113**, 77-86 (1997)

5. I. J. Benjamin and D. R. McMillan, "Stress (heat shock) proteins: molecular chaperones in cardiovascular biology and disease," *Circ. Res.* **83**, 117-132 (1998)

6. K. Tanaka, T. Namba, Y. Arai, M. Fujimoto, H. Adachi, G. Sobue, K. Takeuchi, A. Nakai and T. Mizushima, "Genetic evidence for a protective role for heat shock factor 1 and heat shock protein 70 against colitis," *J. Biol. Chem.* **282**, 23240-23252 (2007)

7. T. Shibata, T. Arisawa, T. Tahara, D. Yoshioka, N. Maruyama, H. Fujita, Y. Kamiya, M. Nakamura, M. Nagasaka, M. Iwata, K. Takahama, M. Watanabe, I. Hirata and H. Nakano, "Protective Role of Genetic Polymorphism of Heat Shock Protein 70-2 for Gastric Cancer Risk," *Digest Dis. Sci.* **54**, 70-74 (2009)

8. L. E. Barrett, J. Y. Sul, H. Takano, E. J. Van Bockstaele, P. G. Haydon and J. H. Eberwine, "Region-directed phototransfection reveals the functional significance of a dendritically synthesized transcription factor," *Nat. Methods.* **3**, 455-460 (2006)

9. X. Tsampoula, V. Garces-Chavez, M. Comrie, D. J. Stevenson, B. Agate, C. T. A. Brown, F. Gunn-Moore and K. Dholakia, "Femtosecond cellular transfection using a nondiffracting light beam," *Appl. Phys. Lett.* **91**, 053902-053903 (2007)

10. S. Ito and M. Takagi, "Correlation between cell cycle phase of adherent Chinese hamster ovary cells and laser phase shift determined by phase-shifting laser microscopy," *Biotechnol. Lett.* **31**, 39-42 (2009)

Appendix A

Materials, cell culturing and microsphere preparation

i. Cell lines used
ii. Cell Culturing
   a) CHO cells
   b) RPE cells
   c) HL60 cells
   d) C2GM cells
iii. Microsphere preparation
iv. Cell-microsphere incubation
v. Statistical analysis of data

Appendix B

Materials, cell culturing and plasmid DNA preparation

i. Cell sample preparation
ii. Cell culturing
iii. Plasmid DNA preparation
iv. Calculation for cell transfection efficiency using $N_{cor} = ((E/D).100)/X_D$
v. Cell synchronization by Thymidine and Colcemid
vi. Preparation of stably transfected HSP-CHO-K1 and HSP-NG108-15 cells
vii. mRNA photo-transfection procedure
viii. Statistical analysis of data

Appendix C

Materials, cell culturing and plasmid DNA preparation for stem cell photo-transfection

i. Experimental setup
ii. Pluripotent stem cells used
iii. Cell culturing
iv. Plasmid DNA preparation

A. Materials, cell culturing and microsphere preparation

i. Cell lines used

A range of cell lines routinely used in both medical and biological research laboratories were used in these studies. For example, Chinese hamster ovary (CHO) cells are widely used as a cell line that grows rapidly as an attached cell population. Retinal pigment epithelial cells (RPE) are an example of a human epithelial cell line that has been immortalized by transduction with human telomerase and retain a near-diploid karyotype. Human promyelocytic leukemia (HL60) cells grow in suspension and are commonly used for studies on drug sensitivity and for investigating factors that induce cell differentiation in leukemia. Haematopoietic FDCP-mix C2GM (C2GM) cells are a murine cell line with stem cell-like properties whose growth is dependent on the presence of growth factors. Both the CHO and HL60 cell lines were purchased from the European collection of cell cultures (ECACC). The RPE cells were donated by Dr. Andrea Bodnar, Geron Corporation, USA and C2GM cells donated by Dr. Elaine Spooncer from the Paterson Institute for Cancer Research, Christie Hospital NHS Trust in Manchester, UK.

Before their incubation with microspheres, the four cell lines were grown at 37^{o}C with 5 % CO_2 and 85 % humidity (optimum growth condition) in T25 vented top tissue culture flasks (Nunc^{TM}) and sub-cultured twice weekly at a ratio 1:4. The different cell lines were also grown in different cell culture media, salts, buffers, antibiotics and growth factors (section ii (a) – (d)). These were supplemented with horse or fetal calf/bovine serum and this is referred to as complete medium.

ii. Cell Culturing

a) CHO cells

CHO cells were grown in minimum essential medium (MEM) (Invitrogen, UK) with 2 mM L-glutamine (Invitrogen, UK), 1 % penicillin–streptomycin (PEST) (Sigma, UK), 0.5 mg/ml geneticin (Invitrogen, UK) and supplemented with 10 % fetal calf serum (FCS) (Sera laboratory Int., UK). These particular cells were used in previous work and

had been photo-transfected with a plasmid containing an antibiotic-resistant gene and a gene encoding a mitochondrially targeted red fluorescent protein (pDsRed2-Mito – Ex 556/Em 586 nm from Clontech Laboratories, Inc), thereby providing an internal fluorescent red marker (1). The reason for using specifically fluorescent cells was to provide ease of detection during performing the characterization experiments mentioned in sections 3.1.2 and 3.1.3. Since these are an adherent cell line, 0.25% (w/v) trypsin–ethylenediaminetetraacetic acid (EDTA) (Sigma, UK), solution was used to harvest the cells for performing experiments.

b) RPE cells

These cells were grown in 10 % FCS Dulbecco's modified Eagle's medium (DMEM) (Invitrogen, UK) supplemented with 10 µg/ml gentamicin (Invitrogen, UK), 0.348 % sodium bicarbonate (w/v) (Sigma, UK), 15 mM 4-(2-hydroxyethyl)-1-piperazineethanesulfonic acid (HEPES) (Sigma, UK) pH 7.4, and 10 µg/ml hygromycin B (Invitrogen, UK) in phosphate buffered saline (PBS) (Sigma, UK). This adherent human epithelial cell line was trypsinised using a 0.25 % (w/v) trypsin–EDTA solution for cell sample preparation prior to optical treatment.

c) HL60 cells

HL60 is a human promyelocytic leukemic cell line that grows in suspension. It was maintained in Roswell Park Memorial Institute (RPMI) (Sigma, UK) 1640 medium supplemented with 10 % FCS and penicillin (50 U/ml) (Sigma, UK), streptomycin (50 µg/ml) (Sigma, UK), and L-glutamine (2 mM).

d) C2GM cells

C2GM cells are a growth-factor dependent haematopoietic stem-cell-like cell line that grows in suspension. These cells are derived from long-term murine bone marrow cultures and have the ability to differentiate into different haematopoietic cells (2). They were cultured in DMEM containing 2 mM L-glutamine, 1 % penicillin–streptomycin, 10 ng/ml murine recombinant granulocyte macrophage colony stimulating factor (GM-CSF) (Invitrogen, UK), and supplemented with 20 % horse serum (Sigma, UK).

iii. Microsphere Preparation

Hard-dyed (internally dyed) green fluorescing (GF) polymer microspheres which have the dye incorporated throughout the polymer matrix (and so are not easily quenched) with diameters 2 µm and 3 µm were purchased from Duke Scientific. The microspheres are made of polystyrene with a density of 1.05 g /cm^3 and a refractive index of 1.59. I used this type of fluorescent microspheres as they emit a bright distinctive green color with an improved contrast and visibility relative to the background material to provide easy detection. The spheres were dyed with fluorescein isothiocyanate (FITC) and had an excitation maximum at 468 nm (blue) and an emission maximum of 508 nm (green). Their stock concentrations were 1.7 X 10^9 and 6.7 X 10^8 spheres/ml (solid 1 %) for the 2 µm and 3 µm respectively. For experimental purposes, these were then further diluted 1:1000 in the different complete growth media (section ii (a) – (d)) depending on the cell line being investigated.

iv. Cell–microsphere incubation

The cells were co-incubated with either 2 or 3 µm GF polymer microspheres within the optimum growth condition stated before (section (i)). The experimental procedure for incubating the adherent cell lines, CHO and RPE cells; approximately 10^5 cells in 2 ml complete medium were seeded onto sterile 30 mm diameter culture plates prior to microsphere treatment. These cells were grown to sub-confluency overnight within optimum growth conditions. The following day (~ 24 hrs post plating), 2 ml of culture supernatant that was left on top of the samples was aspirated and replaced with the same volume of media containing either 2 or 3 µm diameter spheres. For HL60 and C2GM suspension cell lines, seeding was performed at a similar cell concentration as with the other two cell lines: however, these cell samples were grown in microsphere containing media immediately post seeding. 24 hrs following incubation, fluorescence and confocal microscopy were used to confirm microsphere internalization, and trypan blue exclusion tests indicated cell viability. Every experiment was performed in triplicate and repeated five times.

References

1. L. Paterson, B. Agate, M. Comrie, R. Ferguson, T. K. Lake, J. E. Morris, A. E. Carruthers, C. T. A. Brown, W. Sibbett, P. E. Bryant, F. Gunn-Moore, A. C. Riches and K. Dholakia, "Photoporation and cell transfection using a violet diode laser," *Opt. Express.* **13**, 595-600 (2005)

2. I. N. Hampson, M. A. Cross, C. M. Heyworth, L. Fairbairn, E. Spooncer, G. J. Cowling and T. M. Dexter, "Expression and down-Regulation of Cytotoxic-Cell Protease-1 or Granzyme-B Transcripts during Myeloid Differentiation of Interleukin-3-Dependent Murine Stem-Cell Lines," *Blood* **80**, 3097-3105 (1992)

v. Statistical analysis of data

Throughout the data sets presented in this thesis and conducted using MINITAB; analysis of variance (ANOVA), specifically one way ANOVA of the data was run followed by Dunnett's (which compares group means) and Fisher's (a statistical significance test) tests. The error bars in the graphical presentation of all the data in the thesis represents the standard error of the mean (SEM). This was calculated in Microsoft Office Excel using the equation:

$$SEM = STDEV/ SQRT (n)$$

where, STDEV = standard deviation and SQRT (n) = the square root of the number of times the experiment was repeated. Below is full statistical analysis of data presented in chapter 3.

Figure 3.5 (2µm GF microsphere data) **One-Way Analysis of Variance**

```
Analysis of Variance for C2
Source     DF        SS        MS        F        P
C1          5   4044214    808843     6.08    0.001
Error      24   3195107    133129
Total      29   7239321

                                  Individual 95% CIs For Mean
                                  Based on Pooled StDev
Level       N      Mean     StDev  -------+---------+---------+---------
0           5       0.0       0.0  (------*------)
1           5     118.0      40.6     (-----*------)
2           5     185.2     183.1      (------*-----)
3           5    1066.4     835.1                       (-----*------)
4           5     664.8     206.6                 (-----*------)
5           5     512.0     153.6              (-----*------)
                                  -------+---------+---------+---------
Pooled StDev =    364.9               0       500      1000

Dunnett's intervals for treatment mean minus control mean

    Family error rate = 0.0500
Individual error rate = 0.0126

Critical value = 2.70

Control = level (0) of C1

Level        Lower    Center     Upper ---------+---------+---------+--------
1           -505.1     118.0     741.1  (---------*---------)
2           -437.9     185.2     808.3   (---------*---------)
3            443.3    1066.4    1689.5                (----------*---------)
4             41.7     664.8    1287.9           (---------*---------)
5           -111.1     512.0    1135.1        (----------*---------)
                                        ---------+---------+---------+--------
                                                 0       600      1200

Fisher's pairwise comparisons

    Family error rate = 0.338
Individual error rate = 0.0500

Critical value = 2.064

Intervals for (column level mean) - (row level mean)

                    0           1           2           3           4

       1         -594
                  358

       2         -661        -543
                  291         409

       3        -1543       -1425       -1357
                 -590        -472        -405

       4        -1141       -1023        -956         -75
                 -189         -71          -3         878

       5         -988        -870        -803          78        -323
                  -36          82         149        1031         629
```

Figure 3.5 (3µm GF microsphere data) **One-Way Analysis of Variance**

```
Analysis of Variance for C2
Source     DF        SS        MS        F        P
C1          5   4887759    977552     2.46    0.062
Error      24   9537267    397386
Total      29  14425026
                                  Individual 95% CIs For Mean
                                  Based on Pooled StDev
Level       N      Mean     StDev  ---------+---------+---------+-------
0           5       0.0       0.0   (-------*-------)
1           5      10.6      12.3   (-------*-------)
2           5     138.4      45.1     (-------*-------)
3           5    1072.2    1516.6                  (-------*--------)
4           5     746.6     229.2              (--------*-------)
5           5     569.2     171.4           (-------*-------)
                                  ---------+---------+---------+-------
Pooled StDev =    630.4                    0       700      1400

Dunnett's intervals for treatment mean minus control mean

    Family error rate = 0.0500
Individual error rate = 0.0126

Critical value = 2.70

Control = level (0) of C1

Level        Lower    Center     Upper -+---------+---------+---------+------
1          -1065.9      10.6    1087.1 (----------*----------)
2           -938.1     138.4    1214.9   (---------*----------)
3             -4.3    1072.2    2148.7             (----------*---------)
4           -329.9     746.6    1823.1         (---------*----------)
5           -507.3     569.2    1645.7       (----------*---------)
                                     -+---------+---------+---------+------
                                  -1000         0      1000      2000

Fisher's pairwise comparisons

    Family error rate = 0.338
Individual error rate = 0.0500

Critical value = 2.064

Intervals for (column level mean) - (row level mean)

                  0           1           2           3           4

       1        -833
                 812

       2        -961        -951
                 684         695

       3       -1895       -1884       -1757
                -249        -239        -111

       4       -1569       -1559       -1431        -497
                  76          87         215        1148

       5       -1392       -1381       -1254        -320        -645
                 254         264         392        1326        1000
```

Figure 3.10 – Q_{lat} 2µm microsphere data set
C2GM cells
One-Way Analysis of Variance

```
Analysis of Variance for C2
Source     DF        SS        MS        F        P
C1          7  0.025113  0.003588     3.62    0.016
Error      16  0.015858  0.000991
Total      23  0.040971

                                  Individual 95% CIs For Mean
                                  Based on Pooled StDev
Level       N      Mean     StDev  --+---------+---------+---------+----
0           3   0.03325   0.00199   (-------*------)
1           3   0.10492   0.00298                (-------*-------)
2           3   0.11180   0.00788                  (------*-------)
3           3   0.07390   0.06401          (-------*------)
4           3   0.03407   0.05902   (-------*-------)
5           3   0.10826   0.00500                 (-------*------)
6           3   0.06536   0.01576        (-------*-------)
7           3   0.03440   0.00000   (-------*-------)
                                  --+---------+---------+---------+----
Pooled StDev =  0.03148           0.000     0.050     0.100     0.150

Dunnett's intervals for treatment mean minus control mean

    Family error rate = 0.0500
Individual error rate = 0.00993

Critical value = 2.92

Control = level (0) of C1

Level        Lower    Center     Upper ---+---------+---------+---------+----
1         -0.00339   0.07167   0.14673             (------------*-----------)
2          0.00349   0.07855   0.15361               (-----------*------------)
3         -0.03441   0.04065   0.11571        (------------*-----------)
4         -0.07424   0.00082   0.07588  (-----------*------------)
5         -0.00006   0.07500   0.15006              (------------*-----------)
6         -0.04295   0.03211   0.10717       (-----------*------------)
7         -0.07391   0.00115   0.07621  (-----------*------------)
                                  ---+---------+---------+---------+----
                                  -0.060     0.000     0.060     0.120
Fisher's pairwise comparisons

    Family error rate = 0.443
Individual error rate = 0.0500

Critical value = 2.120

Intervals for (column level mean) - (row level mean)

                  0           1           2           3           4           5           6

       1    -0.12616
            -0.01717

       2    -0.13304    -0.06137
            -0.02405     0.04761

       3    -0.09514    -0.02347    -0.01659
             0.01385     0.08552     0.09240

       4    -0.05531     0.01635     0.02323    -0.01467
             0.05367     0.12534     0.13222     0.09432
```

```
       5    -0.12950    -0.05783    -0.05095    -0.08885    -0.12868
            -0.02051     0.05116     0.05804     0.02014    -0.01969

       6    -0.08660    -0.01493    -0.00805    -0.04595    -0.08578    -0.01160
             0.02239     0.09406     0.10094     0.06303     0.02321     0.09739

       7    -0.05564     0.01603     0.02291    -0.01499    -0.05482     0.01936     -0.02353
             0.05335     0.12502     0.13190     0.09400     0.05417     0.12835      0.08546
```

Figure 3.10 – Q_{lat} 2µm microsphere data set
CHO cells
One-Way Analysis of Variance

```
Analysis of Variance for C2
Source     DF        SS        MS        F        P
C1          7   0.03155   0.00451     2.53    0.059
Error      16   0.02852   0.00178
Total      23   0.06006
                                  Individual 95% CIs For Mean
                                  Based on Pooled StDev
Level       N      Mean     StDev  -+---------+---------+---------+-----
0           3   0.05160   0.00000   (--------*--------)
1           3   0.14104   0.00298                  (--------*--------)
2           3   0.16168   0.00596                     (--------*--------)
3           3   0.09105   0.07887          (--------*--------)
4           3   0.05153   0.08926   (--------*--------)
5           3   0.10503   0.00289            (--------*--------)
6           3   0.09460   0.00298          (--------*--------)
7           3   0.08428   0.00298        (--------*--------)
                                  -+---------+---------+---------+-----
Pooled StDev =  0.04222          0.000     0.060     0.120     0.180

Dunnett's intervals for treatment mean minus control mean

    Family error rate = 0.0500
Individual error rate = 0.00993

Critical value = 2.92

Control = level (0) of C1

Level        Lower    Center     Upper -+---------+---------+---------+------
1          -0.01121   0.08944   0.19009           (---------*---------)
2           0.00943   0.11008   0.21073             (---------*---------)
3          -0.06120   0.03945   0.14010      (---------*---------)
4          -0.10072  -0.00007   0.10059   (---------*---------)
5          -0.04722   0.05343   0.15408       (---------*---------)
6          -0.05765   0.04300   0.14365      (---------*---------)
7          -0.06797   0.03268   0.13333     (---------*---------)
                                  -+---------+---------+---------+------
                                 -0.10     -0.00      0.10      0.20

Fisher's pairwise comparisons

    Family error rate = 0.443
Individual error rate = 0.0500

Critical value = 2.120

Intervals for (column level mean) - (row level mean)

             0           1           2           3           4           5        6
```

```
       1   -0.16252
           -0.01637

       2   -0.18316   -0.09372
           -0.03701    0.05244

       3   -0.11253   -0.02309   -0.00244
            0.03362    0.12307    0.14371

       4   -0.07301    0.01643    0.03707   -0.03356
            0.07314    0.16258    0.18322    0.11259

       5   -0.12650   -0.03706   -0.01642   -0.08705    -0.12657
            0.01965    0.10909    0.12973    0.05910     0.01958

       6   -0.11608   -0.02663   -0.00599   -0.07663    -0.11614    -0.06265
            0.03007    0.11952    0.14016    0.06953     0.03001     0.08350

       7   -0.10576   -0.01631    0.00433   -0.06631    -0.10582    -0.05233     -0.06276
            0.04040    0.12984    0.15048    0.07985     0.04033     0.09382      0.08340
```

Figure 3.10 – Q_{lat} 2µm microsphere data set
HL60 cells
One-Way Analysis of Variance

```
Analysis of Variance for C2
Source     DF        SS        MS        F        P
C1          7 0.0162743 0.0023249   415.42    0.000
Error      16 0.0000895 0.0000056
Total      23 0.0163639
                                 Individual 95% CIs For Mean
                                 Based on Pooled StDev
Level       N      Mean     StDev  --+---------+---------+---------+----
0           3  0.034401  0.000000                (*)
1           3  0.040364  0.005164                  (*)
2           3  0.074650  0.002597                              (*)
3           3  0.000000  0.000000   (*)
4           3  0.000000  0.000000   (*)
5           3  0.068458  0.001576                          (*-)
6           3  0.053321  0.002979                     (*)
7           3  0.034401  0.000000                (*)
                                 --+---------+---------+---------+----
Pooled StDev = 0.002366          0.000     0.025     0.050     0.075

Dunnett's intervals for treatment mean minus control mean

    Family error rate = 0.0500
Individual error rate = 0.00993

Critical value = 2.92

Control = level (0) of C1

Level        Lower    Center     Upper -------+---------+---------+---------+
1         0.000323  0.005963  0.011603                (-*--)
2         0.034609  0.040249  0.045889                          (-*-)
```

```
3        -0.040041 -0.034401 -0.028761  (-*-)
4        -0.040041 -0.034401 -0.028761  (-*-)
5         0.028417  0.034057  0.039697                          (--*-)
6         0.013280  0.018920  0.024561                     (--*-)
7        -0.005640  0.000000  0.005640               (-*-)
                                     -------+---------+---------+---------+
                                         -0.025    -0.000     0.025     0.050

Fisher's pairwise comparisons

    Family error rate = 0.443
Individual error rate = 0.0500

Critical value = 2.120

Intervals for (column level mean) - (row level mean)

         0          1           2           3          4           5           6


       1   -0.010058
           -0.001868

       2   -0.044344   -0.038381
           -0.036154   -0.030191

       3    0.030306    0.036269    0.070555
            0.038496    0.044459    0.078745

       4    0.030306    0.036269    0.070555   -0.004095
            0.038496    0.044459    0.078745    0.004095

       5   -0.038152   -0.032189    0.002097   -0.072552   -0.072552
           -0.029962   -0.023999    0.010287   -0.064363   -0.064363

       6   -0.023015   -0.017053    0.017234   -0.057416   -0.057416    0.011041
           -0.014825   -0.008863    0.025423   -0.049226   -0.049226    0.019231

       7   -0.004095    0.001868    0.036154   -0.038496   -0.038496    0.029962   0.014825
            0.004095    0.010058    0.044344   -0.030306   -0.030306    0.038152   0.023015
```

Figure 3.10 – Q_{lat} 2µm microsphere data set
RPE cells
One-Way Analysis of Variance

```
Analysis of Variance for C2
Source     DF        SS        MS        F        P
C1          7  0.038030  0.005433     9.48    0.000
Error      16  0.009167  0.000573
Total      23  0.047197

                                Individual 95% CIs For Mean
                                Based on Pooled StDev
Level       N      Mean     StDev  ------+---------+---------+---------+
0           3   0.03325   0.00199         (-----*-----)
1           3   0.10492   0.00298                    (-----*-----)
2           3   0.11180   0.00788                     (-----*-----)
3           3   0.00000   0.00000  (-----*-----)
4           3   0.03753   0.06500          (-----*----)
5           3   0.11008   0.00596                     (-----*-----)
6           3   0.06536   0.01576               (-----*-----)
7           3   0.03440   0.00000         (-----*-----)
                                ------+---------+---------+---------+
Pooled StDev =  0.02394             0.000     0.050     0.100     0.150
```

```
Dunnett's intervals for treatment mean minus control mean

    Family error rate = 0.0500
Individual error rate = 0.00993

Critical value = 2.92

Control = level (0) of C1

Level        Lower    Center     Upper ------+---------+---------+---------+-
1          0.01460   0.07167   0.12874                   (---------*--------)
2          0.02148   0.07855   0.13562                     (--------*---------)
3         -0.09032  -0.03325   0.02381  (--------*---------)
4         -0.05280   0.00427   0.06134        (---------*--------)
5          0.01976   0.07683   0.13390                   (---------*--------)
6         -0.02496   0.03211   0.08917             (--------*---------)
7         -0.05592   0.00115   0.05821        (--------*---------)
                                       ------+---------+---------+---------+-
                                          -0.060     0.000     0.060     0.120
Fisher's pairwise comparisons

    Family error rate = 0.443
Individual error rate = 0.0500

Critical value = 2.120

Intervals for (column level mean) - (row level mean)

               0           1           2           3           4           5         6

       1  -0.11310
          -0.03024

       2  -0.11998    -0.04831
          -0.03712     0.03455

       3  -0.00818     0.06349    0.07037
           0.07469     0.14635    0.15324

       4   -0.04570    0.02596    0.03284   -0.07896
            0.03716    0.10883    0.11571    0.00391

       5   -0.11826   -0.04659   -0.03971   -0.15152    -0.11399
           -0.03540    0.03627    0.04315   -0.06865    -0.03112

       6   -0.07354   -0.00187    0.00501   -0.10679    -0.06927     0.00329
            0.00933    0.08099    0.08787   -0.02393     0.01360     0.08615

       7   -0.04258    0.02909    0.03597   -0.07583    -0.03831     0.03425    -0.01047
            0.04029    0.11195    0.11883    0.00703     0.04456     0.11711     0.07239
```

Figure 3.11 – Q_{lat} 3µm microsphere data set
C2GM cells
One-Way Analysis of Variance

```
Analysis of Variance for C2
Source     DF        SS        MS        F        P
C1          7  0.065351  0.009336    14.35    0.000
Error      16  0.010409  0.000651
Total      23  0.075759
                                 Individual 95% CIs For Mean
                                 Based on Pooled StDev
Level       N      Mean     StDev  -----+---------+---------+---------+-
0           3   0.05332   0.00298          (----*---)
```

```
1           3   0.16340   0.00788                            (---*----)
2           3   0.13244   0.00298                       (----*---)
3           3   0.04111   0.07121          (----*---)
4           3   0.00000   0.00000    (---*---)
5           3   0.10664   0.00596                   (---*----)
6           3   0.09460   0.00298                (----*---)
7           3   0.02924   0.00298          (---*----)
                                    -----+---------+---------+---------+-
Pooled StDev =  0.02551               0.000     0.070     0.140     0.210
```

Dunnett's intervals for treatment mean minus control mean

```
    Family error rate = 0.0500
Individual error rate = 0.00993

Critical value = 2.92

Control = level (0) of C1

Level        Lower    Center     Upper -----+---------+---------+---------+--
1          0.04927   0.11008   0.17089                       (-------*------)
2          0.01831   0.07912   0.13993                  (-------*------)
3         -0.07302  -0.01221   0.04860         (------*-------)
4         -0.11413  -0.05332   0.00749   (------*-------)
5         -0.00749   0.05332   0.11413                (-------*------)
6         -0.01953   0.04128   0.10209               (------*-------)
7         -0.08489  -0.02408   0.03673      (-------*-------)
                                      -----+---------+---------+---------+--
                                        -0.080     0.000     0.080     0.160
```

Fisher's pairwise comparisons

```
    Family error rate = 0.443
Individual error rate = 0.0500

Critical value = 2.120

Intervals for (column level mean) - (row level mean)

                    0           1           2           3           4           5           6

       1    -0.15423
            -0.06593

       2    -0.12327    -0.01319
            -0.03497     0.07511

       3    -0.03194     0.07814     0.04718
             0.05636     0.16644     0.13548

       4     0.00917     0.11925     0.08829    -0.00304
             0.09747     0.20755     0.17659     0.08526

       5    -0.09747     0.01261    -0.01835    -0.10968    -0.15079
            -0.00917     0.10091     0.06995    -0.02138    -0.06249

       6    -0.08543     0.02465    -0.00631    -0.09764    -0.13875    -0.03211
             0.00287     0.11295     0.08199    -0.00934    -0.05045     0.05619

       7    -0.02007     0.09001     0.05905    -0.03228    -0.07339     0.03325     0.02121
             0.06823     0.17831     0.14735     0.05602     0.01491     0.12155     0.10951
```

Figure 3.11 – Q_{lat} 3µm microsphere data set
CHO cells
One-Way Analysis of Variance

```
Analysis of Variance for C2
Source     DF        SS        MS        F        P
C1          7   0.05459   0.00780     4.61    0.005
Error      16   0.02705   0.00169
Total      23   0.08165

                                  Individual 95% CIs For Mean
                                  Based on Pooled StDev
Level       N      Mean     StDev  ------+---------+---------+---------+
0           3   0.05160   0.00000        (-----*------)
1           3   0.09976   0.00596              (-----*------)
2           3   0.17888   0.00596                        (-----*------)
3           3   0.10110   0.08757              (------*-----)
4           3   0.04300   0.07448       (-----*------)
5           3   0.06364   0.00298          (-----*-----)
6           3   0.05966   0.01523        (-----*------)
7           3   0.01032   0.00000   (-----*------)
                                  ------+---------+---------+---------+
Pooled StDev =  0.04112              0.000     0.080     0.160     0.240

Dunnett's intervals for treatment mean minus control mean

    Family error rate = 0.0500
Individual error rate = 0.00993

Critical value = 2.92

Control = level (0) of C1

Level        Lower    Center     Upper ----+---------+---------+---------+---
1         -0.04988   0.04816   0.14620          (---------*---------)
2          0.02924   0.12728   0.22532                   (---------*---------)
3         -0.04854   0.04950   0.14753          (---------*---------)
4         -0.10664  -0.00860   0.08944    (---------*---------)
5         -0.08600   0.01204   0.11008      (---------*---------)
6         -0.08998   0.00806   0.10610      (---------*---------)
7         -0.13932  -0.04128   0.05676 (---------*---------)
                                  ----+---------+---------+---------+---
                                   -0.10     -0.00      0.10      0.20
Fisher's pairwise comparisons

    Family error rate = 0.443
Individual error rate = 0.0500

Critical value = 2.120

Intervals for (column level mean) - (row level mean)

                  0           1           2           3           4           5           6

       1    -0.11934
             0.02302

       2    -0.19846    -0.15030
            -0.05610    -0.00794

       3    -0.12067    -0.07251     0.00661
             0.02168     0.06984     0.14897

       4    -0.06258    -0.01442     0.06470    -0.01308
             0.07978     0.12794     0.20706     0.12927
```

```
       5    -0.08322    -0.03506     0.04406    -0.03372    -0.09182
             0.05914     0.10730     0.18642     0.10863     0.05054

       6    -0.07924    -0.03108     0.04804    -0.02974    -0.08784    -0.06720
             0.06312     0.11128     0.19040     0.11261     0.05452     0.07516

       7    -0.02990     0.01826     0.09739     0.01960    -0.03850    -0.01786     -0.02184
             0.11246     0.16062     0.23974     0.16195     0.10386     0.12450      0.12052
```

Figure 3.11 – Q_{lat} 3µm microsphere data set
HL60 cells
One-Way Analysis of Variance

```
Analysis of Variance for C2
Source     DF        SS        MS        F        P
C1          7 0.0148063 0.0021152   212.57    0.000
Error      16 0.0001592 0.0000100
Total      23 0.0149655
                                  Individual 95% CIs For Mean
                                  Based on Pooled StDev
Level       N      Mean     StDev  --+---------+---------+---------+----
0           3  0.037382  0.005164                (-*)
1           3  0.053321  0.002979                      (*-)
2           3  0.051601  0.000000                    (-*)
3           3  0.000000  0.000000  (-*-)
4           3  0.000000  0.000000  (-*-)
5           3  0.072242  0.000000                               (-*)
6           3  0.059513  0.004171                          (-*)
7           3  0.040364  0.005164                  (*-)
                                  --+---------+---------+---------+----
Pooled StDev = 0.003154           0.000     0.025     0.050     0.075

Dunnett's intervals for treatment mean minus control mean

    Family error rate = 0.0500
Individual error rate = 0.00993

Critical value = 2.92

Control = level (0) of C1

Level        Lower    Center     Upper --------+---------+---------+---------
1         0.008418  0.015939  0.023460                      (--*--)
2         0.006698  0.014219  0.021740                      (--*--)
3        -0.044903 -0.037382 -0.029861 (--*--)
4        -0.044903 -0.037382 -0.029861 (--*--)
5         0.027339  0.034859  0.042380                               (--*--)
6         0.014610  0.022131  0.029652                          (--*--)
7        -0.004539  0.002981  0.010502                 (--*--)
                                  --------+---------+---------+---------
                                       -0.025    -0.000     0.025
Fisher's pairwise comparisons

    Family error rate = 0.443
Individual error rate = 0.0500

Critical value = 2.120

Intervals for (column level mean) - (row level mean)

                  0           1           2           3           4           5           6

       1   -0.021399
```

```
           -0.010479

       2   -0.019679   -0.003740
           -0.008759    0.007180

       3    0.031922    0.047861    0.046141
            0.042842    0.058781    0.057061

       4    0.031922    0.047861    0.046141   -0.005460
            0.042842    0.058781    0.057061    0.005460

       5   -0.040320   -0.024381   -0.026101   -0.077702   -0.077702
           -0.029399   -0.013460   -0.015180   -0.066781   -0.066781

       6   -0.027591   -0.011652   -0.013372   -0.064974   -0.064974    0.007268
           -0.016671   -0.000732   -0.002452   -0.054053   -0.054053    0.018189

       7   -0.008442    0.007497    0.005777   -0.045824   -0.045824    0.026418    0.013689
            0.002479    0.018418    0.016698   -0.034903   -0.034903    0.037338    0.024610
```

Figure 3.11 – Q_{lat} 3µm microsphere data set
RPE cells
One-Way Analysis of Variance

```
Analysis of Variance for C2
Source     DF        SS        MS        F        P
C1          7 0.0948525 0.0135504   236.90    0.000
Error      16 0.0009152 0.0000572
Total      23 0.0957677
                                  Individual 95% CIs For Mean
                                  Based on Pooled StDev
Level       N      Mean     StDev  --+---------+---------+---------+----
0           3   0.03325   0.00199        (-*)
1           3   0.19264   0.00596                                   (*-)
2           3   0.12384   0.00000                        (-*)
3           3   0.00000   0.00000  (-*-)
4           3   0.00000   0.00000  (-*-)
5           3   0.11352   0.01788                      (-*)
6           3   0.06192   0.00000             (*-)
7           3   0.04587   0.00993          (-*)
                                  --+---------+---------+---------+----
Pooled StDev =  0.00756           0.000     0.060     0.120     0.180

Dunnett's intervals for treatment mean minus control mean

    Family error rate = 0.0500
Individual error rate = 0.00993

Critical value = 2.92

Control = level (0) of C1

Level        Lower    Center     Upper --------+---------+---------+---------
1          0.14136   0.15939   0.17742                              (--*-)
2          0.07256   0.09059   0.10862                       (--*--)
3         -0.05129  -0.03325  -0.01522  (-*--)
4         -0.05129  -0.03325  -0.01522  (-*--)
5          0.06224   0.08027   0.09830                (-*--)
6          0.01064   0.02867   0.04670           (-*--)
7         -0.00542   0.01261   0.03065        (--*-)
                                  --------+---------+---------+---------
                                        0.000     0.070     0.140

Fisher's pairwise comparisons
```

```
    Family error rate = 0.443
Individual error rate = 0.0500

Critical value = 2.120

Intervals for (column level mean) - (row level mean)

                    0           1           2           3           4           5           6

       1    -0.17248
            -0.14630

       2    -0.10368     0.05571
            -0.07750     0.08189

       3     0.02016     0.17955     0.11075
             0.04635     0.20574     0.13693

       4     0.02016     0.17955     0.11075    -0.01309
             0.04635     0.20574     0.13693     0.01309

       5    -0.09336     0.06603    -0.00277    -0.12661    -0.12661
            -0.06718     0.09221     0.02341    -0.10043    -0.10043

       6    -0.04176     0.11763     0.04883    -0.07501    -0.07501     0.03851
            -0.01558     0.14381     0.07501    -0.04883    -0.04883     0.06469

       7    -0.02570     0.13369     0.06488    -0.05896    -0.05896     0.05456    0.00296
             0.00048     0.15987     0.09107    -0.03278    -0.03278     0.08075    0.02914
```

Figure 3.12 – Axial guiding 2µm microsphere data set
C2GM cells
One-Way Analysis of Variance

```
Analysis of Variance for C2
Source     DF        SS        MS         F        P
C1          5   1088.33    217.67    175.77    0.000
Error      12     14.86      1.24
Total      17   1103.19

                                  Individual 95% CIs For Mean
                                  Based on Pooled StDev
Level       N      Mean     StDev  --+---------+---------+---------+----
0           3     0.000     0.000  (-*-)
1           3     8.800     0.300            (-*-)
2           3     9.800     1.114             (-*-)
3           3    12.933     1.415                 (-*-)
4           3    17.067     0.493                      (*-)
5           3    25.333     1.963                           (-*)
                                  --+---------+---------+---------+----
Pooled StDev =    1.113           0.0       8.0      16.0      24.0

Dunnett's intervals for treatment mean minus control mean

    Family error rate = 0.0500
Individual error rate = 0.0133

Critical value = 2.90
```

```
Control = level (0) of C1

Level        Lower    Center     Upper ----------+---------+---------+-------
1             6.165     8.800    11.435 (----*---)
2             7.165     9.800    12.435   (---*----)
3            10.298    12.933    15.568        (----*---)
4            14.432    17.067    19.702             (---*----)
5            22.698    25.333    27.968                       (---*----)
                                       ----------+---------+---------+-------
                                              12.0      18.0      24.0
Fisher's pairwise comparisons

    Family error rate = 0.314
Individual error rate = 0.0500

Critical value = 2.179

Intervals for (column level mean) - (row level mean)

                    0           1           2           3           4

       1     -10.780
              -6.820

       2     -11.780      -2.980
              -7.820       0.980

       3     -14.913      -6.113      -5.113
             -10.953      -2.153      -1.153

       4     -19.047     -10.247      -9.247      -6.113
             -15.087      -6.287      -5.287      -2.153

       5     -27.313     -18.513     -17.513     -14.380     -10.247
             -23.353     -14.553     -13.553     -10.420      -6.287
```

Figure 3.12 – Axial guiding 2µm microsphere data set
CHO cells
One-Way Analysis of Variance

```
Analysis of Variance for C2
Source     DF        SS        MS        F        P
C1          5    1622.0     324.4    18.25    0.000
Error      12     213.3      17.8
Total      17    1835.3
                                  Individual 95% CIs For Mean
                                  Based on Pooled StDev
Level       N      Mean     StDev  -----+---------+---------+---------+-
0           3     0.000     0.000   (---*---)
1           3     4.667     1.069      (----*---)
2           3     7.200     0.964         (---*---)
3           3    11.000     1.212            (---*----)
4           3    15.867     1.963                (---*----)
5           3    29.500     9.962                         (----*---)
                                  -----+---------+---------+---------+-
Pooled StDev =    4.216               0        12        24        36

Dunnett's intervals for treatment mean minus control mean

    Family error rate = 0.0500
Individual error rate = 0.0133

Critical value = 2.90
```

```
Control = level (0) of C1

Level        Lower    Center     Upper -----+---------+---------+---------+--
1           -5.316     4.667    14.649  (-------*-------)
2           -2.783     7.200    17.183    (-------*-------)
3            1.017    11.000    20.983      (-------*-------)
4            5.884    15.867    25.849          (-------*--------)
5           19.517    29.500    39.483                    (--------*-------)
                                     -----+---------+---------+---------+--
                                          0        12        24        36
Fisher's pairwise comparisons

    Family error rate = 0.314
Individual error rate = 0.0500

Critical value = 2.179

Intervals for (column level mean) - (row level mean)

                    0           1           2           3           4

       1     -12.168
               2.834

       2     -14.701     -10.034
               0.301       4.968

       3     -18.501     -13.834     -11.301
              -3.499       1.168       3.701

       4     -23.368     -18.701     -16.168     -12.368
              -8.366      -3.699      -1.166       2.634

       5     -37.001     -32.334     -29.801     -26.001     -21.134
             -21.999     -17.332     -14.799     -10.999      -6.132
```

Figure 3.12 – Axial guiding 2µm microsphere data set
RPE cells
One-Way Analysis of Variance

```
Analysis of Variance for C2
Source     DF        SS        MS        F        P
C1          5   456.151    91.230    93.73    0.000
Error      12    11.680     0.973
Total      17   467.831
                                 Individual 95% CIs For Mean
                                 Based on Pooled StDev
Level       N      Mean     StDev  ---+---------+---------+---------+---
0           3    -0.000     0.000   (-*-)
1           3     5.300     0.100             (--*-)
2           3     5.467     1.901             (--*-)
3           3     7.900     0.265                  (--*-)
4           3    11.467     1.457                        (--*-)
5           3    15.933     0.153                              (--*-)
                                 ---+---------+---------+---------+---
Pooled StDev =    0.987              0.0       5.0      10.0      15.0

Dunnett's intervals for treatment mean minus control mean

    Family error rate = 0.0500
Individual error rate = 0.0133

Critical value = 2.90
```

```
Control = level (0) of C1

Level        Lower    Center     Upper -----+---------+---------+---------+--
1            2.964     5.300     7.636  (----*---)
2            3.131     5.467     7.803  (----*----)
3            5.564     7.900    10.236       (----*---)
4            9.131    11.467    13.803             (----*----)
5           13.597    15.933    18.269                   (----*----)
                                       -----+---------+---------+---------+--
                                          5.0      10.0      15.0      20.0



Fisher's pairwise comparisons

    Family error rate = 0.314
Individual error rate = 0.0500

Critical value = 2.179

Intervals for (column level mean) - (row level mean)

                    0           1           2           3           4

       1      -7.055
              -3.545

       2      -7.222      -1.922
              -3.711       1.589

       3      -9.655      -4.355      -4.189
              -6.145      -0.845      -0.678

       4     -13.222      -7.922      -7.755      -5.322
              -9.711      -4.411      -4.245      -1.811

       5     -17.689     -12.389     -12.222      -9.789      -6.222
              -14.178     -8.878      -8.711      -6.278      -2.711
```

Figure 3.13 – Axial guiding 3µm microsphere data set

C2GM cells

One-Way Analysis of Variance

```
Analysis of Variance for C2
Source     DF        SS        MS         F        P
C1          5   798.945   159.789   324.99    0.000
Error      12     5.900     0.492
Total      17   804.845
                                  Individual 95% CIs For Mean
                                  Based on Pooled StDev
Level       N      Mean     StDev  --+---------+---------+---------+----
0           3     0.000     0.000   (*)
1           3     9.867     0.777                (*)
2           3    11.200     0.000                  (*)
3           3    13.000     0.500                    (-*)
4           3    16.767     1.429                          (*)
5           3    21.667     0.231                                 (*)
                                  --+---------+---------+---------+----
Pooled StDev =    0.701           0.0       7.0      14.0      21.0

Dunnett's intervals for treatment mean minus control mean
```

```
    Family error rate = 0.0500
Individual error rate = 0.0133

Critical value = 2.90

Control = level (0) of C1

Level        Lower    Center     Upper ----------+---------+---------+-------
1            8.206     9.867    11.527  (---*---)
2            9.540    11.200    12.860     (---*---)
3           11.340    13.000    14.660         (---*----)
4           15.106    16.767    18.427                  (---*---)
5           20.006    21.667    23.327                           (---*---)
                                       ----------+---------+---------+-------
                                              12.0      16.0      20.0

Fisher's pairwise comparisons

    Family error rate = 0.314
Individual error rate = 0.0500

Critical value = 2.179

Intervals for (column level mean) - (row level mean)

                    0           1           2           3           4

       1     -11.114
              -8.619

       2     -12.448      -2.581
              -9.952      -0.086

       3     -14.248      -4.381      -3.048
             -11.752      -1.886      -0.552

       4     -18.014      -8.148      -6.814      -5.014
             -15.519      -5.652      -4.319      -2.519

       5     -22.914     -13.048     -11.714      -9.914      -6.148
             -20.419     -10.552      -9.219      -7.419      -3.652
```

Figure 3.13 – Axial guiding 3µm microsphere data set
CHO cells
One-Way Analysis of Variance

```
Analysis of Variance for C2
Source     DF        SS        MS         F        P
C1          5   6830.85   1366.17    758.05    0.000
Error      12     21.63      1.80
Total      17   6852.48

                                  Individual 95% CIs For Mean
                                  Based on Pooled StDev
Level       N      Mean     StDev  -+---------+---------+---------+-----
0           3     0.000     0.000  (*)
1           3    13.600     0.300         (*)
2           3    18.133     2.223           (*)
3           3    23.167     1.102              (*
4           3    33.233     0.874                   (*
5           3    62.467     1.950                                (*)
                                  -+---------+---------+---------+-----
Pooled StDev =    1.342             0        20        40        60

Dunnett's intervals for treatment mean minus control mean
```

```
    Family error rate = 0.0500
Individual error rate = 0.0133

Critical value = 2.90

Control = level (0) of C1

Level        Lower    Center     Upper ----+---------+---------+---------+---
1           10.421    13.600    16.779  (-*-)
2           14.955    18.133    21.312     (-*-)
3           19.988    23.167    26.345        (-*--)
4           30.055    33.233    36.412              (-*-)
5           59.288    62.467    65.645                          (-*-)
                                      ----+---------+---------+---------+---
                                         15        30        45        60

Fisher's pairwise comparisons

    Family error rate = 0.314
Individual error rate = 0.0500

Critical value = 2.179

Intervals for (column level mean) - (row level mean)

                  0           1           2           3           4

       1     -15.988
             -11.212

       2     -20.522      -6.922
             -15.745      -2.145

       3     -25.555     -11.955      -7.422
             -20.778      -7.178      -2.645

       4     -35.622     -22.022     -17.488     -12.455
             -30.845     -17.245     -12.712      -7.678

       5     -64.855     -51.255     -46.722     -41.688     -31.622
             -60.078     -46.478     -41.945     -36.912     -26.845
```

Figure 3.13 – Axial guiding 3µm microsphere data set

RPE cells

One-Way Analysis of Variance

```
Analysis of Variance for C2
Source     DF        SS        MS         F        P
C1          5    595.61    119.12     41.08    0.000
Error      12     34.79      2.90
Total      17    630.41

                                  Individual 95% CIs For Mean
                                  Based on Pooled StDev
Level       N      Mean     StDev  ----+---------+---------+---------+--
0           3     0.000     0.000   (--*--)
1           3     8.100     1.054              (--*--)
2           3     8.567     1.815              (--*--)
3           3    11.100     2.066                  (--*--)
4           3    14.900     1.229                       (--*--)
5           3    18.233     2.686                            (--*--)
                                  ----+---------+---------+---------+--
Pooled StDev =    1.703              0.0       7.0      14.0      21.0
```

Dunnett's intervals for treatment mean minus control mean

```
    Family error rate = 0.0500
Individual error rate = 0.0133

Critical value = 2.90

Control = level (0) of C1

Level        Lower    Center     Upper --+---------+---------+---------+-----
1            4.068     8.100    12.132 (-------*-------)
2            4.535     8.567    12.599  (-------*-------)
3            7.068    11.100    15.132       (-------*-------)
4           10.868    14.900    18.932               (-------*-------)
5           14.201    18.233    22.265                     (-------*--------)
                                     --+---------+---------+---------+-----
                                     5.0      10.0      15.0      20.0
```

Fisher's pairwise comparisons

```
    Family error rate = 0.314
Individual error rate = 0.0500

Critical value = 2.179

Intervals for (column level mean) - (row level mean)

                  0           1           2           3           4

       1     -11.129
              -5.071

       2     -11.596      -3.496
              -5.537       2.563

       3     -14.129      -6.029      -5.563
              -8.071       0.029       0.496

       4     -17.929      -9.829      -9.363      -6.829
             -11.871      -3.771      -3.304      -0.771

       5     -21.263     -13.163     -12.696     -10.163      -6.363
             -15.204      -7.104      -6.637      -4.104      -0.304
```

B. Materials, cell culturing and plasmid DNA preparation

i. Cell sample preparation

All the mammalian cell lines employed in the work presented in chapter 5 were purchased from the European collection of cell cultures (ECACC). The cells were cultured in a 37^{o}C, 5 % carbon dioxide (CO_2) and 85 % humid incubator (optimum growth condition). To prevent detachment of the monolayer, when working with the mouse/rat neuroblastoma x glioma hybrid (NG108-15) and human embryonic kidney (HEK-293) cell lines, the glass surface of the petri dishes was coated with a thin layer of 2 µg/cm^2 laminin (coating procedure similar to that described in sub-section 3.3.1.2) before these cells were seeded. Once the different kinds of culture media used had been modified with antibiotics and supplemented with fetal bovine serum (FBS) (S*era laboratory Int., UK*) they are described as complete medium. For statistical purposes all experiments were done in triplicate and each experiment repeated three times under the same conditions to prove reproducibly. For my investigations, cells were never used post passage number 35 as high culture passage levels may lead to the generation of inaccurate results (1). After assembling and aligning the photo-transfection setup, it was tested by performing dry run experiments where the trypan blue viability dye was introduced into Chinese hamster ovary (CHO-K1) cells.

ii. Cell culturing

The various adherent cell types were grown in T25 vented top culture flasks (*Nunc*^{TM}). Sub-cultured twice weekly at a ratio 1:4, CHO-K1, human neuroblastoma (SK-N-SH) and HEK-293 cells were grown in minimum essential medium (MEM) (*Invitrogen, UK*) with 1 % penicillin-streptomycin (PEST) (*Sigma, UK*) supplemented with 10 % FBS. The NG108-15 cells, were grown in Dulbecco's modified eagle's medium (DMEM) (*Invitrogen, UK*) with 1 % PEST and 10 % FBS. CHO-K1 and NG108-15 cells transfected with the heat shock protein (HSP) 70 promoter gene were designated HSP-CHO-K1 and HSP-NG108-15 respectively. These cells were grown in DMEM with 1 % PEST, 0.5 mg/ml geneticin (*Invitrogen, UK*) and 10 % FBS.

iii. Plasmid DNA preparation

A 4.7 kilobase (kb) plasmid (pDsRed2-Mito from *Clontech Laboratories, Inc*), a mammalian expression vector that encodes a fusion of *Discosoma sp.* red fluorescent protein (DsRed2; 1, 2) and the mitochondrial targeting sequence from subunit VIII of human cytochrome c oxidase (Mito; 3, 4) was used. The enhanced green fluorescent protein plasmid (pEGFP from *Clontech Laboratories, Inc*) carries a red-shifted variant of wild-type GFP which facilitates brighter fluorescence and higher expression in mammalian cells. Additionally, this pEGFP (3.4 kb) encodes the GFPmut1 variant which contains the double-amino-acid substitution of Phe-64 to Leu and Ser-65 to Thr. Both pDsRed2-Mito and pEGFP were prepared from transformed *Escherichia coli* (*E. coli)* cells by utilizing the mini-prep DNA purification system according to the manufacturer's instructions (*Qiagen, UK*). The HSP-70 plasmid was obtained from Mr. Lei Huang (Medical College of Georgia, United States of America). This plasmid is a 5.3 kb DNA containing promoter and 5´-untranslated region of the mouse hsp70.1gene fused with a complementary DNA (cDNA) coding for the GFP with a polyA signal from SV40 large T antigen gene inserted into a pSP72 vector containing a hygromycin resistance gene (2).

iv. Calculation for transfection efficiency using $N_{cor} = ((E/D).100)/X_D$

The transfection efficiency of 63 % given for CHO-K1 cells in table 5.1 (page119) was calculated as follows:

N_{cor} = the population corrected transfection efficiency
E = number of cells transiently expressing the pDNA 48hrs post photo-transfection = 71
D = number of cells dosed (photo-transfected) = 50
X_D = the ratio of proliferation that has occurred in the dosed cells (90 % confluency – 72 hrs post seeding) between dosing (40 % confluency – 24 hrs post seeding) and the measurement of expression = 90/40 = 2.25

Therefore, $N_{cor} = ((71/50).100)/2.25$
$= 63\ \%$

v. Cell synchronization by Thymidine and Colcemid

This work was performed on CHO-K1 as well as HEK-293 cells, where both cell lines were reversibly synchronized at the M and S phases of the cell division cycle independently. In both aspects, cells were plated in complete medium in T25 tissue culture flasks at concentration 10^6 cells/ml and incubated in optimum growth conditions over 48 hours (hrs) prior to arresting. Then, a non-lethal metaphase arrest was induced by treating the cells with 10 µg/ml of colcemid (*Invitrogen, UK*), followed by a further incubation of 6 hrs. Thereafter the cells were harvested using 0.25 % trypsin (*Sigma, UK*) and plated for photo-transfection. In another experiment, the cells were synchronized at the S-phase via a thymidine-1 (TdR) (*Sigma, UK*) double block. Briefly they were treated with 2 mM of TdR for 18 hrs, released into complete medium for 9 hrs and then incubated in medium containing 2 mM TdR a further 18 hrs. After which the cells were again harvested with 0.25 % trypsin. In both cases to ensure that the cells were photo-transfected at the desired stages i.e. M and S phases, the cells plated for photo-transfection were left to recover (incubated for ~ 18 hrs) for one full cell cycle which takes ~ 18 hrs for both CHO-K1 and HEK-293 cells (3-5) before optical treatment at 60 mW and 40 ms.

vi. Preparation of stably transfected HSP-CHO-K1 and HSP-NG108-15 cells

To generate stably transfected cells expressing the HSP-70 promoter, both CHO-K1 and NG108-15 cells were chemically transfected with GeneJammer (*Stratagene, UK*) according to the manufacture's instructions (These cells were transfected in an independent PhD program by Mr. David Carnegie). Briefly, complexes were formed using 2.2 mg/ml of pDNA, 97 µl serum free DMEM and 3 µl GeneJammer. This mixture was incubated at room temperature for approximately 45 min and thereafter added to a 50 % confluent 35 mm petri dish and the cells incubated under optimum growth conditions for 24 – 72 hrs. This was then split 1:4 into growth medium containing the selection antibiotic hygromycin (*Invitrogen, UK*) at a concentration of 0.5 mg/ml. Once stably transfected these cells were labeled HSP-CHO-K1 and HSP-NG108-15.

For optical treatment, cell samples were plated and prepared as mentioned in section B (i) but the cell monolayer was submerged in 60 µl of OptiMEM as opposed to DNA for this experiment.

vii. mRNA photo-transfection procedure

During this project, capped EGFP mRNA was synthesized using the mMESSAGE mMACHINE mRNA synthesis kit (*Ambion, UK*). This was done with extra caution to enhance a nuclease free environment. In brief, pEGFP prepared as described above (section B (iii)) was linearized and used as a template for in vitro transcription via the instruction manual obtained from mRNA synthesis kit. Following successful completion of the capped transcription reaction assembly and subsequent recovery, mRNA was quantified by UV light absorbance using a spectrophotometer. Separate batches of the mRNA produced this way resulted in different quantities with a general amounts ranging between roughly 1.5 – 3.6 µg/µl. CHO-K1 cell culturing and sample preparation for photo-transfection experiments was kept constant to those already mentioned before in section B (i and ii) respectively. For photo-transfection, the CHO-K1 monolayer was bathed in 60 µl of 15 µg/ml EGFP mRNA made up in OptiMEM and targeted photo-transfection of individual cells was then performed via laser irradiation (60 mW, 40 ms) through administering three shots of ultra-short duration while avoiding visual cellular response (i.e. no bubble formation or cellular disruption). After optical treatment the monolayer was rinsed twice in 2 ml of neat OptiMEM each time and then incubated in 2 ml of complete medium under optimum growth conditions.

References

1. P. Hughes, D. Marshall, Y. Reid, H. Parkes and C. Gelber, "The costs of using unauthenticated, over-passaged cell lines: how much more data do we need?," *Biotechniques* **43**, 575-586 (2007)
2. O. Lipan, J. M. Navenot, Z. Wang, L. Huang and S. C. Peiper, "Heat shock response in CHO mammalian cells is controlled by a nonlinear stochastic process," *PLoS Comput. Biol.* **3**, 1859-1870 (2007)
3. A. Sakamoto and K. N. Prasad, "Effect of Dl-Glyceraldehyde on mouse neuroblastoma cells in culture," *Cancer Res.* **32**, 532-534 (1972)
4. R. L. Mellgren, Q. Lu, W. L. Zhang, M. Lakkis, E. Shaw and M. T. Mericle, "Isolation of a Chinese hamster ovary cell clone possessing decreased mu-calpain content and a reduced proliferative growth rate," *J. Biol. Chem.* **271**, 15568-15574 (1996)
5. K. Nehlsen, S. Broll and J. Bode, "Replicating minicircles: Generation of nonviral episomes for the efficient modification of dividing cells - Research article," *Gene Ther. Mol. Biol.* **10B**, 233-243 (2006)

viii. Statistical analysis of data

Figure 5.5 – Photo-transfection parameter data
CHO-K1 cells
One-Way Analysis of Variance

```
Analysis of Variance for C2
Source     DF        SS        MS        F        P
C1         10     11344      1134     4.93    0.001
Error      22      5064       230
Total      32     16408
                                    Individual 95% CIs For Mean
                                    Based on Pooled StDev
Level       N      Mean     StDev  -------+---------+---------+---------
 0          3      0.00      0.00   (-----*-----)
 1          3     40.67     35.57                (------*-----)
 2          3     50.00     17.78                    (-----*-----)
 3          3     62.67      8.33                       (-----*-----)
 4          3     48.00     16.37                   (-----*-----)
 5          3     24.00     14.00           (-----*-----)
 6          3     14.67     13.32        (-----*-----)
 7          3     21.33      5.03          (-----*-----)
 8          3     16.67      3.06        (------*-----)
 9          3     16.67      9.02        (------*-----)
10          3     12.00     11.14       (-----*-----)
                                   -------+---------+---------+---------
Pooled StDev =    15.17                  0        30        60

Dunnett's intervals for treatment mean minus control mean

    Family error rate = 0.0500
Individual error rate = 0.00728

Critical value = 2.96

Control = level (0) of C1

Level        Lower    Center     Upper --------+---------+---------+---------
 1            4.00     40.67     77.33           (----------*---------)
 2           13.33     50.00     86.67              (---------*----------)
 3           26.00     62.67     99.33                 (----------*---------)
 4           11.33     48.00     84.67              (----------*---------)
 5          -12.67     24.00     60.67     (----------*---------)
 6          -22.00     14.67     51.33   (---------*----------)
 7          -15.33     21.33     58.00     (---------*----------)
 8          -20.00     16.67     53.33   (----------*---------)
 9          -20.00     16.67     53.33   (----------*---------)
10          -24.67     12.00     48.67  (---------*----------)
                                       --------+---------+---------+---------
                                               0        35        70
Fisher's pairwise comparisons

    Family error rate = 0.605
Individual error rate = 0.0500

Critical value = 2.074
Intervals for (column level mean) - (row level mean)

             0       1       2       3       4       5       6       7       8       9

      1     -66.36
            -14.97
```

```
 2      -75.69    -35.03
        -24.31     16.36

 3      -88.36    -47.69   -38.36
        -36.97      3.69    13.03

 4      -73.69    -33.03   -23.69   -11.03
        -22.31     18.36    27.69    40.36

 5      -49.69     -9.03     0.31    12.97    -1.69
          1.69     42.36    51.69    64.36    49.69

 6      -40.36      0.31     9.64    22.31     7.64    -16.36
         11.03     51.69    61.03    73.69    59.03     35.03

 7      -47.03     -6.36     2.97    15.64     0.97    -23.03   -32.36
          4.36     45.03    54.36    67.03    52.36     28.36    19.03

 8      -42.36     -1.69     7.64    20.31     5.64    -18.36   -27.69    -21.03
          9.03     49.69    59.03    71.69    57.03     33.03    23.69     30.36

 9      -42.36     -1.69     7.64    20.31     5.64    -18.36   -27.69     -21.03    -25.69
          9.03     49.69    59.03    71.69    57.03     33.03    23.69      30.36     25.69

10      -37.69      2.97    12.31    24.97    10.31    -13.69    -23.03    -16.36    -21.03    -21.03
         13.69     54.36    63.69    76.36    61.69     37.69     28.36     35.03     30.36     30.36
```

Figure 5.6 – Photo-transfection parameter data
HEK-293 cells
One-Way Analysis of Variance

```
Analysis of Variance for C2
Source     DF        SS        MS         F        P
C1         10     11899      1190     10.01    0.000
Error      22      2615       119
Total      32     14514
                                  Individual 95% CIs For Mean
                                  Based on Pooled StDev
Level       N      Mean     StDev  ------+---------+---------+---------+
 0          3      0.00      0.00   (----*----)
 1          3     39.33     18.58                  (----*----)
 2          3     42.00     13.11                   (----*----)
 3          3     44.67      9.02                    (----*----)
 4          3     52.00     15.87                       (----*----)
 5          3     47.33      6.43                     (----*----)
 6          3      6.67     11.55     (-----*----)
 7          3      5.33      6.11     (----*----)
 8          3     14.67     14.05         (----*----)
 9          3     14.33      4.04         (----*----)
10          3      8.00      5.57      (----*----)
                                  ------+---------+---------+---------+
Pooled StDev =    10.90               0        25        50        75

Dunnett's intervals for treatment mean minus control mean

    Family error rate = 0.0500
Individual error rate = 0.00728

Critical value = 2.96

Control = level (0) of C1

Level        Lower    Center     Upper --------+---------+---------+---------
 1           12.99     39.33     65.68             (--------*--------)
 2           15.65     42.00     68.35              (--------*--------)
 3           18.32     44.67     71.01               (--------*--------)
 4           25.65     52.00     78.35                  (-------*--------)
 5           20.99     47.33     73.68                (--------*--------)
 6          -19.68      6.67     33.01  (--------*--------)
```

```
 7          -21.01      5.33     31.68  (--------*--------)
 8          -11.68     14.67     41.01     (--------*--------)
 9          -12.01     14.33     40.68     (--------*--------)
10          -18.35      8.00     34.35   (--------*-------)
                                        --------+---------+---------+---------
                                                0        30        60
Fisher's pairwise comparisons

    Family error rate = 0.605
Individual error rate = 0.0500

Critical value = 2.074

Intervals for (column level mean) - (row level mean)
              0        1        2        3        4        5        6        7        8        9


      1    -57.79
           -20.87

      2    -60.46   -21.13
           -23.54    15.79

      3    -63.13   -23.79   -21.13
           -26.21    13.13    15.79

      4    -70.46   -31.13   -28.46   -25.79
           -33.54     5.79     8.46    11.13

      5    -65.79   -26.46   -23.79   -21.13   -13.79
           -28.87    10.46    13.13    15.79    23.13

      6    -25.13    14.21    16.87    19.54    26.87    22.21
            11.79    51.13    53.79    56.46    63.79    59.13

      7    -23.79    15.54    18.21    20.87    28.21    23.54   -17.13
            13.13    52.46    55.13    57.79    65.13    60.46    19.79

      8    -33.13     6.21     8.87    11.54    18.87    14.21   -26.46   -27.79
             3.79    43.13    45.79    48.46    55.79    51.13    10.46     9.13

      9    -32.79     6.54     9.21    11.87    19.21    14.54   -26.13   -27.46   -18.13
             4.13    43.46    46.13    48.79    56.13    51.46    10.79     9.46    18.79

     10    -26.46    12.87    15.54    18.21    25.54    20.87   -19.79   -21.13   -11.79   -12.13
            10.46    49.79    52.46    55.13    62.46    57.79    17.13    15.79    25.13    24.79
```

Figure 5.7 – Photo-transfection neuroblastoma data
SK-N-SH cells
One-Way Analysis of Variance

```
Analysis of Variance for C2
Source     DF        SS        MS         F        P
C1          5    4153.8     830.8      9.49    0.001
Error      12    1050.7      87.6
Total      17    5204.4

                                  Individual 95% CIs For Mean
                                  Based on Pooled StDev
Level       N      Mean     StDev  ------+---------+---------+---------+
0           3     0.000     0.000  (-----*-----)
1           3    16.667     7.024         (-----*-----)
2           3    24.000    13.115             (-----*-----)
3           3    39.333     8.327                   (-----*-----)
4           3    43.333     7.572                     (-----*-----)
5           3    11.333    13.317        (-----*-----)
                                  ------+---------+---------+---------+
Pooled StDev =    9.357               0        20        40        60

Dunnett's intervals for treatment mean minus control mean
```

```
    Family error rate = 0.0500
Individual error rate = 0.0133

Critical value = 2.90

Control = level (0) of C1

Level        Lower    Center     Upper -----+---------+---------+---------+--
1           -5.489    16.667    38.823    (--------*--------)
2            1.844    24.000    46.156       (--------*-------)
3           17.177    39.333    61.489             (--------*--------)
4           21.177    43.333    65.489              (--------*--------)
5          -10.823    11.333    33.489  (--------*-------)
                                        -----+---------+---------+---------+--
                                             0        25        50        75
Fisher's pairwise comparisons

    Family error rate = 0.314
Individual error rate = 0.0500

Critical value = 2.179

Intervals for (column level mean) - (row level mean)

                    0           1           2           3           4

       1      -33.31
               -0.02

       2      -40.65      -23.98
               -7.35        9.31

       3      -55.98      -39.31      -31.98
              -22.69       -6.02        1.31

       4      -59.98      -43.31      -35.98      -20.65
              -26.69      -10.02       -2.69       12.65

       5      -27.98      -11.31       -3.98       11.35       15.35
                5.31       21.98       29.31       44.65       48.65
```

Figure 5.8 – Photo-transfection neuroblastoma data
NG 108-15 cells
One-Way Analysis of Variance

```
Analysis of Variance for C2
Source     DF        SS        MS        F        P
C1          5      3251       650     4.37    0.017
Error      12      1786       149
Total      17      5037
                                  Individual 95% CIs For Mean
                                  Based on Pooled StDev
Level       N      Mean     StDev  --------+---------+---------+--------
0           3      0.00      0.00  (-------*-------)
1           3     12.00     13.11        (-------*-------)
2           3     14.67      7.57          (------*-------)
3           3     26.67      9.45                (------*-------)
4           3     32.33     22.14                  (-------*-------)
5           3     40.00      9.17                      (-------*-------)
                                  --------+---------+---------+--------
Pooled StDev =    12.20             0        20        40

Dunnett's intervals for treatment mean minus control mean
```

```
    Family error rate = 0.0500
Individual error rate = 0.0133

Critical value = 2.90

Control = level (0) of C1

Level        Lower    Center     Upper -------+---------+---------+---------+
1          -16.89     12.00     40.89 (-----------*----------)
2          -14.22     14.67     43.55  (-----------*----------)
3           -2.22     26.67     55.55       (-----------*----------)
4            3.45     32.33     61.22         (-----------*----------)
5           11.11     40.00     68.89            (-----------*-----------)
                                      -------+---------+---------+---------+
                                             0        25        50        75
Fisher's pairwise comparisons

    Family error rate = 0.314
Individual error rate = 0.0500

Critical value = 2.179

Intervals for (column level mean) - (row level mean)

                    0           1           2           3           4

       1      -33.71
                9.71

       2      -36.37      -24.37
                7.04       19.04

       3      -48.37      -36.37      -33.71
                -4.96       7.04        9.71

       4      -54.04      -42.04      -39.37      -27.37
               -10.63        1.37        4.04       16.04

       5      -61.71      -49.71      -47.04      -35.04      -29.37
               -18.29       -6.29       -3.63        8.37       14.04
```

Figure 5.9A – Passage Number data
CHO-K1 cells
One-Way Analysis of Variance

```
Analysis of Variance for C2
Source     DF        SS        MS        F        P
C1          5      7495      1499     4.25    0.019
Error      12      4229       352
Total      17     11724
                                  Individual 95% CIs For Mean
                                  Based on Pooled StDev
Level       N      Mean     StDev  --------+---------+---------+--------
0           3      0.00      0.00  (-------*-------)
1           3     40.67     35.57                (-------*------)
2           3     50.00     17.78                   (-------*-------)
3           3     62.67      8.33                       (-------*-------)
4           3     48.00     16.37                    (-------*-------)
5           3     24.00     14.00          (-------*-------)
                                  --------+---------+---------+--------
Pooled StDev =    18.77                   0        30        60

Dunnett's intervals for treatment mean minus control mean
```

```
    Family error rate = 0.0500
Individual error rate = 0.0133

Critical value = 2.90

Control = level (0) of C1

Level        Lower    Center     Upper ------+---------+---------+---------+-
1            -3.79     40.67     85.12      (------------*-----------)
2             5.55     50.00     94.45         (-----------*------------)
3            18.21     62.67    107.12            (------------*------------)
4             3.55     48.00     92.45        (------------*-----------)
5           -20.45     24.00     68.45 (------------*------------)
                                       ------+---------+---------+---------+-
                                             0        35        70       105




Fisher's pairwise comparisons

    Family error rate = 0.314
Individual error rate = 0.0500

Critical value = 2.179

Intervals for (column level mean) - (row level mean)

                    0           1           2           3           4

       1      -74.07
               -7.27

       2      -83.40      -42.73
              -16.60       24.07

       3      -96.07      -55.40      -46.07
              -29.27       11.40       20.73

       4      -81.40      -40.73      -31.40      -18.73
              -14.60       26.07       35.40       48.07

       5      -57.40      -16.73       -7.40        5.27       -9.40
                9.40       50.07       59.40       72.07       57.40
```

Figure 5.9B – Passage Number data
HEK-293 cells
One-Way Analysis of Variance

```
Analysis of Variance for C2
Source     DF        SS        MS         F        P
C1          5      4516       903      7.44    0.002
Error      12      1456       121
Total      17      5972
                                  Individual 95% CIs For Mean
                                  Based on Pooled StDev
Level       N      Mean     StDev  ------+---------+---------+---------+
0           3      0.00      0.00  (-----*-----)
1           3     28.67     11.85             (----*-----)
2           3     33.33      2.52               (----*-----)
3           3     36.00      5.29                (----*-----)
4           3     52.00     14.42                      (-----*----)
```

```
5           3     39.33     18.58                  (-----*----)
                                        ------+---------+---------+---------+
Pooled StDev =    11.02                       0        25        50        75

Dunnett's intervals for treatment mean minus control mean

    Family error rate = 0.0500
Individual error rate = 0.0133

Critical value = 2.90

Control = level (0) of C1

Level        Lower    Center     Upper ---------+---------+---------+--------
1             2.58     28.67     54.75 (------------*------------)
2             7.25     33.33     59.42    (------------*------------)
3             9.92     36.00     62.08     (------------*------------)
4            25.92     52.00     78.08              (------------*------------)
5            13.25     39.33     65.42       (------------*------------)
                                        ---------+---------+---------+--------
                                                20        40        60
Fisher's pairwise comparisons

    Family error rate = 0.314
Individual error rate = 0.0500

Critical value = 2.179

Intervals for (column level mean) - (row level mean)

                    0           1           2           3           4

       1      -48.26
               -9.07

       2      -52.93      -24.26
              -13.74       14.93

       3      -55.60      -26.93      -22.26
              -16.40       12.26       16.93

       4      -71.60      -42.93      -38.26      -35.60
              -32.40       -3.74        0.93        3.60

       5      -58.93      -30.26      -25.60      -22.93       -6.93
              -19.74        8.93       13.60       16.26       32.26
```

Figure 5.11 – Cell Synchronization data
CHO-K1 cells
One-Way Analysis of Variance

```
Analysis of Variance for C2
Source     DF        SS        MS        F        P
C1          3   10062.0    3354.0   186.33    0.000
Error       8     144.0      18.0
Total      11   10206.0
                                  Individual 95% CIs For Mean
                                  Based on Pooled StDev
Level       N      Mean     StDev  ---+---------+---------+---------+---
0           3     0.000     0.000   (-*-)
1           3    41.000     3.606                 (-*--)
2           3    62.000     6.557                       (-*-)
3           3    77.000     4.000                             (-*-)
                                  ---+---------+---------+---------+---
```

```
Pooled StDev =    4.243               0        25        50        75

Dunnett's intervals for treatment mean minus control mean

    Family error rate = 0.0500
Individual error rate = 0.0205

Critical value = 2.88

Control = level (0) of C1

Level        Lower    Center     Upper ----------+---------+---------+-------
1           31.023    41.000    50.977  (-----*------)
2           52.023    62.000    71.977                (-----*------)
3           67.023    77.000    86.977                        (-----*------)
                                       ----------+---------+---------+-------
                                                 45        60        75
Fisher's pairwise comparisons

    Family error rate = 0.176
Individual error rate = 0.0500

Critical value = 2.306

Intervals for (column level mean) - (row level mean)

                    0           1           2

       1      -48.99
              -33.01

       2      -69.99      -28.99
              -54.01      -13.01

       3      -84.99      -43.99      -22.99
              -69.01      -28.01       -7.01
```

Figure 5.11 – Cell Synchronization data
HEK-293 cells
One-Way Analysis of Variance

```
Analysis of Variance for C2
Source     DF        SS        MS         F        P
C1          3    5270.9    1757.0    24.95    0.000
Error       8     563.3      70.4
Total      11    5834.2
                                  Individual 95% CIs For Mean
                                  Based on Pooled StDev
Level       N      Mean     StDev  -----+---------+---------+---------+-
0           3     0.000     0.000   (---*---)
1           3    24.000     5.568            (----*---)
2           3    32.333    15.308               (----*---)
3           3    58.667     4.041                        (---*----)
                                  -----+---------+---------+---------+-
Pooled StDev =    8.391                0        25        50        75

Dunnett's intervals for treatment mean minus control mean

    Family error rate = 0.0500
Individual error rate = 0.0205

Critical value = 2.88

Control = level (0) of C1
```

```
Level        Lower    Center     Upper --------+---------+---------+---------
1             4.267    24.000    43.733 (---------*---------)
2            12.601    32.333    52.066     (---------*---------)
3            38.934    58.667    78.399                (---------*---------)
                                        --------+---------+---------+---------
                                               20        40        60
Fisher's pairwise comparisons

    Family error rate = 0.176
Individual error rate = 0.0500

Critical value = 2.306

Intervals for (column level mean) - (row level mean)

                    0           1           2

       1      -39.80
               -8.20

       2      -48.13      -24.13
              -16.53        7.47

       3      -74.47      -50.47      -42.13
              -42.87      -18.87      -10.53
```

C. Materials, cell culturing and plasmid DNA preparation for stem cell photo-transfection

i. Experimental setup

During all the pluripotent stem cell studies, the fs laser beam profile as well as pulse duration were measured as mentioned in subsections 5.2.1 and 5.2.2 (page 112-113) of this thesis. The photo-transfection setup was also arranged and aligned the same as previously described (subsection 5.2.3, page 113). For statistical purposes all experiments were done in triplicates and each experiment repeated three times under the same conditions. In addition throughout my experiments, the transfection efficiency (%) was calculated according to Tsukakoshi et al, 1984 (1) and Stevenson et al, 2009 (2) (appendix B (iv) page B2).

ii. Pluripotent stem cells used

The pluripotent mES cells utilized during my studies and presented in the data within chapter 6 are called E14g2a cells. These cells were obtained as a kind donation from Dr. Judith Sleeman (University of St. Andrews, School of Biology, Scotland). Although these cells are not specifically a cell line, in that they have not been transformed and do not have longevity genes required to make permanent immortal cell line, they divided frequently when cultured in the presence of the leukemia inhibitory growth factor (LIF). LIF is an interleukin 6 class cytokine, which is a chemical that affects cell growth, development and influences embryogenesis. Since embryonic stem cells arise from the ICM at the blastocyst stage, their removal from this location results in their removal from their natural supply and source of LIF. Consequently, removal of LIF imposes stem cell differentiation. Therefore, during *in vitro* culturing of mES cells LIF supplementation is crucial to maintain the stem cells in an undifferentiated state.

iii. Cell Culturing

The E14g2a cells were always cultured in a 37^{o}C, 5 % carbon dioxide (CO_2) and 85 % humid incubator (optimum growth condition). These adherent cells were grown in 0.2 % gelatin (Sigma, UK) coated on the surface of a T25 vented top culture flasks (*Nunc*^{TM}). They were sub-cultured twice weekly at a concentration of 1 X 10^6 cells/ml in complete growth medium constituting of Knockout DMEM (KDMEM) (*Invitrogen, UK*) modified with 1 % non-essential amino acids (*Invitrogen, UK*), 1 % L-glutamine (*Invitrogen, UK*), 1 % sodium pyruvate (*Invitrogen, UK*), 0.1 % β-mercaptoethanol (Si*gma, UK*), supplemented with LIF (*Millipore, UK*) and 10 % FBS (*Biosera, UK*).

iv. Plasmid DNA Preparation

The same 4.7 kb plasmid (pDsRed2-Mito) as used previously was used for stem cell photo-transfection (appendix B (iii) page B2). To differentiate the E14g2a cells, a transcription factor Gata-6 gene was obtained a kind gift from Dr. Josh Brickman (University of Edinburgh, Scottish Centre for Regenerative Medicines, Scotland) which was already introduced into an 8.6 kb pCAGSIH vector resistant to hygromycin. This plasmid was also multiplied in *E. coli* and thereafter purified using the mini-prep kit from Qiagen. Expression of Gata-6 in embryonic stem cells is sufficient to trigger the proper differentiation program towards ExE (3).

References

1. Tsukakoshi, Kurata, Nomiya, Ikawa and Kasuya, "A novel method of DNA transfection by laser microbeam cell surgery," *Appl. Phys. B-Photo.* **35**, 135-140 (1984)
2. D. Stevenson, F. Gunn-Moore, C. Campbell and K. Dholakia, "Transfection by optical injection," *The Handbook of Photonics for Biomedical Science,* **Chapter 3**, 87-117 (2010)
3. J. Fujikura, E. Yamato, S. Yonemura, K. Hosoda, S. Masui, K. Nakao, J. Miyazaki and H. Niwa, "Differentiation of embryonic stem cells is induced by GATA factors," *Genes Dev.* **16**, 784-789 (2002)